

The Role of Heparan Sulphate Proteoglycans in Extracellular Vesicle-Mediated Growth Factor Delivery



Sara Isabel Ferreira Veiga

Division of Cancer and Genetics

School of Medicine

Cardiff University

*Thesis submitted for the degree of
Doctor of Philosophy*

August 2021

Acknowledgements

Firstly, I would like to thank Cancer Research Wales for funding my research. This project would not have been possible without their support, and I am incredibly grateful for this opportunity.

To my supervisors, Dr Jason Webber and Professor Aled Clayton, I would like to thank you for introducing me to the amazing EV field, and for all the guidance and encouragement throughout my PhD. You pushed me to always be better and helped me growing as a scientist; plus, you were always extremely patient in answering my millions of questions. I would also like to extend my appreciation to Professor Rachel Errington and Dr Zsuzsanna Tabi for all your contributions to this project.

During my PhD studies I have been extremely lucky to be able to be part of such a supportive and encouraging group as TMEG. I would like to thank Dr Alex Cocks and Dr Alexandra Shephard for teaching me the ways of the lab and helping me set up when I first started my PhD. I owe an extra special thank you to Alex Cocks for his help in some of my experiments and for keeping up the good spirit in the lab. To Dr Lauren Evans (!), your friendship and your wonderful contributions to our PhD shrine were essential to keep me motivated during these years. I also love all the new British expressions you taught me during these years. Working alongside you was a pleasure, and I had a really good time being your lab mate. Dr Andreia de Almeida, thank you for being an awesome friend and for always having an encouraging word. Your enthusiasm for science is inspiring and I was really lucky to be able to collaborate with you in so many fun projects. Dr Kate Milward, thank you so much for all the training and help you provided me during some of the most challenging times of my thesis. Your patience, enthusiasm and very thoughtful advice, were crucial to keep me pushing towards the end. Dr Chris Burton, who would have guessed that you joining our lab would have such a huge impact in my own scientific career? I am so happy to have been able to work alongside you and thankful for all the good times we had in the lab. Mark Gurney, Thea Konstantinou and Muireann Ni Bhaoighill, I am really thankful for all the times one of you helped me solve an EV-related enigma or helped me to deal with lab equipment and particular experiments. I would also like to thank Marie Wiltshire, for safely and quickly getting the PhD students back in the lab, after all the COVID-19 challenges, as well as Dr Dimitris Parthimos and Dr Rachel Howard Jones for their ongoing support throughout my PhD.

While away from home, I was incredibly fortunate to have a wonderful and supportive group of friends here in Cardiff. To Ana, I took my first steps in science with you, years back in Portugal, and I was able to have you supporting me throughout my PhD journey. How lucky am I?! There will never be enough words or thank yous to summarize and truly appreciate how important you are to me, and how incredibly grateful I am to have you in my life. Thank you for everything! To Aleksandra, thank you for your friendship, all your support and constant reassurance. You have helped me with so many different things throughout my PhD; I cannot thank you enough! You are a wonderful friend, and I am very lucky to have been able to share all these years with you.

To my housemates, Dave, Neil, Shane, and Jenni, you guys made our house in Crwys Road a home away from home. You have been such amazing housemates during these years! Thank you so much for putting up with all my PhD talk and struggles and for always having an encouraging word. Movie night is resuming shortly! Dave, I want to especially thank you for everything you have done for me. You have made this journey so much easier, and I will never be able to thank you enough for all the things you do to see me happy. Your words of encouragement have been essential to keep me pushing, especially towards the end.

To all my friends back in Portugal, thank you for always being there for me. To João and Catarina, you guys are my best cheerleaders. Thank you!

Finally, I want to thank my brother and parents for their continued and unconditional support. You have always been there for me throughout my many adventures around the world. Knowing that I can always count on you makes all this so much easier. Thank you for all your love and for believing in me.

Summary

The crosstalk between cells in the tumour microenvironment is important for disease progression. Prostate cancer cells secrete extracellular vesicles (EVs), which play a key role in regulating the phenotype of local fibroblasts. Heparan sulphate (HS) glycosaminoglycan (GAG) chains, associated with heparan sulphate proteoglycans (HSPGs), have previously been implicated in EV-mediated communication; in delivery of transforming growth factor beta-1 (TGF- β 1) to fibroblasts and in triggering a distinctive myofibroblast differentiation. HSPGs, however, are known to bind a variety of other growth factors and cytokines, and we hypothesise that vesicular-associated HS plays an important role in the simultaneous delivery of complex factors to recipient cells. We anticipated that removal of EV-associated HS would result in attenuated delivery of factors and altered biology.

Removal of HS-GAG chains by heparinase III digestion, or selective attenuation of single-HSPG core proteins by genetic manipulation, did not grossly impact biophysical measurements of vesicles. Nonetheless, differences in protein expression between control vs. HS and HSPG-modified EVs were certainly apparent. Removal of HS resulted in loss of several factors from the EV surface. Manipulating core proteins, however, produced complex data with examples of both loss and gain of factors, likely due to the roles of HSPGs in cargo loading during biogenesis. Functional enrichment analysis of these factors suggests roles in cancer-relevant processes such as angiogenesis, tumour invasion and immune function. Loss of EV-associated HS was functionally impactful, with a demonstrable attenuation of fibroblast to myofibroblast differentiation, and attenuated several EV-mediated signalling pathways. EV-activated fibroblasts were further shown to secrete different pro- and anti-inflammatory cytokines following HS modulation of EVs. To explore the immune effects and inflammatory characteristics promoted by EVs, THP-1 cells were used as a model for myeloid polarisation. Preliminary data points to a fibroblast secretome capable of inducing an anti-inflammatory THP-1 phenotype.

This study provides insight into the complex modalities by which HSPGs control the phenotype of EVs and emphasises the importance of this mechanism of growth factor delivery in processes such as stromal modulation in cancer.

Scientific contributions

Manuscripts in preparation

Veiga, S.; Shephard, A.; Cocks, A. Clayton, A.; Webber, J. Heparan sulphate proteoglycans are required for EV-mediated delivery of growth factors that modulate fibroblast function (working title). *In preparation.*

Shephard AK.; **Veiga S.**; Cocks A.; Errington RJ.; Clayton A.; Webber, JP. EV-associated heparan sulphate proteoglycans drive prostate cancer progression and can predict aggressive disease. *In preparation.*

Burton, C.; **Veiga, S.**; De Almeida, A.; Milward, K.; Ni Bhaioighill, M.; Evans, L.; Konstantinou, T.; Mikhailov, R.; Wu, F.; Yang, C.; Errington, E.; Webber, J.; Clayton, A. Eeve - "the 3D-EV". A handheld model representing an Extracellular Vesicle, as a public engagement tool. *In preparation.*

Alexander Cocks; Jason P. Webber; **Sara Veiga**; Peter Watson; Arwyn T. Jones; Juan Manuel Falcon-Perez; Pierre Riskallah; Maria Harkiolarki; Rachel J. Errington; Aled Clayton. Assessing endocytosis of cancer-vesicles by stromal fibroblasts; evidence for mitochondrial delivery of luminal cargo. *In preparation.*

Abstracts published in indexed journals

Sara Veiga, Alex Shephard, Alex Cocks, Aled Clayton and Jason Webber. Heparan sulphate proteoglycans are required for EV-mediated delivery of multiple growth factors (OP2.06 = PF17.06) J Extracell Vesicles. Volume 9, 2020 - Issue sup1: ISEV2020: Abstract Book.

Christian Burton, **Sara Veiga**, Jason Webber, Kate Milward, Muireann Ni Bhaioighill, Lauren Evans, Andreia De Almeida, Rachel J. Errington and Aled Clayton. 3D-printed model to represent the structure and nature of extracellular vesicles, for public engagement and education events (PT08.01). J Extracell Vesicles. Volume 9, 2020 - Issue sup1: ISEV2020: Abstract Book.

Sara Veiga, Alex Shephard, Alex Cocks, Aled Clayton and Jason Webber. Heparan sulphate glycosaminoglycans on the extracellular vesicle surface bind a variety of proteins (OF19.02). J Extracell Vesicles. 2019; 8(Suppl 1): 1593587.

Oral presentations - selected abstracts

Heparan sulphate proteoglycans are required for EV-mediated delivery of multiple growth factors. ISEV 2020 Annual Meeting, virtual meeting, July 2020. *Oral presentation with Poster.*

Introduction to SNEV. ISEV 2020 Annual Meeting, virtual meeting, July 2020. Current EVents session.

Heparan sulphate glycosaminoglycans on the extracellular vesicle surface bind a variety of proteins. ISEV 2019 Annual Meeting, Kyoto, Japan. April 2019.

Conference posters

A 3D-printed model to represent the structure and nature of extracellular vesicles, for public engagement and education events. ISEV 2020 Annual Meeting, virtual meeting, July 2020. *Outstanding Poster Abstract Award winner.*

Heparan sulphate proteoglycans at vesicle surface are important for cell-to-cell communication and cancer progression. GW4 Nanomedicine Conference and Workshop. Exeter, UK. July 2019. *One minute flash presentation.*

Defining Proteins Associated with Heparan Sulphate Proteoglycans on the Exosome Surface. 33rd Annual School of Medicine and Dentistry Research Day, Cardiff, UK. January 2019. *Poster and poster with pitch presentation.*

Defining Proteins Associated with Heparan Sulphate Proteoglycans on the Exosome Surface. UKEV Forum 2018, Sheffield, UK. December 2018.

Funding and awards

Travel grants

Cardiff Institute for Tissue Engineering and Repair (CITER) Travel Bursary to attend the 9th Annual Meeting of the International Society for Extracellular Vesicles (ISEV) in Philadelphia, USA. 2020 - later moved online.

William Morgan Thomas Fund Travel Bursary to attend the 9th Annual Meeting of the International Society for Extracellular Vesicles (ISEV) in Philadelphia, USA. 2020 - later moved online.

UK Society for Extracellular Vesicles (UKEV) Forum 2019 Travel Grant.

M Banfill Fund Travel Bursary to attend the 8th Annual Meeting of the International Society for Extracellular Vesicles (ISEV) in Kyoto, Japan. 2019.

William Morgan Thomas Fund Travel Bursary to attend the 8th Annual Meeting of the International Society for Extracellular Vesicles (ISEV) in Kyoto, Japan. 2019.

Table of Contents

Acknowledgements	iii
Summary	v
Scientific contributions	vii
Table of Contents	ix
List of Figures	xiii
List of Tables	xvii
List of Appendices	xix
Abbreviations	xxi
1 Introduction.....	1
1.1 Extracellular Vesicles.....	1
1.1.1 Defining EVs – The rise of the extracellular vesicle field	1
1.1.2 EV Biogenesis & composition	2
1.1.2.1 EV biogenesis.....	2
1.1.2.2 The complex molecular composition of a vesicle	6
1.1.3 EV isolation methods and EV characterisation	9
1.1.3.1 EV isolation methods.....	9
1.1.3.2 EV characterisation	12
1.1.4 General properties of EV interactions with recipient cells	14
1.2 EVs in the tumour microenvironment	18
1.2.1 Overview of the tumour microenvironment	18
1.2.2 EVs in tumour-to-tumour communication	23
1.2.3 EVs in tumour-to-fibroblasts communication.....	24
1.2.4 EVs in tumour-to-endothelial cells communication	25
1.2.5 Cancer-derived EVs modulate immune response.....	26
1.2.6 Tumour EVs help to set up the pre-metastatic niche	28
1.3 EV-associated HSPGs within the tumour microenvironment	32
1.3.1 HSPG structure	32
1.3.2 HSPGs bind growth factors.....	35
1.3.3 HSPGs in cancer.....	37
1.3.4 HSPGs in EV biogenesis	39
1.3.5 HSPGs in EV uptake	41
1.3.6 The roles of EV-associated HSPGs in cancer	44
1.4 Hypothesis and aims.....	46
2 Materials and Methods.....	47
2.1 Cell culture	49
2.1.1 Monolayer cell culture	49
2.1.2 shRNA-mediated knockdown of HSPGs within DU145 cells	50
2.1.3 High-density bioreactor culture of DU145 cells	51
2.2 EV isolation	52
2.2.1 Isolation of EV by ultracentrifugation on a sucrose cushion.....	52
2.3 EV characterisation	52
2.3.1 Bicinchoninic acid protein assay	52
2.3.2 Western blotting	53
2.3.2.1 Sample preparation	53
2.3.2.2 Bradford assay	53

2.3.2.3	Polyacrylamide gel electrophoresis	53
2.3.2.4	Protein transfer and detection	54
2.3.3	Nanoparticle tracking analysis	56
2.3.4	Microplate immunophenotyping assay for EV analysis	56
2.3.5	Cryo-electron microscopy	57
2.4	Modification of EV-associated HSPGs.....	57
2.4.1	Heparinase III digestion of HS-GAG chains	57
2.5	Proteomic analysis of HSPG-modified EVs.....	58
2.5.1	Olink Proximity Extension Assay	58
2.5.2	Olink data analysis	59
2.5.3	Functional enrichment analysis	60
2.5.4	Validation & quantification of selected protein targets by Enzyme-Linked Immunosorbent Assay (ELISA)	60
2.6	Assessment of EV function	64
2.6.1	Fibroblast differentiation	64
2.6.2	Uptake of EVs.....	64
2.6.2.1	Fluorescent labelling	64
2.6.2.2	Detection of cellular uptake of fluorescent EVs by fluorescent microscopy	65
2.6.2.3	Detection of cellular uptake of fluorescent EVs by flow cytometry.....	65
2.6.3	Assessment of EV-mediated signalling and cytokine production in recipient fibroblasts	68
2.6.3.1	Proteome Profiler Human Phospho-Kinase Array Kit (R&D Systems)	68
2.6.3.2	Proteome Profiler Human XL Cytokine Array (R&D Systems).....	68
2.6.3.3	Measuring cytokine production in recipient fibroblasts	69
2.6.4	Monocytic differentiation, and macrophage polarisation and activation studies	70
2.6.4.1	THP-1 differentiation into macrophage-like cells	70
2.6.4.2	THP-1 stimulation with fibroblast derived cell conditioned medium	70
2.6.4.3	THP-1 stimulation with EVs treated with active HEPHIII, heat-inactivated HEPHIII or no enzyme.....	71
2.6.4.4	Macrophage stimulation with fibroblast derived cell conditioned medium	71
2.6.4.5	Macrophage stimulation with EVs treated with active HEPHIII, heat-inactivated HEPHIII or no enzyme	71
2.6.5	Flow cytometry analysis	72
2.6.5.1	Labelling of cell surface antigens for surface and intracellular staining	72
2.6.5.2	General gating strategy.....	73
2.6.6	Measuring cytokine production from THP-1 and macrophage stimulated cells.....	75
2.7	Statistical analysis.....	76
3	Characterisation of prostate cancer cell-derived extracellular vesicles	77
3.1	Introduction.....	79
3.2	Aims & Objectives	82
3.3	Characterisation of DU145-derived EVs	84
3.3.1	Vesicle morphology	84
3.3.2	Vesicle size distribution and purity assessment	86
3.3.3	Quality assessment by vesicle protein	89
3.4	Removal of HS-GAG chains from the EV surface.....	91
3.4.1	Heparinase III digestion of HS-GAG chains on DU145 EVs	91
3.4.2	Assessment of off-target effects associated with heparinase III digestion of vesicles	

3.5 Knockdown of vesicular-associated HSPGs	97
3.5.1 Confirmation of HSPG knockdown on DU145 cells	97
3.5.2 Assessment of the effects on EVs due to HSPG knockdown	101
3.6 Discussion	105
4 Defining the repertoire of proteins tethered to the surface of extracellular vesicles by heparan sulphate proteoglycans	111
4.1 Introduction.....	113
4.1.1 Aims & Objectives	116
4.2 Exploring the profile of vesicular HSPG-associated proteins	117
4.2.1 Discovery of HS-associated factors in DU145 extracellular vesicles	117
4.2.2 Functional enrichment analysis of HEPHIII-digested vesicles	121
4.2.3 Selecting protein candidates for validation.....	128
4.2.4 ELISA validation of selected proteins in DU145 EVs	130
4.2.5 ELISA validation of selected proteins in HEPHIII-treated EVs	132
4.2.6 Perturbation of HSPG core proteins on vesicles and their impact on EV-associated factors	135
4.2.7 Analysis of EV changes due to HSPG core protein loss.....	142
4.2.8 Functional enrichment analysis of the of HSPG-deficient EVs	147
4.2.9 ELISA validation of proteins in HSPG-deficient extracellular vesicles	156
4.2.10 Comparison of proteins with altered expression following either HEPHIII treatment or attenuation of specific HSPGs	162
4.3 Discussion	167
5 Exploring the impact of heparan sulphate-deficiency on extracellular vesicle function	175
5.1 Introduction.....	177
5.1.1 Aims & Objectives	180
5.2 The impact of HS removal on vesicle uptake by fibroblast cells.....	181
5.2.1 Imaging of EV uptake by fluorescent microscopy	181
5.2.2 Semi-quantitative analysis of EV uptake by flow cytometry	183
5.3 HS-mediated regulation of EV-related functions.....	185
5.3.1 Fibroblast differentiation	185
5.3.1.1 Induction of an α SMA-positive myofibroblast-like phenotype.....	185
5.3.2 The impact on fibroblast function	188
5.3.2.1 Impact of vesicles on common signalling pathways.....	188
5.3.2.2 Impact of vesicles on fibroblast cytokine secretion.....	194
5.3.2.3 Secretion of growth factors by EV-activated fibroblasts	199
5.3.3 The conversation between EV-activated stroma and immune cells.....	201
5.3.3.1 Characterisation of macrophage subsets in THP-1 cells.....	202
5.3.3.2 Differentiation and polarisation responses induced by EV activated fibroblasts	207
5.3.3.3 Differentiation and polarisation responses induced directly by EVs	216
5.3.4 Assessment of cytokine secretion by stimulated THP-1 cells	224
5.4 Discussion	229
6 Discussion	235

6.1 General discussion 237
6.2 Future Directions 241
6.3 Concluding Remarks 242
Appendices 243
References 257

List of Figures

Figure 1.1. Extracellular vesicle biogenesis process.	5
Figure 1.2. Molecular composition of vesicles of endosomal origin.	8
Figure 1.3 Processes of cellular communication.	17
Figure 1.4. Tumour-derived EVs in the tumour microenvironment.	31
Figure 1.5. Examples of Heparan sulphate proteoglycans present at the surface of cells and extracellular vesicles.	33
Figure 1.6. Heparan sulphate biosynthesis.	34
Figure 1.7. Roles of HSPGs in EV biogenesis and uptake.	43
Figure 2.1. Overview of the PEA technology for Olink Target 96.	59
Figure 2.2. Representative standard curves for each of the ELISAs used to validate and quantify proteins identified from the Olink analysis, on the EV surface.	63
Figure 2.3. Gating strategy used for analysis of uptake of fluorescent EVs by fluorescent microscopy.	67
Figure 2.4. Representative standard curves for each of the ELISAs used to assess cytokine production in recipient fibroblasts.	69
Figure 2.5. Gating strategy used for analysis of monocytic differentiation and macrophage activation studies.	74
Figure 2.6. Representative standard curves for each of the ELISAs used to assess cytokine production from THP-1 and macrophage stimulated cells.	76
Figure 3.1. Enzymatic digestion with Heparinase III.	83
Figure 3.2. Schematic representation of Heparinase I, Heparinase II and Heparinase III cleavage sites.	83
Figure 3.3. Cryo-EM of purified DU145 EVs.	85
Figure 3.4. Size distribution of DU145 derived EVs.	86
Figure 3.5. Distribution of particle to protein (P:P) ration over time.	89
Figure 3.6. Characterisation of DU145 derived EVs by Western Blot.	90
Figure 3.7. Detection of tetraspanins present in DU145 derived EVs by a plate-based immunophenotyping assay.	91
Figure 3.8. Confirmation of HEP III digestion of heparan sulphate on DU145 EVs.	93
Figure 3.9. Tetraspanins expression on EVs after HEP III enzymatic digestion.	94
Figure 3.10. Size distribution of DU145 EVs after HEP III enzymatic digestion.	95
Figure 3.11. Recovery yield obtained for different HEP III enzymatic digestions carried.	96

Figure 3.12. HSPG expression in DU145 cells, at the mRNA level, following knockdown of each HSPG with 5 different shRNA sequences.	98
Figure 3.13. HSPG knockdown specificity in DU145 cell lines, assessed through non-targeted HSPG expression, at mRNA level.	99
Figure 3.14. HSPG protein expression on the surface of EVs from HSPG-modified DU145 cell lines.	100
Figure 3.15. Impact of HSPGS-knockdown on size and EV phenotype of vesicles obtained from cell conditioned media.	101
Figure 3.16. Impact of HSPGS-knockdown on size and phenotype of EVs isolated through sucrose cushion method.	103-104
Figure 4.1. Enzymatic removal of HS side chains alters the protein profile of DU145 vesicles.	120
Figure 4.2. Top 10 biological pathways provided by FunRich for proteins associated with HS-GAG chains in HEP111 treated vesicles.	123
Figure 4.3. Additional significantly enriched associations (not in the top 10).	124
Figure 4.4. Functional enrichment analysis of biological pathways by FunRich for list of proteins randomly selected from the cardiovascular III, inflammation, and oncology II panels.	127
Figure 4.5. Validation of selected proteins detectable on the EV surface.	131
Figure 4.6. Impact on protein concentration upon HS-chains removal from DU145 vesicles.	134-135
Figure 4.7. Removal of specific HSPGs from DU145 vesicles produces vesicles with distinct protein profiles.	139-141
Figure 4.8. Venn diagram and list showing the associations between proteins elevated in HSPG-deficient vesicles.	143
Figure 4.9. Venn diagram and table showing the associations between proteins decreased in HSPG-deficient vesicles.	146
Figure 4.10. Top 10 biological pathways provided by FunRich for the differently expressed proteins associated with vesicular HSPGs.	151
Figure 4.11. Common pathways attributable to both HSPG-deficient and HEP111-digested EVs (not in the top 10).	152
Figure 4.12. Functional enrichment analysis of biological pathways by FunRich for list of proteins randomly selected from the cardiovascular III panel, inflammation panel, and oncology II panel.	155

Figure 4.13. Validation of targets identified in HSPG-deficient vesicles on DU145 EVs.	158
Figure 4.14. Quantification of different proteins at the surface of HSPGs-deficient vesicles.	161
Figure 4.15. Validation of targets identified in HSPG-deficient vesicles on HEPIII-treated DU145 EVs.	163
Figure 4.16. Venn diagrams show common proteins with altered expression following HEPIII-treatment of EVs or modification of EV-associated HSPGs.	165-166
Figure 5.1. Uptake of Alexa-594 labelled EVs by fibroblasts.	182
Figure 5.2. Quantification by flow cytometry of the uptake of Alexa-633 labelled EVs by fibroblasts.	184
Figure 5.3. Myofibroblast differentiation induced by EVs.	187
Figure 5.4. Tyrosine kinase receptors activation in fibroblasts treated with prostate cancer EVs, compared with untreated cells.	189
Figure 5.5. EVs promote phosphorylation of proteins not constitutively active in fibroblast cells.	190
Figure 5.6. Removal of HS-GAG chains alters receptor activation promoted by EVs.	192
Figure 5.7. Detection of VEGF and FGF on vesicle surface.	193
Figure 5.8. Proteins produced by fibroblasts treated with prostate cancer EVs, compared with untreated cells.	195
Figure 5.9. EVs promote production of different cytokines by fibroblast cells.	197
Figure 5.10. Removal of HS-GAG chains alters cytokine production promoted by EVs.	198
Figure 5.11. Secretion of FGF, VEGF and HGF by EV activated fibroblasts.	200
Figure 5.12. Characterisation of CD14 ⁺ population in THP-1 cells by flow cytometry.	203
Figure 5.13. Characterisation of CD68 ⁺ cells in the THP-1 population by flow cytometry.	204
Figure 5.14. Characterisation of CD14 ⁺ CD80 ⁺ , CD14 ⁺ CD86 ⁺ , CD14 ⁺ CD163 ⁺ and CD14 ⁺ CD206 ⁺ population in THP-1 cells by flow cytometry.	205-206
Figure 5.15. Schematic representation of indirect EV-stimulation of THP-1 cells and THP-1 cells previously primed with PMA.	207
Figure 5.16. Characterisation of CD14 ⁺ population in THP-1 and THP-1+PMA cells after indirect EV-stimulation through fibroblast conditioned media.	209
Figure 5.17. Characterisation of CD68 ⁺ population in THP-1 and THP-1+PMA cells after indirect EV-stimulation through fibroblast cell conditioned media.	210

Figure 5.18. Characterisation of CD14 ⁺ CD80 ⁺ , CD14 ⁺ CD86 ⁺ , CD14 ⁺ CD163 ⁺ and CD14 ⁺ CD206 ⁺ population in THP-1 cells after indirect EV-stimulation through fibroblast conditioned media.	211-212
Figure 5.19. Characterisation of CD14 ⁺ CD80 ⁺ , CD14 ⁺ CD86 ⁺ , CD14 ⁺ CD163 ⁺ and CD14 ⁺ CD206 ⁺ population in THP-1+PMA cells after indirect EV-stimulation through fibroblast conditioned media.	214-215
Figure 5.20. Schematic representation of direct EV-stimulation of THP-1 cells and THP-1 cells previously primed with PMA.	216
Figure 5.21. Characterisation of CD14 ⁺ population in THP-1 and THP-1+PMA cells after direct EV-stimulation.	218
Figure 5.22. Characterisation of CD68 ⁺ population in THP-1 and THP-1+PMA cells after direct EV-stimulation.	219
Figure 5.23. Characterisation of CD14 ⁺ CD80 ⁺ , CD14 ⁺ CD86 ⁺ , CD14 ⁺ CD163 ⁺ and CD14 ⁺ CD206 ⁺ population in THP-1 cells after direct EV-stimulation.	220-221
Figure 5.24. Characterisation of CD14 ⁺ CD80 ⁺ , CD14 ⁺ CD86 ⁺ , CD14 ⁺ CD163 ⁺ and CD14 ⁺ CD206 ⁺ population in THP-+PMA cells after direct EV-stimulation.	222-223
Figure 5.25. Secretion of IL-1 β , TNF- α , VEGF and TGF- β by THP-1 and THP-1+PMA cells directly or indirectly stimulated by EVs.	225-228

List of Tables

Table 2.1. Cell line culture conditions.	50
Table 2.2. Primary antibodies.	55
Table 2.3. Antibodies used to confirm successful digestion of HS-GAG chains by HEP111.	58
Table 2.4. Flow cytometry antibodies and stains.	73
Table 3.1. Purity assessment of DU145 derived EVs isolated by the sucrose cushion method.	88
Table 4.1. Summary of the number of proteins included in the Olink analysis from the three panels.	118
Table 4.2. List of protein and corresponding gene names input in FunRich software for enrichment analysis.	122
Table 4.3. List of 33 genes identified in the biological pathways database from FunRich.	122
Table 4.4. List of randomised proteins and corresponding gene names for the randomised list input in FunRich software for enrichment analysis.	126
Table 4.5. List of 32 genes identified in the biological pathways database for the randomised list input in FunRich software for enrichment analysis.	126
Table 4.6. Proteins chosen for further validation by ELISA.	129
Table 4.7. Number of growth factors from cardiovascular III panel included in analysis.	136
Table 4.8. Number of growth factors from inflammatory II panel included in analysis. .	136
Table 4.9. Number of growth factors from oncology II panel included in analysis.	136
Table 4.10. Number of proteins increased and decreased in each specific HSPG-deficiency.	137
Table 4.11. Proteins increased and decreased for each specific HSPG-deficiency. ...	138
Table 4.12. Calculated fold increase for GD15, MMP-1 and t-PA relative to non-mammalian control EVs.	144
Table 4.13. Calculated fold decrease for CYR61, TFPI and ABL1.	147
Table 4.14. List of proteins and corresponding gene name input in FunRich software for enrichment analysis.	148

Table 4.15. List of 70 genes identified in the biological pathways database for the randomize list input in FunRich software for enrichment analysis.	149
Table 4.16. List of proteins and corresponding gene name for the randomize list input in FunRich software for enrichment analysis.	153
Table 4.17. List of 76 genes identified in the biological pathways database for the randomize list input in FunRich software for enrichment analysis.	154
Table 4.18. Proteins from the Olink analysis of HSPG-deficient vesicles selected for further validation by ELISA.	156

List of Appendices

Appendix 4.1. Biomarkers in Olink Panels.	245
Appendix 4.2. Venn diagram showing the overlap between Cardiovascular III, Inflammation.	246
Appendix 4.3. Standard curve for CXCL10 MCP-1 and IL-18 ELISA and absorbance readout detected for DU145 EVs	247
Appendix 4.4. The abundance of proteins in control and HSPG-deficient vesicles can be translated in the strength of signal detected by the Olink assay.	248-250
Appendix 4.5. (A). Standard curve for MMP-1 ELISA and absorbance readout detected for DU145 EVs.	251
Appendix 4.5. (B). Quantification of MMP-1 on DU145 EVs.	251
Appendix 4.5. (C). Quantification of MMP-1 on HSPG deficient EVs.	252
Appendix 4.5. (D). Standard curve for ABL1 ELISA and absorbance readout detected for DU145 EVs.	252
Appendix 4.5. (E). Standard curve for ABL1 ELISA and absorbance readout detected for 4 µg of HSPG-deficient EVs.	253
Appendix 4.5. (F). Standard curve for ABL1 ELISA and absorbance readout detected for 4 µg of HEP III treated and untreated EV conditions.	253
Appendix 5.1. Coordinates identifying the target-proteins represented by each pair of dots on the Human Phospho-RTK profiler array.	254
Appendix 5.2. Coordinates identifying the target-proteins represented by each pair of dots on the Human XL cytokine profiler array.	255
Appendix 5.3. Standard curve for HGF ELISA and absorbance readout detected for 4 µg of no enzyme, heat inactivated HEP III and active HEP III treated EV conditions. ...	256
Appendix 5.4. Standard curve for IL-1α and IL-17A ELISA and absorbance readout detected from assayed conditioned media from fibroblasts.	266

Abbreviations

Δ	Delta
α SMA	alpha smooth muscle actin
ABL1	Tyrosine-protein kinase ABL1
AF4	Asymmetrical-flow field-flow fractionation
ALIX	Accessory protein ALG-2 interacting protein X (also known as programmed cell death 6-interacting protein)
ARF6	ADP ribosylation factor 6
ATP	Adenosine triphosphate
BGLY	Betaglycan
BGLY-def	Betaglycan-deficient EVs
BSA	Bovine serum albumin
c-Met	Hepatocyte growth factor receptor
CAFs	Cancer associated fibroblasts
CCL20	C-C motif chemokine 20
CCM	Cell conditioned media
CD	Cluster of differentiation
CHMP	Charged multivesicular body protein
CM	Conditioned media
Cryo-EM	Cryogenic electron microscopy
CS	Chondroitin sulphate
CSF-1	Colony-stimulating factor-1
CST	Cytometry signalling and tracking
CSTB	Cystatin-B
CTFs	C-terminal fragments
CTSV	Cathepsin L2
CXCL10	C-X-C motif chemokine 10
CY561 member 1)	Cysteine-rich angiogenic inducer 61 (also known as CCN family member 1)
D ₂ O	Deuterium Oxide
DAPI	4',6-diamidino-2-phenylindole
DCs	Dendritic cells
DC-HIL	Dendritic cell-associated HSPG-dependent integrin ligand
DNA	Deoxyribonucleic acid
ECM	Extracellular matrix
EGF	Epidermal growth factor
EGFRvIII	Epidermal growth factor receptor variant III
ELISA	Enzyme-Linked Immunosorbent Assay
EM	Electron microscopy
EpCAM	Epithelial cell adhesion molecule
EphA	Ephrin type A receptor
EphB	Ephrin type B receptor
ESCRT	Endosomal sorting complex required for transport
EVs	Extracellular vesicles
EXT	Exostosin-like protein
FACS	Fluorescence-Activated Cell Sorting
FAK	Focal adhesion kinase
FBS	Fetal bovine serum
FBS ^{EV-}	FBS depleted of EVs

FC	Fold change
FGF-2	Fibroblast growth factor (also known as FGF basic (bFGF))
FGFR	FGF receptor
FMO	Fluorescence minus one
FSC	Forward scatter
GAG	Glycosaminoglycan
Gal	Galectin
GAPDH	Glyceraldehyde-3-Phosphate Dehydrogenase
GDF-15	Growth/differentiation factor 15
GDNF	Glial cell-derived neurotrophic factor
GlcA	Glucuronic acid
GlcNAc	N-acetylglucosamine
GMCSF	Granulocyte-macrophage colony-stimulating factor
GPC1	Glypican-1
GPC1-def	Glypican-1-deficient EVs
GPC6	Glypican-6
GPC6-def	glypican-6-deficient EVs
GPI	Glycosylphosphatidylinositol
GRP94	Glucose-regulated protein 94
HB-EGF	Heparin binding EGF-like growth factor
HBSS	Hanks's balanced salt solution
HEP III	Heparinase III
HGF	Hepatocyte growth factor
HRP	Horseradish peroxidase
HS	Heparan sulphate
HSPG	Heparan sulphate proteoglycan
ICAM	Intercellular adhesion molecule
IFN γ	Interferon gamma
IGF-1 R	Insulin-like growth factor 1 receptor
IGFBP2	Insulin Like Growth Factor Binding Protein 2
IL	Interleukin
ILVs	Intraluminal vesicles
ISEV	International Society for Extracellular Vesicles
ITGB3	Integrin Subunit Beta 3
LAMP	Lysosomal associated protein
LDS	Lithium dodecyl sulphate
LOD	Limit of detection
LPS	Lipopolysaccharides
MB	Myoglobin
MCP-1	Monocyte chemoattractant protein-1 (also known as CCL2)
MDR-1/P-gp	P-glycoprotein
MDSC	Myeloid-derived suppressor cell
MFG-E8	Milk fat globule-EGF factor 8
MFI	Mean fluorescent intensity
MHC	Major histocompatibility complex
MID	Mean integrated density
MIF	Macrophage migration inhibitory factor
miRNA	Microribonucleic acid
MISEV	Minimal Information for Studies of Extracellular Vesicles
MK	Midkine
MMPs	Matrix metalloproteinases
MOI	Multiplicity of Infection

mRNA	Messenger ribonucleic acid
MS	Mass spectrometry
MVEs	Multivesicular endosomes
NCR	Natural toxicity receptors
NDST	N-deacetylase/N-sulfotransferase
NK	Natural killer
NKG2D	Natural killer group 2 member D
NMC	Non-mammalian (NM)-control
NPX	Normalized Protein eXpression
NTA	Nanoparticle tracking analysis
OPCs	Oligodendrocyte precursor cells
P:P	Particle:Protein ratio
p53	tumour protein P53
PBMCs	Peripheral blood mononuclear cells
PBS	Phosphate Buffered Saline
PCR	Polymerase chain reaction
PD-1	T-cell inhibitor receptor programmed death-1
PD-L1	Programmed death ligand 1
PDGF	Platelet-derived growth factor
PEA	Proximity extension assay
PFA	Paraformaldehyde
PLA	Phospholipase A
PLP2	Phospholipase D2
PMA	Phorbol of 12-myristate 13-acetate
PMSF	Phenylmethane sulfonyl fluoride
PS	Phosphatidylserine
PSGL-1	P-selectin glycoprotein ligand-1
PVDF	Polyvinylidene fluoride
qPCR	real time quantitative PCR
Rab	RAS-related protein
rhTGF- β 1	Recombinant human TGF β 1
RIPA	Radioimmunoprecipitation assay
RT	Room temperature
RT-qPCR	Quantitative reverse transcription PCR
RTKs	Receptor tyrosine kinases
SCF	Stem cell factor
SDC1	Syndecan-1
SDC1-def	Syndecan-1-deficient EVs
SDC3	Syndecan-3
SDC3-def	Syndecan-3-deficient EVs
SDC4	Syndecan-4
SDC4-def	Syndecan-4-deficient EVs
SDF-1	Stromal-derived growth factor-1
SDS	Sodium dodecylsulphate
SEC	Size exclusion chromatography
shRNAs	Short hairpin ribonucleic acid
SNAP	Soluble N-ethylmaleimide sensitive fusion attachment protein
SNARE	SNAP receptor (SNARE)
SSC	Side scatter
STAT3	Signal Transducer and Activator Of Transcription 3
sTGF- β 1	Soluble TGF- β 1
Sulf	Sulfatase

TAMs	Tumour associated macrophages
TF	Tissue factor
TFPI	Tissue factor pathway inhibitor
TGF- β 1	Transforming growth factor beta 1
TLR	Toll-like receptor
TNF- α	Tumour necrosis factor α
TNFRSF1A	TNF Receptor Superfamily Member 1A
tPA	Tissue plasminogen activator
TRAIL	Tumor necrosis factor (TNF)-related apoptosis-inducing ligand
TRF	Time-resolved fluorescence
TSG101	Tumour susceptibility 101
TSPN6	Tetraspanin 6
TSPN8	Tetraspanin 8
uPA	Urokinase (also known as urokinase-type plasminogen activator)
VCAM-1	Vascular cell adhesion protein 1
VEGF	Vascular endothelial growth factor
VEGFR	VEGF receptor
VIM	Vimentin
WFDC2	WAP four-disulphide core domain protein 2
WIF1	WNT Inhibitory Factor 1

Chapter 1

Introduction

1.1 Extracellular Vesicles

1.1.1 Defining EVs – The rise of the extracellular vesicle field

The history of extracellular vesicles (EVs) started in 1946 when Chargaff and West described that a fraction of plasma free of platelets was able to maintain clotting properties, and these were diminished after high-speed centrifugation that sedimented a fraction with coagulatory activity (Chargaff and West, 1946). In 1967, Peter Wolf published the first electron microscopy images showing what he called “platelet dust”, lipid rich particles obtained from platelets by ultracentrifugation (Wolf, 1967). Two decades later, in the early 1980s, the term exosome was first used to describe secreted vesicles from the plasma membrane involved in transport of substances or nutrients. These vesicles consisted of populations of heterogeneous sizes, a small population of around 40 nm and another one with sizes between 500 and 1000 nm (Trams et al., 1981). A few years later, Philip Stahl’s group first identified small vesicles in maturing red blood cells as a mean of recycling of transferrin and its receptor (Harding et al., 1983). In 1987, Johnstone and colleagues, while studying reticulocyte maturation, published the first report including the term exosomes to refer to intraluminal vesicles (ILVs) that are secreted by multivesicular endosomes (MVEs) upon fusion with the plasma membrane (Johnstone et al., 1987). These studies laid the first understanding of the intracellular pathways involved in the biogenesis of small vesicles. The interest in these vesicles continued to grow and in the mid-1990s a key discovery by Raposo *et al.* demonstrated that vesicles derived from B cells through a similar endocytic route, play a role in antigen presentation (Raposo et al., 1996), and could stimulate memory T cell responses in a peptide and major histocompatibility complex (MHC) restricted fashion. The same observation in manipulating dendritic cell-derived exosomes (Zitvogel et al., 1998) revealed antigen presentation functions *in vivo*. Hence the groundwork indicating that vesicles could play important roles in cell-to-cell communication was set, demonstrating that vesicles were not just a mechanism to remove unwanted cellular components.

As the field grew, other types of plasma membrane-derived vesicles with larger sizes > 200nm were reported. EVs were then named based on their size and mechanism by which they were produced, and different names started appearing in the literature, such as microvesicles (Heijnen et al., 1999), ectosomes (Hess et al., 1999), and vesicles released by dying cells but distinct from exosomes were termed apoptotic vesicles (Théry et al., 2001). A particular type of EV released by cancer cells was initially

Chapter 1 - Introduction

oncosome at first (Al-Nedawi et al., 2008) and large oncosome in later studies (Minciacchi et al., 2015). While the term exosome was used to refer mostly to small vesicles derived from MVEs, it has also been reported that small vesicles can also derive directly from the plasma membrane (Booth et al., 2006). In fact, as of 2014 the term exosome was the most popular term to describe EVs in studies (Lotvall et al., 2014), independently of their biogenesis or isolation methods, but it should be a specific term for vesicles of endosomal origin and not for those of plasma membrane origin. Currently, limitations such as lack of consensus on markers, variety of isolation protocols and techniques for characterisation does not fully allow for a distinction between the different types of vesicle. This is mainly due to similar morphology, molecular content and overlapping range of sizes. As a result, the nomenclature used is imperfect and open to debate; consequently the term “extracellular vesicles” was encouraged to describe all secreted vesicles (Gould and Raposo, 2013). Recently, the International Society for Extracellular Vesicles (ISEV) published a position paper “Minimal information for studies of extracellular vesicles (MISEV)” to attempt to improve the rigor and the reproducibility of studies in the EV field, in what concerns the documenting of specific EV-associated activities and distinctions between EV populations (Théry et al., 2018). For the vesicles isolated and used in this thesis, the term EVs will be used, and it refers to a population of small vesicles < 200nm, whose exact subcellular origin cannot be defined.

1.1.2 EV Biogenesis & composition

1.1.2.1 EV biogenesis

Cells can secrete EVs by direct budding from the plasma membrane or fusion of MVEs with the cell surface, releasing the ILVs contained within. Therefore, it is likely that the machineries involved in their biogenesis and release are different, although common characteristics can be shared. These shared mechanisms blur the distinction between the different vesicle sub-populations (Raposo and Stoorvogel, 2013).

For small vesicles of endosomal origin, it all starts with the genesis of an early endosome from the plasma membrane, which after maturation becomes a late endosome (Stoorvogel et al., 1991). Here, a stepwise process starts to generate ILVs via the inward budding of the endosome limiting membrane, creating an endosome that can hold hundreds of small intraluminal vesicles, termed multivesicular endosomes (MVEs). This process involves a large group of proteins from the endosomal sorting complex required

for transport (ESCRT), that starts with ESCRT-0 recruiting ubiquitylated cargo at the endosomal membrane and ESCRT-I. ESCRT-I and ESCRT-II will assist the budding of the membrane and recruitment of ESCRT-III finalises the process with scission of the small vesicles, forming an ILV (Hurley, 2008).

However, alternative mechanisms, independent of ESCRT machinery may exist, as cells depleted of key subunits of the four ESCRT complexes were still able to generate cluster of differentiation (CD) 63-positive ILVs within MVEs (Stuffers et al., 2009). Ceramide was shown to be required for the formation of ILVs within lipid rich regions in the endosomal membrane (Trajkovic et al., 2008). The structure of ceramide would cause the membrane in these regions to project inward, leading to the creation of MVEs. In fact, artificial MVE were generated in the study by mixing lipids, cholesterol, sphingomyelin and the critical enzyme in this process, sphingomyelinase 2, which generates ceramide. In addition, proteins of the tetraspanin family have also shown to be involved in this ESCRT-independent endosomal sorting. Tetraspanin-enriched microdomains form associations with different proteins, suggesting a sorting role into domains that will later bud into small vesicles (Perez-Hernandez et al., 2013). Recently, tetraspanin 6 (TSPN6) was described as an important factor in EV biogenesis through association with syntenin and the heparan sulphate proteoglycan (HSPG) syndecan-4 (Ghossoub et al., 2020). Years before, HSPGs had been revealed as a central piece in an alternative biogenesis pathway, involving the association of syndecans with syntenin and ESCRT accessory protein ALG-2 interacting protein X (ALIX; also known as programmed cell death 6-interacting protein) (Baietti et al., 2012). The syndecan-syntenin-ALIX pathway was not entirely dependent on the ESCRT complex but requires the accessory protein ALIX and the availability of ESCRT-III sub-units. This mechanism will be explained in more detail later in this thesis. Furthermore, the GTPase ADP ribosylation factor 6 (ARF6) and phospholipase D2 (PLP2) were also implicated in syntenin-ALIX exosome biogenesis and budding. ARF6 depletion from MCF-7 cells was associated with a reduction of syndecan-1, syntenin and ALIX, and prevented exosome release induced by syntenin overexpression. As CD63 internalisation was not affected by ARF6 depletion, ARF6 does not seem to be related with cargo loading into exosomes, but rather with ILVs budding from late endosomes, together with PDL2 (Ghossoub et al., 2014).

MVEs must translocate to and fuse with the plasma membrane to release the ILVs into the pericellular space, and thus this is the secretion of small EVs. RAS-related protein

Chapter 1 - Introduction

(RAB) GTPases are involved in mobilizing the secretory MVEs towards the cell periphery. Perturbing Rab11 (Savina et al., 2002), Rab35 (Yeung et al., 2018) and Rab27a and Rab27b (Ostrowski et al., 2010) attenuates small EV secretion. It should be noted that inhibition of one of these Rab proteins, only partially impacted the EV quantity, indicating that other mechanisms and routes of MVE or distinct types of MVE may exist. These processes are in addition to the secretion of small EVs arising directly from the plasma membrane. Yeung *et al.* demonstrated that in prostate cancer cell-derived EVs, knockdown of Rab35 or Rab11 had a modest impact, attenuating about 20% of vesicle output. Rab35 knockdown, but not that of Rab11b, led to vesicles that were not capable of driving myofibroblast differentiation. The study suggested that different populations of vesicles might be regulated by different Rab mechanisms (Yeung et al., 2018), and such sub-populations exert functionally distinctive effects.

The final step in small EV biogenesis involves the fusion of MVEs with the plasma membrane. This process is not well defined yet, but it is dependent on soluble N-ethylmaleimide sensitive fusion attachment protein (SNAP) receptor (SNARE) complexes. These regulate the secretion of lysosome-related organelles (Rao et al., 2004), and have been shown to be involved in small EV release (Wei et al., 2017, Verweij et al., 2018). The EV biogenesis process is shown in **Figure 1.1**.

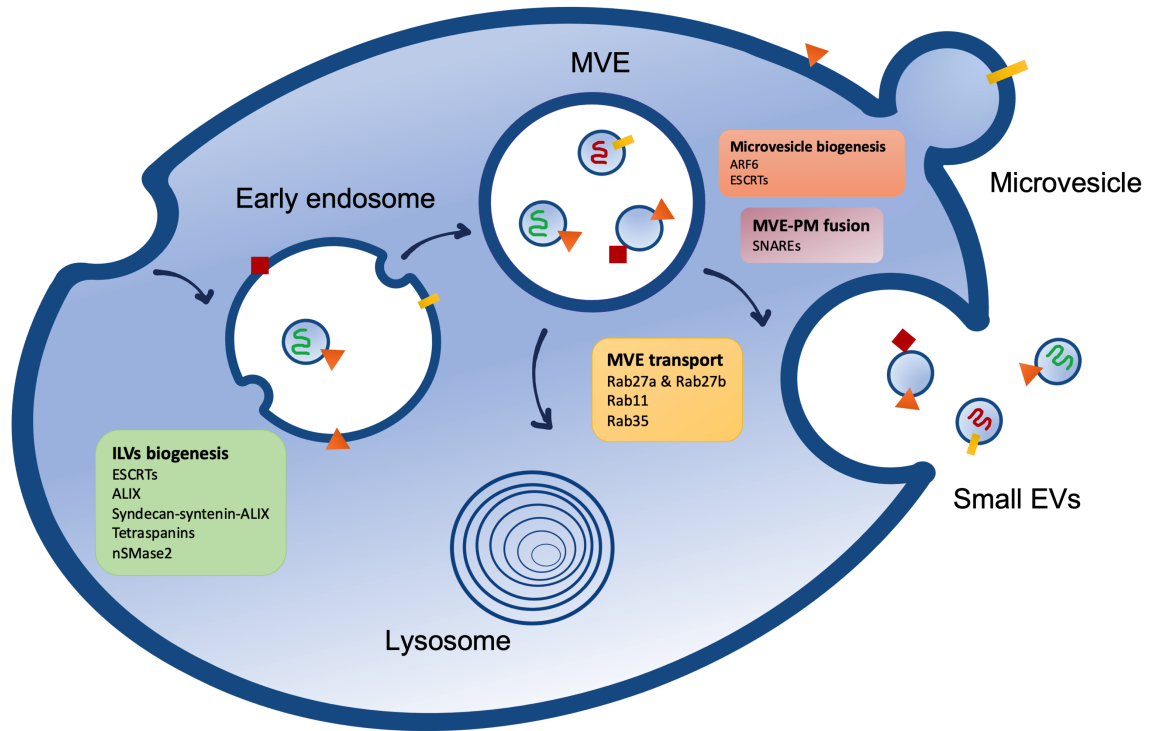


Figure 1.1. Extracellular vesicle biogenesis process. The inward budding of early endosomal membrane generated intraluminal within multivesicular endosomes/late endosomes. This process is regulated by components of the ESCRT complex as well as tetraspanins and syndecans. The MVE can fuse with the plasma membrane, releasing the internal vesicles and originating small EVs (exosomes). Fusion is regulated by a multistep process including MVE movement along microtubules and docking to the plasma membrane. These are supported by several Rab proteins. Membrane fusion is possible with the contribution of SNARE proteins, ARF6, and ESCRTs. Alternatively, MVE can fuse with the lysosome for degradation of their cargo. Adapted from Bebelman et al., 2018.

1.1.2.2 *The complex molecular composition of a vesicle*

Considering their origin, small EVs originating from MVEs are expected to contain proteins associated with the endosomal pathway. Therefore, EVs are expected to be enriched in components of the ESCRT mechanism, such as ALIX and tumour susceptibility 101 (TSG101), and proteins associated with endosomal maturation such as lysosomal associated protein 1 (LAMP1) (Wolfers et al., 2001) and 2 (LAMP2) (Kowal et al., 2016). Tetraspanins, known to cluster into microdomains at the plasma membrane or endosomes (Perez-Hernandez et al., 2013), including CD9, CD63 and CD81, are usually enriched in EVs and used as markers (Kowal et al., 2016). Proteins involved in antigen presentation such as MHC class I (MHCI) and class II (MHCII) are also enriched in EVs (Raposo et al., 1996, Lamparski et al., 2002, Kowal et al., 2016). These proteins are usually found at a higher density on the EVs than on the limiting membrane of MVEs, indicating that there is an active incorporation process of these components during EV biogenesis. Proteins from the endoplasmic reticulum like glucose-regulated protein 94 (GRP94) (Kowal et al., 2016) and calnexin (Webber et al., 2014) are mostly absent from endosomal derived vesicles, and analyses such as western blots that demonstrate the absence of such elements can be helpful in determining the quality of the EV isolate.

EVs can also contain proteins that are specific to their parent cells, for example, epithelial cell adhesion molecule (EpCAM) is commonly found on EVs derived from epithelial carcinomas (Tauro et al., 2013) and used to immunocapture cancer cell-derived EVs (Campos-Silva et al., 2019, Zhang et al., 2019). The presence of TCR/CD3/ ζ Complex also suggests EVs derived from activated T cells (Blanchard et al., 2002). CD3 is only expressed in T lymphocytes, and immunocapture of CD3⁺ EVs from cancer patient plasma allowed to identify their protein content and the functionality of the parent T cells (Theodoraki et al., 2018). EV membranes consist of a lipid bilayer similar to that of cell plasma membrane. However, EVs are enriched in cholesterol, sphingomyelin and ceramide (Llorente et al., 2013). Ceramide plays a central role in ESCRT-independent MVEs formation mechanism (Trajkovic et al., 2008) and ILVs within MVEs contained most of the cholesterol detected in the endocytic pathway, showing a preferential association with secretory MVEs (Möbius et al., 2003).

Besides carrying proteins and lipids, a major contribution to the field was the discovery that EVs can carry as part of the overall cargo nucleic acids such as messenger ribonucleic acid (mRNA) and microribonucleic acid (microRNA), and that mRNA could be translated into functional proteins within recipient cells (Ratajczak et al., 2006, Valadi et al., 2007, Skog et al., 2008). These studies also showed that certain forms of RNAs isolated from EVs were found to be enriched in relation to the originating cells, suggesting that these molecules are also selectively incorporated into EVs, and these patterns of expression may serve as potential markers for diagnosis and prognosis of different diseases. The presence of fragments of small non-coding RNAs (van Balkom et al., 2015, Nolte-t Hoen et al., 2012a) as well as genomic and mitochondrial deoxyribonucleic acid (DNA) have also been reported (Thakur et al., 2014, Sansone et al., 2017). Although the nature of the vesicles, or vesicle subpopulations that harbour DNA remains a little controversial. Transport of these nuclease-sensitive molecules within EVs comes with the advantages of protecting them from the extracellular environment, ensuring their stability in the extracellular space and facilitating the delivery of nucleic acid from cell to cell in a protected package. Recent studies have also pointed to the presence of metabolites in EVs. One study showed that cancer associated fibroblasts (CAFs) can supply tumours with nutrients through EVs (Zhao et al., 2016) and EVs derived from mesenchymal stem cells carry metabolites such as glutamic acid and lactic acid both of which are associated with tumour proliferation (Vallabhaneni et al., 2014). Metabolomics analysis of urinary EVs showed that the metabolite steroid hormone dehydroepiandrosterone sulphate (DHEAS) could provide a prostate cancer marker and be a useful means of monitoring disease (Clos-Garcia et al., 2018).

After the first study by Théry et al. using mass spectrometry-based proteomics to characterize EVs derived from mouse dendritic cells (DC) cultures (Théry et al., 1999), other studies followed (Théry et al., 2001, Lamparski et al., 2002) and the data have now been assembled on publicly available databases such as Exocarta (Keerthikumar et al., 2016) and Vesiclepedia (Pathan et al., 2019). Collectively, these works clearly identify EVs as distinct sub-proteomes/ transcriptomes of the parent cell with some common “house-keeping” like features as well as cell/tissue and context specific compositions. A graphical example of the molecular components found in vesicles of endosomal origin and their topography is provided in **Figure 1.2**.

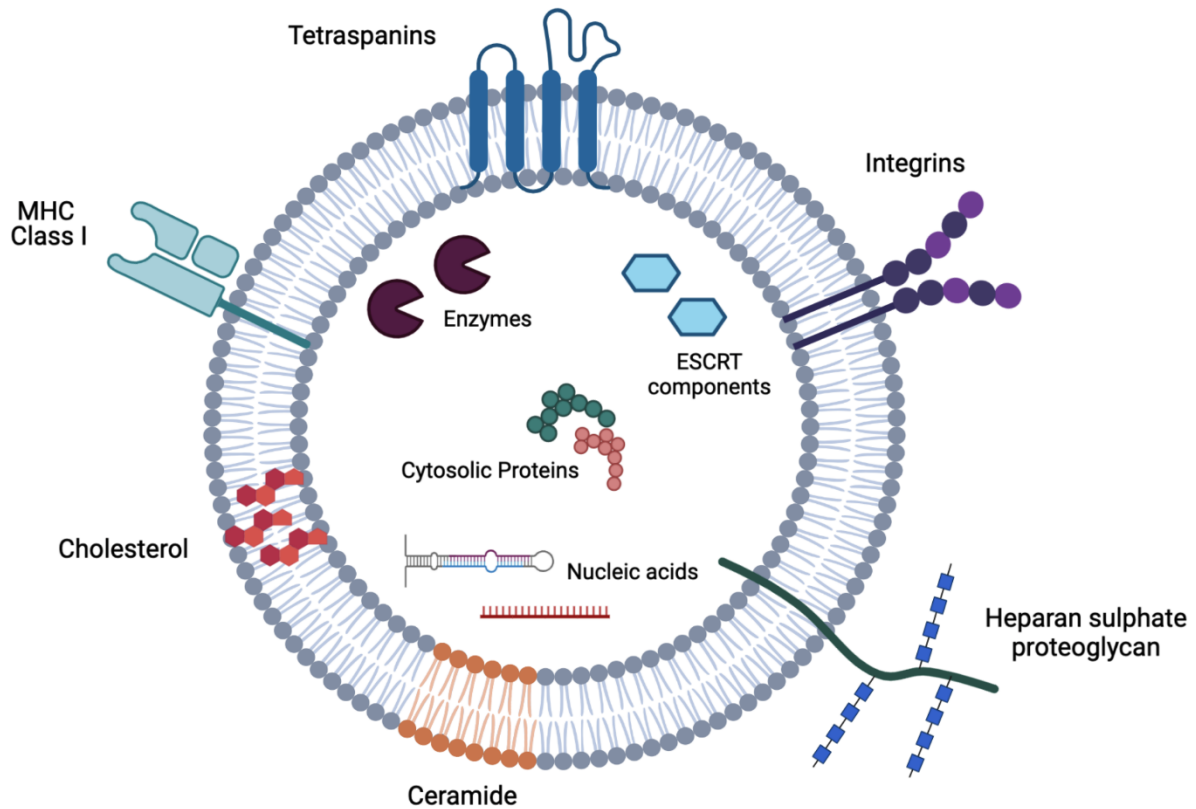


Figure 1.2. Molecular composition of vesicles of endosomal origin. Schematic representation of composition of nanosized vesicles with a lipid bilayer. Membrane-associated proteins represented consist in tetraspanins, such as CD9, CD63 and CD81, integrins, MHC I molecules and HSPGs. Intraluminal cargo represents different proteins and various RNA species. Image produced using Biorender software.

1.1.3 EV isolation methods and EV characterisation

1.1.3.1 EV isolation methods

Within the EV field, addressing EV heterogeneity is a major challenge. In addition approaches to improve and standardize EV isolation and characterisation are often debated (Théry et al., 2006). In earlier studies, the general protocol to isolate small EVs was based on serial centrifugation steps to remove cellular debris, and microvesicles, followed by high speed ultracentrifugation at 100,000 x g, that pellets small EVs (Johnstone et al., 1987). Some protocols include the use of 0.22 µm filters prior to pelleting to separate the small and large EV subpopulations. However, this method can also co-isolate other EV types with overlapping sizes and can co-isolate non vesicular components like proteins aggregates, as well as some lipoproteins that sediment at similar speeds. Using a continuous sucrose density gradient, Raposo *et al.* defined that EVs float at a density of 1.1-1.2 g/mL, and this method provides a route for a more refined and purer EV isolate (Raposo et al., 1996). An alternative to the sucrose density method is loading the sample on top of a 30% sucrose deuterium oxide (D₂O) cushion prior to ultracentrifugation (Lamparski et al., 2002). The resulting sucrose cushion has a density similar to EVs (1.21 g/mL) which prevents small EV (of density <1.2g/mL) from pelleting, being retained instead in the isotonic cushion. The sucrose is then washed and the pelleted EVs collected. This method was developed to isolate clinical grade exosomes and is more practical as a preparative scale approach than the sucrose gradients. Alternative, and arguable superior density matrices are available, providing greater resolving power than sucrose. The use of OptiPrep™, an iodixanol based solution for density gradient isolation, seems to be preferable to sucrose-based gradient to obtain purer EV preparations (Lobb et al., 2015), however, with the caveat that it is a complex, laborious and time consuming technique.

The rotor type, relative centrifugal fields, as well as centrifugation times used in EV isolation are very important to improve purity as well as yield (Cvjetkovic et al., 2014). Nevertheless, the literature often lacks these critical details, partly perhaps because researchers do not fully appreciate the concept of method-bias on the eventual EV isolate. The EV-TRACK paper (Van Deun et al., 2017) highlights these issues clearly, with over 200 different protocols that describe an ultracentrifugation based EV isolation method; hence each study creates a slightly different EV-isolate that might be

Chapter 1 - Introduction

functionally distinct. These are ongoing reproducibility and validation challenges for the EV field, with still no general consensus on “the” method of choice.

Protocols based on immunoaffinity, developed using antibody-coated beads (Clayton et al., 2001) or latex beads (Lamparski et al., 2002), have also been used to isolate different populations of EVs. These rely on the expression of specific proteins at the EV surface that will be captured by antibody-coated beads and analysed by flow cytometry. However, due to the lack of specific markers for distinct EV populations, these protocols cannot really differentiate between different subpopulations nor exclude a certain population that is negative for the target protein. This protocol is also limited by the difficulty in separate EVs from the beads to be used in further functional studies. Thus, the protocol remains more relevant in identifying the markers presents in a sample and is best suited as a bulk-population analytical tool.

Ultrafiltration (Lamparski et al., 2002) and tangential flow filtration (Busatto et al., 2018) can be used to isolate EVs from large volumes of fluid; however, because these methods are based on membrane size to capture the vesicles, this might also co-isolate contaminants of the same size. Size exclusion chromatography (SEC) also seems to be one of the most elected methods of isolation by researchers, due to its convenience, reproducibility, and highly efficiency in eliminating non-vesicular contaminants from biological fluids such as plasma (Théry et al., 2006, Welton et al., 2015). Again, however, the method suffers from co-isolation of particulate entities, such as lipoproteins that have similar sizes. The combination of multiple techniques, despite more laborious, provides superior methods for purity. Different studies have combined SEC with other techniques, as to overcome SEC limitations and improve EV purity. For instance, combination of SEC with density cushion provided a significant separation of EVs from lipoproteins in plasma samples (Karimi et al., 2018). Iodixanol density gradient ultracentrifugation, followed by an EV-capture technique, such as bind-elute chromatography (BEC), separated with high efficiency protein contaminants from EVs isolated from blood plasma, however, it also resulted in a reduced EV yield (Onódi et al., 2018).

At the moment, there are various commercial kits available for EV isolation, with the goal of making the process fast and practical, and hopefully reproducible. The use of precipitation kits such as ExoQuick (System Biosciences) and Total Exosome Isolation kits (TEI, Invitrogen) has been reported, and even compared with other kits, such as SEC

columns qEV (iZON) and *Exo-spin*[™] (Cell Guidance Systems) or methods based on membrane affinity binding, such as exoEasy (Qiagen) (Buschmann et al., 2018, Brennan et al., 2020). For biological samples, precipitation and membrane affinity were apparently better at distinguishing healthy donors from patients; moreover SEC had higher purity, even if lower yield (Buschmann et al., 2018). Nonetheless, the sizes, yield, and co-isolated contaminants were different between methods. The MISEV2018 survey showed that 97% of the researchers that answered the survey agreed that being cautious when using these kits was essential as they have very poor vesicle specificity (Théry et al., 2018).

An emerging technology useful for the isolation and analysis of EVs are the microfluidic chips which allow for immune capture using specific antigens or markers of interest. Some allow for the elution of EVs for downstream analysis, for instance, EGFRvIII EVs can be isolated and quantified from glioblastoma patient plasma and further eluted for RNA sequencing (Reátegui et al., 2018). Such approaches are somewhat idiosyncratic and not widely available for community-wide testing and validation. Furthermore, they are limited in scale and throughput, and may only be applicable for certain small volume applications.

Another of the most recent developments in terms of EV isolation is the particle drag-based fractionation technique, asymmetrical-flow field-flow fractionation (AF4), a type of flow field-flow fractionation (FFF) that has been gaining popularity in the EV field. AF4 can be used to fractionate subpopulations of EVs with high resolution (Zhang et al., 2018). A combination of a perpendicular cross flow and parabolic flow profile carries smaller EVs, followed by larger ones, to the detectors, providing information about size distribution. Additionally, distinct subpopulations can also be collected for additional studies (Zhang and Lyden, 2019). This technique has many benefits, including avoiding exposure of EVs to high external forces, preserving their integrity, being highly reproducible and with an efficient recovery, as well as providing a large dynamic range of size separation. However, only small quantities of sample can be used, and the sample collected is quite diluted and might require pre-concentration prior to use. In addition, the technology platform is expensive and hence available to only a few laboratories.

Chapter 1 - Introduction

ISEV recommends choosing the technique according to the type of biofluid EVs are being isolated from and the final use of the collected EVs. In addition, the selection must consider the recovery rate and specificity of the method, and characterisation details of final EV preparations should be provided (Théry et al., 2018).

1.1.3.2 EV characterisation

Equally as important as selecting an EV isolation and purification method is the characterisation of EVs in terms of defining the product specification. This will usually be done by multiple and complementary techniques to ascertain the degree of purity of the isolated content, and the molecular and morphological nature of the isolate. This is key to increasing the confidence of the data arising, where findings are attributed to properties or functions of EVs (Théry et al., 2018).

Quantification of EVs themselves is difficult, but quantification of EV structural content such as protein, lipids and nucleic acids can be used by proxy, and provide a rough estimate of EV quantity. Additionally, a combination of methods can be used to estimate the purity of the EV isolation. For example, measuring particle:protein (P:P) ratios (Webber and Clayton, 2013), protein:lipid ratio (Osteikoetxea et al., 2015) and protein:RNA ratio (Cvjetkovic et al., 2014) can provide an estimation of EV isolation quality. Visualization of EVs within an EV isolate by cryogenic (cryo)-electron microscopy (EM) provides evidence of the native vesicle structures, and size and often the extent of amorphous aggregates of non-vesicular material within the sample can be imaged. The instantly vitrified vesicles present a perfectly round shape by cryogenic electron microscopy (cryo-EM), delimited by a lipid bilayer (Conde-Vancells et al., 2008). This technique is much better at maintaining the real structure of vesicles, unlike the EM first used to characterize EVs that erroneously showed a cup shaped morphology (Raposo et al., 1996), arising as an artefact of fixation. In some examples, immuno-gold labelling of vitrified vesicles has been achieved providing information about the distribution of particular proteins amongst the entire EV population (Brisson et al., 2017). However, these seem particularly challenging from a technical perspective and very few groups are able to achieve this reliably.

Nanoparticle tracking analysis (NTA) is a light scatter-based technique that allows the determination of size and concentration of particles in solution. Since particle velocity in

solution is related to size, viscosity and temperature, measuring EV velocity optically can be useful (Gardiner et al., 2013). A limitation of this technique is that it cannot distinguish between EVs and non-vesicular nanoparticles, which might be significant constituents of samples such as plasma. Also, scattered light is limited for particles, such as vesicles, that have a low refractive index, and therefore smaller vesicles < 50nm are difficult to detect. NTA invariably underestimates the total concentration of particles in the sample, and overestimates the proportion of larger vesicles, that scatter more light. While conventional flow cytometry is not sensitive enough to detect individual EVs, high resolution flow cytometry methods have been developed for analysis of antibody or dye labelled nanosized vesicles (Nolte-t Hoen et al., 2012b, Morales-Kastresana et al., 2017). Similarly, immunolabeling of EVs with antibodies against proteins known to be present on vesicular surface has been suggested before for EM microscopy (Théry et al., 2006).

Currently, there remains a lack of universal markers for the different types of EVs, specially to distinguish MVE-derived EVs from other small EVs. The MISEV 2018 guidelines recommend that the characterisation of isolated EVs be based on demonstrating the presence of EV markers and the absence of common protein contaminants (Théry et al., 2018). For this, three main categories are proposed: 1) transmembrane or glycosylphosphatidylinositol (GPI)-anchored proteins associated to the plasma membrane and/or endosomes, such as tetraspanins CD9, CD63 and CD81; 2) cytosolic proteins recovered in EVs such as ALIX, TSG101, ARF6 and syntenin; 3) major components of non-EV co-isolates structures, such as lipoproteins and ribosomal proteins. Two additional categories can be included; one for the study of small EVs not originating from plasma membrane or endosomes and another for secreted proteins recovered with EVs (their association with EVs being demonstrated further).

Several standard protein detection methods can be used to provide information on the enrichment of proteins on EVs. Western blotting is perhaps the more conventional method, being widely used to compare protein content between cell lysates and EV isolates. Proteins from endoplasmic reticulum origin, such as calnexin and GRP94, should be absent from isolates containing small EVs as these proteins are not present in either MVEs or plasma membrane-derived EVs (Théry et al., 2006). Other approaches such as bead-based flow cytometry use beads coated with antibodies against proteins typically found on the EV surface (Théry et al., 2006), and multiplex approaches allow

for the capture of EVs on bead arrays prior to detection with varied antibodies by flow cytometry (Koliha et al., 2016). These increase the possibility of discriminating between different sub populations of EVs and contributes to a better understanding of EV heterogeneity. In June 2021, Raghu Kalluri's group published a quantitative proteomics analysis that identified syntenin-1 as consistently abundant in the proteome of exosomes from different cellular origins and biofluids, and using different isolation methods (Kugeratski et al., 2021). This highlights a putative universal marker that could be used to distinguish a particular EV population.

As the field evolves and the techniques of isolation and characterisation become more advanced, the possibilities of categorizing the different EV populations become more real. But the key to this is the capability of single vesicle analysis, for example, by super-resolution imaging techniques, cryo-EM methods, or very high sensitivity flow cytometry.

1.1.4 General properties of EV interactions with recipient cells

Once released into the extracellular space, EVs are able to mediate cell-cell signalling locally and systemically by interacting with recipient cells, eliciting functional responses and phenotypical changes. The understanding that EVs could play essential roles in cellular communication came with the observation that EVs derived from B cells can have cell activating roles by containing MHC class II complexes that are functional in antigen presentation, leading to T cell stimulation (Raposo et al., 1996). In addition to the presentation of ligands to receptors on the recipient cell surface, EVs can also transfer molecular cargo into recipient cells. A well accepted example is the delivery of miRNA and mRNA (Valadi et al., 2007, Skog et al., 2008). Others reported the transfer of oncogenic receptors, such as EGFRvIII (Al-Nedawi et al., 2008), and more recently, the transfer of metabolites (Zhao et al., 2016, Vallabhaneni et al., 2014). EVs can also transfer cytosolic proteins, lipids and enzymes (Zaborowski et al., 2015).

For EV communication to occur, vesicles are required to dock to the plasma membrane of recipient cells, and this can lead to activation of plasma membrane receptors, triggering an intracellular signalling response and/or internalization through distinct endocytic pathways. EVs can also fuse with the cell membrane, releasing its cargo directly on the cell cytoplasm, a mechanism that can also occur inside the endosome,

allowing the release of the cargo of endocytosed vesicles (van Niel et al., 2018, Mulcahy et al., 2014).

Several adhesion molecules are involved in binding of EVs to the surface of recipient cells, such as integrins, immunoglobulins, tetraspanins and HSPGs (Mulcahy et al., 2014, Buzás et al., 2018). Integrins on the EV surface have a key role in directing EV adhesion to specific cell types (Hoshino et al., 2015) and can interact with molecules such as intercellular adhesion molecules (ICAMs) at the surface of DC cells, while tetraspanins CD9 and CD81 can contribute to binding to DC cells as well (Morelli et al., 2004). In addition, the presence of tetraspanin Tspan8-CD49d complex on the EV surface facilitated EV adhesion to endothelial cells (Nazarenko et al., 2010). DC-derived EVs carrying MHC-complexes and ICAM-1 can be captured more efficiently by CD8⁺ DCs compared to CD8⁻ DCs. This requires LFA-1 integrin, without the need for internalisation and reprocessing, resulting in presentation of vesicular MHC complexes by DCs (Segura et al., 2007).

The externalisation of phosphatidylserine (PS), leading to exposure of this negatively charged lipid on the EV surface, can facilitate its recognition by plasma membrane receptors either directly or indirectly through its binding with bridging proteins. PS on microvesicles is suggested to have a critical role for incorporation of vesicles into HUVEC cells, by directly binding to the PS receptor on these cells (Wei et al., 2016). PS also binds to the Tim4 receptor (Tietjen et al., 2014) that has been used to capture PS-exposing EVs (Nakai et al., 2016). The interaction of PS with milk fat globule-EGF factor 8 (MFG-E8) forms a bridge between PS and integrins, such as $\alpha_v\beta_3$. EV-MFG-E8 has been found to be secreted by bone marrow-derived DCs (BMDCs) and the possibility of it being important for EV capture by DC cells has been reported (Véron et al., 2005). The role of HSPGs in EV attachment to recipient cells will be explored later in this thesis.

There are many examples of vesicles delivering a receptor-ligand engagement event that elicits some form of intracellular signalling response, and downstream functional consequence. For example, EVs expressing Fas-ligand on their surface were able to activate Fas-positive lymphocytes, inducing apoptosis in these cells (Andreola et al., 2002), and the delivery of Delta-like IV by tumour EVs is able to inhibit Notch signalling in endothelial cells, affecting vessel sprouting and branching (Sheldon et al., 2010). Other studies show that association of the IFN- γ / IFNGR1 complex with EVs activates

Chapter 1 - Introduction

STAT1 in target cells (Cossetti et al., 2014), tetraspanin complexes are able to induce endothelial cell activation (Nazarenko et al., 2010) and B cell-derived EV-integrins produce strong adhesive interactions with TNF- α activated fibroblast and induce calcium signalling events (Clayton et al., 2004). Furthermore, vesicular delivery of TGF- β 1 to its receptor induces activation of SMAD signalling pathway, resulting in fibroblast differentiation (Webber et al., 2010).

EVs can also directly deliver their cargo content in the cytosol, by fusing with the recipient cell membrane. This was demonstrated by the use of EVs labelled with lipophilic dye octadecyl rhodamine B (R18), which is at higher concentration on the EV membrane but dilutes upon fusion with unlabelled recipient membranes, allowing for visualization of membrane fusion (Montecalvo et al., 2012). Microvesicles bearing tissue factor (TF) and P-selectin glycoprotein ligand-1 (PSGL-1) are able to fuse with platelet membrane, transferring both protein and lipid to the platelet surface (del Conde et al., 2005).

So far, endocytosis seems to be the most common mode of EV internalisation, and different mechanisms of endocytic processes have been described for different cell types (Mulcahy et al., 2014). Caveolin and clathrin dependent endocytosis are more specialised and receptor dependent. These require the binding of EVs to receptors placed in caveolin or clathrin rich pits in the plasma membrane and are mediated by dynamin. Impairment of clathrin coated pits or caveolae (caveolin invaginated vesicles) formation affected EV uptake (Escrevente et al., 2011, Nanbo et al., 2013), and dynamin inhibition has also shown to decrease EV uptake (Feng et al., 2010), implicating a role of these mechanisms in EV internalisation. The role of caveolin in EV uptake remains unclear, as it was also found to be a negative regulator of EV uptake in fibroblasts and glioma cells, while internalisation mainly occurred by lipid raft-mediated endocytosis (Svensson et al., 2013). The authors suggested that caveolin-1 could act as a stabilizer of lipid rafts, negatively contributing to EV uptake. Internalisation of EVs has also been reported to happen through phagocytosis by cells with phagocytic phenotype such as macrophages (Feng et al., 2010) as well as by macropinocytosis in microglia (Fitzner et al., 2011). Some of the processes of EV interactions with recipient cells are shown in **Figure 1.3**.

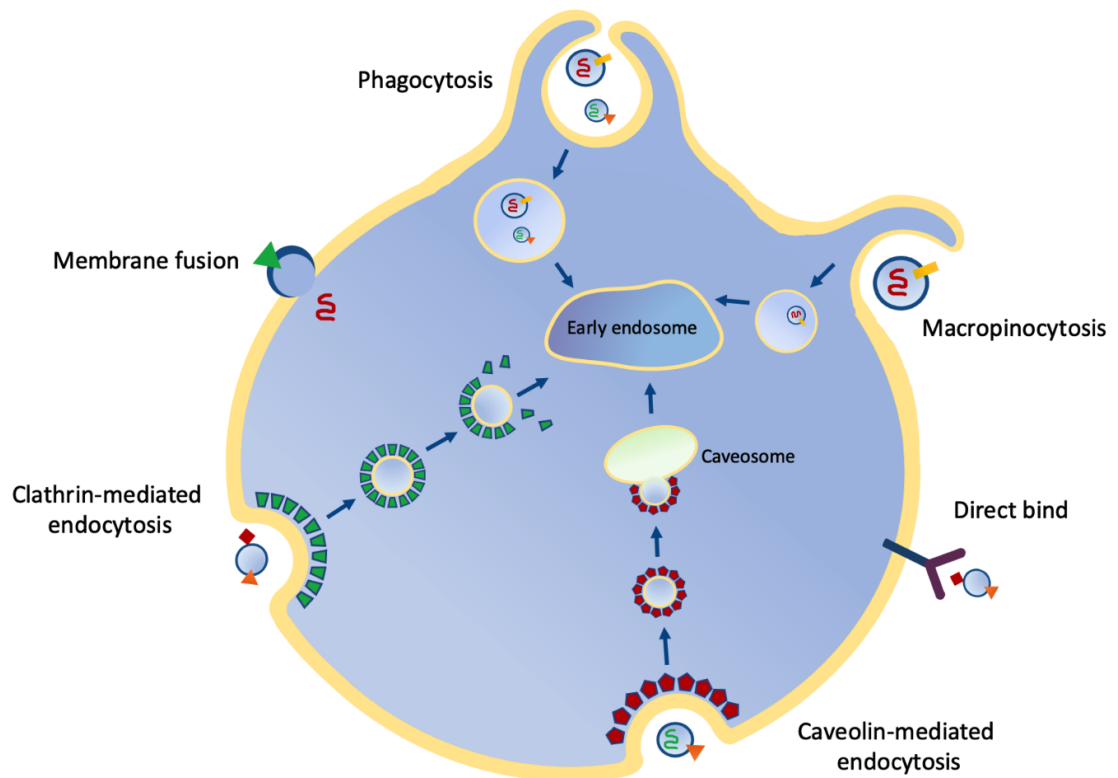


Figure 1.3. Processes of cellular communication. EVs can transfer their cargo into recipient cells by different mechanisms, including membrane fusion and various endocytic pathways. Distinct machinery is involved in the different endocytic processes that can be clathrin-dependent or caveolin-dependent. Clathrin-caveolin independent processes also exist, such as receptor and lipid-raft mediated processes (not represented). In specialized cells, extracellular material can be endocytosed by macropinocytosis and phagocytosis. EVs can also trigger intracellular signalling of recipient cells via direct binding with surface receptors. Internalized EVs can back-fuse with the membrane of MVE, releasing the cargo in the cytoplasm or can be recycled from recipient cells, as well as be degraded after fusion of MVE with lysosomes (not shown). Adapted from Mulcahy et al., 2014.

Chapter 1 - Introduction

After internalisation vesicles follow the typical endosomal pathway, fusing with early endosomes and then late endosomes and MVEs which can fuse with the lysosomes (Parolini et al., 2009, Chen et al., 2018a, Tian et al., 2013). EVs can also fuse with the endosomal membrane and release their contents in the cytosol. The fusion process is still unclear but has been visualised in two different studies using EVs labelled with fluorescent R18 lipid probe (Parolini et al., 2009, Montecalvo et al., 2012). Additionally, a study tracking miR-21 loaded EVs in live cells showed that it could be gradually released from the endosome as no overlapping was seen between miR-21 and EVs, and it also did not accumulate in lysosomes (Chen et al., 2018a). EVs can also have a “contactless” effect by altering the components of the extracellular space in the vicinity of cells through the actions of vesicular enzymes. Such an example can be seen by EVs that may use CD73 and CD39 phosphatases present on their cellular surface to aid the production of extracellular adenosine, which contributes to the negative regulation of T cell function (Clayton et al., 2011). The involvement of EVs in these cell-interaction processes described above is most likely to result in a cellular response as they do not engage with the endosomal-lysosomal pathway.

1.2 EVs in the tumour microenvironment

1.2.1 *Overview of the tumour microenvironment*

Cancer is a leading cause of mortality worldwide, responsible for nearly 10 million deaths in 2020 (World Health Organization). In the UK alone, prostate cancer is responsible for more than 11,000 deaths a year (Cancer Research UK, 2016-2018), but the survival rate is high, with 77.6% of men diagnosed surviving their disease for ten years or more (Cancer Research UK, 2013-2017). Nonetheless, men presenting with advanced disease that has escaped the confines of the organ have a disease that is essentially incurable.

In 2000, Hanahan and Weinberg published a review article comprising six hallmarks of cancer essential to confer cells the abilities to sustain tumour growth and metastatic dissemination. These hallmarks represent some characteristics intrinsic to the cancer cell, such as resistance to cell death, insensitivity to anti-growth signals, sustained proliferation, inducing angiogenesis, activation of invasion and metastasis, and limitless replicative potential (Hanahan and Weinberg, 2000). Then, in a follow-up review in 2011,

the authors included two emerging hallmarks and two enabling characteristics of the cancer development process. The first emerging hallmark involved the metabolic reprogramming in order to support cell growth and proliferation, and the second is related with the ability of cancer cells to evade immune system destruction. The acquisition of these hallmarks of cancer are enabled by the development of genomic instability in cancer cells, originating random mutations, together with tumour promoting inflammation, driven by immune cells (Hanahan and Weinberg, 2011).

Contrary to what was initially thought, cancers do not consist only in masses of malignant transformed cells but are, in reality, complex structures that can recruit non-transformed neighbouring cells, driving them to support tumorigenesis, creating the tumour microenvironment. The collaborative interactions between neoplastic cancer cells and their supporting stroma promote cancer dissemination and growth (Baghban et al., 2020). The role of the tumour microenvironment and its constituents has therefore gained increased recognition in the past decade. Still, some aspects of the stroma have long been appreciated, such as the contributions of tumour angiogenesis, matrix remodelling and immune regulation. Furthermore, the altered stroma in the tumorigenesis process has been compared with the wound healing scenario, with tumours being nicknamed “wounds that do not heal” (Dvorak, 1986).

Once a tumour starts growing, the need for oxygen and nutrients to fuel the metabolic needs is increased and an extended blood supply is required. In 1971, Judah Folkman proposed the hypothesis that tumours require angiogenesis for their growth, not being able to grow more than a few millimetres without its induction, and that the tumours secrete a diffusible substance that would stimulate endothelial cell proliferation and recruitment (Folkman, 1971). Several pro-angiogenic factors were identified such as fibroblast growth factor (FGF-2 (bFGF)) (Presta et al., 1986), vascular endothelial growth factor (VEGF) (first identified as vascular permeability factor (VPF) (Dvorak et al., 1992, Kim et al., 1993), and platelet derived growth factor (PDGF) (Keck et al., 1989). The secretion of these factors, together with anti-angiogenic factors, quickly becomes dysregulated and leads to abnormal vasculature in tumours. This is characterised by excessive branching, blind ends, discontinuous endothelial lining and defective pericyte and basement membrane coverage. This eventually leads to poor vessel functionality, disordered perfusion and increased vascular leakiness, which contributes to tumour cell extravasation and metastasis (De Palma et al., 2017). With the tumour continuous

Chapter 1 - Introduction

growth, this irregular vascularisation leads to poor blood supply and consequent restricted access to oxygen, giving rise to hypoxic regions. Hypoxia induces the secretion of hypoxia-inducible factors (HIFs) by both tumour and stroma cells. These pro-angiogenic factors, such as VEGF-A and CXCL12, stimulate neovascularization in an attempt to increase oxygen delivery to the cells (Petrova et al., 2018).

Immune evasion and inflammation have emerged as a key components of cancer progression. The immune system is known to fight invading pathogens and remove damaged cells, however, in cancer, immune cells have the ability to both control or prevent tumour initiation and progression, but also facilitate neoplastic transformation, by promoting tumour inflammation (Hanahan and Weinberg, 2011). Tumour associated macrophages (TAMs) are a key component of the tumour microenvironment. They can be either transformed tissue resident macrophages or circulating monocytic-derived macrophages recruited to the tumour location by growth factors and chemokines (Noy and Pollard, 2014). When within the tumour microenvironment, macrophages can be skewed from the classically activated (M1) towards an alternatively activated (M2) phenotype. While M1 macrophages are typically associated with an inflammatory and immune-promoting situation, the M2 subset promotes reparatory and regulatory functions. This shift in phenotype is motivated by signals derived from the tumour and other cells in the microenvironment as well as physiological conditions that elicit M2 activation in established progressing tumours (Qian and Pollard, 2010, Mantovani et al., 2017). M1 macrophages are typically associated with the expression of markers such as CD80 and CD86, as well as secretion of pro-inflammatory cytokines such as interleukin (IL)-1 β , IL-6, tumour necrosis factor α (TNF- α) and M2 can express CD163, CD200R and CD206 and secrete IL-10, VEGF and transforming growth factor beta (TGF- β) (Chen et al., 2019, Jayasingam et al., 2020). However, it should be noted that this classification while useful, does not fully convey the complexity of macrophage activation, and macrophages can express both M1 and M2 markers, presenting a mixed phenotype (Pettersen et al., 2011, Murray et al., 2014). Tumour supporting macrophages produce anti-inflammatory cytokines that help to support the tumour, inducing angiogenesis, matrix remodelling, invasion, and metastasis. M2 macrophages, apart from secreting VEGF, supporting angiogenesis in the tumour environment (Linde et al., 2012, Jetten et al., 2014), can also make it available by expressing matrix metalloproteinases (MMPs), such as MMP-9 that releases matrix bound VEGF, stimulating angiogenesis as well as tumour invasion (Bergers et al., 2000, Du et al., 2008). In an experimental model of

metastatic breast cancer, tumour cells synthesize colony-stimulating factor-1 (CSF-1) that stimulates macrophages to produce epidermal growth factor (EGF), that in turn activates tumour cell migration (Wyckoff et al., 2004). The immunosuppressive tumour microenvironment created by the tumour also leads to evading immune mechanisms. For example, TGF- β has the ability to suppress effector T cells cytotoxicity (Thomas and Massagué, 2005), limiting their ability to induce apoptosis in tumour cells, and IL-10 secreted by macrophages can abolish IL-12 production by DCs, altering their function (Ruffell et al., 2014).

Extracellular matrix (ECM) remodelling is critical for tumour progression. The ECM is composed by collagen (its most abundant element), elastin, fibronectin, laminins, tenascin C, as well as proteoglycans (chondroitin sulphate and heparan sulphate) and glycosaminoglycans (hyaluronic acid) (Theocharis et al., 2016). Besides providing biochemical and structural support, this dynamic structure is continuously remodelled, to maintain tissue homeostasis. ECM remodelling consists in processes of deposition, modification, degradation, and organization, that once deregulated can lead to pathological conditions (Winkler et al., 2020). In cancer there is a deposition of ECM that can lead to tumour stiffness (Acerbi et al., 2015) and can determine tumour aggressiveness and clinical outcome (Bergamaschi et al., 2008). Cancer associated fibroblasts (CAFs) are a key player in ECM remodelling, by secreting large quantities of ECM proteins, growth factors and remodelling enzymes (Liu et al., 2019). Furthermore, secretion of remodelling enzymes by CAFs can lead to the loss of architecture seen in cancer, that contributes to disease progression. Proteases, including MMPs, degrade the surrounding matrix and remove barriers that allow for tumour cell migration and invasion (Winkler et al., 2020). The deposition of ECM components by CAFs was shown to be involved with the creation of tracks that guide cancer cell invasion (Gaggioli et al., 2007). Additionally, increased stiffness of the ECM contributes to increased production of TGF- β and mechanical tension necessary for fibroblast differentiation (Tomasek et al., 2002).

In the process of wound healing, fibroblasts have the ability to be activated and become myofibroblasts (Gabbiani et al., 1971). Once wound healing is resolved, these myofibroblasts undergo apoptosis (Desmoulière et al., 1995). However, in the inflammatory tumour microenvironment, these myofibroblasts are hijacked and kept in a persistent wound healing state (Dvorak, 1986), which has been reported in the prostate

Chapter 1 - Introduction

cancer reactive stroma (Olumi et al., 1999, Tuxhorn et al., 2002). Here, the smooth muscle cells, abundant in healthy prostate tissue, are replaced by myofibroblasts (Tuxhorn et al., 2002). These myofibroblasts present a contractile phenotype associated with the expression of alpha smooth muscle actin (α SMA), a cytoskeletal protein associated with smooth muscle cells, and can be induced by tumour-derived TGF- β (Rønnov-Jessen and Petersen, 1993, Desmoulière et al., 1993). Verona *et al.* showed that TGF- β signalling has a crucial role in generating tumour supporting stroma. To generate this stroma, TGF- β binds to TGF- β type II receptor, which in turn recruits the TGF- β type I receptor, leading to phosphorylation of SMAD2 and SMAD3. These complex with SMAD4 and translocate to the nucleus, where they act as transcription factors and regulate expression of tissue remodeling genes (Verona et al., 2007).

Within the tumour microenvironment, myofibroblasts are one of the biggest contributors towards promotion of angiogenesis by secreting elevated levels of growth factors such as hepatocyte growth factor (HGF), VEGF, PDGF and stromal-derived growth factor-1 (SDF-1) (Brown et al., 1999, Dong et al., 2004, Orimo et al., 2005, Webber et al., 2015b). In an elegant study examining fibroblast-epithelial interactions, it was demonstrated, both *in vitro* and *in vivo*, that CAFs were able to induce tumorigenesis in a non-initiated prostate epithelial cell line while normal fibroblasts did not elicit the same response (Olumi et al., 1999). In the *in vivo* component of the study, fibroblasts (either normal or tumour-associated) were mixed with epithelial cells (normal or initiated) and co-implanted as xenografts in immune-deficient mice. In addition to the enhanced proliferation of prostate cancer cells, as seen *in vitro*, myofibroblasts were able to induce a greater number of blood vessels, demonstrating an essential role for these cells in promoting angiogenesis, which was not observed in tissue containing normal fibroblasts.

CAFs also have the ability to affect tumour immunity due to their immunomodulatory secretome (Torres et al., 2013, Takahashi et al., 2017). In prostate cancer, CAFs secretion of SDF-1 seems to be crucial to recruit and induce M2 polarization (Orimo et al., 2005, Comito et al., 2014). Monocyte chemoattractant protein-1 (MCP-1/CCL2) is a known macrophage chemoattractant and has the capacity to induce infiltration of monocytes in breast CAF spheroids (Ksiazkiewicz et al., 2010). CAFs secretome can also contribute to escape from immune surveillance by reducing infiltration of CD8⁺ T cytotoxic cells (Cohen et al., 2017). Therefore, these cells emerge as important players in orchestrating tumour-immunity.

Cancer-derived EVs have been shown to contribute to both recruitment and activation of fibroblasts. Additionally, tumour EVs have emerged as key players in the microenvironment, modulating tumour cells, angiogenesis, and tumour immune response (Bebelmann et al., 2018). These will be described in more detail in the next sections.

1.2.2 EVs in tumour-to-tumour communication

Tumour cells can transfer their oncogenic properties to other tumour cells within the primary tumour via EVs. Al-Nedawi *et al.* demonstrated that glioma cells expressing a highly oncogenic variant of epidermal growth factor receptor, called EGFRvIII, secreted microvesicles harbouring this variant and were able to transfer it to non-EGFRvIII expressing cancer cells within the tumour. The recipient cells were later able to express the mutated receptor leading to increased proliferation and tumour growth (Al-Nedawi et al., 2008). Later, vesicles containing EGFRvIII mRNA were shown to induce morphological changes and anchorage-independent growth in recipient tumour cells (Skog et al., 2008). Furthermore, treatment of mice with melanoma EVs, expressing high levels of Met, facilitated Met expression in Met-low cells, supporting their metastatic capacity in the lungs (Adachi et al., 2016). EVs have also been implied in efficient transfer of integrin $\alpha_v\beta_6$ between different prostate cancer cell lines, that co-localized to the cell surface. Recipient cells treated with EVs containing $\alpha_v\beta_6$ were able to migrate to a greater extent than cells treated with EVs where $\alpha_v\beta_6$ was downregulated (Fedele et al., 2015). Besides effects in migration and metastasis, this horizontal transfer of molecules by EVs has also been implicated in resistance to therapy. Corcoran and colleagues reported that EVs are able to transfer Docetaxel resistance in prostate cancer (Corcoran et al., 2012) suggesting an involvement of the drug efflux pumps such as MDR-1/P-gp (P-glycoprotein), that was present in the prostate cancer cells-derived EVs. Later findings suggested that multidrug resistant osteosarcoma cells were able to transfer drug resistance to sensitive cells via EV-mediated delivery of MDR-1 mRNA or its product, the P-glycoprotein (Torreggiani et al., 2016). The transfer of miRNAs by EVs has also been implicated in drug resistance (Chen et al., 2014) and proliferation (Singh et al., 2014, Felicetti et al., 2016). Taken together, these reports show the various roles of cancer EVs in acquisition and horizontal transfer of malignant traits.

1.2.3 EVs in tumour-to-fibroblasts communication

Tumour-derived EVs can communicate with neighbouring stromal cells and have been shown to be important modulators in the activation of fibroblasts, contributing to the formation of the tumour reactive stroma.

The first report of cancer EVs involvement in driving differentiation of fibroblast into a disease supporting phenotype was documented in a prostate cancer model by Webber *et al.* (Webber *et al.*, 2015b). Previous studies from our group have shown that EVs, produced from a variety of cancer cell lines, expressing high levels of TGF- β 1, can trigger fibroblast differentiation to myofibroblasts, as shown by the presence of structural α SMA (Webber *et al.*, 2010), and gain of pro-angiogenic function resulting in enhanced tumour growth *in vivo* (Webber *et al.*, 2015b). EVs from cancer cell lines with lower/undetectable levels of TGF- β 1, were unable to trigger these phenotypical changes. Additionally, soluble recombinant human TGF- β 1 (rhTGF- β 1) could not reproduce these effects to the same extent, underlying the importance of EV-bound TGF- β 1 to enhance its functional activity. Myofibroblasts generated with vesicular TGF- β 1 secreted pro-angiogenic growth factors such as FGF-2, HGF and VEGF, which were significantly different from myofibroblasts generated with rhTGF- β 1, and secretion was abrogated by blocking TGF- β 1 signalling (Webber *et al.*, 2015b). These vesicular induced myofibroblasts were also able to support migration of endothelial cells and formation of vessel-like structures, as well as recapitulate disease phenotype and functions. The vesicular generated stroma is also able to support tumour growth *in vivo* (Webber *et al.*, 2015b). Similarly, prostate cancer EVs carrying TGF- β 1 were able to regulate the differentiation of bone marrow mesenchymal stem cells, promoting a disease supporting myofibroblast-like phenotype. This phenotype was also not supported by rhTGF- β 1, highlighting the contributions of EVs in promoting CAFs within the tumour microenvironment (Chowdhury *et al.*, 2015). More recently, EVs with characteristics of microvesicles, isolated from ovarian cancer cells, were described with the ability to modulate the behaviour of fibroblasts towards a CAF state and instil a secretome able to promote proliferation, motility and invasion of tumour and endothelial cells (Giusti *et al.*, 2018).

In addition, EVs derived from prostate cancer stem cells and EVs derived from bulk tumours have been compared, and differences in miRNA content were found. Nonetheless, highly abundant EV-miRNAs from both cell types are able to increase

MMPs and RANKL expression in fibroblasts, increasing their metastatic potential (Sánchez et al., 2016). Furthermore, EVs released from prostate cancer cells in hypoxic conditions were found to carry a higher number of proteins comparing to EVs obtained from the same cells in normoxic conditions and demonstrated higher MMP activity. EVs secreted from cells in hypoxia were able to induce activation of prostate fibroblasts with higher expression of α -SMA and were also able to enhance motility on another prostate cancer cell line, different from that of their origin (Ramteke et al., 2015).

EVs can also transfer characteristics of tumour cells to fibroblasts. For example, EVs derived from a T cell leukaemia cell line can transfer hTERT mRNA, the transcript of the enzyme telomerase, to telomerase-negative fibroblasts. This transfer leads to an increase in telomerase protein and activity in recipient cells and further increases life span and proliferation of fibroblasts (Gutkin et al., 2016). These studies suggest that cancer cells can dictate their surroundings via EVs and create a suitable microenvironment able to support cancer survival and progression.

1.2.4 EVs in tumour-to-endothelial cells communication

Endothelial cells are key components of the tumour microenvironment and are susceptible to modelling by tumour-derived EVs. Al-Nedawi and colleagues showed that besides the horizontal transfer of the oncogenic EGFRvIII among cancer cell subsets (Al-Nedawi et al., 2008), microvesicles can also transfer this receptor to nearby endothelial cells. This leads to VEGF expression by recipient cells, activating autocrine VEGF signalling and stimulating angiogenesis (Al-Nedawi et al., 2009). Furthermore, mRNA, miRNA, and angiogenic proteins, contained in glioblastoma microvesicles, are taken up by recipient cells and translated into proteins that promote primary tumour growth and endothelial cell proliferation (Skog et al., 2008). Highly malignant glioblastoma multiform cells, growing in hypoxic conditions, produce EVs containing hypoxia-regulated mRNAs and proteins, reflecting the hypoxic status of the secretory cells, and these EVs promote angiogenesis as well as endothelial cell stimulation of pericyte proliferation (Kucharzewska et al., 2013). EVs can also carry hypoxia regulating miRNAs that can affect endothelial function, again reflecting the hypoxic status of their secretory cells (Umezu et al., 2014, Hsu et al., 2017). The tetraspanin8 (TSPN8) (formerly D6.1A (rat)/CO-029 (human)), packed in EVs derived from rat pancreatic adenocarcinoma, was found to strongly induce angiogenesis *in vivo* as well as

endothelial cell branching, proliferation, and migration *in vitro* (Gesierich et al., 2006). In endothelial cells, TSPN8-CD49d complex containing EVs induced regulation of several angiogenesis-related genes such as macrophage migration inhibitory factor (MIF), von Willebrand factor, VEGF and VEGFR2 enhancing proliferation, migration and sprouting of endothelial cells (Nazarenko et al., 2010). It has also been demonstrated that upregulation of heparanase in myeloma and breast cancer cells is associated with enhanced secretion of EVs containing syndecan-1, VEGF and HGF, leading to endothelial invasion via the ECM and consequent angiogenic activity (Thompson et al., 2013). Additionally, tumour-derived EVs can modify vascular permeability, which can facilitate the escape of tumour cells from primary sites and their entrance into distant metastatic tissues. For example, metastatic melanoma derived EVs (Peinado et al., 2012) and breast cancer derived EVs (Hoshino et al., 2015) were both able to induce vascular permeability in the lung, and lung, liver and brain (Zhou et al., 2014).

1.2.5 Cancer-derived EVs modulate immune response

Evasion of immune surveillance is one of the hallmarks of cancer (Hanahan and Weinberg, 2011). Several studies investigating the role of tumour-derived EVs indicate that the interactions between tumour EVs and the immune system can act to both support and suppress tumour development. It has been reported that EVs can carry tumour antigens and induce efficient anti-tumour responses. For example, melanoma derived EVs express MHC class I molecules and tumour antigens (such as Mart-1/MelanA) that are delivered to DCs for cross presentation to cytotoxic T lymphocytes (CD8⁺ T cells) (Wolfers et al., 2001, André et al., 2002), modulating responses that suppress tumour growth *in vivo* (Wolfers et al., 2001). EVs could, therefore, be involved in sampling antigens to DCs. Other studies have addressed the relationship between tumour-derived EVs and natural killer (NK) cell activity, with EVs containing HSP70 heat shock protein stimulating NK cell activity leading to apoptosis in tumour cells (Gastpar et al., 2005).

However, tumour EVs appear to mostly promote immunosuppressive effects that support tumour progression and metastasis. In this setting, tumour-derived EVs have been shown to be involved in the polarisation status of macrophages. Several studies showed the involvement of tumour-derived EVs in delivering miRNAs that induce the pro-tumorigenic M2 macrophage phenotype (Ying et al., 2016, Shinohara et al., 2017, Hsu

et al., 2018, Chen et al., 2018c). Lung derived EVs containing miR-21 and miR-29a are able to bind to Toll-like receptor (TLR) 8, present on macrophages at the tumour interface, activating NF- κ B and promoting the secretion of inflammatory cytokines TNF- α and IL-6 (Fabbri et al., 2012). Activation of TLR2 by breast cancer EVs also leads to NF- κ B pathway activation in macrophages, and secretion of pro-inflammatory cytokines IL-6, TNF- α , GCSF, and CCL2. This TLR2-dependent-macrophage-stimulated effect appears to be mediated by proteins associated with the vesicle surface (Chow et al., 2014). Recently, it was demonstrated that chemotherapy induced increased secretion of heparanase rich EVs, which modulated ECM to promote macrophage migration and secretion of TNF- α , which is essential for promoting myeloma growth (Bandari et al., 2018).

Tumour-derived EVs are also able to hijack the immune system and promote the escape of tumour cells. The cytotoxic function of NK cells in response to IL-2 was impaired when lymphocytes were exposed to tumour-derived EVs, while CD4⁺CD25⁺ regulatory cells (Tregs) remained IL-2 responsive through induction of Foxp3 expression. EV treatment by itself was also able to boost Treg suppressive function (Clayton et al., 2007). These effects were observed with mesothelioma, and prostate cancer cell-derived EVs. The data revealed a role of tumour EVs in driving immune responses away from cytotoxic effector mechanisms while supporting Treg activities, in a process favoured in part by EV-membrane bound TGF- β 1 delivered to lymphocytes. Administration of TGF- β 1 neutralizing antibody to lymphocytes treated with IL-2 and EVs partially restored their proliferative activity, revealing TGF- β 1 could act as a contributor towards the suppressive functions promoted by Tregs (Clayton et al., 2007). A few years later, an independent study reported similar observations, with EVs promoting stimulatory effects in Tregs but inducing apoptosis in CD8⁺ T lymphocytes (Wieckowski et al., 2009). A follow-up study by Clayton *et al.* demonstrated that TGF- β 1 had a role in down-regulating NKG2D expression in either NK or CD8⁺ T cells, leading to a decrease in IFN γ production and impaired activation of these effector cells (Clayton et al., 2008b). EV-bound NKG2D ligands had previously been associated with this mechanism (Clayton and Tabi, 2005) but the dominant effect is due to vesicular TGF- β 1. Other groups have also reported the importance of vesicular ligands such as FAS and programmed death ligand 1 (PD-L1). FAS ligand has been associated with inducing of apoptosis in lymphocytes (Taylor et al., 2003) whilst PD-L1 bearing vesicles hinder CD8⁺ T cell activation that could be reversed with anti-PD1 antibody treatment (Chen et al., 2018b, Poggio et al., 2019).

Nonetheless, EVs also have the capacity to modulate immune responses by modulating the tumour interstitial fluid environment and not just by direct interaction with the immune cells. Cancer EVs expressing CD39 and CD73 were reported to suppress T cells through adenosine production, by dephosphorylating exogenous adenosine triphosphate (ATP) and 5'AMP (Clayton et al., 2011). This EV-generated adenosine inhibits T cells by signalling through the adenosine A_{2A} receptor. More recently, a study suggested that perforin secreted by CD8⁺ T cells was able to disrupt the membrane of EVs, releasing the adenosine contained inside that would act as an immunosuppressive metabolite and inhibit T cells response by binding to its adenosine receptor (Tadokoro et al., 2020). Collectively, tumour-derived EVs exploit diverse mechanisms that contribute to an immunosuppressive environment and tolerance, which all support tumour progression.

1.2.6 Tumour EVs help to set up the pre-metastatic niche

In 1889, Stephen Paget proposed the “seed and soil” hypothesis of cancer metastasis after noticing that different tumour types tend to metastasize to specific organs. He suggested that this was not a random process and that certain tumour cells, “the seed”, had an affinity for the environment of specific organs, “the soil” (Paget, 1989). In 2003, Fidler added a refinement to Paget’s hypothesis by suggesting that the metastatic process is selective for cells that can successfully migrate to the distal organ and encounter a microenvironment that is suitable for the success of metastatic cell proliferation (Fidler, 2003). This process starts with the development of vascular leakiness, followed by alteration of the resident cells at the distant place and sequent attraction of bone marrow-derived cells to the pre-metastatic site, which all together will recruit circulating tumour cells (Psaila and Lyden, 2009).

In the past decade, the role of EVs in the communication between the primary tumour and the pre-metastatic niche has been gaining recognition, placing them as regulatory mechanisms used by tumour cells to prime specific organs to facilitate metastasis. Peinado and colleagues provided one of the first reports that EVs promote pre-metastatic niche formation. The group showed that EVs derived from highly metastatic melanoma cells enhance metastasis to the lung by transferring MET oncoprotein to bone marrow progenitor cells, mobilising and educating them to a pro-metastatic phenotype that supports tumour vasculogenesis (Peinado et al., 2012). Furthermore, these EVs were also able to enhance lung endothelial permeability in mice, a process essential to start

the metastatic process. The concept of a stepwise promotion of pre-metastatic niche formation by EVs was further explored by Costa-Silva *et al.* who showed that EVs secreted by pancreatic tumour cells containing high levels of MIF induce upregulation of TGF- β production in Kupffer cells in the liver leading to fibronectin production. This results in a fibrotic liver environment that attracts bone-derived macrophages and promotes a pre-metastatic environment suitable for liver metastasis (Costa-Silva *et al.*, 2015). Soon after, the same group showed that specific groups of integrins present on cancer EVs directed them to specific organs, establishing their metastatic organotropism. For example, EVs expressing integrin $\alpha_v\beta_5$ specifically bind to Kupffer cells, promoting liver metastasis, while integrins $\alpha_6\beta_1$ and $\alpha_6\beta_4$ bind to lung fibroblasts and epithelial cells, mediating metastasis to the lungs (Hoshino *et al.*, 2015). However, it remains unknown if the organ-specific tropism is solely determined by EV integrin repertoire. In the study, vascular leakiness was also observed as a first EV-mediated step, suggesting a vesicular role in starting the metastatic cascade.

When on-site, EVs target non-transformed cells in pre-metastatic organs and transform them to support the tumorigenic process. Brain metastatic breast cancer cell derived-EVs are able to transfer miR-181c into endothelial cells, resulting in the breakdown of the blood-brain barrier and extravasation of metastatic cancer cells to the brain (Tominaga *et al.*, 2015). Renal cancer stem cell-derived EVs contain miRNAs for growth factors, such as VEGF, MMP-2 and MMP-9, which contribute to pre-metastatic niche formation in the lung (Grange *et al.*, 2011), whereas miRNAs in EVs from prostate cancer contributed to osteoblast differentiation, driving metastasis to the bone (Sánchez *et al.*, 2016). In addition, EVs can also reprogramme the metabolism in the tumour microenvironment. Breast cancer cell derived-EVs containing miR-122 can suppress glucose uptake by non-tumour cells in the pre-metastatic niche, such as fibroblasts, but do not seem to increase glycolysis in cells in the primary tumour microenvironment. This leads to an augmentation in glucose availability, accommodating the massive energy needs of cancer cells during metastatic growth (Fong *et al.*, 2015). However, EVs are also able to suppress pre-metastatic niche formation and metastasis. One study showed that EVs from poorly metastatic melanoma cells were able to inhibit lung metastasis, by inducing the expansion and recruitment of the patrolling monocyte at the pre-metastatic niche, resulting in tumour cell clearance (Plebanek *et al.*, 2017). This is not surprising, considering the evidence of anti-tumour effects of EVs in the immune system, addressed in the previous section. Thus, it might be possible at in early phase anti-tumour

Chapter 1 - Introduction

mechanisms are more abundant, and as the cancer sets in, processes to support cancer growth and metastasis take over.

Much is still unknown about the role of tumour EVs in the metastatic process. Therefore, it is of great importance to understand the mechanisms by which EVs promote tumorigenesis, which EV cargo are relevant for these processes, as well as address the contributions of particular tumour cell subpopulations. A summary of the different roles of tumour EVs in modulating tumour responses, angiogenesis and immune responses is shown in **Figure 1.4**.

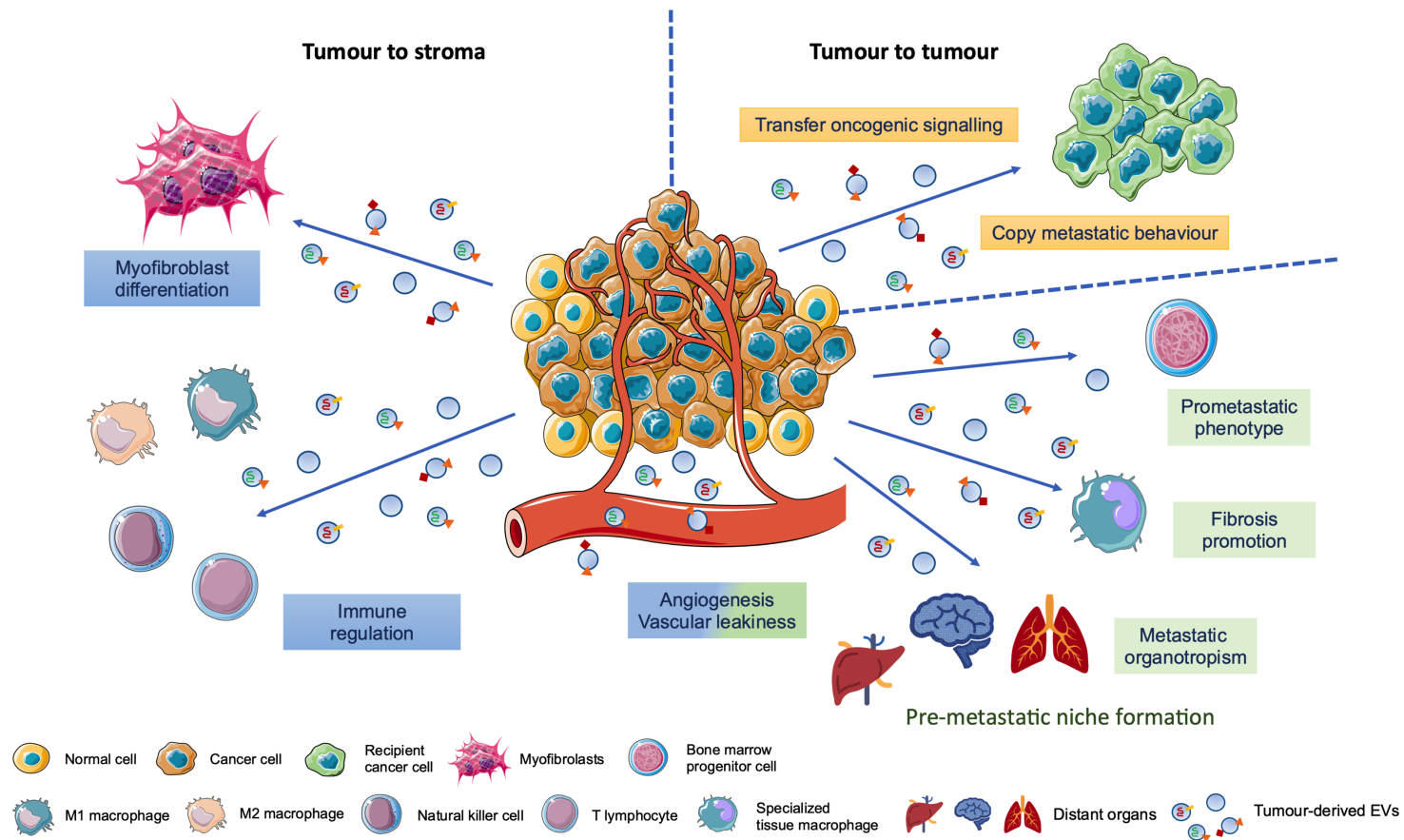


Figure 1.4. Tumour-derived EVs in the tumour microenvironment. Tumour EVs function in tumour-to-stroma and tumour-to-tumour communication. EVs released by cancer cells have several roles within the tumour microenvironment by educating different types of stromal cells. EVs act by promoting angiogenesis, pro-metastatic phenotypes, and regulating immune response. In addition, cancer EVs can help to set up the pre-metastatic niche by altering bone marrow-derived progenitor and resident cells, as well as influencing metastasis in specific organs. Cancer EVs can also transfer malignant traits between different tumour cell subpopulations helping tumour progression and resistance to therapy. Adapted from Bebelman et al., 2018. Figure created using Servier Medical Art templates.

1.3 EV-associated HSPGs within the tumour microenvironment

HSPGs have had an emerging role in the EV field, namely in biogenesis and uptake. Syndecans were shown to play a central role in EV biogenesis through the syndecan-syntenin-ALIX pathway shown by Guido David and Pascal Zimmerman (Baietti et al., 2012), and most recently syndecan-4 involvement in EV biogenesis has also been described (Ghossoub et al., 2020). In addition, cell surface syndecans, as well as glypicans, were shown to play a role in EV uptake by recipient cells (Christianson et al., 2013). All these mechanisms have raised the importance of better understanding the involvement of HSPGs and their GAG content in EV functions and will be further described later.

1.3.1 HSPG structure

Heparan sulphate proteoglycans (HSPGs) are specialized glycoproteins with a core protein, which is covalently attached to one or more heparan sulphate (HS) glycosaminoglycan (GAG) chains. HSPGs can be grouped in three distinct classes according to their location and core protein structure. The membrane-associated HSPGs include the glyicans with a transmembrane domain such as syndecans (syndecan 1-4) and betaglycan, and the GPI-anchored glypicans (glypican 1-6). The secreted ECM HSPGs consist of perlecan, agrin and collagen type XVIII. Lastly, the secretory vesicle proteoglycan serglycin, found in intracellular granules in mast and hematopoietic cells, carries heparin chains, which is an unusually extended and highly sulphated form of HS (Sarrazin et al., 2011).

This thesis will focus on membrane-associated HSPGs (**Figure 1.5**), as their location at the cell surface is more likely to later lead to their incorporation on the surface of endosomal derived EVs during the biogenesis process. All four members of the syndecan family contain HS-GAG chains, but syndecan-1, -3 and -4 also contain chondroitin sulphate (CS) (Chernousov and Carey, 1993, Ueno et al., 2001, Deepa et al., 2004), which in syndecan-4 are suggested to cooperate with HS-GAG chains in binding midkine and pleiotrophin (Deepa et al., 2004).

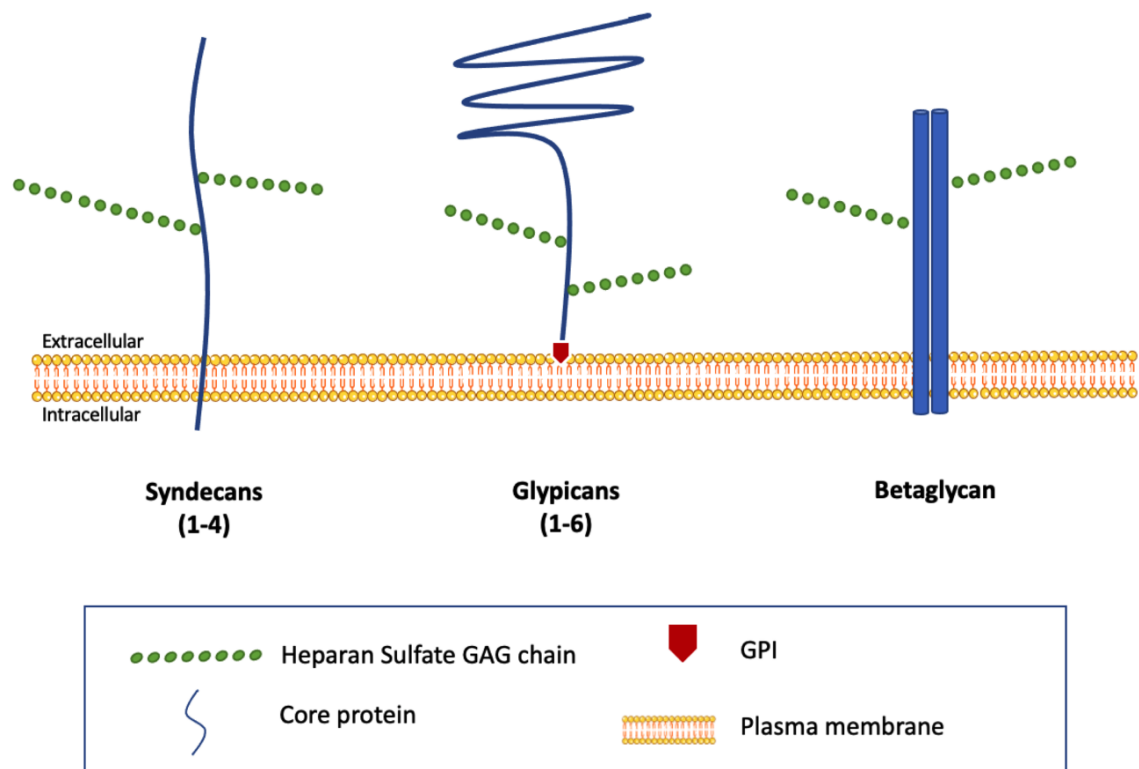


Figure 1.5. Examples of Heparan sulphate proteoglycans present at the surface of cells and extracellular vesicles. Representation of transmembrane syndecans and betaglycan and glycosylphosphatidylinositol (GPI)-anchored glypicans. Green dotted line represents intact glycosaminoglycan chains attached to the protein core (blue).

The HS-GAG chains of HSPGs are synthesised in the Golgi apparatus through the coordinated action of different enzymes. HS biosynthesis starts with the formation of a tetrasaccharide linker, consisting of xylose, galactose and glucuronic acid (GlcA), attached to specific serine residues on the core protein. Attachment of *N*-acetylglucosamine (GlcNAc) starts chain elongation, which is continued by stepwise addition of GlcNAc and GlcA residues, in a process aided by members of the exostosin glycosyltransferase family, such as exostosin-like protein (EXT) 1 and EXT2 (Kitagawa et al., 1999, Kreuger and Kjellén, 2012). As the chain elongates, a series of modifications take place. Different sulfotransferases, such as *N*-deacetylase/*N*-sulfotransferase (NDST) and 2-*O*-, 3-*O*- and 6-*O*-sulfotransferases (2OST, 3OST and 6OST), as well as C5-epimerase (GLCE), will catalyse deacetylation, sulphation, and epimerization reactions (respectively) in specific residues. The synergic action of these enzymes affects the composition and characteristics of HS chains and creates regions of sulphated residues (NS domains) separated by non-sulphated regions (NA domains). A general overview of HS biosynthesis and structure is shown in **Figure 1.6**. Once at the

cell surface, HS chains can be further modified by two endosulfatases (Sulf1 and Sulf2) or by action of heparanase and/or extracellular proteases (Annaval et al., 2020). All of these processes make HS-GAG chains highly heterogeneous, and because the mechanisms behind the regulation of these enzymes are largely unknown, the specific heparome in a cell at a given time is unpredictable.

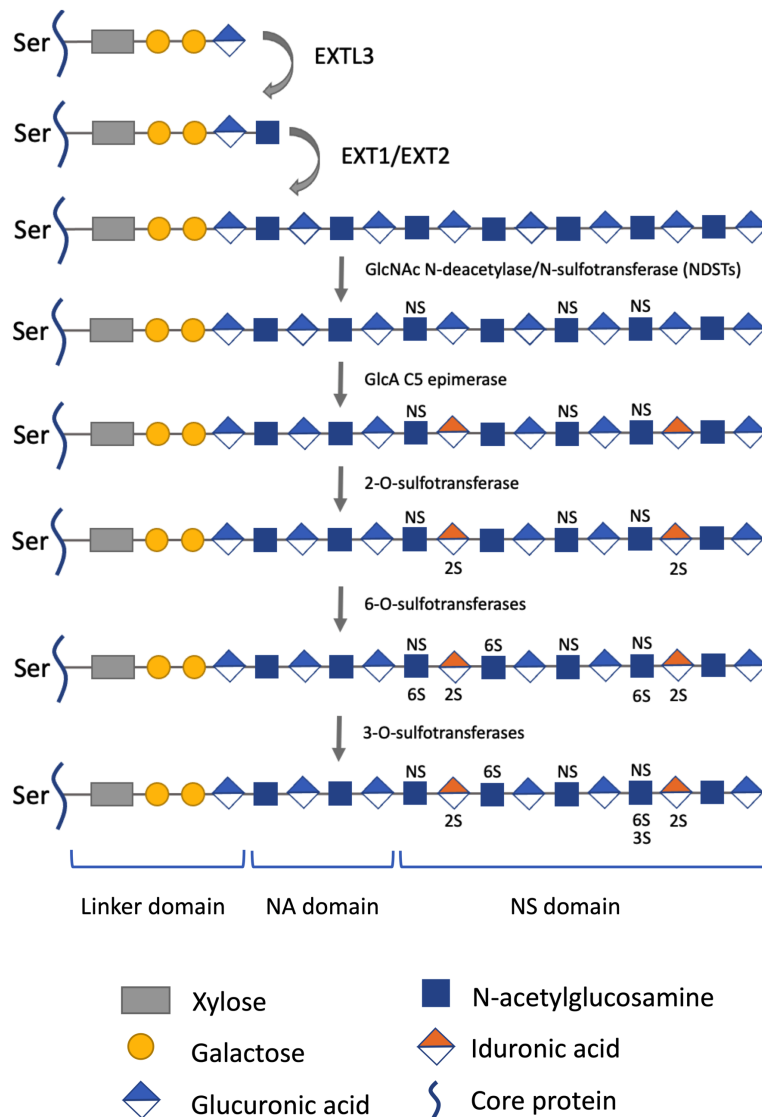


Figure 1.6. Heparan sulphate biosynthesis. Representation of the stepwise production of HS GAG chains. Biosynthesis starts with the production of the linker domain, covalently attached to serine residues on the core protein. Initiation starts with attachment of *N*-acetylglucosamine (GlcNAc) by EXTL3 enzyme and chain elongation results from continuous addition of GlcNAc and glucuronic acid (GlcA) residues by EXT1 and EXT2 enzymes. De-acetylation and sulphation are carried out by NDSTs, and glucuronic acid can be epimerised by C5 epimerase to give origin to iduronic acid. Sulphate groups can then be modified by 2ost, 3OST and 6OST. The resulting chain is constituted with regions of high sulphation (NS domain) and low sulphation (NA domains). Exostosin-like protein (EXTL), exostosin (EXT), N-deacetylase/N-sulphotransferase (NDST), 2-O-sulphotransferase (2OST), 6-Osulphotransferase (6OST) and HS 3-O-sulphotransferase (3OST). Adapted from Kreuger and Kjellén, 2012.

1.3.2 HSPGs bind growth factors

HSPGs are known to bind a variety of ligands such as morphogens, cytokines, growth factors, and enzymes. Furthermore, they can also act as co-receptors (Ori et al., 2011, Sarrazin et al., 2011, Bishop et al., 2007). FGF was the first factor to be shown to depend on HS to interact with its receptor (Yayon et al., 1991, Rapraeger et al., 1991). Since then, HSPGs have been shown to be important in Wnt signalling (Ai et al., 2003) and modulating the activity of hedgehog (Hh) (Capurro et al., 2005), TGF- β (López-Casillas et al., 1991), HGF (Derksen et al., 2002) and VEGF (Jung et al., 2016), amongst others. While syndecans seem to be mostly involved in processes related with cell adhesion to the ECM and cell signalling to the cell interior, glypicans appear to be involved in regulating morphogen gradients and signalling of morphogen receptors (Sarrazin et al., 2011). These apparently different functions between syndecans and glypicans might be related to location of the HS-GAG chains. In glypicans, and contrary to syndecans, these are located in close proximity to the juxtamembrane region, and therefore, closer to the cell surface (Iozzo and Schaefer, 2015). Additionally, binding of proteins to HS-GAG chains restricts their diffusion and allows for their concentration at the cell surface.

The sulphation pattern of the HS-GAG chains present on HSPGs is responsible for the negative charge that determines their binding to functional ligands, largely through electrostatic reactions, mostly occurring in NS domains. Heparin, a highly sulphated form of HS, has been extensively used to purify growth factors, often described as “heparin binding proteins”, through affinity chromatography. However, most functionally relevant protein interactions bind HS rather than heparin (Ori et al., 2011). Some of these interactions require specific sequences and sulfation patterns to be present in HS-GAG chains for the association with proteins ligands to occur. For example, macrophage inflammatory protein 1 α (MIP1 α) was found to bind more strongly to larger S-domains present in HS, which are more enriched in 6-O-sulfate, and 6-O-sulphation of HS appears to be important for MIP1 α biological activity (Stringer et al., 2002), as well as FGF-2 (Maccarana et al., 1993) and VEGF (Robinson et al., 2006).

The binding of proteins to HSPGs can also involve the cytoplasmatic domains, such as the interactions of syntenin with syndecan-1 cytoplasmatic domain, shown to be crucial for EV biogenesis (Baietti et al., 2012, Roucourt et al., 2015). The ectodomain of syndecan-1 also seems to be required for integrin-related cell adhesion. Syndecan-1 association with $\alpha_v\beta_3$ integrin activity was demonstrated to be required for spreading in

Chapter 1 - Introduction

human breast carcinoma cells (Beauvais and Rapraeger, 2003). In another study, both the HS chains and ectodomain of syndecan-1 were shown to be required for the full activity of syndecan-1 in regulating ECM alignment in human mammary fibroblasts (Yang and Friedl, 2016). This ECM aligned fibre architecture was dependent on the association of syndecan-1 ectodomain with $\alpha_v\beta_3$ integrin, modulating fibronectin fibrillogenesis. Additionally, syndecan-1 HS chains interaction with fibronectin may also help to modulate this process. This ECM remodelling promoted the migration and invasion of breast cancer carcinoma cells.

Nevertheless, most interactions with HSPGs and ligands are related to the HS-GAG chains, and this is perhaps their most fundamental role. The size of HS-GAG chains (40–160 nm) allows binding of multiple ligands, assimilating them from the soluble phase and concentrating them at a specific location in the extracellular space. This contributes to the increase of their lifetime by protecting them from protease degradation (Sadir et al., 2004). HS-GAG chains can also contribute towards the diffusion of HS-binding ligands. Duchesne *et al.* explored how FGF-2 diffuses along the HS-GAG chains, by using transmission electron microscopy and photothermal heterodyne imaging. Through these techniques, it was observed that FGF-2 distribution around the cell is highly heterogenous. While some FGF-2 molecules remain immobile or in confined motion (range of movement ~ 100 nm), others display substantial translocation across several micrometres, even in fixed cells, where movement of HSPGs in the membrane is impeded. Considering that this distance is greater than the length of HS chains, this movement most likely occurs through dissociation and re-tethering of FGF-2 in nearby sites in different HS chains (Duchesne et al., 2012). HSPGs can also bind proteins in *trans*, acting from the cell harbouring the HSPG core protein to a receptor present in another cell. Jakobsson *et al.* described how VEGF interactions with its receptor in endothelial cells could be supported by HSPGs present in adjacent perivascular smooth muscle cells. These HSPGs would bind to the VEGF receptor and delay its internalisation, prolonging receptor tyrosine phosphorylation and transduction of biological responses (Jakobsson et al., 2006).

Remodelling of HSPGs can have an important impact on proteoglycan functions and ligand diffusion. Syndecans and glypicans can be shed from the cell surface and impact the signalling events mediated by HSPGs (Ding et al., 2005, Matsuda et al., 2001, Iozzo and Schaefer, 2015). On the other hand, heparanase, the sole mammalian heparan

sulphate-degrading enzyme, is responsible for trimming the heparan sulphate chains on HSPGs, liberating the growth factors from core proteins and allowing them to diffuse at a long distance (Sanderson et al., 2005, Goodall et al., 2014). Heparanase has also been shown to have a crucial role in EV biogenesis and cargo loading, as discussed later in this thesis (Thompson et al., 2013, Roucourt et al., 2015). Additionally, heparanase has been shown to be involved in many processes in cancer progression that will be explored further in the next section.

1.3.3 HSPGs in cancer

Due to their highly heterogenous structure and involvement in regulation of biological activities, HSPGs are important contributors to tumour progression. As one of the major constituents of basement membranes (Yurchenco and Schittny, 1990), cleavage of HS-GAG chains from HSPGs by heparanase, alters the architecture of the ECM, decreasing its stiffness and facilitating tumour cell invasion and angiogenesis.

Syndecan-1 is one of the most studied HSPGs in what concerns cancer progression. Heparanase seems to have a powerful effect on syndecan-1 functions by means of trimming the HS chains from syndecan-1 core protein, exposing the core protein and allowing for increased cleavage by MMPs (Ramani et al., 2012, Yang et al., 2007). In myeloma, heparanase-stimulated upregulation of the expression of MMP-9, a syndecan-1 sheddase, resulted in increased syndecan-1 shedding (Purushothaman et al., 2008), and consequent syndecan-1 availability in soluble form, resulting in increased growth of myeloma tumours *in vivo* (Yang et al., 2002). One study hypothesises that shedding of syndecan-1 by MMP-9 allows for its binding to integrin $\alpha_4\beta_1$ and VEGFR2, present on myeloma and endothelial cells, promoting an invasive phenotype and endothelial cell activation (Jung et al., 2016).

The binding of growth factors to HS in HSPGs has an important role in oncogenic signalling. For example, lack of glypican-1 in breast cancer cell lines was associated with attenuation of proliferation effects promoted by factors, such as heparin binding EGF-like growth factor (HB-EGF), FGF-2, and HGF. Additionally, this HSPG seems to prolong signalling by enhancing the interaction of these factors with their receptors (Matsuda et al., 2001). Furthermore, HGF association with syndecan-1 in multiple myeloma cells promotes HGF-mediated signalling through its c-Met receptor, activating

Chapter 1 - Introduction

phosphatidylinositol 3-kinase/protein kinase B and Ras/mitogen-activated protein (MAP) kinase pathways, which promote cell survival and proliferation respectively (Derksen et al., 2002).

Angiogenesis, a key element in cancer growth and progression, seems to be highly modulated by HS and HSPGs, due to the association of HS with angiogenic factors such as FGF, HGF, and VEGF. Endothelial cells are activated in response to these pro-angiogenic factors secreted by tumour and stromal cells and promote vascularisation and tumour growth. Cleavage of HS-GAG chains by heparanase seems to improve the likelihood of the formation of active FGF-2-FGR complex, stimulating FGF-2 activity and enhancing FGF-mediated angiogenesis in melanoma. These effects were dependent on the heparanase concentrations used (Reiland et al., 2006). Heparanase activity has been shown to increase microvessel density (Kelly et al., 2003) and stimulate endothelial invasion (Purushothaman et al., 2010). The release of heparanase from myeloma cells leads to shedding of intact syndecan-1, in concert with VEGF, and this complex activates integrins and VEGF receptors on adjacent endothelial cells, stimulating angiogenesis and endothelial invasion (Purushothaman et al., 2010). HSPGs role in delaying VEGFR receptor internalisation also contributes towards promoting angiogenesis by enhancing VEGF signalling in endothelial cells from multiple myeloma patients (Lamorte et al., 2012). These studies show the role of HSPGs in tumour progression and the importance of heparanase in modulating invasion of both tumour and endothelial cells.

Besides heparanase, sulfation enzymes such as Sulf1 and Sulf2, responsible for removing 6-*O*-sulfate groups from HS-GAG chains, can also play a role in modulating ligand binding to HSPGs. Distinct to the heparanase role described before (Reiland et al., 2006), Sulf1 partakes in reducing affinity of FGF-2 to FGFR (Lai et al., 2003, Narita et al., 2006) as well as attenuating VEGF165-mediated signalling in endothelial cells (Narita et al., 2006). Sulf2 seems to have the opposite effect, promoting FGF-2 signalling in hepatocellular carcinoma (Lai et al., 2008), and is required for the interaction of VEGF with HS-GAGs (Uchimura et al., 2006). In prostate cancer cell lines DU145 and PC3, Sulf2 overexpression suggests a possible pro-tumorigenic effect of this enzyme by increasing cell migration and epithelial-mesenchymal transition (Vicente et al., 2015). Sulf1 and Sulf2 seem to have different biological functions, with Sulf1 most likely playing an anti-tumour role, whereas Sulf2 has pro-tumour effects (Hammond et al., 2014).

HSPGs also seem to play an important role in modulation of tumour immunity, particularly in immune evasion and promotion of an anti-inflammatory tumour microenvironment. Dendritic cell-associated HSPG-dependent integrin ligand (DC-HIL), is an immune suppressive molecule that abrogates T cell responses via binding to syndecan-4 at the cell surface, reducing pro-inflammatory cytokine secretion (Chung et al., 2007, Chung et al., 2009). Further studies showed that myeloid-derived suppressor cell (MDSC) expression of DC-HIL is crucial for melanoma immune evasion through inhibition of T cell responses and blocking DC-HIL/syndecan-4 interaction enhanced T cell response (Chung et al., 2014). However, the innate immune response to cancer cells by NK cells can also be modulated by the interaction of natural cytotoxicity receptors (NCR) with HSPGs at the tumour cell surface, mediating NK cell target recognition and anti-tumour response (Hecht et al., 2009). Once again highlighting the importance of heparanase remodelling of HSPGs, HS fragments arising from heparanase activity have been shown to stimulate the release of pro-inflammatory cytokines such as cytokines IL-1 β , IL-6, IL-8, IL-10 and TNF by human peripheral blood mononuclear cells (PBMCs) through the TLR-4 (Goodall et al., 2014). This receptor has also been shown to be activated in dendritic cells by HS fragments, promoting their maturation and an inflammatory response (Johnson et al., 2002).

Collectively, these studies show that HSPGs can regulate immune mechanisms and contribute to cancer initiation and progression. This knowledge can provide interesting targets for development of therapeutics to fight cancer growth and progression.

1.3.4 HSPGs in EV biogenesis

In the past decade, HSPGs have been found to be intrinsically linked with EV biogenesis. In 2012, Guido David and Pascal Zimmermann were the first to describe the syndecan-syntenin-ALIX pathway for EV biogenesis (Baietti et al., 2012), shown to be associated particularly with the secretion of small vesicles of endosomal origin, commonly referred to as exosomes. For this, the cytoplasmatic domain of syndecan connects with the cytosolic adaptor syntenin that interacts, through its N-terminal, with ALIX. ALIX is an auxiliary component of the ESCRT machinery that supports the budding of the ILVs within the endosomal membrane. This process seems to be dependent on ESCRT-III components Snf7/ charged multivesicular body protein (CHMP)4 and Vps2/CHMP2, but not Vps24/CHMP3 or Vps20/CHMP6. Considering that ceramide is involved in EV

Chapter 1 - Introduction

biogenesis, the study used RNA-mediated interference (RNAi) to target neutral sphingomyelinase-2 (an enzyme involved in ceramide production) in MCF-7 cells, resulting in decreased detection of syndecan, CD63, syntenin, and ALIX, further confirming their involvement in this mechanism. Additionally, in the MCF-7 breast cancer cell lines used in the study, CD63 loading seemed to be particularly dependent on syndecan-syntenin-ALIX. Depletion of any one of these three proteins within MCF-7 cells resulted in a reduced accumulation of CD63 within the exosomes. Knockdown of CD63, on the other hand, had little effect in exosomal levels of syndecan, syntenin and ALIX. The HS contributions for syndecan clustering and oligomerisation were also explored in the study. Disrupting the HS structure either by knockdown of enzymes involved in HS biogenesis and sulfation, such as EXT1/2 and NDST1/2, markedly reduced the number of exosomes released by the cells. The addition of heparitinase (also known as heparinase III (HEPIII)) to the cell culture media, to digest HS-side chains, had a similar effect. The work also demonstrated that while isolated exosomes contain mostly C-terminal syndecan fragments (CTFs), compared with intact syndecans, syndecan-CTFs alone failed to sustain exosome formation and exosomal accumulation of syntenin and CD63 in syndecan-depleted cells. Nevertheless, its production might be required for exosome formation, along with clustering of syndecans (Baietti et al., 2012).

Supporting these findings, in a study by the same group, Roucourt *et al.* showed that trimming of HS on syndecans by heparanase facilitates exosome biogenesis (Roucourt et al., 2015). They speculate that trimming of HS chains is somehow responsible for clustering of syndecans, which had previously been shown to support EV production (Baietti et al., 2012). By reducing the size of the HS-GAG chains, syndecans can come close together and accumulate within the endosome. Furthermore, once HS is removed, protease cleavage sites on syndecans become exposed, facilitating the formation of CTFs, which are commonly identified in exosome composition (Baietti et al., 2012, Roucourt et al., 2015). Additionally, heparanase had no effect on the secretion of EVs containing markers like CD9 and CD81. Still, it stimulated the release of EVs containing CD63, being perhaps involved in targeting specific cargo in exosomes, and supporting the idea that several different mechanisms might be involved in EV cargo loading and biogenesis. This study supports the previous findings by Thompson *et al.* showing that heparanase activity is related to increased release of EVs by tumour cells, as well as EV composition and function (Thompson et al., 2013).

In 2020, Zimmermann and colleagues showed that syndecan-4 is involved in EV biogenesis through association with tetraspanin 6 (TSPN6) (Ghossoub et al., 2020). TSPN6 reduces the exosomal release of syntenin and syntenin cargo. TSPN6 has also been shown to interact with syndecan-4 and syntenin, acting as a negative regulator of exosome release, supporting the lysosomal degradation of syndecan-4 and syntenin. The lysosomal degradation of syntenin seems to rely particularly on syndecan-4 opposed to other syndecans previously shown to interact with syntenin, such as syndecan-1, which had no impact on TSPN6-mediated syntenin degradation. TSPN6 also inhibits shedding of syndecan-4 ectodomain and supports lysosomal degradation of cleaved syndecan-4 and syndecan-4 associated cargo. Overall, the study shows that TSPN6 can have a fundamental role in the sorting towards degradative endosomes, rather than secretory late endosomes. These mechanisms seem to place HSPGs as important players in EV biogenesis and shed light on how specific cargos may be sorted into EVs.

1.3.5 HSPGs in EV uptake

HSPGs have been shown to be important for uptake of macromolecular cargo and complexes, such as lipoproteins, and viral particles rely on HSPGs to enter cells. However, the role of HSPGs in EV uptake is ill-defined and does not seem to be restricted to one particular pathway, varying with cellular context and type of ligand (Christianson and Belting, 2014, Wittrup et al., 2009, Belting, 2003).

The uptake of EVs by recipient cells is a crucial step in EV-cell communication, and HSPGs at the surface of recipient cells have been found to be associated with this process. Several studies have shown that cell uptake of tumour-derived EVs can be blocked by heparin (Atai et al., 2013, Christianson et al., 2013, Franzen et al., 2014). One study showed that whilst heparin can block uptake of both tumour and non-tumour-derived EVs, by tumour and non-tumour recipient cells alike, this effect is much more accentuated for tumour EVs/cells. Nevertheless, the study also demonstrated that heparin was most likely blocking EV uptake at the level of cell binding and not internalisation (Atai et al., 2013).

In another study, the use of cell mutants with attenuated HSPG synthesis revealed a reduced capacity for EV internalisation. These results were confirmed using xylosides to inhibit HSPG biosynthesis, resulting again in reduced EV internalisation (Christianson et

Chapter 1 - Introduction

al., 2013). Additionally, EV-associated HSPGs were considered not essential for EV uptake. Even if syndecans and glypicans were detected at the EV surface, removal of HS from the EV surface, with heparinase I and III, did not affect uptake (Christianson et al., 2013). However, treating EVs with heparin prior to their addition to cell cultures seemed to promote a small decrease in uptake (Atai et al., 2013, Franzen et al., 2014), perhaps by blocking ligands necessary for EV binding to the cell surface, such as fibronectin. Fibronectin was previously shown to be important for docking of EVs to the cell surface, and it was proposed that HSPGs play a role in both EV binding and uptake by recipient cells, however, uptake was not explored in this study (Purushothaman et al., 2016). More recently, fibronectin on the surface of microvascular endothelial cell-derived EVs was shown to mediate EV internalisation by oligodendrocyte precursor cells (OPCs). This mechanism was dependent on the binding of vesicular fibronectin to HSPGs at the surface of OPCs, promoting cell survival and proliferation. Treatment of EVs with heparin greatly reduced incorporation of EVs by the cells, most likely by blocking fibronectin attachment to cell-surface HSPGs (Osawa et al., 2017). However, in all these studies, EV uptake is not completely inhibited, suggesting the existence of HSPG-independent modes of internalisation and alternative uptake pathways, such as those previously discussed in this chapter. Overall, vesicular entry seems to rely more on cell surface HSPGs than EV-associated HSPGs.

Recently, two studies were published describing new contributions of HSPGs to EV uptake. Fuentes *et al.* demonstrated that integrin subunit beta 3 (ITGB3), an integrin present on the recipient cell surface, is required for the uptake of EVs in breast cancer cells through ITGB3-interacting HSPGs present on the EV surface. This mechanism is related with the process of integrin endocytosis, where ITGB3 interaction with focal adhesion kinase (FAK) starts the endocytic process (Fuentes et al., 2020). Another study by Mattias Belting's group showed that hypoxia in glioma cells contributed to increased vesicular uptake through an HSPG dependent mechanism and lipid raft-mediated endocytosis (Cerezo-Magaña et al., 2021). EVs, syndecan-1 and membrane raft marker CtxB all co-internalised in hypoxic cells, and treatment with a membrane raft-mediated endocytosis inhibitor significantly decreased internalisation. This hypoxia induced uptake led to an EV-mediated lipid drop formation that contributes to a metabolic phenotype involved in the malignant behaviour of several tumour types

Many factors, including the abundance and structure of HSPGs, vesicular HSPG-associated ligands, and cell-specific uptake mechanisms, can all influence the EV-cell interactions and explain the differences observed between cell types. Therefore, the identification of EV-associated ligands required for EV-cell interaction, and also EV uptake, will be of high interest to the field. **Figure 1.7** shows how HSPGs can be implicated in EV biogenesis and uptake by recipient cells.

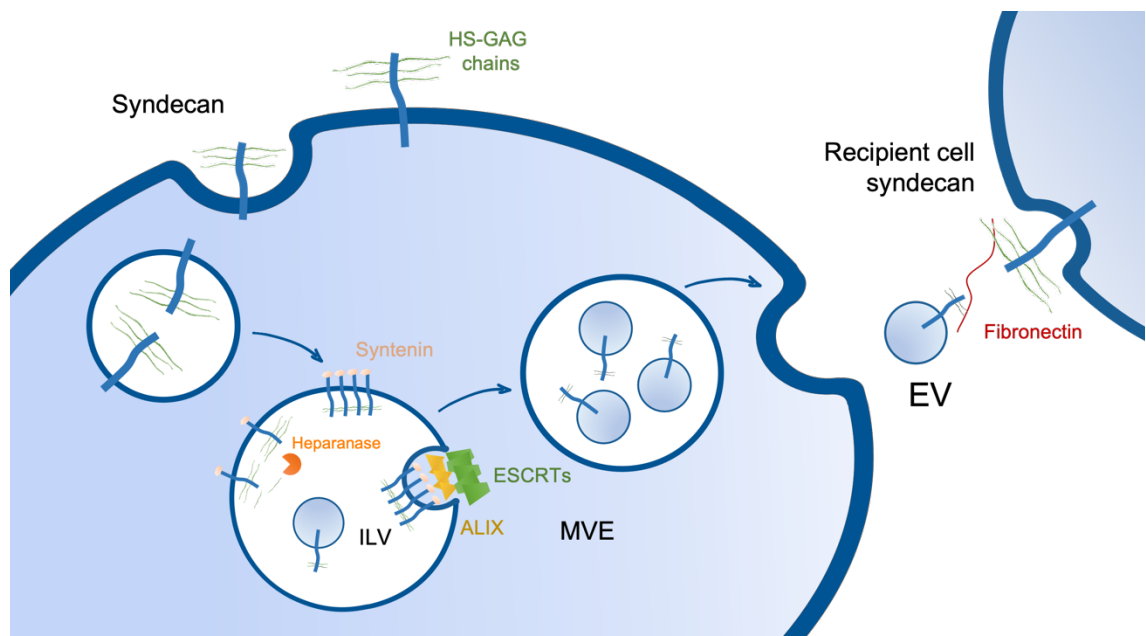


Figure 1.7. Roles of HSPGs in EV biogenesis and uptake. Syndecans and HS-associated cargo are internalized by endocytosis. In endosomes, the cytoplasmic part of syndecans interacts with syntenin and heparanase trims its HS components, allowing for clustering of several syndecans on the endosomal membrane. Syntenin interaction with ALIX, recruits other ESCRT components that stimulate endosomal budding and ILV formation. This process is associated with CD63 enriched EVs. After release, HS present on the EV surface can interact with fibronectin associated with recipient cell surface HSPGs, leading to EV docking and uptake. Image created based on Roucourt et al., 2015 and Buzás et al., 2018.

1.3.6 The roles of EV-associated HSPGs in cancer

EVs have a significant impact in cancer progression, and due to their unique interactive surface area, they can establish contact and mediate communication between cancer cells and the surrounding microenvironment. As described before, vesicular HSPGs have been found on EVs and have relevant functions (Baietti et al., 2012, Christianson et al., 2013). Moreover, HSPGs bind several proteins, such as VEGF and HGF (Reiland et al., 2006, Matsuda et al., 2001), and EVs enriched in these proteins can contribute to tumour progression (Thompson et al., 2013). It is therefore conceivable that EV-associated HSPGs can bind to a variety of additional proteins, and that EVs act as a means of distributing these proteins throughout the tumour microenvironment and beyond.

Previous research by Webber *et al* showed that betaglycan was essential for tethering of TGF- β 1 to the EV surface (Webber et al., 2010). Cleavage of betaglycan induced by pervanadate and selective knockdown of this HSPG resulted in reduced vesicular TGF- β 1 detection. In a follow-up study by the group, the HSPG HS side chains, present at the EV surface, were found to be required for the functional delivery of TGF- β 1. Enzymatic digestion of HS side chains by means of HEP1III did not affect the levels of TGF- β 1 detected on vesicle surface. However, HS side chain loss led to an attenuation of the SMAD-dependent TGF- β signalling in recipient fibroblasts, resulting in abrogation of differentiation to an α SMA-positive phenotype. Furthermore, removal of EV-associated HS resulted in failure of EVs to induce pro-angiogenic function of the recipient fibroblasts (Webber et al., 2015b). This demonstrated that HS side chains were required for TGF- β 1 ability to enlist a disease-promoting fibroblast phenotype.

As mentioned before, the negatively charged HS side chains on HSPGs have an affinity for positively charged protein that contributes to their binding to several different factors. Nucleic acids such as miRNA and mRNA, for example, are negatively charged and were demonstrated to be carried by EVs and involved in cell-cell communication triggering pro-tumorigenic effects (Skog et al., 2008, Fong et al., 2015, Sánchez et al., 2016). Therefore, EV-associated HSPGs could serve as carriers for nucleic acids providing a stable way of transport away from the degradative enzymes. Furthermore, the presence of miRNA on the outer side of EVs also makes it easier to conceptualise how EV-associated miRNAs are able to bind and activate TLRs present in endosomes in the

recipient cell, following internalisation to the endosomal compartment, inducing a pro-metastatic inflammatory response (Fabbri et al., 2012). Additionally, it is also suggested that they could activate TLR present on the surface of recipient cells (Cerezo-Magaña et al., 2020).

Besides being a way of increasing protein distribution and presentation, the vesicular HSPGs can be released in the microenvironment together with its bound factors by the action of degrading enzymes, such as heparanase and MMPs (Yang et al., 2007, Purushothaman et al., 2008, Ramani et al., 2012). This further facilitates the distribution of signalling ligands, increasing the area where these molecules can promote their actions, possibly contributing to signalling at distance. Furthermore, these enzymes have also been found to be present on EVs (Hakulinen et al., 2008, Bandari et al., 2018, Sanderson et al., 2019) and can contribute to the remodelling of the ECM, promoting invasion and proliferation. For example, heparanase found in EV surface may release the HS-bound growth factors present in the ECM, increasing their availability within the tumour microenvironment and signalling at distance, as well as enhancing cell migration by removing structural barriers (Bandari et al., 2018). Both signalling at distance and ECM remodelling could be significant in setting up pre metastatic niches in distant organs.

Finally, vesicular-associated HSPGs have a great potential as cancer biomarkers for liquid biopsy diagnosis. Glypican-1 enriched in cancer cell-derived EVs has been reported as a potential biomarker for detection of early-stage pancreatic cancer (Melo et al., 2015), and syndecan-1 in vesicles, isolated from patient plasma, can discriminate between glioblastoma multiforme and low-grade glioma with strong evidence that these EVs provide directly from glioblastoma tumours (Indira Chandran et al., 2019).

Much is still unknown about the mechanisms by which EVs transfer their cargo and target specific cells, and the implications for EV tropism and biodistribution in cancer remain to be elucidated. Therefore, studies to explore and target the vesicular heparome would be essential to shed light on these mechanisms and uncover the roles of EV-associated HSPGs in cancer.

1.4 Hypothesis and aims

The ability of prostate cancer-derived EVs to induce a physiologically relevant form of fibroblast to myofibroblast differentiation was previously shown to be highly dependent on vesicular associated HSPGs.

In this thesis I hypothesise that HSPGs present on the surface of EVs are required for EV-mediated delivery of a repertoire of growth factors to fibroblasts. Together, these act in a coordinated manner to generate a myofibroblast phenotype that might influence the microenvironment, including immune cells, in a tumour-promoting fashion.

The study involves direct processing of isolated EVs to modify their HS-composition, as well as genetic manipulation of prostate cancer cells with the intention of generating EVs deficient in HSPG core proteins. Using such tools, the overarching aims of the study are as follows:

1. To explore the impact of HS/HSPG modification on the general biophysical properties of EVs, such as their structure, in order to establish whether HS/HSPGs are necessary for small EVs to physically exist.
2. To define the repertoire of growth factors and cytokines tethered to EVs via HS/HSPG dependent mechanisms, and to perform in silico exploration on the biological roles of such EV-related elements.
3. To establish the functional importance of HS/HSPG modifications on their fibroblast and myeloid cell modulating activities, in an effort to understand if HS/HSPG dependent constituents of EVs are required for such functional responses.

Chapter 2

Materials and Methods

2.1 Cell culture

2.1.1 *Monolayer cell culture*

The cell line DU145 (LGC Standards (ATCC), Middlesex, UK), obtained from a prostate cancer brain metastasis was used in this study as source of EVs. Cells were cultured in RPMI-1640 media (Gibco -Thermo Fisher Scientific, Gloucester, UK) supplemented with 100 µg/mL streptomycin (Sigma-Aldrich, Dorset, UK), 100 U/mL penicillin (Sigma-Aldrich, UK), 2 mM L-glutamine (Sigma-Aldrich). This will hereafter be called complete media. RPMI-1640 complete media is further supplemented with 10% fetal bovine serum (FBS) (Thermo Fisher Scientific) depleted of EVs, as needed. FBS was depleted of EVs to prevent any contamination of cell conditioned media (CCM) by bovine derived EVs. This was achieved by ultracentrifugation of FBS for 18 hours at 100,000 x g. This depleted serum is referred to as FBS^{EV-}. Primary human lung fibroblasts (AG02262; Corriell Institute for Medical Research, New Jersey, USA), of apparently healthy origin, were used in this study to model EV-stromal cell interactions typically occurring within the tumour microenvironment. Fibroblasts were supplied at passage six, and all experiments were performed on fibroblasts at passages of ten or less. Fibroblasts were cultured in DMEM/F-12 (1:1 v/v) complete media (Gibco - Thermo Fisher Scientific) and supplemented with 10% FBS^{EV-} (Thermo Fisher Scientific), as needed. THP-1 human immortalized monocytic-like cell line (ATCC, Virginia, USA) derived from acute monocytic leukaemia was used to study monocyte/macrophage function. Cells were cultured in RPMI-complete media, further supplemented with 10 mM HEPES solution (Sigma-Aldrich), 1 mM Sodium Pyruvate (Sigma-Aldrich) and 10% FBS^{EV-}, as needed. All cells were cultured in a 95% humidified incubator at 37°C and 5% CO₂. MycoAlert™ detection kits (Lonza, Lancashire, UK) were used to test for mycoplasma regularly. Cell lines culture conditions are summarized in **Table 1.1**.

Table 2.1. Cell line culture conditions

Cell line	Description	Media	Conditions	Source
DU145	Prostate cancer cells from brain metastasis	RPMI-1640	10% v/v FBSEV • 2 mM L-Glu* • 100 µg/mL strep** • 100 U/mL pen***	ATCC
AG02262	Primary lung fibroblasts	DMEM/F12	10% v/v FBSEV • 2 mM L-Glu* • 100 µg/mL strep** • 100 U/mL pen***	Corriel Institute for Medical Research
THP-1	Immortalized monocytic-like cell line	RPMI-1640	10% v/v FBSEV • 2 mM L-Glu* • 100 µg/mL strep** • 100 U/mL pen*** • 10 mM HEPES solution • 1 mM Sodium Pyruvate	ATCC

L-glutamine; *streptomycin; *penicillin

2.1.2 *shRNA-mediated knockdown of HSPGs within DU145 cells*

DU145 prostate cancer cells with altered heparan sulphate proteoglycan (HSPG) expression profiles were provided by Dr Jason Webber (Cardiff University). To selectively knockdown specific HSPGs, a lentiviral based delivery of short hairpin ribonucleic acids (shRNAs) (Mission, Sigma-Aldrich) was used as per the manufacturer's protocol. Briefly, wild type DU145 cells were seeded into 96-well flat-bottomed plates at 5,000 cells/well. The following day, cells were stably transduced with MISSION® shRNA lentiviral transduction particles, using a Multiplicity of Infection (MOI) of 20, in the presence of hexadimethrine bromide (8 µg/ml) (Sigma-Aldrich). After 24 hours, puromycin (1.25 µg/ml) (Sigma-Aldrich) was added at a dose predetermined to be cytotoxic to the cells, and media was changed daily. The specific HSPG targeted for knockdown were selected based on previous HSPG expression profiling of DU145-derived EVs, and these included syndecan-3, syndecan-4, glypican-1, glypican-6 and betaglycan. An irrelevant shRNA targeting non-mammalian RNA, termed non-mammalian (NM)-control (NMC), was used as a transduction control. Attenuation of specific HSPGs, relative to cells infected with the NMC shRNA, was assessed by quantitative reverse transcription polymerase chain reaction (RT-qPCR). To achieve maximal possible knockdown, 5 shRNA sequences per target were tested, and cell lines

showing best attenuation of target expression, based on downregulation of messenger ribonucleic acid (mRNA), were taken forward for further study. Transduced cells were cultured in the presence of puromycin until passage six, when deemed free of lentiviral particles, prior to experimental use. HSPG-modified DU145 cells were investigated to determine the impact of HSPG-knockdown on cell viability, proliferation, and EV secretion based on particle counting using nanoparticle tracking analysis (NTA). Cells were expanded in CELLline bioreactors flasks and modified EVs (HSPG deficient) were isolated from cell conditioned media as described below.

2.1.3 High-density bioreactor culture of DU145 cells

DU145 cells and HSPG-modified DU145 were maintained in CELLline bioreactors flasks (Sigma -Aldrich), to ensure high density cell cultures for production of large quantities of EVs for analysis. The bioreactor flask consists of two chambers separated by a 10 kDa semipermeable membrane, allowing movement of nutrients and O₂/CO₂, but not EVs, between the two chambers. 30x10⁶ cells were initially seeded into the inner chamber, in 15 mL of RPMI-1640 complete media, supplemented with 5% FBS^{EV-}. The outer chamber was filled with 500 mL of RPMI-1640 complete media with 5% regular (non-EV-depleted) FBS. The high volume of media maintains the large density of DU145 cells, whilst every week the secreted EVs were collected from the 15 mL cell supernatant from inner chamber. The use of these flasks generates cell conditioned media that has 8 to 10 times more concentrated EVs compared to standard 2D flasks (Clayton et al., 2008a). Every week, the CELLline bioreactor cell conditioned media was collected from the inner chamber of the flask and replaced with 15 mL of fresh complete media supplemented with FBS^{EV-}, whilst media in the outer chamber was replaced with 500 mL of fresh complete media supplemented with FBS. The collected cell conditioned media was pre-cleared of cells and cellular debris by sequentially centrifugation, twice at 400 x g for 6 minutes and then once at 2000 x g for 15 minutes. After this last centrifugation the media was filtered through a 0.22 µm Millex GP syringe filter unit (Merck, Dorset, UK). Filtered supernatants were stored at -80°C.

2.2 EV isolation

2.2.1 *Isolation of EV by ultracentrifugation on a sucrose cushion*

Pre-cleared and filtered supernatant, from DU145 and HSPG-deficient DU145 cells, obtained from bioreactor flasks, were thawed in a water bath at 37°C. EVs were then isolated by ultracentrifugation on a sucrose cushion. Ultracentrifuge tubes (Beckman Coulter, Wycombe, UK) were loaded with the collected supernatant, and underlain with 4 mL of 30% sucrose/D₂O solution (Sigma- Aldrich). Tubes were heat sealed and loaded into a SW32 swing rotor (Beckman Coulter). Centrifugation was performed at 100,000 x g (calculated based on the radius maximum rMax) for 90 minutes at 4°C. The sucrose, containing the EVs, was collected and diluted in excess PBS (Phosphate Buffered Saline) (Sigma-Aldrich), then loaded into new ultracentrifuge tubes. A fixed angle 70Ti rotor (Beckman Coulter) was used for a second centrifugation at 100,000 x g (r max) for 90 minutes, at 4°C, to pellet the EVs. EV pellets were resuspended in 500 µL PBS and aliquoted in 30 µL, 10 µL or 5 µL, to facilitate use and avoid freeze/thaw cycles. Samples were stored at -80°C, until required.

2.3 EV characterisation

2.3.1 *Bicinchoninic acid protein assay*

Unless otherwise stated, a MicroBCA Protein Assay kit (Thermo Fisher Scientific) was used to quantify EVs based on protein content. A standard curve was generated by 12-point serial dilution of bovine serum albumin (BSA) from 2000 µg/mL BSA to 0 µg/mL. EVs were diluted 1:8 by adding 10 µL of DU145 EVs to 70 µL of PBS, or 1:16 by adding 5 µL of heparinase III (HEPIII) treated or digestion control EVs to 75 µL PBS. After incubation with the kit components (Buffers “A”, “B” and “C”) to allow colour development (37°C; 35 minutes) absorbance was read at 562 nm using a PHERAstar FS Microplate plate reader (BMG Labtech, Aylesbury, UK). The absorbance values of known EV specimens were extrapolated from the standard curve.

2.3.2 Western blotting

2.3.2.1 Sample preparation

Cell lysates were prepared using radioimmunoprecipitation assay (RIPA) lysis buffer containing: 1x protease inhibitor cocktail, 200 mM phenylmethane sulfonyl fluoride (PMSF), 100 nM sodium orthovanadate and 1X lysis buffer (all from Santa Cruz Biotechnology, California, USA). Samples were centrifuged at 10,000 x g for 10 minutes at 4°C, to remove insoluble components, and split into aliquots stored at -80°C for future use. Cell lysates were directly compared to EV samples, normalised based on protein loading. Protein determination for the cell or EV lysates for western blots was performed by Bradford Assay (BioRad, Watford, UK).

2.3.2.2 Bradford assay

Bradford protein assay was performed according to manufacturer's protocol. An 8-point standard curve was established by serial dilution of BSA (2000 µg/mL). 5 µL of samples diluted in 15 µL of sterile H₂O (1:4 dilution). Bradford Protein Assay was diluted 1:3 in sterile reverse osmosis (RO) H₂O and 250 µL were mixed with 5 µL of diluted sample/BSA protein and incubated 5 minutes at room temperature (RT). Samples and standards are run in duplicate. Absorbance values were measured at 570 nm using a PHERAstar FS Microplate plate reader.

2.3.2.3 Polyacrylamide gel electrophoresis

20 µg of cell lysates or vesicles were boiled in lithium dodecyl sulphate (LDS) sample buffer (ThermoFisher Scientific), with or without 20mM dithiothreitol (DTT; Santa Cruz Biotechnology) reducing agent. Boiled samples and molecular weight markers (Magic Mark™ XP and SeeBlue® Plus 2 Precision Stain; (ThermoFisher Scientific) were loaded onto NuPAGE™ precast 4-12% Bis-Tris gradient gels (Life Technologies) and subjected to electrophoresis at a constant voltage of 180V for 45 minutes in 1x NuPAGE™ MOPS sodium dodecyl sulphate (SDS) running buffer (Life Technologies) using an Invitrogen™ PowerEase® 500 (Thermo Fisher Scientific) power supply.

2.3.2.4 Protein transfer and detection

A BioRad Mini Trans-Blot Electrophoretic Transfer cell (BioRad) and 25 mM Tris, 192mM glycine (both from Sigma-Aldrich) were used to transfer proteins into methanol activated polyvinylidene fluoride (PVDF) membranes (GE Life Sciences), and blots run for 90 minutes at a constant 80V, at ice cold conditions. Membranes were then blocked overnight at 4°C using 5% (w/v) non-fat powdered milk (Marvel, UK) in PBS containing 0.5% (w/v) Tween®20 (Sigma-Aldrich). The next day, membranes were incubated with primary antibodies (**Table 2.2**) typically at 1 µg/mL for 2 hours at RT. Membranes were subjected to 3x 5 minutes washes with 0.5% Tween®20 (Sigma-Aldrich) in PBS. Next, membranes were incubated with goat anti-mouse-horseradish peroxidase (HRP) conjugate (Santa Cruz Biotechnology) for 1 hour at RT. After another 3x 5 minutes washes, a chemiluminescent substrate (Li-Cor, Nebraska, USA) was used to detect the protein bands using a C-Digit blot scanner (Li-Cor).

Table 2.2. Primary antibodies. All primary antibodies used for Western Blot, ELISA-like immunofluorescence plate assays and functional assays.

Primary antibody	Isotype	Company	Catalogue number	Application	Concentration (µg/mL)
ALIX	IgG ₁	Santa Cruz	Sc-166952	Western blot	1
TSG101	IgG _{2a}	Santa Cruz	Sc-7964	Western blot	1
GAPDH	IgG ₁	Novus Biologicals	NBP1-47339	Western blot	1
GRP94	IgG _{2a}	Santa Cruz	Sc-32249	Western blot	1
CD9	IgG _{2b}	R&D Systems	MAB1880	Immunophenotyping assay for EV analysis	1
CD63	IgG ₁	Bio-Rad	MCA2142	Immunophenotyping assay for EV analysis	1
CD81	IgG ₁	Bio-Rad	MCA1847 EL	Immunophenotyping assay for EV analysis	1
αSMA	IgG ₁	Santa Cruz	Sc-32251	Fibroblast expression, fluorescence microscopy	2

2.3.3 Nanoparticle tracking analysis

NTA is a method that allows for the visualization and analysis of nanometre sized particles (< 1µm) in a solution. The light scattering of particles is used to track their movement under Brownian motion and then calculate particle size using the Stokes-Einstein equation:

$$Dt = \frac{TK_B}{3\pi\eta d}$$

Dt: Diffusion constant (product of diffusion coefficient D and time t)

T: Sample temperature

K_B: Boltzmann's constant

η: Solvent viscosity

d: Diameter of spherical particle

EV containing samples were analysed using the NanoSight™ NS300 platform (Malvern Instruments, UK). But before measuring samples, 100 nm and 80 nm latex beads (Malvern Instruments) are measured to confirm that NTA measurements are accurate. Samples (EVs/beads) were diluted in particle-free water (Fresenius Kabi, Cheshire, UK) and run at a constant flow rate (set to 50) using a NanoSight™ syringe pump (Malvern Instruments, Malvern, UK) for 5x30 second captures at 25°C. Videos were captured using a sCMOS camera system (OrcaFlash 2.8, Hamamatsu Photonics, Japan) and analysed using the NTA 3.1 software (version 3.1 build 3.1.54). Camera sensitivity was set at 14-16 and detection threshold at 1-3, to reveal the small particles. Concentration, size distribution, mean and mode sizes are calculated for the EVs by the software, and concentrations were further used with protein concentrations to calculate the particle:protein (p:p) ratios to gain a sense of EV purity (Webber and Clayton, 2013).

2.3.4 Microplate immunophenotyping assay for EV analysis

Vesicle concentrates were diluted in PBS and bound onto high protein binding ELISA strip 96-well plates (Greiner Bio-One, Stonehouse, UK), at a dose of 1 µg/well and incubated at 4°C overnight. Wells were washed 3 times with Wash Concentrate 29 (Kaivogen, Turku, Finland), to remove unbound particles, and blocked with 1% BSA/PBS (Reagent Diluent Concentrate 2 (10% BSA solution): R&D Systems, Biotechne,

Abingdon, UK) for 2 hours at RT, before being washed 3 times again. Primary antibodies were added at a concentration typically around 1 µg/mL (**Table 2.1**) for 2 hours at RT. Wash was repeated 3 times, and goat anti-mouse biotinylated antibody (Perkin Elmer, Buckinghamshire, UK) (diluted in 0.1% BSA/PBS), at 200 ng/mL working concentration, was used for 1 hour at RT, to detect the primary antibody. Wells were washed 3 times before adding 1:1000 europium-streptavidin conjugate (Perkin Elmer) in assay buffer (Kaivogen), for 45 minutes at RT. After 6 further washes, enhancement intensifier (Kaivogen) was added for 5 minutes at RT. Signal was detected by time-resolved fluorescence (TRF) on a PHERAstar FS Microplate (BMG Labtech, Aylesbury, UK), Optic module (337/615 A). Integration time 400 µs.

2.3.5 Cryo-electron microscopy

Cryo-EM was performed in collaboration with Professor Juan Falcon-Perez at the microscopy facility at CIC bioGUNE, Spain. EVs were adsorbed onto glow-discharged holey carbon grids (QUANTIFOIL, Großlobichau, Germany). Samples were vitrified by rapid immersion into liquid ethane using a VITROBOT (Maastricht Instruments BV, Maastricht, NL). Samples were then imaged at liquid nitrogen temperatures (approx. -195°C), using a JEM-2200FS/CR Transmission Electron Microscope (JEOL, Tokyo, Japan), equipped with a field emission gun and operated at an acceleration voltage of 200 kV. Image J software was used to analyse exported tiff images. The size of the different morphologic structures was determined, by measuring the diameter at the widest point of the structures, and averages plotted using GraphPad Prism 8.4.3 (471) software. Data was based on 329 total structures counted across 20 different fields of view.

2.4 Modification of EV-associated HSPGs

2.4.1 Heparinase III digestion of HS-GAG chains

Previous studies have demonstrated that EV-associated heparan sulphate can be digested using the enzyme heparinase III (HEPIII) (Christianson et al., 2013, Baietti et al., 2012). HEPIII digests the heparan sulphate side chains of the proteoglycan, releasing them from the core protein. It cleaves heparan sulphate by digestion between N-Acetyl-D-glucosamine and D-glucuronic acid. To determine the role of HS in EV-mediated growth factor delivery in this study, EVs were incubated with active HEPIII (Amsbio,

Chapter 2 – Materials and Methods

Abingdon, UK), at a concentration of 0.6 U/mL for 3 hours at 37°C in HEP111 buffer (0.1% Triton, 0.1 M NaCl, 1 mM CaCl₂, 50 mM 6-aminohexanoic acid and 50 mM HEPES, at pH 7). HEP111 digested EVs were compared to EVs treated with a matched concentration of heat-inactivated HEP111 (inactive HEP111; achieved by heating samples at 90°C for 10 minutes), or untreated (no enzyme) (EVs incubated in the absence of HEP111), for 3 hours at 37°C in HEP111 buffer. After incubation, with or without enzyme, vesicles were washed, by centrifugation at 100,000 x g for 90 minutes (Optima™ MAX-XP ultracentrifuge. TLA 110 rotor (Beckman Coulter)), to remove digested HS-GAG chains. Pelleted EVs were resuspended in PBS. Confirmation of digestion was achieved by microplate immunophenotyping assay (section 2.3.4) using HS (F58-10E4) primary antibody and western blot using ΔHS (F69-3G10) antibodies (**Table 2.3**).

Table 2.3 Antibodies used to confirm successful digestion of HS-GAG chains by HEP111.

Primary antibody	Clone	Isotype	Company	Catalogue number	Concentration (µg/mL)
HS	F58-10E4	IgM	Amsbio	370255-1	1
ΔHS	F69-3G10	IgM	Amsbio	370260-1	1

2.5 Proteomic analysis of HSPG-modified EVs

2.5.1 Olink Proximity Extension Assay

Vesicle concentrates from DU145 with HS-GAG and HSPG-core protein modifications were lysed in RIPA buffer prior to analysis by a multiplex proximity extension assay (PEA) (Olink Bioscience, Uppsala, Sweden), configured in an array form. Three predetermined Olink panels were used, as designed by the manufacturer: Cardiovascular III, Inflammation and Oncology II panels. These comprise 92-related protein biomarkers in each panel. This gives a broad coverage of potentially relevant factors, together with very high sensitivity due to a polymerase chain reaction (PCR)-like amplification of signal. Briefly, 1 µL of sample was incubated in the presence of a pair of antibodies, linked to unique oligonucleotides (Proseek probes). These probes pair-wise bind to the respective protein target present in the sample. When the two probes are in close proximity, they hybridize to each other. Only correct matched sequences hybridize. In

the presence of DNA polymerase, the hybridizing oligo-tails form an PCR target sequence. The resulting sequence was subsequently detected by and quantified using standard real time quantitative PCR (qPCR), using a microfluidics device (**Figure 2.1**).

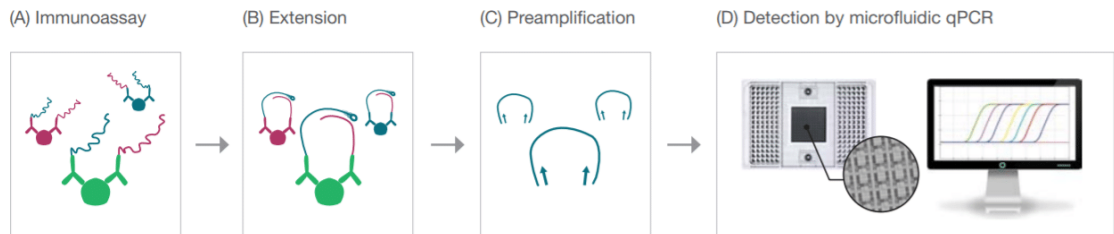


Figure 2.1. Overview of the PEA technology for Olink Target 96. (A) 92 Antibody pairs linked to unique DNA oligonucleotides (Proseek probes), bind target antigen in the sample. **(B)** Oligonucleotides in close proximity hybridize, and an amplicon is created in the presence of DNA polymerase. **(C)** This newly created piece of DNA barcode is amplified by real-time PCR. **(D)** The amount of each DNA barcode is quantified by microfluidic qPCR. (Image and information obtained from Olink website).

The generated fluorescent signal directly correlates with protein abundance. The pre-processed data was provided in the arbitrary unit Normalized Protein eXpression (NPX) on a log₂ scale, which was then linearized by using the formula 2^{NPX} . A high NPX value corresponds to a high protein concentration. However, the value is a relative quantification meaning that no comparison of absolute levels between different proteins can be made. The limit of detection (LOD) was calculated separately by Olink for each sample plate and assay, based on the background, estimated from negative controls included in each plate. Values below this limit were reported by Olink as < LOD.

2.5.2 Olink data analysis

Following receipt of data from Olink, any proteins that could not be detected within any of the experimental groups were removed prior to further analysis. For all other proteins, fold change in HEP111 treated EVs was calculated relative to inactivate HEP111 treated EVs. For HSPG-core protein modified EVs the comparison was made in relation to the NMC condition. Statistical significance of change in protein expression was assessed using the students t test, corrected for multiple testing using Benjamini-Hochberg adjustment. Selection of proteins for further analysis was achieved by taking fold-change and statistical significance into consideration.

2.5.3 Functional enrichment analysis

Functional enrichment analysis was performed for biological pathways using FunRich (<http://www.funrich.org>), FunRich is an open access, standalone functional enrichment and network analysis tool, that provides tools for functional enrichment analysis. Analysis was performed against the FunRich background database, which is exclusively human specific. This database comprises annotations collated from ExoCarta (Keerthikumar et al., 2016) and Vesiclepedia (Pathan et al., 2019), and therefore encapsulates identifications arising from proteomics analysis of EVs. Protein names were transformed into corresponding gene names, to be input in the software. For each list of genes introduced in FunRich, a biological pathway analysis was generated. Information about the number of genes in the input dataset which are available in the biological pathway database is provided, as well as the number of genes in the background of the pathway analysis. The output list was arranged in order of p-value (low to high), and statistically significant pathways ($p < 0.05$, using corrected values from the Benjamini-Hochberg method, for false discovery rate control during multiple comparisons) were then sorted into fold enrichment score (high to low).

2.5.4 Validation & quantification of selected protein targets by Enzyme-Linked Immunosorbent Assay (ELISA)

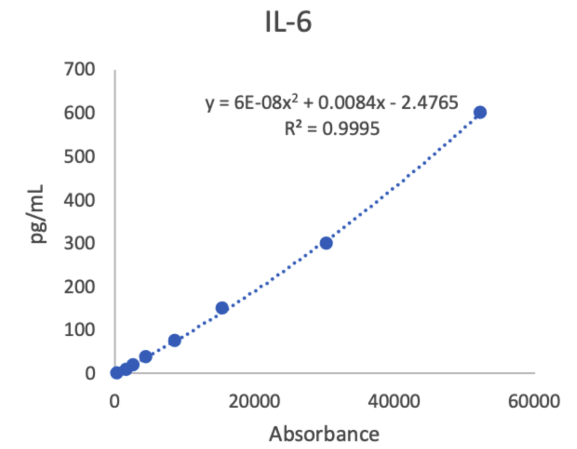
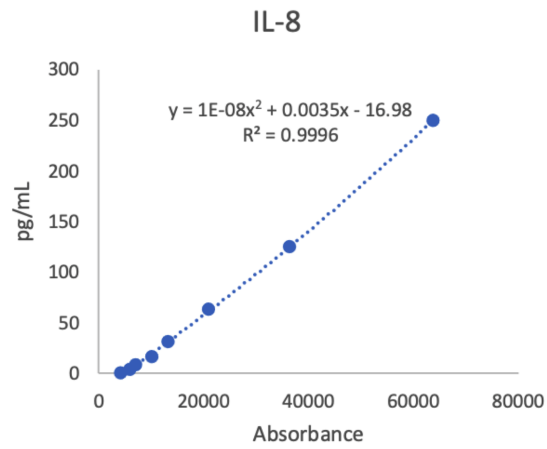
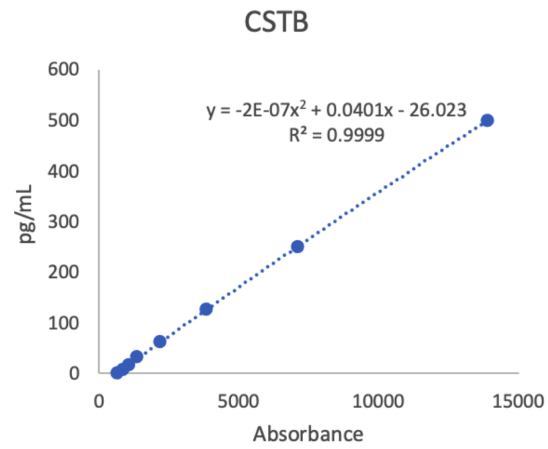
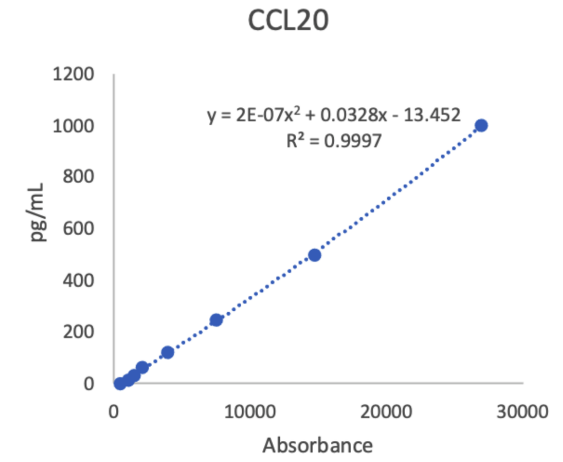
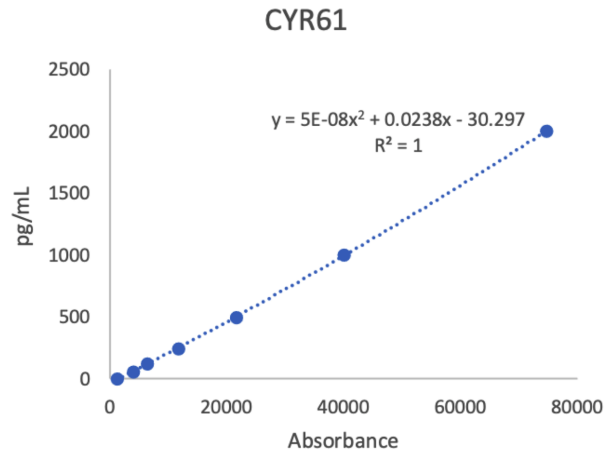
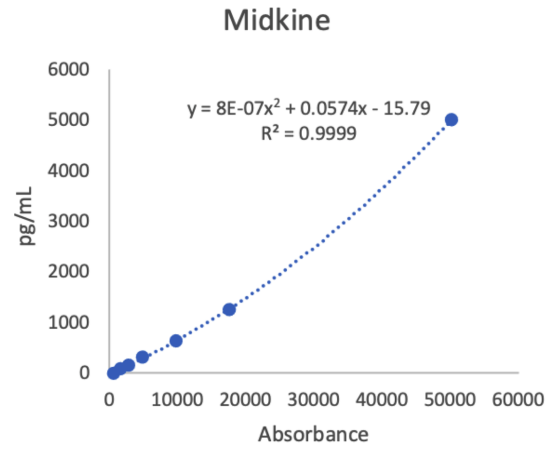
Proteins selected for validation were assayed using the DuoSet ELISA Development System (R&D Systems), with the exception of ABL1. The manufacturer's instructions were followed except for the detection of the colorimetric change in the substrate solution that was substituted for Europium-streptavidin conjugate. This change eliminated an enzyme-driven colorimetric reaction which is a kinetic process and has a very limited dynamic range. Instead, the readout was thus replaced for a non-kinetic endpoint with high dynamic range and superior sensitivity, measuring TRF (as in section 2.3.4).

High protein binding ELISA strip 96-well plates were coated with the required capture antibody, diluted as recommended by the manufacturer. Diluted capture antibodies (100 μL per well) were added, and plates incubated overnight at RT. Wells were washed 3 times with wash buffer (Kaivogen) to remove unbound antibody. Wells were blocked by adding 300 μL of reagent diluent (1%BSA in PBS; R&D Systems) and incubated at RT for 1 hour. Wells were washed 3 times, prior to the addition of 100 μL of sample or standard (serial dilution to create an 8-point standard curve) and subsequent incubation

for 2 hours at RT. Wells were washed and detection antibody (100 μ L/well), diluted as recommended by the manufacturer, was added before incubation for 2 hours at RT. Wells were washed 3 times, before detection using europium-streptavidin conjugate was carried as stated in previous section 2.3.4.

Quantification of ABL1 was assayed using the ABL1 ELISA Kit (Human) (OKCA01575) from Aviva Systems Biology (USA). This kit provided a 96-well-plate pre-coated with an antibody specific for ABL1. Manufactures instructions were followed. Samples and standards were incubated in the pre-coated plate and washed, and after, wells were incubated with a biotinylated detector antibody specific for ABL1. After wash, Avidin-Peroxidase Conjugate was added, incubated and unbound conjugate is washed away. MB substrate is added and catalysed by HRP, turning blue and indicating the presence of the protein. Acidic stop solution is added to stop the reaction and absorbance is read at 450 nm.

For all ELISAs, values obtained from absorbance readings were extrapolated from the standard curve to calculate the analyte concentration in each sample, using a 2nd order polynomial equation. If the analyte level was below the lowest point on the standard curve, the analyte was considered undetectable, and a value of 0 pg/mL was assigned. In a similar way, if the value detected for the protein was above the highest point in the standard curve, the highest concentration value was assigned to that sample. In such an event, this was made clear by stating that the recorded value was greater than the highest standard and the true value was therefore ambiguous. Due to scarcity of EV material, it was not always possible to perform extensive dilution series to fit the specimen to the standard curve, hence occasional issues of this nature were encountered. **Figure 2.2** shows a representative example of standard curves obtained for each of the assayed proteins. The equation of the curve and R^2 , to demonstrate curve fit, are both shown



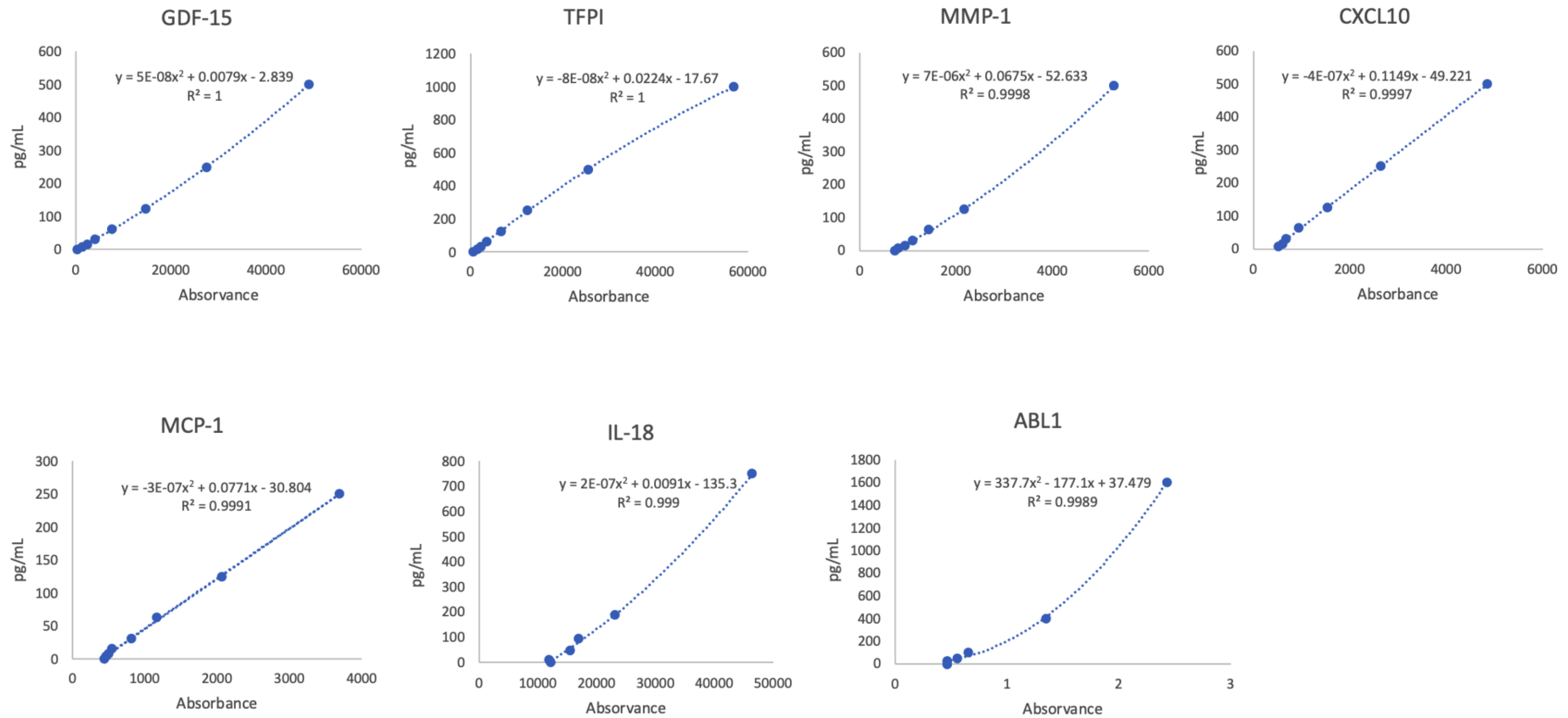


Figure 2.2. Representative standard curves for each of the ELISAs used to validate and quantify proteins identified from the Olink analysis, on the EV surface. Standard curves generated by graphing the mean absorbance of each sample (x axis) vs. the standard concentration (y-axis) of at least 5 points obtained from a serial dilution. The 2nd order polynomial equation and R² values obtained for each curve are shown as well. Absorbance was read at 337/615, except for ABL1, which was read at 450 nm.

2.6 Assessment of EV function

2.6.1 *Fibroblast differentiation*

Primary human fibroblasts (AG02262) were seeded in a 48 well glass-bottomed plates (Greiner Bio-One, Germany) at 25,000 cells/well in DMEM/F12 complete media as described in section 2.1.1. Once cells were around 80% confluent, they were grown for 48 hours in serum-free media to allow depletion of any remainder growth factors in the media, that could influence fibroblasts capacity to express α SMA. Fibroblasts were incubated with either 1.5 ng/mL of sTGF β , 200 μ g/mL of DU145 native EVs or EVs previously treated with active HEP13, inactive HEP13 or no enzyme, in DMEM/F12 without FBSEV⁻, for a further 72 hours. Cells grown just in media were used as control. Following treatment, cells were fixed in ice-cold acetone/methanol (1:1) for 5 minutes. Acetone/methanol was then removed, and wells left to dry for 30 minutes at RT. Wells are hydrated with PBS, washed and blocked with 1% BSA/Hanks's balanced salt solution (HBSS; Sigma), for 1 hour at room temperature, before washing and incubation with primary antibody (anti- α SMA; Santa Cruz) (**Table 2.2**) in 0.1% BSA/HBSS for 2 hours at RT. Cells were then incubated with Alexa488 conjugated goat anti-mouse secondary antibody (Thermo Fisher Scientific) at 10 μ g/mL in 0.1% BSA/HBSS, for 1 hour in the dark, at RT. For nuclei staining, cells were incubated with 4',6-diamidino-2-phenylindole (DAPI), from a 14.3 mM stock, diluted 1:50,000 times in PBS (0.3 μ M,) for 5 minutes in the dark at RT. Cells were visualised using Alexa488 and DAPI filters on the Axio Observer Z1 with a ZEISS Plan Aplanachromat 20x/0.8 ∞ 0,17 lens. Cells were automatically counted using MATLAB software, with a pre-set threshold defined for α SMA positivity.

2.6.2 *Uptake of EVs*

2.6.2.1 *Fluorescent labelling*

EV samples (30 μ L aliquots) were incubated with Alexa Fluor 594 C₅ maleimide dye (working concentration 200 μ g/mL; Thermo Fisher Scientific), made up to 50 μ L with PBS, on a shaker for 1 hour in the dark at RT. Exosome Spin Columns MW3000 (Thermo Fisher Scientific) were prepared according to manufacturer's instructions. To rehydrate the powder in the columns, 650 μ L PBS were added, for 15 minutes at RT. Columns need to be gently tapped to ensure no bubbles of air are formed in the gel during this

time. Excess PBS was removed by centrifugation of the column at 750 x g for 2 minutes. Fluorescently labelled EVs were added to the top of the gel in the column. Columns were further centrifuged for 3 minutes at 750 x g to separate the labelled EVs from the unbound Alexa Fluor 594 maleimide dye. The unbound dye will be trapped in the column. The collected solution will have the labelled EVs. Alexa Fluor 594 maleimide dye not incubated with EVs but centrifuged through the column has been used as a control for the amount of non-captured free dye and efficiency of this column capture process (Roberts-Dalton et al., 2017). A Nanodrop™ 2000 Spectrometer (Thermo Scientific, UK) was used to determine the concentration of EVs after the labelling process, because it only requires 2 µL of sample. This concentration was used to set EV doses when treating fibroblasts.

2.6.2.2 Detection of cellular uptake of fluorescent EVs by fluorescent microscopy

Fibroblasts were seeded at 10,000 cells per well in 96 glass-bottomed plates (175 µm thick glass) (Greiner Bio-One) and cultured until 80% confluent. Cells are then starved for 24 hours and incubated with 25 µg/mL of fluorescently labelled EVs in DMEM/F12 complete media in the absence of added FBS, for 1 hour at 37°C. Previous studies from the group have indicated excellent uptake can be visualised from 30 minutes to 4 hours or longer. At 1 hour there is unambiguous levels of cell entry under these conditions (personal communication Prof Aled Clayton). Cells were then washed with PBS and fixed with 4% PFA for 20 minutes at RT. After a wash, cells were permeabilized with 0.1% triton X-100 for 5 minutes at RT. Cells were washed and stained with Actin Green (AlexaFluor™ 488 phalloidin: Thermo Fisher Scientific), prepared with 1 drop/mL PBS, for 30 minutes. Actin Green was removed and to reveal nuclei, cells were stained with NucBlue™ Fixed Cell ReadyProbes™ Reagent (DAPI; Thermo Fisher Scientific), prepared at 2 drops/mL PBS. Plates were immediately imaged without removal of the DAPI stain. Fibroblasts containing labelled EVs are visualised on the Axio Observer Z1 microscope with a ZEISS Plan Apochromat 63x/ 1.4 Oil lens, using Alexa488/594 and DAPI filters.

2.6.2.3 Detection of cellular uptake of fluorescent EVs by flow cytometry

Fibroblasts were seeded in 48 well cell culture plates (Greiner Bio-One) at 20,000 cells/well and cultured until 80% confluent. Cells were growth arrested for 24 hours in serum free media, and then treated with 25 µg/mL of labelled EVs in DMEM/F12

Chapter 2 – Materials and Methods

complete media 0% FBS, for 1 hour at 37°C. Following treatment, cells were washed with PBS and stripped from the plate surface with 150 µL/well of trypsin at 37°C until detached. The cell suspension was added to flow cytometry tubes (StemCell Technologies, Cambridge, UK), and then 300 µL PBS were used to remove remaining cells in each well and added to flow cytometry tubes. The volume was made up to 500 µL. Cells were pelleted by centrifugation at 400 x g for 6 minutes. Pelleted cells were resuspended in 100 µL of PBS per tube and put on ice. A Fluorescence-Activated Cell Sorting (FACS) cytometer (BD Biosciences, Berkshire, UK) was calibrated using cytometry signalling and tracking (CST) beads (BD Biosciences). Cell populations were firstly gated based on their forward scatter (FSC) area (-A) and height (-H) assessment to exclude debris and doublets (**Figure 2.3 A**). Doublet cells occupy double the area to height and appear off the diagonal of the gated singlet cell population and were excluded from analysis. Next, the population of interest was selected based on their granularity, under x-axis set to FSC-A and y-axis set to side scatter (SSC)-A (**Figure 2.3 B**). These cells were then analysed considering their fluorescence intensities following uptake of Alexa Fluor 594 C5 maleimide-labelled EVs. Examples of a positive (**Figure 2.3 C**) and negative (**Figure 2.3 D**) cells population are shown. Data were analysed using FACS-DIVA software v8.0.1 (BD Biosciences). Mean fluorescent intensity (MFI) was used to represent the general fluorescent levels in the population.

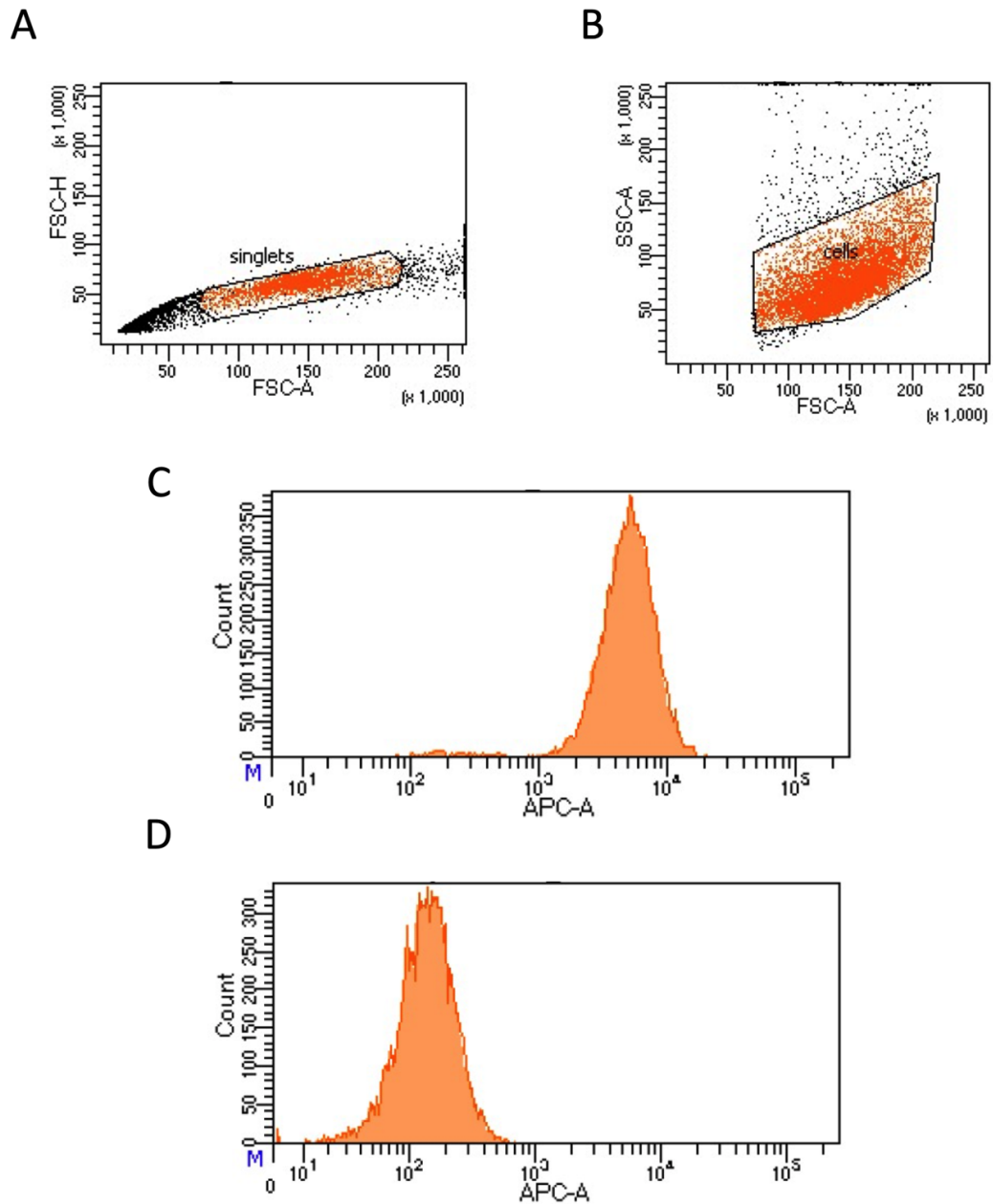


Figure 2.3. Gating strategy used for analysis of uptake of fluorescent EVs by fluorescent microscopy. Representative gating strategy and associated dot plots for the flow cytometry analysis of uptake of Alexa Fluor 594 C5 maleimide-labelled EVs. **(A)** Doublet cells were excluded with the x-axis set to FSC area (-A), and the y-axis set to FSC height (-H). **(B)** Single cells gated based on size and granularity with the x-axis to FSC-A, and the y-axis to SSC-A. **(C, D, E)** Histograms show cell count based on negative (D), positive (D) or positive-high (E) incorporation of fluorescent EVs detected by allophycocyanin (APC) laser lines at 594 and 633 nm.

2.6.3 Assessment of EV-mediated signalling and cytokine production in recipient fibroblasts

2.6.3.1 Proteome Profiler Human Phospho-Kinase Array Kit (R&D Systems)

Fibroblasts were seeded in 24 well cell culture plates at 50,000 cells/well and serum starved for 48 hours. Cells were then incubated with 200 µg/mL of EVs treated with active HEP III or no enzyme, in DMEM/F12 (without FBS) for 2 hours. Following treatment cells were lysed with RIPA lysis buffer and protein quantified by Bradford assay as previously described in section 2.3.2.2. The proteome profiler was performed following manufacture instructions, with the exception of the use of Chemi Reagent Mix that was substituted by chemiluminescent substrate Li-Cor, prior to detection of phosphorylated proteins using the C-Digit blot scanner (Li-Cor). ImageJ software was used to assess the densitometry of the dots on the membranes.

2.6.3.2 Proteome Profiler Human XL Cytokine Array (R&D Systems)

Fibroblasts were seeded in 24 well cell culture plates at 50,000 cells/well and serum starved for 48 hours. Cells were then incubated with 200 µg/mL of EVs treated with active HEP III or no enzyme, in DMEM/F12 (without FBS) for 72 hours. Stimulated cells were incubated with Golgi-Stop and Golgi-Plug (BD Biosciences) for 18 hours previous to lysis, to prevent cytokine secretion. Following treatment cells were lysed with RIPA lysis buffer and protein quantified by Bradford assay as previously described in section 2.3.2.2. The protocol was performed following manufacture instructions, with the exception of the use of Chemi Reagent Mix, that was substituted by chemiluminescent substrate Li-Cor and detected by a C-Digit blot scanner (Li-Cor). ImageJ was used to assess the densitometry of the dots on the membranes.

2.6.3.3 Measuring cytokine production in recipient fibroblasts

To investigate if the cytokines identified from experiments in sections 2.6.3.1 and 2.6.3.2, were secreted by fibroblasts stimulated with HS-modified EVs at 72 hours, DuoSet ELISA Development System (R&D Systems) were used as described in section 2.5.4 to assay IL-1 α , IL-17, FGF-basic, VEGF, and HGF. TRF values were extrapolated from the standard curve to calculate the protein concentration in each sample, using a 2nd order polynomial equation. As before, if the protein level was below the lowest point on the standard curve, the analyte was considered undetectable, and a value of 0 pg/mL was assigned. Total cell conditioned media was used whenever possible. Otherwise, the dilution factor was included in the calculation to obtain protein concentration. **Figure 2.4** shows a representative example of standard curve obtained for each of the assayed proteins. Equations and R² are shown.

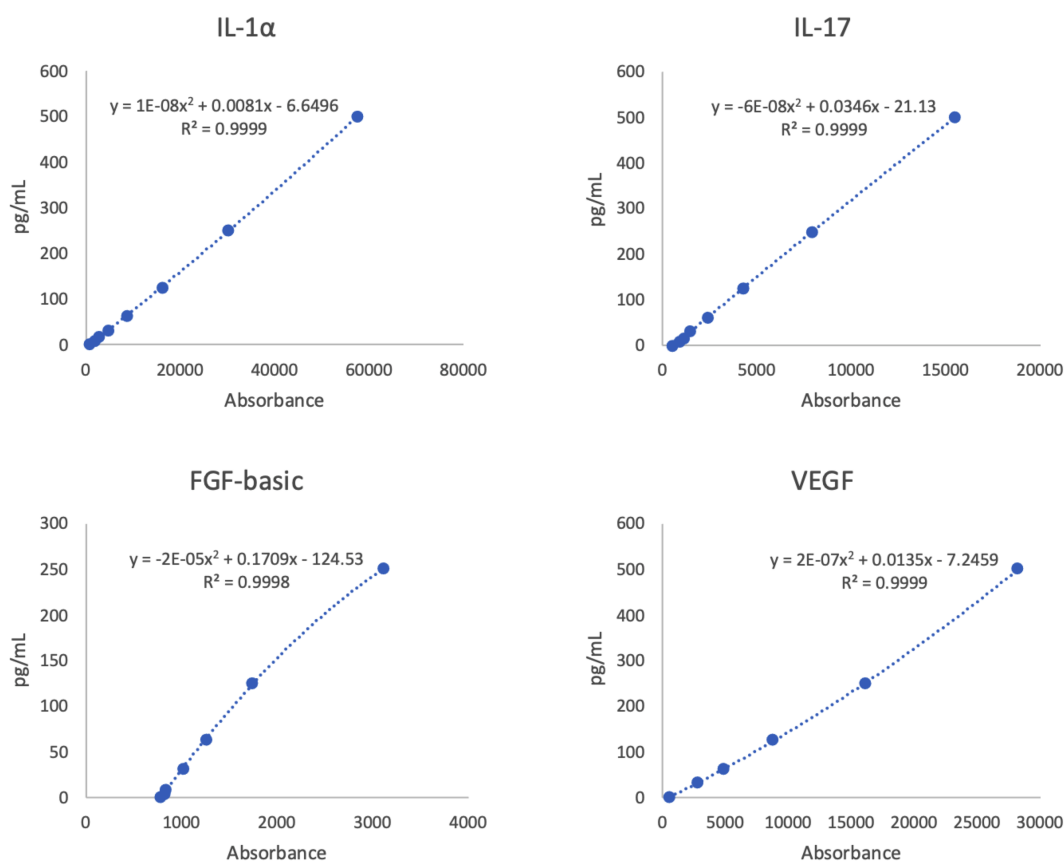


Figure 2.4. Representative standard curves for each of the ELISAs used to assess cytokine production in recipient fibroblasts. Standard curves generated by graphing the mean absorbance of each sample (x axis) vs. the standard concentration (y-axis) of at least 5 points obtained from a serial dilution. The 2nd order polynomial equation and R² values obtained for each curve are shown as well. Absorbance read at 337/615.

2.6.4 Monocytic differentiation, and macrophage polarisation and activation studies

2.6.4.1 THP-1 differentiation into macrophage-like cells

For macrophage differentiation of THP-1 cells towards macrophage-like cells, THP-1 were treated with 80nM of Phorbol of 12-myristate 13-acetate (PMA; Merck) for 48 hours. PMA treatment was removed and replaced with fresh RPMI1640 complete media 10% FBS^{EV-} for a further 72 hours to allow for maturation of differentiated cells. Differentiation was assessed by flow cytometry (section 2.6.5). Wells were incubated with 100 µL PBS containing 2% FBS and 1 mM EDTA for 5 minutes (37°C), before being gently pipetted to detach adherent macrophages from the plate. Detached cells were added to the corresponding flow cytometry tubes.

2.6.4.2 THP-1 stimulation with fibroblast derived cell conditioned medium

THP-1 cells were seeded in 48 well-plate at 100,000 cells/well and co-incubated with 50% cell conditioned media collected from fibroblast differentiation assays (section 2.6.1), and 50% RPMI-complete media, 10% FBS^{EV-}, during 72 hours prior to flow cytometry. To establish myeloid cell controls, THP-1 were incubated with classical M1 and M2 promoting cytokines. M1 control included incubating cells with interferon gamma (IFN γ) (20 ng/mL, PBL Assay Science, New Jersey, UK) and lipopolysaccharides (LPS) (10 pg/mL, Sigma Aldrich), and M2 was established through 72 hours incubation with IL-4 (20 ng/mL, PeproTech, New Jersey, USA) IL-13 (PeproTech, 20 ng/mL), IL-10 (10 ng/mL, R&D Systems). As THP-1 are grown in RPMI-complete media and fibroblasts in DMEM/F12 complete media, to mimic these growing conditions, wells were established were 50% of RPMI and 50% DMEM/F12 complete media with 10% FBS^{EV-}, were added to cells. When harvesting, suspension myeloid cells were transferred to sterile flow cytometry tubes. To detach adherent differentiated cells from the plate, wells were incubated with 200 µL PBS containing 2% FBS and 1 mM EDTA for 10 minutes (37°C), before being gently pipetted to detach cells. Detached cells were added to the corresponding flow cytometry tubes. Differentiation (CD14⁺, CD68⁺) and polarisation (CD80⁺, CD86⁺, CD163⁺, CD206⁺) was assessed by flow cytometry (section 2.6.5).

2.6.4.3 THP-1 stimulation with EVs treated with active HEP111, heat-inactivated HEP111 or no enzyme

THP-1 cells were seeded in 48 well-plates at 100,000 cells/well and were treated with either 1.5 ng/mL of sTGF β or 200 μ g/mL of EVs previously treated with active HEP111, inactive HEP111 or no enzyme, in RPMI complete media supplemented with 5% FBS^{EV-} for 72 hours. Myeloid controls were established as in section 2.6.4.2 as well as harvesting. Differentiation and polarisation were assessed by flow cytometry (section 2.6.5).

2.6.4.4 Macrophage stimulation with fibroblast derived cell conditioned medium

THP-1 cells were seeded in 48 well-plates at a concentration of 400,000 cells/ well and treated with 80 nM of PMA, for 48 hours, as described in section 2.6.4.1. After the 72 hours to allow for maturation of polarized cells, media was removed from wells and cells were co-cultured with 50% cell conditioned media collected from fibroblasts differentiation assay (section 2.6.1) and 50% RPMI complete media, 10% FBS^{EV-}, during 72 hours prior to flow cytometry. Controls were established as in section 2.6.4.2, as well as harvesting. Differentiation and polarisation were assessed by flow cytometry (section 2.6.5).

2.6.4.5 Macrophage stimulation with EVs treated with active HEP111, heat-inactivated HEP111 or no enzyme

THP-1 cells were seeded in 48-well plates at a concentration of 400,000 cells/ well and treated with 80nM of PMA, for 48 hours, as described in section 2.6.4.1. After the 72 hours to allow for maturation of polarized cells, media was removed from wells and cells were treated with either 200 μ g/mL active HEP111, heat inactivated HEP111, no enzyme (untreated) vesicles or sTGF- β 1 (1.5 ng/mL) in RPMI164, 5% FBS^{EV-}, for 72 hours. Myeloid controls were established as in section 2.6.4.2, as well as harvesting. Differentiation and polarisation were assessed by flow cytometry (section 2.6.5).

2.6.5 Flow cytometry analysis

FACSVerse cytometer (BD Biosciences), with 3-lasers, and up to 8-colour configuration was used for flow cytometry analysis. The instrument runs the FACSuite v1.2.1 software (BD Biosciences) and is calibrated using cytometry CST beads (BD Biosciences). Data were analysed using FACS-DIVA software v8.0.1 (BD Biosciences).

2.6.5.1 Labelling of cell surface antigens for surface and intracellular staining

After cell harvesting, as previously indicated, cells were washed with PBS, by adding 1 mL of PBS to each tube and centrifuging samples at 600 x g for 5 minutes. The supernatant was discarded, and cells were blocked with 2% mouse serum (Sigma Aldrich) in PBS, in the residual tube volume, for 15 minutes at RT. This was done to prevent unspecific binding to Fc receptors. All staining was performed in the dark to preserve fluorescence and prevent photobleaching. Cells were stained with the indicated volumes of fluorophore-conjugated primary antibodies (**Table 2.4**) in the residual blocking volume, for 30 minutes, at 4°C. Cells were then washed with 1 mL PBS, to remove unbound antibodies/dye, and supernatant discarded. Cells were then prepared for intracellular staining, being resuspended by gently pipetting 100 µL of IC fixation buffer (eBioscience, Thermo Fisher Scientific). Cells were left to incubate for 30 minutes at RT. After, cells underwent 2x 1 mL washes with 1x permeabilization buffer (10x; eBioscience, Thermo Fisher Scientific) supernatant from the last wash is discarded and 2% mouse serum is added to residual volume for 15 minutes at RT, in the dark. Intracellular antibody is added to the cells for 30 minutes at RT, and afterwards washed with 1 mL PBS. Cells are resuspended in 100 µL of fix buffer (prepared from 1:4 dilution of IC fixation buffer), for analysis. In all experiments, unstained cells were used as a negative control, and fluorescence minus one (FMO) controls were used to help gating strategy.

Table 2.4 Flow cytometry antibodies and stains Antibodies and fluorescent viability dye used in flow cytometry experiments. Cells were stained with antibodies according to surface and intracellular staining protocols.

Antigen/ Antibody	Fluorophore	Clone	Supplier	Surface/ Intracellular stain	Volume per tube (μ L)
Primary antibodies					
CD14	PE-Cy7	63D3	BioLegend	Surface	1.5
CD11b	BV510	ICRF44	Biolegend	Surface	1.5
CD86	PE	IT2.2	BioLegend	Surface	1.5
CD80	PerCP-Cy5	2D10	BioLegend	Surface	1.5
CD163	APC	eBioGH1/61	Thermo Fisher Scientific	Surface	1.5
CD206	BV421	19.2	BD Biosciences	Surface	1.5
CD68	FITC	Y1/82A	BioLegend	Intracellular	1.5
Fluorescent viability dye					
Fixable viability dye	eFluor™ 780 (~APC-Cy7)	NA	Thermo Fisher Scientific	Performed at same time as surface staining	0.5

2.6.5.2 General gating strategy

The voltages for the FSC and SSC were adjusted based on cell size and granularity, respectively. Prior to analysis, the following gating strategy was used to include or exclude cells from analysis (**Figure 2.5**). First, cell debris were excluded based on their granularity following x axis set to FSC-A and y axis set to SSC-A (**Figure 2.5 A**). When analysing differentiated populations, this gate helps to select the appropriate cell population for analysis. Because some conditions would shift and change the population, this gate was established at the start, to set the population of interest and the consequent analysis. Next, doublets were excluded based on FSC area (-A) and height (-H). Doublet cells occupy double the area to the height, so these larger cells appearing off the diagonal of the gated singlet cell population and were excluded from analysis (**Figure 2.5 B**). Finally, cells were stained with Fixable viability dye eFluor™ 780 (eBioscience,

Chapter 2 – Materials and Methods

Thermo Fisher Scientific) to eliminate the dead (positive stained) cells (**Figure 2.5 C**). The viability dye is an impermeable stain, which works by binding to intracellular amines in dead cells. Dead cells have their membrane integrity compromised, which allows for the intracellular action of this dye. Cells present in the final live cell inclusion gates were then analysed or used as further parent gate for other markers of interest. Data were analysed using FACS-DIVA software v8.0.1 (BD Biosciences). Marker expression was analysed considering percentage/proportion of cells expressing the marker within the parent population.

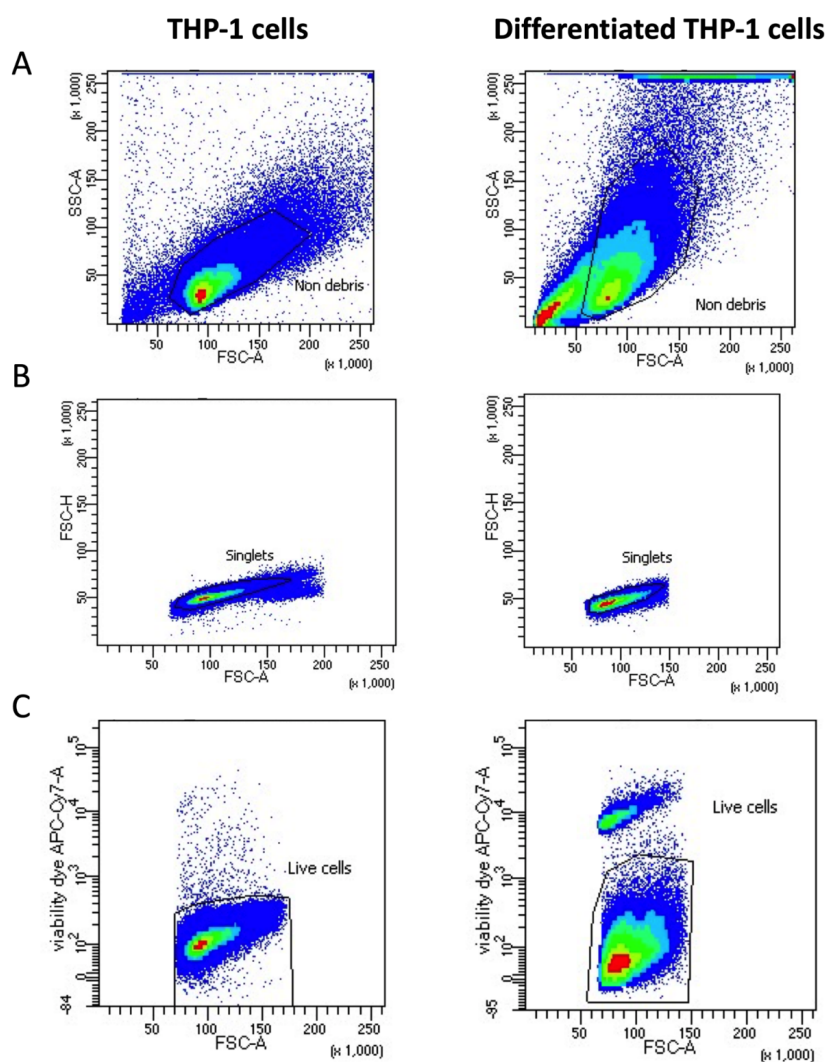


Figure 2.5. Gating strategy used for analysis of monocytic differentiation and macrophage activation studies. Representative gating strategy for the flow cytometry analysis of THP-1 and differentiated THP-1 cells. **(A)** Cell debris were excluded based on size and granularity with the x-axis to FSC-A, and the y-axis to SSC-A. **(B)** Single cells gated with the x-axis set to FSC area (-A), and the y-axis set to FSC height (-H). **(C)** Fixable viability dye eFluor™ 780 (y-axis) was used to exclude dead cells, which would contribute to non-specific positive staining.

2.6.6 Measuring cytokine production from THP-1 and macrophage stimulated cells

To investigate if the experimental conditions described in sections 2.6.4.2, 2.6.4.3, 2.6.4.4 and 2.6.4.5, were able to promote differentiation and polarization of myeloid cells, cytokines typically associated with M1- or M2-like macrophages were assayed in cell conditioned media obtained after 72 hours. DuoSet ELISA Development System (R&D Systems) were used as described in section 2.5.4 to assay IL-1 β , TNF- α , VEGF and TGF- β 1 (Sawa-Wejksza et al., 2018).

Latent TGF- β 1 requires activation to the immunoreactive form that is detectable by the TGF- β 1 DuoSet ELISA kit. Cell conditioned media obtained from the experimental conditions described before were acid activated using 20 μ L of 1M hydrochloric acid (HCL), incubated for 10 minutes at RT. The acidified samples were neutralised by adding 20 μ L of 1.2N sodium hydroxide (NaOH)/0.5M HEPES. Once neutralised, 100 μ L of sample were added to the wells and incubated for 2 hours at RT. Wells were washed and detection antibody (100 μ L/well) added, and remaining protocol followed as in described in 2.5.4. TRF values were extrapolated from the standard curve to calculate the protein concentration in each sample. Total cell conditioned media was used whenever possible. Otherwise, the dilution factor was included in the calculation to obtain protein concentration. **Figure 2.7** shows a representative example of standard curve obtained for each of the assayed proteins. Equation and R² are shown to demonstrate curve fit quality.

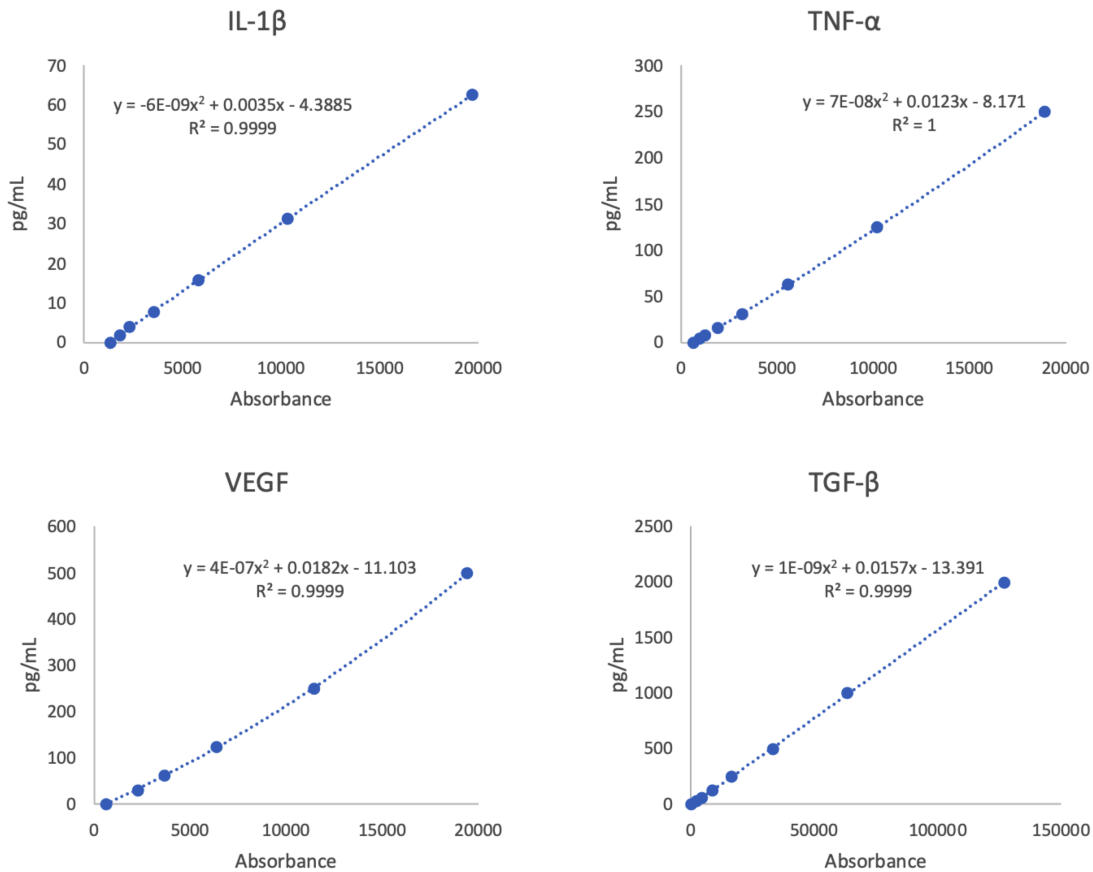


Figure 2.6. Representative standard curves for each of the ELISAs used to assess cytokine production from THP-1 and macrophage stimulated cells. Standard curves generated by graphing the mean absorbance of each sample (x-axis) vs. the standard concentration (y-axis) of at least 5 points obtained from a serial dilution. The 2nd order polynomial equation and R² values obtained for each curve are shown as well. Absorbance read at 337/615.

2.7 Statistical analysis

Statistical analyses were performed using GraphPad Prism 9 Software v9.1.0 (GraphPad, San Diego, USA). Experiments with two experimental groups were evaluated using students t-test. For experiments with more than two experimental groups, statistical analysis was performed using One-Way ANOVA with a Tukey post-hoc test. P values less than 0.05 were considered statistically significant (*p<0.05, **p<0.01, ***p<0.001, ****p<0.0001). Graphs depict mean \pm SD, from a representative experiment of at least three similar experiments, unless stated otherwise.

Chapter 3

Characterisation of prostate cancer cell-derived extracellular vesicles

3.1 Introduction

The tumour microenvironment exhibits a complex biology, consisting not only of cancer cells, but several other elements such as extracellular matrix, blood vessels, fibroblasts and immune cells. The interactions between the different components of the tumour microenvironment are crucial to create the conditions required for disease progression (Balkwill et al., 2012). It is known that intercellular communication can be mediated through cell-cell contact or secretion of soluble factors, and most recently, the role of EVs has been put into play. These vesicles, released from various cell types, have attracted considerable attention and have been implicated in the functional delivery of proteins and nucleic acids to recipient cells (Raposo and Stoorvogel, 2013, Maia et al., 2018, Lo Cicero et al., 2015). Examples have been described of the capacity of EVs to carry both mRNA and miRNA, that modulate the recipient transcriptome (Valadi et al., 2007) , as well as the delivery of growth factors and cytokines including TGF- β 1, that has previously been shown to play a role in modulation of the tumour microenvironment (Webber et al., 2010). This ability of EVs to facilitate message exchange between cells, delivering a complex assortment of molecules in concert, places these EVs as important and highly sophisticated mediators of cell-cell communication, but their full role in disease remains unclear.

When studying EVs, in terms of their molecular composition and functional effects, it is fundamentally important to perform adequate purification of vesicles from the complex assortment of factors present within cell supernatant or biological fluids. Such source material is complex and will contain a diverse repertoire of secreted factors as well as multiple vesicle sub-types of varied origins. Purification is distinct from concentration, and defining what an acceptably pure EV isolate is, continues to be a much-debated topic in this research field. Although general guidelines from ISEV are available (Théry et al., 2018, Lotvall et al., 2014), these rightly evolve as the field matures and may not always be successful in clarifying certain controversies. The MISEV 2018 guidelines provide guidance on experimental methods and minimal information when reporting EV studies. It recommends the demonstration of structural morphology, size, and expression of typical EV-related proteins to clearly define the population in study. Topology is also an important recommendation as part of vesicle characterisation, with indications to identify where in or on a vesicle the target of interest is located, as this can be important in what concerns to vesicle function. As it remains difficult to truly distinguish EV sub-types, or even if an element is genuinely EV-related, the importance of assessing

Chapter 3 - Results

contaminants, and its contribution to ascribing a specific function to EVs, is also raised. MISEV 2018 recommends the functional analysis of the “non-EV” fraction to confirm and attribute a specific function to EVs or a particular sub-type of EVs. Nonetheless, when considering elements that might be rather loosely tethered to the EVs, for example through HSPG-mediated interactions, these questions can be challenging to fully address. Considering EVs are dynamic and change with their environment, as well as taking into account the limited knowledge we have in what relates to their machinery of biogenesis, cargo loading and release, the MISEV guidelines might not always hold true.

Cell surface HSPGs have been emerging as important contributors to EV-mediated cell-to-cell signalling as well as their intracellular biogenesis. Internalisation of EVs was shown to be partly mediated by HSPGs such as syndecans and glypicans at the recipient cell surface (Christianson et al., 2013), as well as through the interaction between cell surface and EV-associated HSPGs, aided by a fibronectin-bridge (Purushothaman et al., 2016). Moreover, the syndecan-syntenin-ALIX complex, formed upon internalisation of syndecans from the cell surface, has been described as an important mechanism for EV cargo selection and EV biogenesis (Baietti et al., 2012). It is therefore conceivable that HSPGs will remain at the surface of secreted EV and play multiple roles in EV activities. One such aspect includes the known ability for HSPGs to interact with multiple proteins through their HS-GAG chains and act as high capacity/low affinity mobile reservoirs of ligands. For that reason, the HSPG repertoire of EVs and their assortment of associated factors are hypothesised as important in the overall proteome of EVs and their subsequent intercellular communication functions.

Here, in this chapter, we will characterise EVs secreted by a prostate cancer cell line; DU145. This has been well explored previously by the group in terms of the proteome (Webber et al., 2014), influence on immune modulation (Clayton et al., 2007), and in activating mesenchymal stroma cells (Webber et al., 2015b, Chowdhury et al., 2015). Exploring HSPGs in the context of this model system is novel, and to address this topic two approaches were used to perturb the HSPGs status in the vesicles. Firstly, isolated vesicles were subjected to enzymatic digestion by exogenous addition of heparinase III. This protease-free enzyme preparation was aimed at removing the HS-GAG chains from the HSPGs-core proteins present at the surface of EVs (**Figure 3.1**), as previously described (Baietti et al., 2012, Webber et al., 2015b). There are three kinds of heparinase enzyme produced by *Flavobacterium heparinum*. While Heparinase I and II cleave both

heparin and heparan sulphate chains, heparinase III cleaves exclusively heparan sulphate and does not cleave unfractionated heparin or low molecular weight heparins (Sasisekharan et al., 1995). This enzyme specifically cleaves the 1-4 linkages between hexosamine and glucuronic acid residues in heparan sulphate, via an elimination mechanism (**Figure 3.2**). This method, despite being very selective for HS-GAG chains, does not discriminate between specific HSPGs, such as syndecan-1 or glypican-3, for example, as it will cleave HS-GAG chains irrespective of the nature of the core protein. As such, this approach confers a total removal of these chains and would be expected to drastically remove any factors that are tethered through interaction with HS-GAG chains. The second approach, aimed to address the specificity of the core protein, utilises lentiviral-based delivery of shRNAs to generate DU145 cell variants deficient in a particular HSPG core protein, such as betaglycan. In theory, therefore, vesicles released from these cells would also exhibit attenuated levels of betaglycan at their surface. As a consequence, such EVs would have lost the factors associated with this specific HSPG. Nonetheless, the potential broader consequences for attenuating a specific HSPG core protein in DU145 cells needed to be explored, given the presumed role for certain HSPG in the biogenesis and loading of components into EVs (Baietti et al., 2012). It may be that such manipulations of the parent cell will lead to unpredictable events, modulating the quantity and cargo of EVs in more profound ways. In addition, many HSPG core proteins share regions of homology or will exhibit similar GAG-sequences. For these reasons, the loss of a given core protein might be mitigated by such homology with other HSPGs, presenting challenges due to functional redundancy.

Throughout this thesis, EV isolation was achieved by ultracentrifugation of pre-cleared cell conditioned media, from DU145 wild-type and HSPG-deficient cells, overlaid onto a 30% sucrose/D₂O cushion (Théry et al., 2006). This method was adapted and simplified, from an FDA-approved protocol for biomanufacturing of clinical-grade vesicles (exosomes), used as therapeutic vaccines for cancer patients (Lamparski et al., 2002). This approach of separating a distinct class of vesicles, based on their biophysical density, may indeed omit some types of EVs. While it can exclude, for example, large dense vesicles originating from the plasma membrane, the advantage of floatation is in the superior elimination of non-vesicular elements, such as soluble cytokines, that do not co-isolate at these densities. A good example of this is shown in Webber *et al.* (Webber et al., 2010), where the separation of EV using a continuous sucrose gradient identified a form of cell derived TGF- β 1 separating at densities of 1.1-1.2 g/mL. In contrast

Chapter 3 - Results

recombinant TGF- β 1 floated at much lower density. Hence this floatation approach can be successful in discriminating elements that are genuinely vesicle-associated from those that potentially co-isolate when using simpler pelleting approaches.

3.2 Aims & Objectives

The overall aim of this chapter is to characterise DU145 derived extracellular vesicles according to the MISEV guidelines, and most importantly, assess the impact of HSPG modifications on EV morphology.

The main goals for this chapter were:

- Characterise biophysical features of native EVs from DU145 cells.
- Investigate expression of expected markers and absence of potential contaminants.
- Explore the consequence of HS-GAG chain, or HSPG core protein, manipulation on EV features.

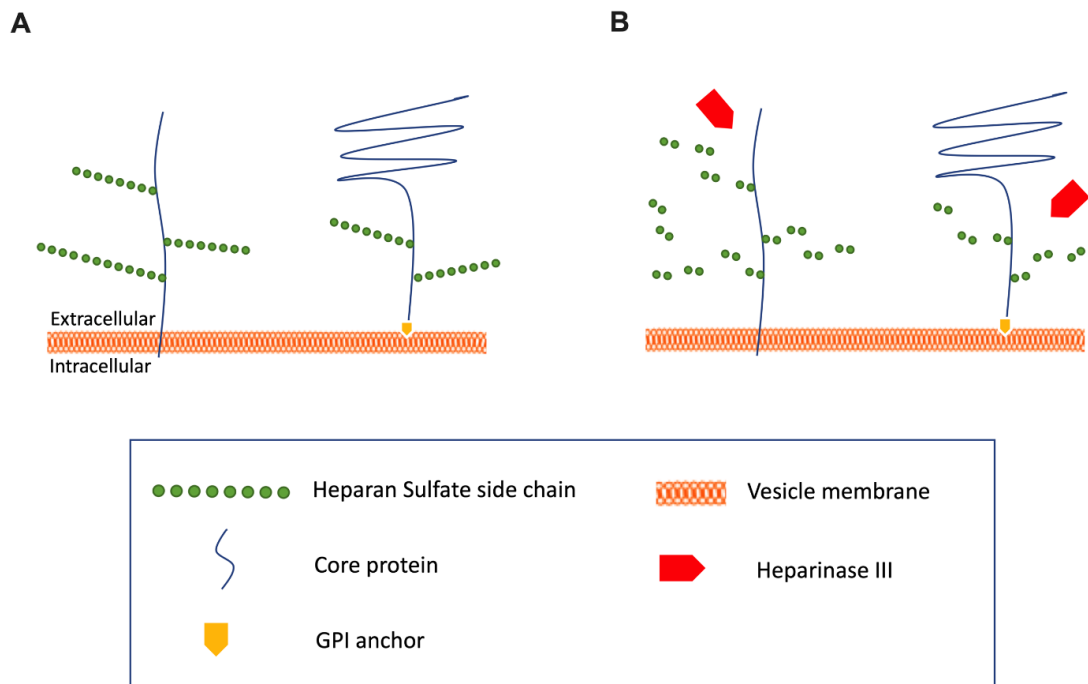


Figure 3.1. Enzymatic digestion with Heparinase III. (A) Schematic representation depicting a transmembrane HSPG (e.g., syndecans; left) and a glycosylphosphatidylinositol (GPI)-anchored HSPG (e.g., glypicans; right). Green dotted line represents intact glycosaminoglycan chains attached to the protein core (blue). (B) Addition of Heparinase III leads to cleavage of the elongated GAG chains, in the 1-4 linkages between hexosamine and glucuronic acid residues, and their eventual removal by washing. Short stubs remain to the core protein, which can be detected by a specific antibody (Δ -HS; clone 3G10). Intact HS-GAG chains can be detected by a HS antibody (clone 10E4).

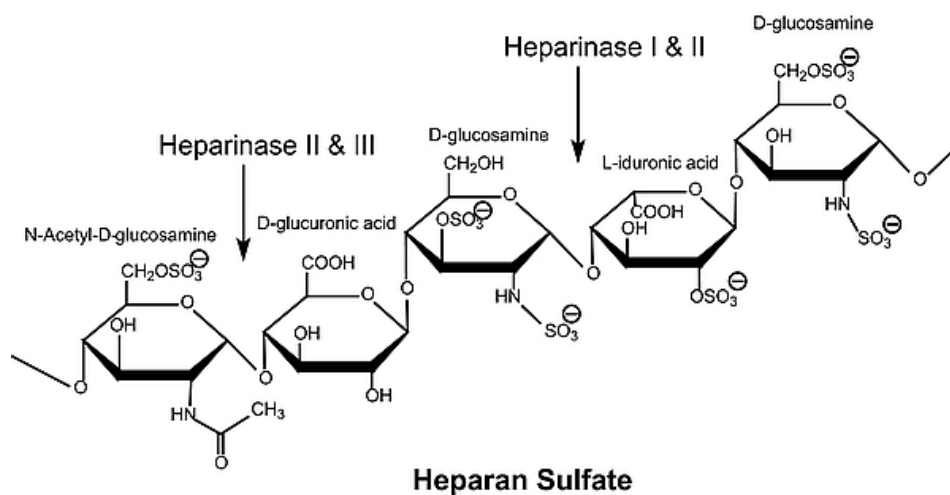


Figure 3.2. Schematic representation of Heparinase I, Heparinase II and Heparinase III cleavage sites. Adapted from Sigma-Aldrich.

3.3 Characterisation of DU145-derived EVs

3.3.1 Vesicle morphology

Vesicles used in these studies were derived from the DU145 prostate cancer cell line, (ATCC, USA), originally isolated from a brain metastasis (Stone et al., 1978). DU145 cells were cultured in small-scale integra bioreactors, as described in the methods section 2.1.3 (Chapter 2). EVs were isolated from the cell conditioned media by combining differential centrifugation, filtration, and a density cushion-based ultracentrifugation using 30% sucrose/D₂O.

To examine the morphology of isolated EVs, cryo-EM was carried out by Prof. Juan Falcon-Perez (CIC-bioGUNE, Spain). Briefly, specimens are vitrified in ethane pre-cooled with liquid nitrogen. Vitrified samples are imaged without any fixatives or labelling to reveal native, biologically relevant structures. In past studies, the reliance on fixation is acknowledged as an issue generating structural artefacts, such as the appearance of “cup shaped vesicles” (Raposo et al., 1996). Cryo-EM images reveal a heterogenous population of vesicle structures, with a clearly delineated border, indicative of a lipid bilayer (**Figure 3.3 A**). Several distinct structures were apparent in the isolates (**Figure 3.3 B**), and these were briefly classified based on shape, similar to the approach of Zabeo *et al.* (Zabeo et al., 2017). The majority of structures are described as small (< 100 nm) vesicles exhibiting a clear single-bilayer membrane. These represented 94% of the total structures counted (**Figure 3.3 C**) and had a mean size around 58 nm (**Figure 3.3 D**). The presence of larger unilamellar vesicles (> 200 nm) was rare, as was the presence of irregular sacks that appear to contain smaller vesicles and other amorphous material as intraluminal cargo. Vesicles with multi-membranes, i.e., apparent vesicles within vesicles, were equally rare (< 1%) events. Analysis of a total of 20 microscopic fields for this preparation demonstrated that these other structures represent less than 6% of the total events (**Figure 3.3 A**). Their presence suggests that the EV isolation procedure is not perfect in generating fully homogeneous vesicle structures, but the vast majority observed in the cryo-EM images indicates that there is a successful enrichment for smaller vesicles in the EV preparations.

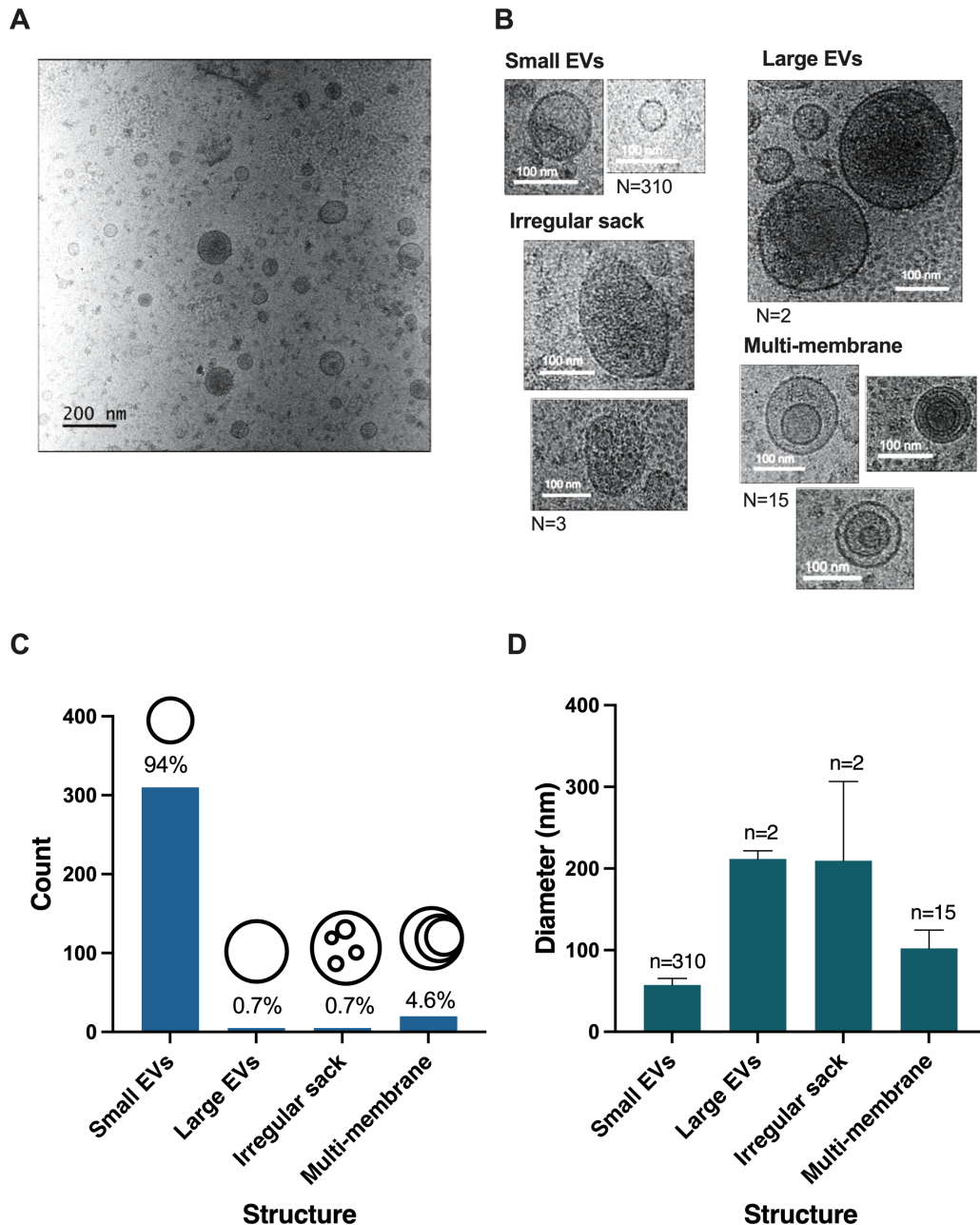


Figure 3.3. Cryo-EM of purified DU145 EVs. Cryo-EM was performed on DU145 EVs, isolated using the sucrose cushion method. **(A)** Image represents a typical microscopic field, revealing a variety of structures in terms of size and shape. **(B)** Structures were classified as distinct entities by size and shape and specific examples of these distinct shapes are highlighted at higher magnification. A graphical representation is shown for clarity and the number of events is specified for each. **(C)** A cartoon schematic is shown to help define these structural categories, and they are purely arbitrary but similar to published reports. Distinct categories of vesicles were counted and the relative frequency of these are shown as a %, while bars represent event counts. **(D)** The diameter at the widest point was measured for each event and the mean \pm SD of n events is shown. These data are based on 329 total structures counted across 20 different fields of view.

3.3.2 Vesicle size distribution and purity assessment

Nanoparticle tracking analysis (NTA), using the NanoSight NS300 platform, was performed to assess the particle size distribution within EV isolates (**Figure 3.4**). The isolated EVs had a modal diameter of around 92 nm, which falls in the range of small EVs as defined by ISEV (Théry et al., 2018), and is roughly comparable with the cryo-EM images presented in **Figure 3.3**, which show the majority of particles to be < 200 nm. The size distribution in the histogram obtained by NTA is typical of a DU145 EV preparation (Yeung et al., 2018, Webber and Clayton, 2013). There is a range of particle sizes detectable, some up to 600 nm, with several peaks < 200 nm. Whilst these might suggest distinct sub-populations, in reality, NTA is notoriously poor at discriminating particles of different sizes in a mixture such as polystyrene beads and care must be taken in interpreting multiple peaks. These are relatively low in number and represent only a minor portion of the overall population. The majority of particles detected by NTA were similar in size to those observed in cryo-EM images (**Figure 3.3 A**). The very small particles seen in cryo-EM, however, are not represented in the histogram, as NTA is most likely less sensitive at detecting particles < 90 nm (Gardiner et al., 2013), and consequently NTA has a tendency to overestimate the actual size distribution.

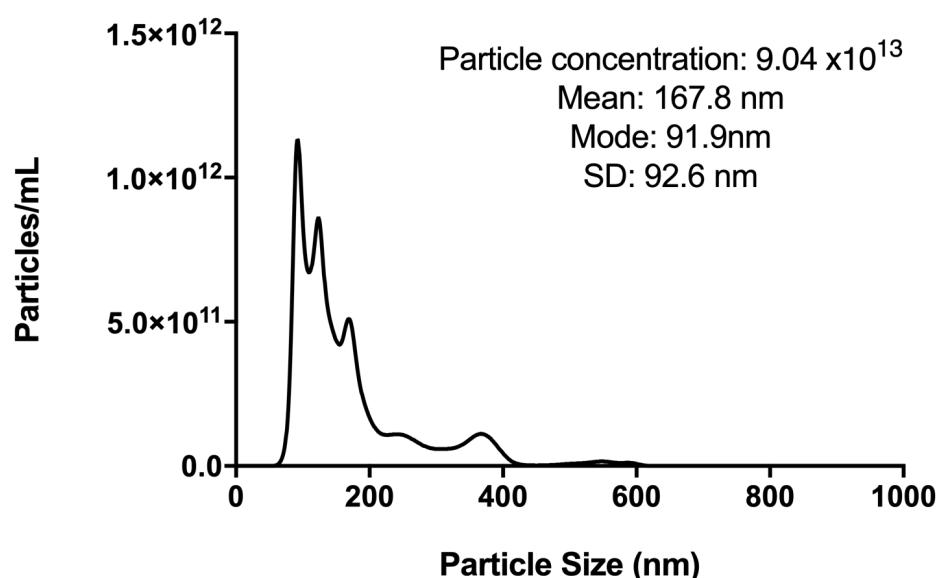


Figure 3.4. Size distribution of DU145 derived EVs. Nanosight™ based NTA histogram shows the size distribution profile of a typical EV isolate. Particle counts (particles/mL) and size distribution (nm) is represented in the histogram. Presented histogram is based on summary data from 5 videos, each video tracks particles for 30 seconds, and accumulating > 2500 number of completed tracks. The data collected allows for the calculation of particle concentration of the sample, as well as mode and mean size of particles.

By comparing the number of particles detected per μg of protein quantified in a given sample, the particle to protein (P:P) ratio can infer an estimation of purity of the isolated EVs (Webber and Clayton, 2013). For this, a combination of NTA and BCA protein assay is used. NTA provides the particles/mL of EVs present in a preparation, while BCA determines the concentration of particles in the EVs isolates in terms of $\mu\text{g/mL}$. BCA results are used to normalise vesicle concentrations used in later experiments. In the original article (Webber and Clayton, 2013), the authors demonstrate that an increase in soluble (non-particulate) protein contaminants will reduce the particle to protein ratio. Therefore, tracking this measurement can be useful as part of a routine quality assurance process in EV studies.

For this study, an arbitrary threshold of 1×10^{10} particle/ μg protein was applied, which is indicative of an isolation of good purity, mostly devoid of contaminants. The quality of EVs preparations was routinely assessed, and example of preparations are listed in **Table 3.1**. Differences between preparations can be noted, both in particle and protein concentrations, but most have consistent quality, exceeding the threshold of 1×10^{10} particle/ μg protein, and longitudinal tracking of the preparations highlighted that an occasional drop in purity was independent of time (**Figure 3.5**). Variation from preparation to preparation can be representative of day-to-day variations, not only in the methods used for quantification and in the experimental aspects of isolation but may also reflect variation of the culture environment within the DU145 cell bioreactors. Preparations with P:P ratios of $< 1 \times 10^{10}$ were indicative of a certain degree of protein contamination that could potentially be explained by issues arising during harvesting of EVs from the sucrose cushion, where perhaps some of the pellet or supernatant was inadvertently collected. However, the consistent P:P ratios obtained for these preparations show that the sucrose cushion method used here for vesicle isolation, is generally consistent in providing isolates of high purity, with low protein contamination.

Table 3.1. Purity assessment of DU145 derived EVs isolated by the sucrose cushion method. Protein and particle concentrations of DU145 derived EVs were measured by BCA and Nanosight™ NTA and used to calculate the P:P ratio. Some variability between the preparations can be seen. P:P ratios of $< 1 \times 10^{10}$ were indicative of a certain degree of protein contamination in the EVs preparations and are shown in red. These would be examples of isolations that had failed this quality control-criterion and would not be used in experiments.

Date EV isolation	Protein concentration (µg/mL)	Particle concentration (particles/mL)	P:P ratio (particles/µg)	Quality control
31/5/2018	2111.4	4.31×10^{13}	2.04×10^{10}	PASS
11/6/2018	3382.0	6.48×10^{13}	1.92×10^{10}	PASS
2/10/2018	5847.0	1.15×10^{13}	1.97×10^{10}	PASS
22/10/2018	4218.0	9.04×10^{13}	2.14×10^{10}	PASS
9/4/2019	4919.8	4.14×10^{13}	8.41×10^9	FAIL
24/5/2019	3788.7	2.25×10^{13}	5.94×10^9	FAIL
3/6/2019	5963.7	2.09×10^{14}	3.50×10^{10}	PASS
19/6/2019	7887.3	9.50×10^{13}	1.20×10^{10}	PASS
17/9/2019	6431.0	5.76×10^{13}	8.96×10^9	FAIL
13/12/2019	3893.8	6.83×10^{13}	1.75×10^{10}	PASS
30/1/2020	2145.4	2.36×10^{13}	1.10×10^{10}	PASS
7/2/2020	1260.5	1.69×10^{13}	1.34×10^{10}	PASS

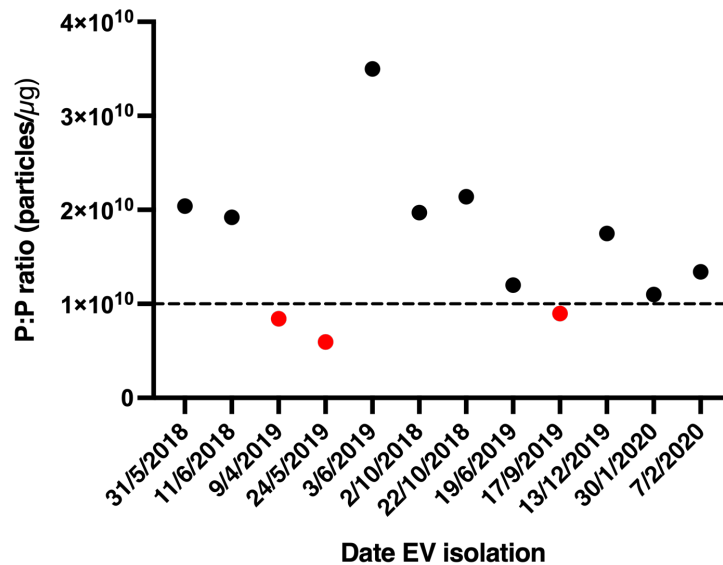


Figure 3.5. Distribution of particle to protein (P:P) ration over time. Protein to particle concentrations of DU145 derived EVs are shown with respective date of EV preparation. The dotted line corresponds to the 1×10^{10} purity threshold, with date points below the threshold shown in red.

3.3.3 Quality assessment by vesicle protein

To better define the nature of the vesicles being studied it is important to explore the expression of specific protein markers known to be enriched in EVs. Typically, several EV-associated proteins are expected to be present in a preparation, but it is also important to investigate the presence of proteins not expected to be enriched in EVs or not expected in an EV isolate, as these may represent non-vesicular contamination within the preparation. (Lotvall et al., 2014, Théry et al., 2018).

For this study, the expression of known EV-associated markers, such as ALIX and TSG101, was assessed. Both of these proteins are involved in endosomal maturation and are expected to be enriched in small EVs of endosomal origin. However, such factors may also be incorporated into small EVs derived from plasma membrane budding, and for this reason do not exclusively and clearly indicate endosomal manufacture (Nabhan et al., 2012, Booth et al., 2006). The levels of GRP94, an endoplasmic reticulum protein, and GAPDH, a cytosolic protein, were also evaluated. The expression of ALIX, TSG101, GRP94 and GAPDH was carried out by western blot to compare the relative levels of these markers in EV lysates compared to that observed within whole cell lysates (**Figure 3.6**). Despite ALIX and TSG101 being components of the cell, their clear enrichment in

Chapter 3 - Results

EVs is evident. In contrast, GRP94 was only present in the cell lysates and was not at detectable levels in EVs. This suggests that EVs within the preparation are devoid of contamination from cellular compartments such as the endoplasmic reticulum. GAPDH, as a cytosolic marker, was expected to be found both in cell and EV lysates, which was confirmed.

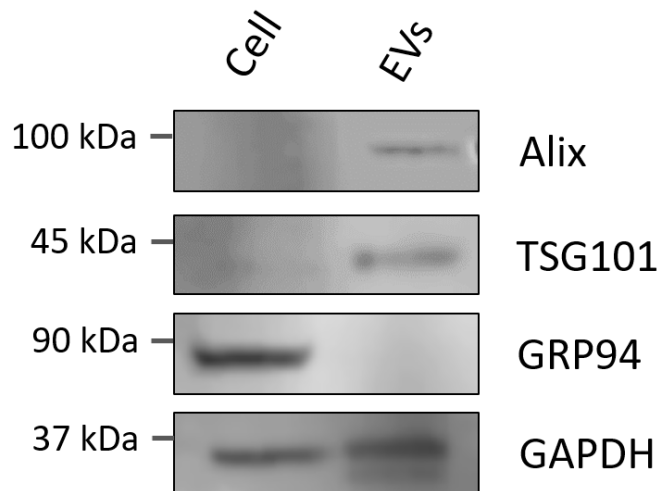


Figure 3.6. Characterisation of DU145 derived EVs by western blot. 20 µg of EV and DU145 cell lysates were subjected to SDS-PAGE and western blotting. The presence of ALIX and TSG101 was detected in EVs. GRP94, an endoplasmic reticulum marker, was chosen as the non-endosomal origin protein and was not detected in EVs. GAPDH, a cytosolic marker, was detected both in cell and EV lysates.

The expression of classical EV-related tetraspanins, CD9, CD63 and CD81 was assessed by an immunophenotyping plate assay. Isolated EVs were plated immobilised onto high-protein binding plates, prior to labelling with specific antibodies, and subsequent detection by TRF. The approach identifies targets at the outer EV surface. Isolates were strongly positive for these tetraspanins (**Figure 3.7**).

The combined data from the western blot and plate-based immunophenotyping assay agree with the high purity determined by the P:P ratio and show the effective removal of potentially co-isolated cell components from EVs isolates.

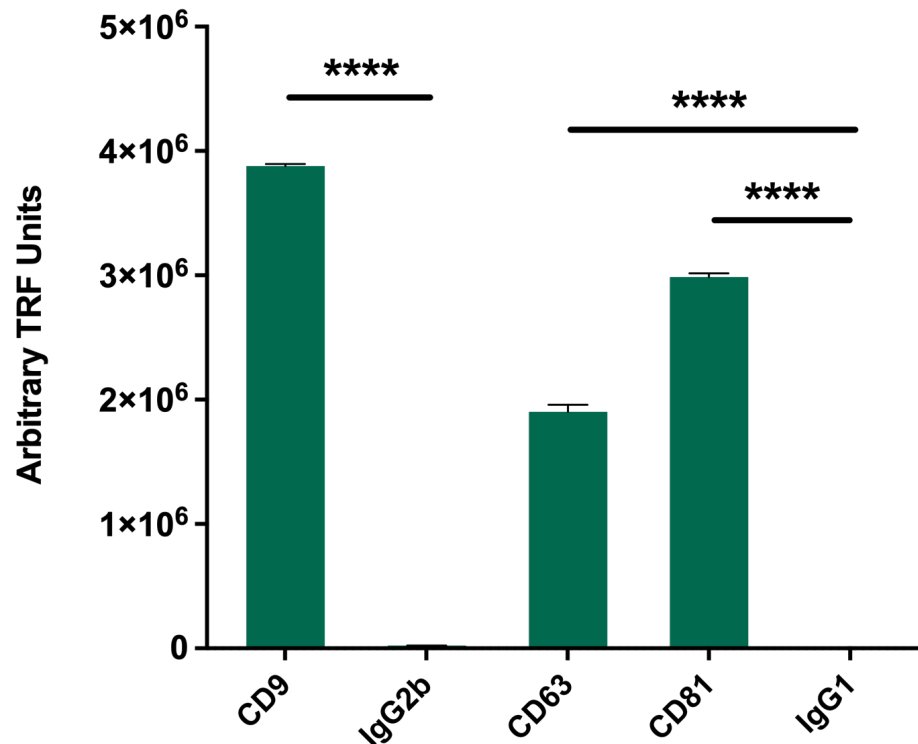


Figure 3.7. Detection of tetraspanins present in DU145 derived EVs by a plate-based immunophenotyping assay. DU145 EVs were captured onto a high protein binding ELISA plate (1 µg/well). Expression of surface EV-associated tetraspanins CD9, CD63 and CD81 were detected using target-specific antibodies. IgG1 was used as an isotype control for CD9 and IgG2b for CD63 and CD81. Graph shows arbitrary time-resolved fluorescent (TRF) levels (mean ± SD), based on triplicate wells, and a representative of three independent experiments. ****p<0.0001, one-way ANOVA with Tukey's multiple comparison test.

3.4 Removal of HS-GAG chains from the EV surface

3.4.1 Heparinase III digestion of HS-GAG chains on DU145 EVs

In order to disrupt the HSPGs on the EV surface, enzymatic digestion of the HS-GAG chains was carried out using HEP III enzyme, as previously described (Webber et al., 2015b). DU145 EVs used for these experiments are subjected to different treatments, one involving addition of an active form of HEP III enzyme, another with the same enzyme heat-inactivated at 90°C for 10 min, and finally, a untreated (no enzyme) control condition where vesicles do not receive enzyme but are simply incubated in the enzyme-free buffer system. After incubation, EVs are washed in order to remove the enzyme and the cleaved products, and re-pelleted by ultracentrifugation. EV concentration was re-confirmed by BCA assay to account for potential losses due to the washing step.

Chapter 3 - Results

Confirmation of successful HS removal was achieved using the aforementioned plate-based immunophenotyping assay but using a HS-specific antibody (anti-heparan sulphate; clone F58-10E4), in this instance. This antibody binds to the N-sulphated glucosamine residues present in the sample and allows the general detection of HS-GAG chains. As expected, HS was readily detectable on EVs treated with no enzyme and also those treated with inactive HEP111 enzyme. For EVs treated with active HEP111, the signal for HS was 10 times lower than that of the non-digested and dropped below that of the control (IgM) antibody, suggesting complete removal of EV-associated HS from the vesicles (**Figure 3.8 A**). EVs treated identically to active HEP111, but with heat-inactivated enzyme as a control, had equally high signal as EVs treated with no enzyme, indicating the presence of the enzyme does not interfere with the capacity to detect HS in this assay. This experiment was conducted ten times, with similar results.

Removal of EV-associated HS was further validated by western blot analysis, and the detection of HS neo-epitopes exposed by digestion by HEP111 (shown in **Figure 3.1**), was achieved by using the Δ HS antibody (clone 3G10). Such epitopes are not available for antibody binding in the control treatments; however, the appearance of the available binding sites is evident following treatment with active HEP111. **Figure 3.8 B** shows distinct bands of different molecular weights, which reflect the HS epitopes present on various HSPGs-core proteins. This data highlights the presence of multiple HSPG-core proteins with surface exposed HS-GAG chains and is consistent with our previous studies (Webber et al., 2015b). GAPDH was used here as a loading control, and the treatments did not have an impact on this band, indicative of equal lane loading.

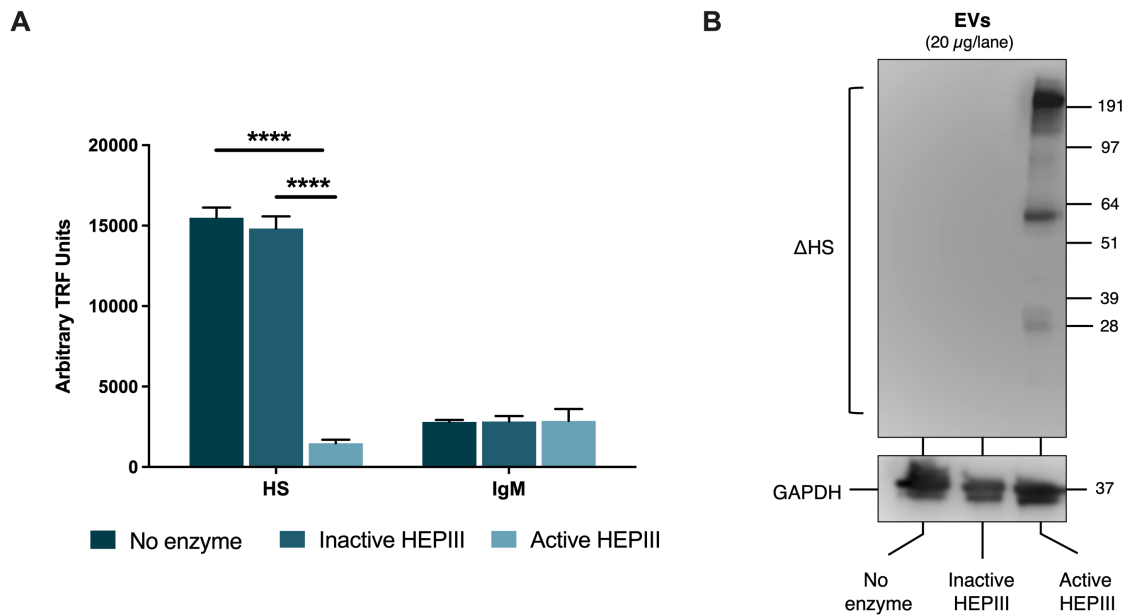


Figure 3.8. Confirmation of HEP111 digestion of heparan sulphate on DU145 EVs. DU145 EVs were previously treated with heat-inactivated HEP111, active HEP111, or no enzyme. **(A)** A plate-based immunophenotyping assay was used to assess the levels of HS present on EVs. Graph represents arbitrary time-resolved fluorescent units (mean \pm SD), based on triplicate wells, and are representative of ten independent experiments. **** $p < 0.0001$ control EVs vs. active HEP111, one-way ANOVA with Tukey's multiple comparison test. IgM was used as isotype control for HS antibody. **(B)** Treated vesicles were loaded (20 μ g/lane) for western blotting and run on a MOPS SDS gel. Blots were stained with Δ HS or GAPDH specific antibodies. In this example, the intensity of GAPDH band serves as a loading control. SeeBlue® Plus 2 Precision Stain was used as a molecular weight marker.

3.4.2 Assessment of off-target effects associated with heparinase III digestion of vesicles

The integrity of the vesicles is fundamental for any future functional work, so it was very important to assess if the effect of HEP111 could jeopardize the physical structure /membrane integrity and biophysical quality of EVs. For this, a variety of general characterisation assays were performed, comparing the three aforementioned vesicle conditions.

Initially tetraspanin expression levels across the treatments was explored. Treatment of EVs for removal of HS did not affect CD9, CD63 and CD81 signal at the surface of the vesicles, maintaining similar detection levels in the presence or absence of HEP111 (**Figure 3.9**). The plate assay requires 1 μ g per well to be loaded, and for each treatment an equivalent tetraspanin signal was generated.

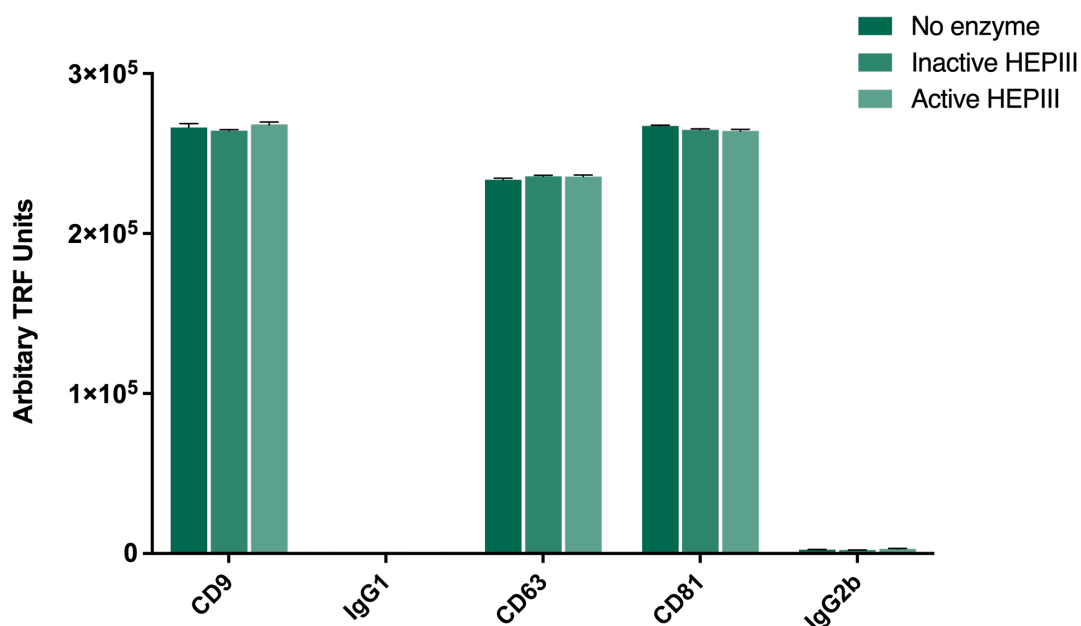


Figure 3.9. Tetraspanins expression on EVs after HEP111 enzymatic digestion. An immunophenotype plate assay was used to detect the surface expression of EV-associated tetraspanins CD9, CD63 and CD81, following removal of heparan surface from the surface of EVs. EVs had been previously treated with heat-inactivated HEP111, active HEP111, or no enzyme, and were captured onto a high protein binding ELISA plate (1 μ g/well). IgG1 was used as an isotype control for CD9 and IgG2b for CD63 and CD81. Graph shows mean \pm SD, based on triplicate wells, and a representative of three independent experiments. Statistical analysis, one-way ANOVA with Tukey's multiple comparison test.

The impact on size after the removal of HS from the surface of vesicles was also assessed. While the preference would have been to employ cryo-EM for this, unfortunately, the repertoire of samples needed would have made this difficult and resource consuming. Therefore, the Nanosight™ NTA system was elected with a realisation of its limitations, particularly with smaller EVs. There were no significant differences in size distribution in the vesicles treated or untreated with HEP111 enzyme (**Figure 3.10 A**) and an overlap of size range from the treated and untreated conditions can be observed (**Figure 3.10 B**). The modal diameter was within 120-135 nm, which is comparable with sizes observed in previous EVs preparations, indicating that removal HS from the surface of vesicles does not affect size in a significant way.

Overall, the data shows that HEP111 enzymatic digestion is able to significantly remove HS from the surface of EVs, without grossly affecting the integrity of the vesicle. Moreover, the similar tetraspanin levels observed here indicate the effectiveness of the protein quantitation after HEP111 washing, and that the digestion does not grossly strip away significant amounts of protein from the vesicle.

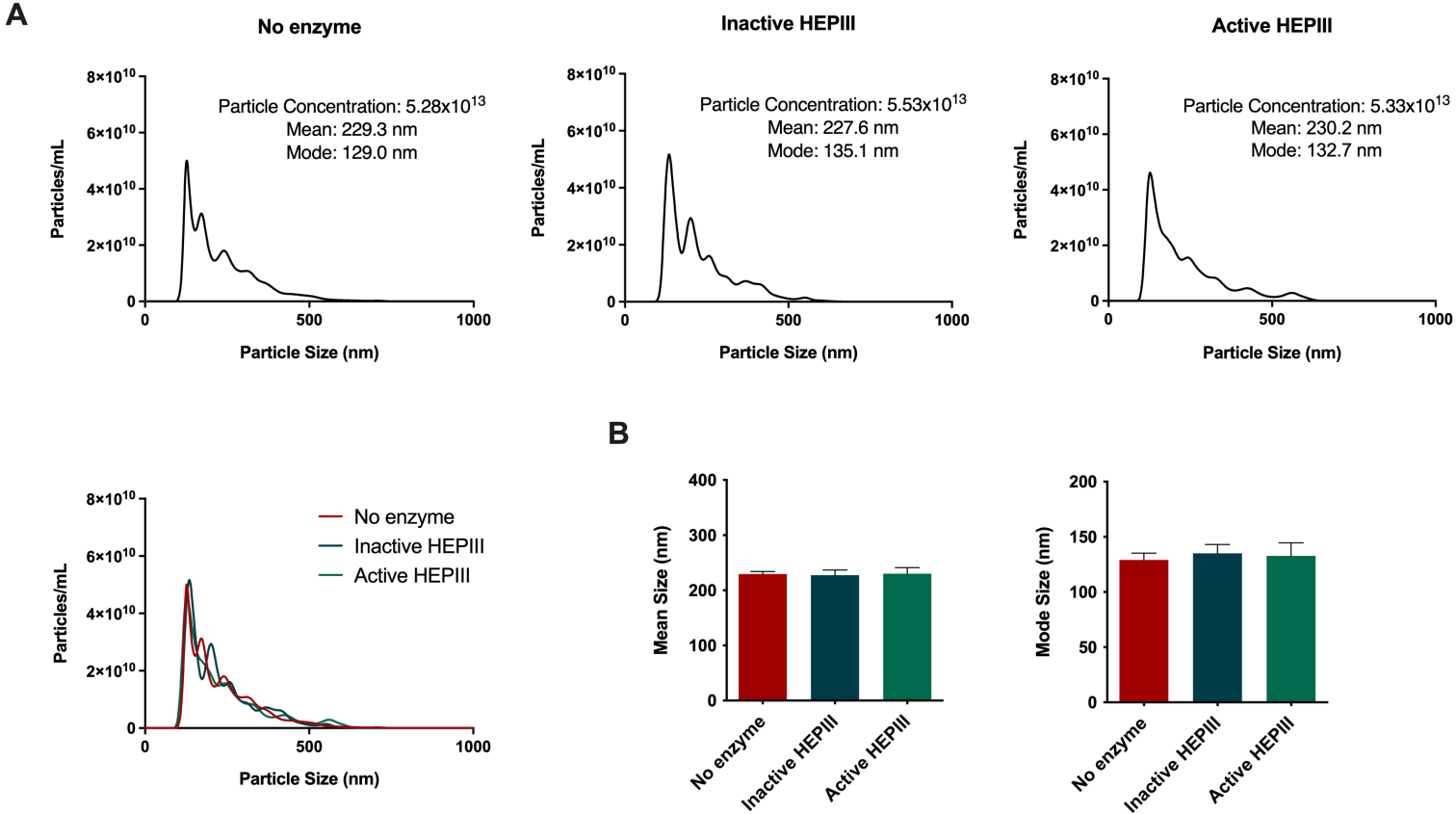


Figure 3.10. Size distribution of DU145 EVs after HEP111 enzymatic digestion. Nanosight™ NTA was used to assess size distribution of untreated (no enzyme), active HEP111, or inactive HEP111 treated DU145 EVs. **(A)** Nanosight™ NTA histograms shows the typical size distribution representative of each condition. Particle counts (particles/mL) and size distribution (nm) is represented in the histogram. Presented histogram is based on summary data from 5 videos, each video tracks particles for 30 seconds, and accumulating > 5000 number of completed tracks. Size distribution of EVs under different treatment conditions were overlaid to show consistency of sizes across all conditions. **(B)** Bar graphs show mean ± SD of mode and mean sizes, of the Nanosight™ NTA histograms. Statistical analysis one-way ANOVA with Tukey’s multiple comparison test.

Chapter 3 - Results

Due to the different treatments the EVs are subjected to, potential alteration of the properties of vesicles can occur, and it is to be expected that the input concentration of EVs incubated with the different conditions will not be the same following recovery by ultracentrifugation. The recoverable yield was very variable following the wash step. **Figure 3.11** shows the variability of recovery yields over the course of the study. Differences can perhaps be explained by user handling of samples; however, it is possible to notice an improvement in recovery percentages that went from 20% to over 50%, as I got more familiar with this technique throughout my PhD. Low recovery yields might also be the result of low or altered pelleting efficiency leading to loss of material. Alternatively, the low volume of initial sample treated with the HEP III enzyme, combined with the consequent ultracentrifugation step, which will lead to incremental loss of material, can be to blame. There is no defined pattern in recovery, which means that enzymatic digestion is not adversely affecting sedimentation in any predictable way. Moreover, this low recovery yield provides lower quantity of material to work with on future experiments making the follow-on experiments rather challenging.

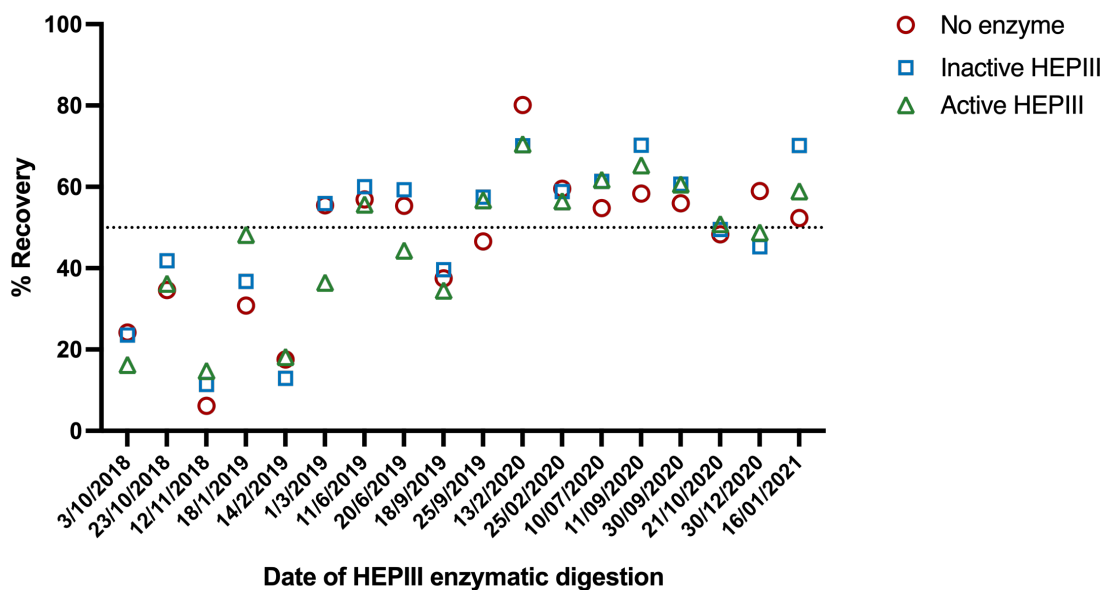


Figure 3.11. Recovery yield obtained for different HEP III enzymatic digestions carried. The percentage of EVs recovered from ultracentrifuge-based washing of EVs. Data show all EV treatments, and the tracking of recovery throughout a 27-month period. Dotted line marks the 50% recovery yield.

3.5 Knockdown of vesicular-associated HSPGs

The method of using HEP1III to enzymatically remove the HS-GAG chains from the surface of EVs, will target every HS chain available at the surface of EVs, and not discriminate between distinct HSPGs. To better understand the roles of individual HSPGs in EV-mediated growth factor delivery, several modified DU145 cell lines were generated (by Dr Jason Webber). Transduction of DU145 cells was achieved using lentiviral particles to deliver shRNAs targeting a specific HSPG core protein. Developing these more specific tools would help to better ascertain the role of each individual HSPG in the context of EVs. As previously mentioned, HSPGs within the EV-generating cell play important roles in the biogenesis and cargo-loading of EVs, prior to their release (Baietti et al., 2012). Therefore, it is important to assess how knocking down particular HSPGs in the parent cell, might affect the release of EVs in a general sense.

3.5.1 Confirmation of HSPG knockdown on DU145 cells

Recent, unpublished data from our group (generated by Dr Jason Webber) has shown syndecan-3 (SDC3), syndecan-4 (SDC4), glypican-1 (GPC1), glypican-6 (GPC6), and betaglycan (BGLY) to be the most abundant HSPGs on the surface of DU145 EVs. In order to ensure maximal attenuation of HSPGs, five shRNA sequences were tested against each of these HSPG core protein targets. A shRNA that selectively targets an irrelevant non-mammalian target (non-mammalian control; NMC) was also used to account for any potential unexpected effects that might arise due to lentiviral transduction. The resultant transduced cells were assessed for target HSPG expression at the mRNA level, and cells with the greatest target attenuation were expanded for further studies (**Figure 3.12**).

SDC3 mRNA expression was extremely well (> 98%) attenuated within DU145 cells by all of the shRNA sequences screened. For the other HSPGs, there were different levels of efficacy for the different shRNA sequences. SDC4 attenuation was best achieved using shRNA #9098, generating a knockdown of 95% compared to NMC levels. For GPC1, GPC6, and BGLY, the shRNAs that resulted in the lowest mRNA expression in the cells were #2911, #3096 and both #001 and #081, respectively, providing a knockdown of at least 87%.

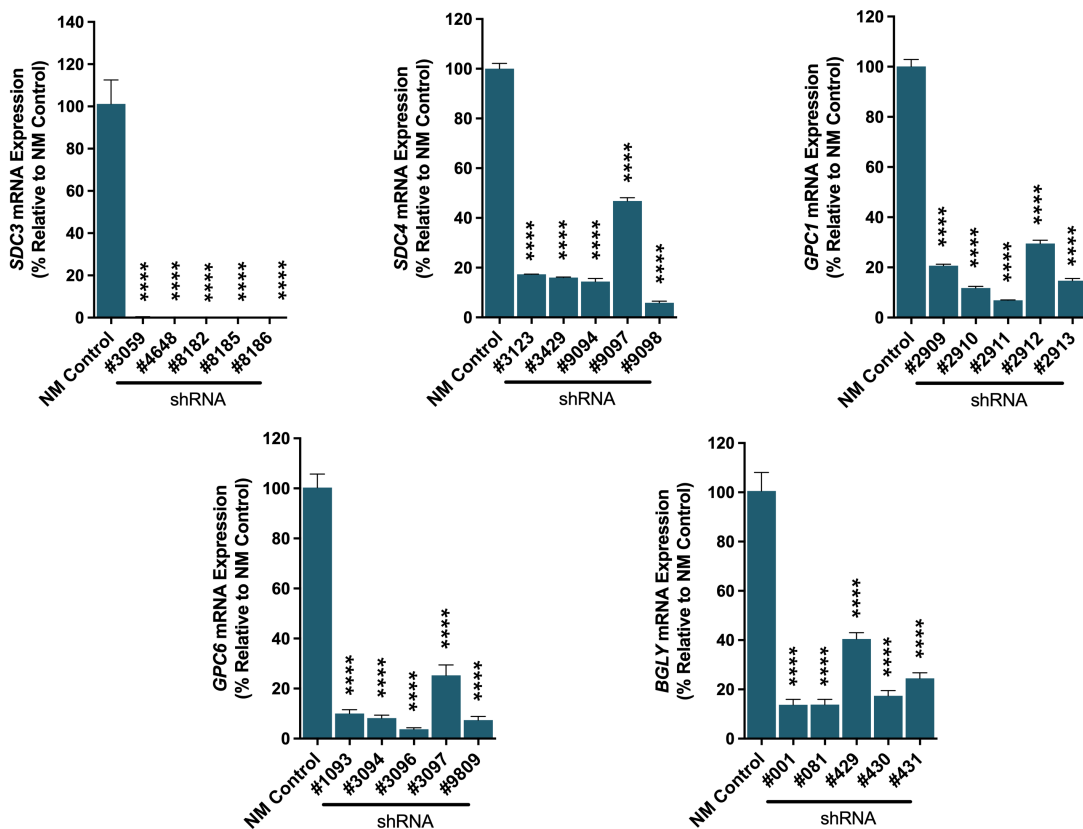


Figure 3.12. HSPG expression in DU145 cells, at the mRNA level, following knockdown of each HSPG with 5 different shRNA sequences. Targeted knockdown of specific HSPGs was achieved by lentiviral-based delivery of shRNAs, assessing five individual shRNA sequences (indicated by #) per target. The mRNA expression of targeted HSPGs was assessed by TaqMan gene expression assays, normalised against GAPDH, using the $\Delta\Delta C_t$ method. Bar graphs shows mean \pm SD of mRNA levels for each HSPG gene, relative to non-mammalian (NM) control, following lentiviral transduction with 5 different shRNA. *SDC3* (syndecan-3), *SDC4* (syndecan-4), *GPC1* (glypican-1), *GPC6* (glypican-6) and *BGLY* (betaglycan) **** $p < 0.0001$, one-way ANOVA with Tukey's multiple comparison test. Data from Dr Jason Webber.

Due to the potential homology between HSPG core proteins, it is possible that targeting of one HSPG may inadvertently impact other core proteins. Therefore, it was important to establish the specificity of the different shRNA for their intended target. To achieve this, mRNA expression levels of the non-targeted HSPGs were assessed by qPCR in each of the HSPG-deficient cell lines. The data in **Figure 3.13** identifies low cross-reactivity for all the HSPGs under attention here, except GPC6. This sequence strongly attenuated GPC1, in addition to a comparable level as GPC6 (> 90% knockdown), and hence the GPC6 knockdown presented in this chapter in fact represents strong attenuation of both GPC1 and -6. For the remainder, the knockdowns had limited effects

on the non-targeted HSPG. In some cases, it was apparent that knockdown of a given HSPG resulted in elevated expression of mRNA for non-targeted HSPG. A notable example is betaglycan mRNA levels on vesicles derived from SDC3 knockdown cell lines, which appears to be more expressed than the NMC. These were not entirely expected and may represent compensatory changes in the DU145 cells that make up for loss of a particular core protein. This aspect is not well understood, and apart from documenting this change, it was not pursued further in this thesis.

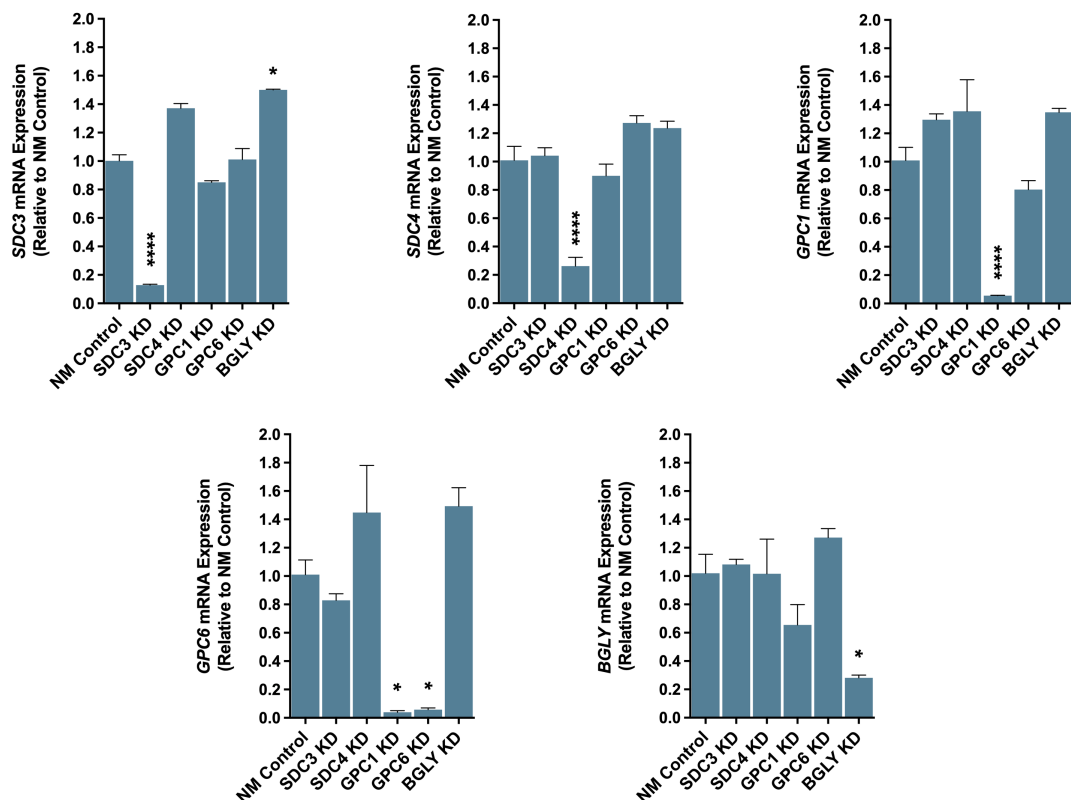


Figure 3.13. HSPG knockdown specificity in DU145 cell lines, assessed through non-targeted HSPG expression, at mRNA level. To confirm specificity of shRNA-induced knockdowns, the mRNA expression of each HSPG target was compared across all of the generated HSPG-deficient cell lines and is plotted relative to DU145 cells treated with an irrelevant control shRNA. HSPG mRNA expression was assessed by TaqMan gene expression assays and is normalised to GAPDH, using the $\Delta\Delta C_t$ method. Bar graphs shows mean \pm SD of mRNA levels for non-targeted HSPG, relative to control, in each HSPG-modified DU145 cell line. Cell line tested: SDC3 KD (syndecan-3 knockdown), SDC4 KD (syndecan-4 knockdown), GPC1 KD (glypican-1 knockdown), GPC6 KD (glypican-6 knockdown) and BGLY KD (betaglycan knockdown). ** $p < 0.01$; *** $p < 0.001$, one-way ANOVA with Tukey's multiple comparison test. Data from Dr Jason Webber.

Chapter 3 - Results

The confirmation of attenuation of specific HSPGs at the surface of EVs was important and was assessed using the plate-based immunophenotyping assay, as previously detailed, but using antibodies against individual HSPG core proteins (**Figure 3.14**). These data confirm the successful generation of EVs exhibiting deficiencies in specified HSPG core proteins. The diminished expression levels were at least 60% reduced compared to the NMC. Although it was hoped the attenuation would be stronger than this and align to the strongly attenuated mRNA in the parent cells, this was unfortunately not the case. Nevertheless, the approach has generated altered EVs with attenuated levels of specific HSPG core proteins on their outer membrane surface, providing tools for further exploring HSPG importance in EV-biology.

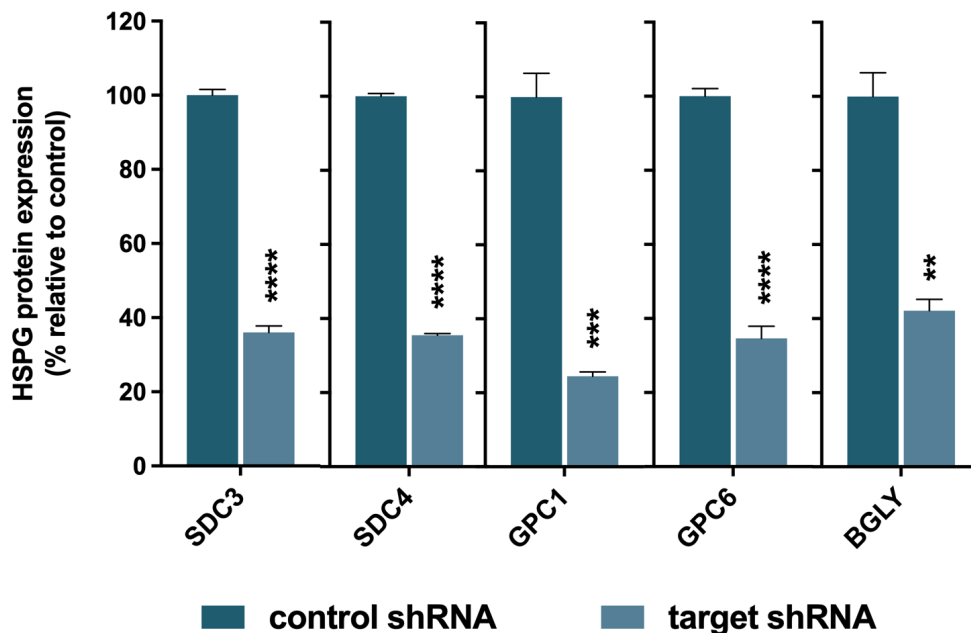


Figure 3.14. HSPG protein expression on the surface of EVs from HSPG-modified DU145 cell lines. EVs were isolated from HSPG-deficient cell lines (obtained with shRNA-induced knockdown of individual HSPGs) and DU145 cells treated with an irrelevant control shRNA (NMC). 1 μ g of EVs were immobilised onto high-binding 96 well plates and HSPG expression, on the surface of EVs, was assessed by plate-based immunophenotyping assay using antibodies specific to individual HSPGs. Bar graphs shows mean \pm SD of protein levels from EVs derived from each HSPG-modified DU145 cell line, for targeted shRNA, in relation to control shRNA. SDC3 (syndecan-3), SDC4 (syndecan-4), GPC1 (glypican-1), GPC6 (glypican-6) and BGLY (betaglycan). ** $p < 0.01$; *** $p < 0.001$, unpaired t test. Data from Dr Jason Webber.

3.5.2 Assessment of the effects on EVs due to HSPG knockdown

In order to understand the impact of HSPGs-core protein attenuation on some of the general features of vesicles, an assessment of general EV characteristics was again conducted. Experiments included evaluation of potential changes in EV secretion, as well as vesicle size, and the expression of EV-associated tetraspanins, on EVs isolated by ultracentrifugation using the sucrose cushion method.

To assess vesicle secretion, HSPG-attenuated DU145 cells were seeded at a density of 100,000 cells/well and the cell conditioned media collected after 48 hours of culture. EVs present in the cell conditioned media were not subjected to any isolation process and were assessed directly, by Nanosight™ NTA, to determine the concentration of vesicles, normalised per cell, present within the cell conditioned media. There was no detectable impact on the number of particles present within cell conditioned media from any of the five HSPG-deficient cells compared to that of the DU145 control cells (**Figure 3.15**), suggesting the shRNA treatment did not have an adverse impact on the capability of the parent cells to produce small vesicles.

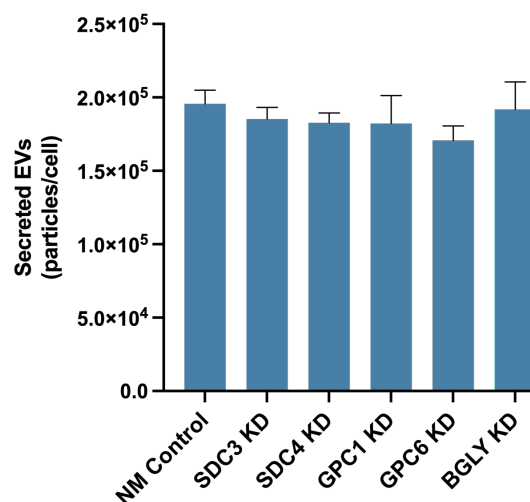


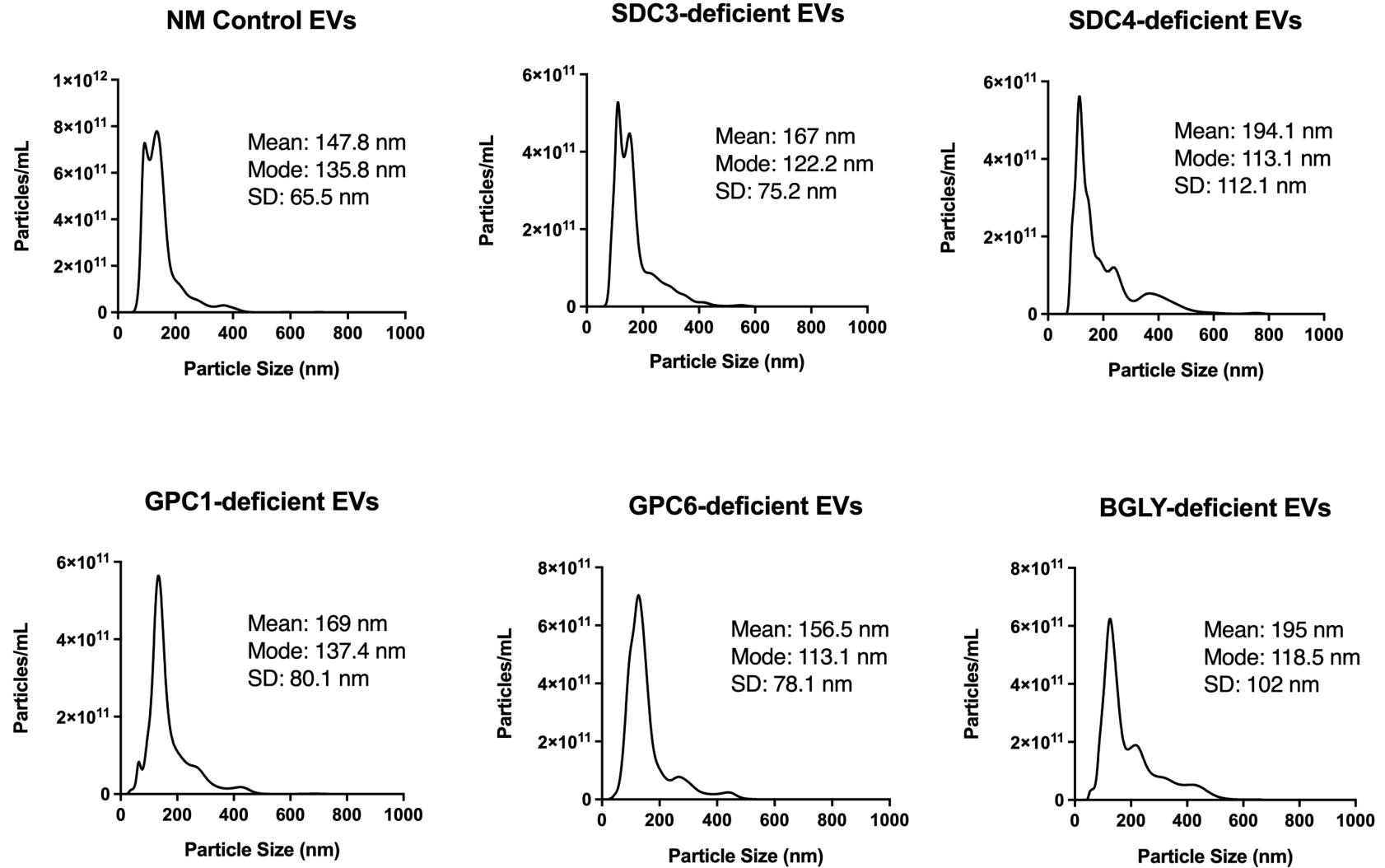
Figure 3.15. Impact of HSPGs-knockdown on size and EV phenotype of vesicles obtained from cell conditioned media. HSPG-deficient DU145 cells were seeded at a density of 100,000 cells/well, and cell conditioned media collected after 48 hours culture. Nanoparticle tracking analysis was used to measure the size and secreted particles. Bar graph represents mean \pm SD of secreted particles per cell. Data shown is based on summary data from 5 videos, each video tracks particles for 30 seconds, accumulating > 5000 number of completed tracks. The data collected allows for the calculation of particles concentration of the sample, as well as mode and mean size of particles. Cell line tested: SDC3 KD (syndecan-3 knockdown), SDC4 KD (syndecan-4 knockdown), GPC1 KD (glypican-1 knockdown), GPC6 KD (glypican-6 knockdown) and BGLY KD (betaglycan knockdown). Statistical analysis; one-way ANOVA with Tukey's multiple comparison test. Data from Dr Jason Webber.

Chapter 3 - Results

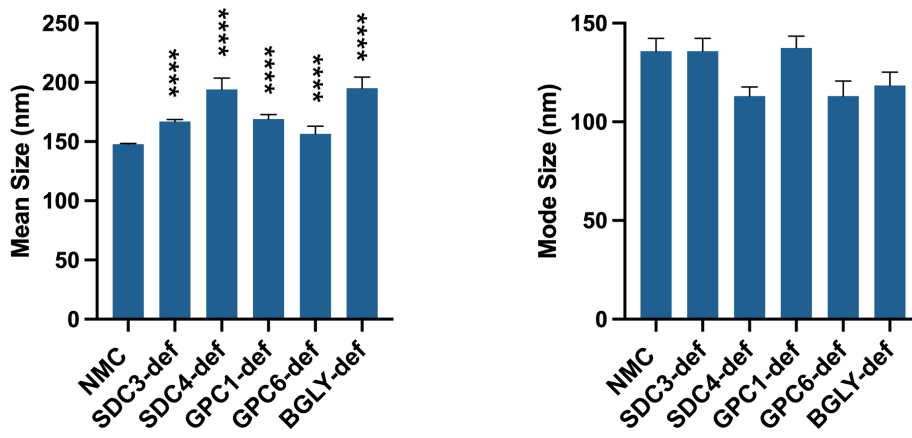
EVs isolated from control and HSPG-deficient DU145 cells using the sucrose cushion method, were assessed by NTA to determine the vesicles size (**Figure 3.16 A**). The size distribution is similar to those previously observed for EVs isolated from DU145 cells and consistent with isolation of small EVs (**Figure 3.4**). However, statistically significant differences can be observed in the mean size distribution for all of the HSPG-deficient EVs compared to the NMC, up to 1.3-fold. In contrast there seems to be no difference in the mode size of isolated vesicles (**Figure 3.16 B**). Next, the consequence of HSPG attenuation on EV-related tetraspanin levels was explored, again using the plate immunophenotyping assay method. Knockdown of HSPGs from cells did indeed have an effect on the expression of CD9, CD63 and CD81 tetraspanins on the surface of EVs. Some of these differences were not trivial, with almost a 2-fold difference between CD63 levels on GPC1 deficient EVs compared with BGLY deficient EVs. The overall significance of these general changes remains unknown, but they are indicative of likely contributions of specific HSPG core proteins to the manufacture and loading of components into/onto EVs during their biogenesis. (**Figure 3.16 C**).

To conclude, the range of approaches employed here to modulate the HSPG repertoire of EVs have been very successful; either in eliminating HS-GAG chains or in the specific attenuation of core-proteins. Although these treatments largely maintain the integrity of the vesicles, they are not entirely inert and there are examples where the modifications are not exclusively focused to HSPGs alone, and general impacts on the EV population arising are evident.

A



B



C

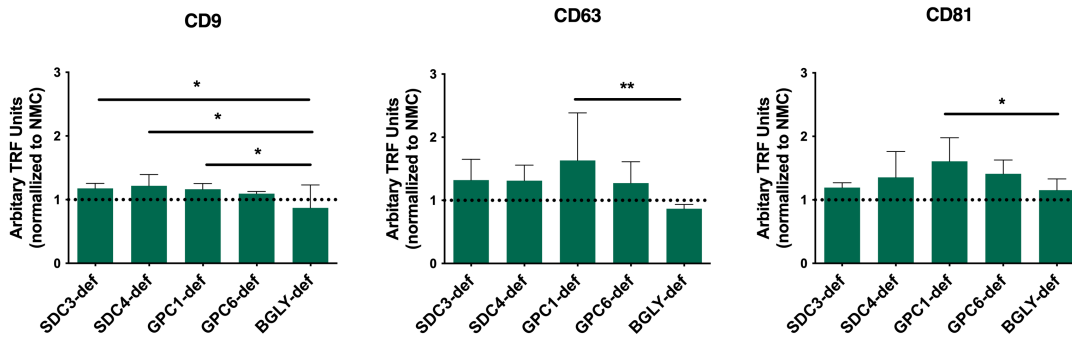


Figure 3.16. Impact of HSPGS-knockdown on size and phenotype of EVs isolated through sucrose cushion method. EVs from each of the five specific HSPG-deficient DU145 cell lines and control were isolated using the sucrose cushion method. **(A)** Nanosight™ NTA histograms shows the typical size distribution representative of each condition. **(B)** Bar graphs show mean \pm SD of mode and mean sizes, of the Nanosight™ NTA histograms, for each of the experimental conditions. Data shown is based on summary data from 5 videos, each video tracks particles for 30 seconds, accumulating > 3000 number of completed tracks. The data collected allows for the calculation of mode and mean size of particles. **(C)** EVs were characterised by plate-based immunophenotype assay to analyse the expression of CD9, CD63 and CD81. Bar graphs show mean \pm SD based on triplicate wells, and a representative of three independent experiments. All 5 knockdown conditions were normalised to the non-mammalian control (NMC). SDC3-def (syndecan-3-deficient EVs), SDC4-def (syndecan-4-deficient EVs), GPC1-def (glypican-1-deficient EVs), GPC6-def (glypican-6-deficient EVs) and BGLY-def (betaglycan-deficient EVs). * $p < 0.05$, ** $p < 0.01$, **** $p < 0.0001$ one-way ANOVA with Tukey's multiple comparison test.

3.6 Discussion

In this chapter, the manufacture of EVs from a prostate cancer cell line (DU145) is described and the nature of the EV-product generated is defined by a series of physical and molecular analyses. Furthermore, the EV product was subject to either direct enzymatic modification to remove HS-GAG chains, or alternatively DU145 cells were subject to shRNA-based attenuation of HSPG core proteins. The consequence of these interventions on the nature of EVs produced was also examined.

The capacity to separate EVs from other structures or soluble components present in the cell conditioned medium can be achieved by a variety of different techniques with variable results (Konoshenko et al., 2018). Currently, there is no optimal technique that allows the absolute isolation of EV structures from other entities and their concentration from a source material. Differential ultracentrifugation is one of the most commonly used EV separation and concentration methods used in the field (Raposo et al., 1996, Théry et al., 2006, Witwer et al., 2013). However, variable specificity and recovery of the method has resulted in refinement of such techniques with the goal to improve purity. Here, the use of the sucrose cushion ultracentrifugation method for isolation produces a heterogenous population of mostly small vesicles of similar morphology and with high particles to protein ratios, which are indicative of low levels of non-vesicular protein contaminants. The analysis of these isolates also highlighted the enrichment in typical EV-associated endolysosomal markers, such as ALIX and TSG101, and high signals for surface tetraspanins. The apparent absence of ER-marker GRP94 indicates that general intracellular contents are absent from the preparations, and the molecular contents of the EV isolates are highly distinct from those representing general lysed cells.

The quantification of EVs is difficult and there is not a single method that provides an accurate assessment of EV concentration. However, evaluation of different components of EVs, such as proteins, lipids, and nucleic acids, can be used indirectly to measure EVs and provide a rough estimate of EV quantity. Moreover, the ratios between the different quantification methods can provide a useful measure for purity. Particle:protein ratio (Webber and Clayton, 2013), protein:lipid ratio (Osteikoetxea et al., 2015) and protein:RNA ratio (Cvjetkovic et al., 2014) are also employed in an effort to evaluate the general purity of EV isolation. Each of these have their advantages and limitations. Protein concentration was measured by BCA protein assay, and this was used to

Chapter 3 - Results

normalise EVs used in experiments. Nonetheless, this method does not come without problems, and due to the difficulty in distinguish vesicles from non-vesicular material, there is an assumption made when using this technique, that is, that all detected protein is vesicular, which might lead to an overestimation of the number of vesicles present in the sample. Furthermore, there may be a variety of non-vesicular nano-particulate present, such as protein aggregates or lipoproteins (from FBS), for example, that may be included in an NTA based vesicle count. Additionally, limitation of light scatter, with hollow and very small vesicles, make these analyses underrepresent the small vesicles present. With these caveats in mind, a simple estimation of purity by P:P ratio remains a useful internal quality control step and can underline occasional isolations that are atypical and suspect. Overall, few isolations had to be discarded in the study due to the suspicion of overly high protein contamination, and the system was tractable in terms of identifying poor preparations and allowing selection of only good quality EVs for this study (Webber and Clayton, 2013).

Direct high-resolution imaging of immobilized EVs, using techniques such as cryo-EM, is one of the best methods to determine the size and morphology of individual EVs, as it analyses them in their native state, and applying this method to an EV isolates gives a greater representation of vesicle heterogeneity present (Arraud et al., 2014). Images obtained through cryo-EM show various structures, delineated by lipid bilayers, similar to small EVs identified in other studies (Arraud et al., 2014, Zabeo et al., 2017). Additionally, it is possible to identify several other structures/amorphous materials in the samples. Vesicular structures appearing to depict membranes within membranes were observed as well as nano-vesicles of size greater than 200 nm. The presence of these large structures is unexpected, considering the usage of 220 nm-pore filters in the steps that precede the isolation using the sucrose cushion method. Vesicles may, however, be prone to some level of deformation during pressure-driven filtration without rupture, and their malleability may allow for a deformation of their shape, being then able to pass through such pores. The presence of larger vesicles in isolates is not unusual and has been documented by others (Arraud et al., 2014, Zabeo et al., 2017), and might be caused by aggregation due to the high-speed ultracentrifugation process (Linares et al., 2015). Even so, this highlights that floatation-based protocols are not fully able to generate a monodispersed vesicle population, as other structures seem to co-isolate at this density. Overall, despite the heterogeneity in the EV samples, the majority (94%) of the population comprises unilamellar nanovesicles of < 100 nm size. Nonetheless, it is

important to recognise the presence of these other structures, as they reflect the content of the EV preparations and partially reflect the vesicle output of the DU145 cells. Currently, an extensive analysis of EV heterogeneity by cryo-EM is outside the scope of this thesis. It would require substantially more imaging and forms of automated signal processing in order to generate data based on several thousand events, as opposed to just a few hundred EVs manually analysed herein. Although NTA presents many limitations, it nonetheless can explore a greater number of nanoparticulate events, and for this reason, it can be useful to give an overall exploration of vesicles in a sample. Because of its availability and relative tractability, this platform was used to examine the impact of EV modifications on vesicle sizing and quantity. At least by this tool, HEP1III digestion showed little effect on EV size. Additionally, evaluating changes in tetraspanins indicated little impact, pointing to a very selective and non-destructive effect of HEP1III enzyme on the EVs.

This is somewhat in marked contrast to the alternative approach used for EV modification. Attenuating HSPG core proteins in the parent cells appeared to increase the EV size (NTA mean) for all targeted HSPGs, and also exhibited altered levels of tetraspanins. A comprehensive proteomics study from 2016 by Kowal *et al.* showed that tetraspanins were particularly useful to differentiate EVs subsets (Kowal *et al.*, 2016). This seemed to support the hypothesis raised in a study by Rana & Roller from 2012, that EVs are generated through tetraspanin networks (Rana *et al.*, 2012). Alteration of HSPGs on EVs during their biogenesis in DU145 cells might, therefore, also alter the expression of particular tetraspanins on the secreted vesicles. This might be a general effect, or an aspect restricted to EV subsets represented by the differential expression of certain tetraspanins. Surprisingly perhaps, given some of the above changes, there seemed to be limited impact on the overall vesicle output from cell variants, with an identical amount of vesicle output per cell at least during the 48 hours of EV accumulation we tested. This does not necessarily mean that secretion is unaffected. The quantity of extracellular EVs is a balance between production, degradation extracellularly, and autocrine uptake /processing. Any of these elements may be affected by the attenuation of HSPG core proteins. However, the observation of no global changes for the entire set of knockdowns here, more likely indicates that secretion quantity rate is independent of HSPG inclusion, and that the vesicle impact we see mostly relates to the EV-molecular content and size. Clearly, however, and as part of this, attenuation of HSPG mRNA levels in the parent cell is likely to have effects beyond the selected HSPG core protein only,

Chapter 3 - Results

and potentially fundamentally alter the cargo-load of EVs. This is an aspect to consider in the subsequent chapters.

Establishment of DU145 cell lines with stable knockdown of specific HSPG core proteins was very successful. Several of the shRNA used were capable of attenuating target expression, but only the ones with the greatest attenuation were used to establish cell lines that were later used for collection and isolation of EVs. The GPC6 knockdown from the cells was not specific, as mRNA expression of both GPC6 and GPC1 were decreased in the cells. This is most likely attributed to homology in the core-protein sequence between GPC1 and 6, which the shRNA against GPC6 is targeting. Documenting this is important, as it does not make it possible to guarantee that any result attributed to the GPC6 deficient EVs is specifically related to GPC6 loss. To tackle this, a different shRNA, for example, the second-best shRNA silencing GPC6, could have been selected to further expand and establish the cell line in the lab. However, this is a time consuming and laborious process, hence why this approach was not taken throughout my PhD. Another interesting idea could have been the use of CRISPR/cas9 method. CRISPR, however, would knockout the targeted gene from the cells rather than knockdown. Considering HSPGs are relevant in EV biogenesis, the effect this could have in the cell is not clear, and off-target effects could also arise.

Overall, this chapter describes the successful isolation, quantification, and characterisation of DU145 derived EVs. It also addresses the different methods used to determine EV morphology, phenotype and concentration. Most importantly, this chapter demonstrates the successful establishment of cell lines that release EVs that lack one targeted HSPGs on their surface or a more vesicle-preserving approach if using HEPIII based surface digestion. The impact this will have on the ability of EVs to deliver growth factors, as well as the functional consequences, will be investigated in the subsequent chapters.

Summary of objectives met:

- This chapter describes the successful isolation, quantification, and characterisation of DU145 derived EVs.
- Successful removal of HS-GAG chains from the EV surface was achieved using HEP111 based surface digestion without this majorly impacting vesicular integrity.
- EVs derived from cell lines established in the laboratory showed that the shRNA approach chosen was successful in the attenuation of specific HSPGs expressed on the EV surface. However, this approach had a minor effect on EV size and tetraspanin loading.

Chapter 4
Defining the repertoire of proteins
tethered to the surface of extracellular
vesicles by heparan sulphate
proteoglycans

4.1 Introduction

Cells within the tumour microenvironment can communicate by a variety of mechanisms, including transferring soluble factors, cell-to-cell contact, and transfer of complex molecular cargo via secretion and reciprocal receipt of EVs.

The intercellular communication mediated by secreted EVs is a means of transporting specific biomolecules from cell to cell (Valadi et al., 2007, Sullivan et al., 2017, Naito et al., 2017) and instils EVs with the ability to alter the tumour microenvironment by regulating the cross-talk between different cellular components. EVs have the capacity to modulate immunity (Raposo et al., 1996), angiogenesis (Ludwig and Whiteside, 2018), and promote metabolic reprogramming of recipient cells (Yang et al., 2020) as well as other processes, such as cell motility and invasion, ultimately supporting metastatic spread, and in some cases, disease progression (Zhang and Yu, 2019, Webber et al., 2015a). The signalling potential of EVs does not depend solely on the uptake and transfer of luminal cargo to receptor cells. The true definition of EV-cargo relates to the molecular material within the vesicles but also the factors at the outer surface of the vesicle, which can also have important signalling roles by interacting with diverse receptors present on the surface of recipient cells.

HSPGs are known to bind a plethora of ligands, such as growth factors and chemokines, either by association with their HS-GAG chains, or to their core protein (Bishop et al., 2007, Sarrazin et al., 2011). This provides them with the ability to be dynamic mobile reservoirs of multiple signal-initiating molecules. Furthermore, the specific sulphation and structure of their GAG chains determines the interaction with various protein ligands, as well as conferring protection from proteolytic degradation in the microenvironment. This increases their half-life (Cerezo-Magaña et al., 2020) but potentially also offers an avidity effect upon handover to recipient cell receptors (Yayon et al., 1991).

We have previously shown that DU145 prostate cancer cells produce EVs with strong stroma-activating roles, capable of inducing differentiation of stromal fibroblasts to an α SMA positive myofibroblastic cell phenotype. These myofibroblasts are phenotypically and functionally distinct when compared to myofibroblasts generated by stimulation with soluble TGF- β 1. Specifically, the EV-generated myofibroblasts exhibit pro-angiogenic effects and, moreover, support tumour growth in xenografts (Webber et al., 2015b). Myofibroblast differentiation by EVs is mediated at least in part by TGF- β 1 tethered to

Chapter 4 - Results

the EV surface via betaglycan, a transmembrane HSPG. Loss of betaglycan, mediated by enzymatic cleavage, and the resulting decrease in TGF- β 1 levels, attenuated EV-mediated myofibroblast differentiation, indicating an important role of vesicular betaglycan in the delivery of functional TGF- β 1 (Webber et al., 2010). The importance of HS-GAG chains associated with betaglycan in handing over TGF- β 1 to other TGF- β receptors was considered, and selective removal of HS from the surface of DU145 cell-derived EVs identified the vital role of HS-GAG chains (Webber et al., 2015b). Although the levels of TGF- β 1 present were not impacted by the removal of HS-GAG chains, there was a significant loss of function, with attenuated differentiation and an abrogation of pro-angiogenic behaviours. Clearly, the vesicle delivery of TGF- β 1 involving HSPGs is markedly different from the classical paradigm of soluble TGF- β 1 reaching the recipient cell surface. In particular, it is important to consider that this unique form of delivering TGF- β 1 also co-delivers other molecular components to recipient cells, and the variety of cargo delivered at the same time as TGF- β 1 is likely relevant in generating the aforementioned myofibroblast phenotype and function. It is also noteworthy that primary stromal cells isolated from patients with prostate cancer exhibited a very similar phenotype and function to the EV-induced myofibroblasts. This points to a likely role of EVs in educating stromal cells and skewing their function towards pro-tumoral actions, *in vivo*.

We hypothesised that additional growth factors and cytokines could also be carried on the surface of EVs in association with surface HSPGs, and delivered to recipient cells, constituting an interesting mechanism by which EVs can co-deliver multiple factors altogether. This may allow EVs to exert a fine control over cellular responses, providing a nuanced and distinctive response not possible when considering random diffusion of soluble factors within the secretome, as the EVs bring these elements to the recipient surface in concert. However, our focus herein relates to the nature of HSPG on EVs and the repertoire of factors tethered to these on EV surfaces. Currently, this sub-proteome of the EV-surface has never before been explored.

It is important to be mindful of the fact that detection of growth factors in EV samples can be extremely challenging, as their abundance amongst the diverse EV population is likely to be very low. Moreover, it is also important to consider potential co-isolated protein contaminants that can influence sample purity. Therefore, the choice of an adequate isolation method to minimize this is crucial. The isolation method used throughout this thesis, consisting of ultracentrifugation-based floatation of EVs within a sucrose cushion,

increases the overall purity and limits the likelihood of soluble contaminants being co-isolated in our EV preparations (Théry et al., 2006).

Mass spectrometry (MS) is the most common method for protein profile investigations, and hundreds if not thousands of proteins have been identified in association with EVs through this technique (Pocsfalvi et al., 2016). But detection of less abundant proteins in complex mixtures can be difficult, where low abundant components are often not identified due to the presence of a few, yet highly abundant, EV constituents. In consequence, mass spectrometry requires considerable efforts in sample preparation, fractionation, and high sensitivity instrumentation to detect relatively low abundant components. In this study, we elected to employ a non-MS approach and explored the utility of a multiplex protein array developed by Olink™. This very sensitive PEA technology uses pairs of oligonucleotide-labelled matching antibodies that, upon binding to a target protein and being in proximity, hybridize to each other. Only correct matched sequences hybridize. In the presence of DNA polymerase, the hybridizing oligo tails form an amplicon that acts as a unique marker for the specific antigen. The resulting sequence is subsequently amplified and detected by quantitative real-time PCR. The generated signal is proportional to the initial protein concentration in the sample, and although analyte dependent, sensitivities down to 0.06 pg/mL can be achieved as described by the manufacture (Olink). This technology confers greater stability, expanded target range, and improved affinity for the target proteins, decreasing the problems associated with other antibody-based arrays (Assarsson et al., 2014). Nonetheless, this is a focussed assay that incorporates pre-selected analyte sets and therefore is limited to 92 analytes for sample in the current configuration. In this aspect, mass spectrometry methods are less restrictive and allow for a broader generation of discovery data to identify highly novel factors.

This chapter addresses the hypothesis that HSPGs are responsible for tethering multiple growth factors at the surface of EVs. Through the use of the above very sensitive technology, we set out to define the repertoire of vesicular-HSPG related factors and to explore their potential relevance in specific biological processes through functional enrichment analyses.

4.1.1 Aims & Objectives

The aim of this chapter was to deal with the aforementioned hypothesis that HSPGs present on cancer EVs act as a low affinity, high capacity, means to tether growth factors and cytokines to the surface of EVs.

It is proposed that disruption of the HS-GAG chains or the HSPG system imposes significant changes in the repertoire of factors carried by EVs and a change in their delivery and functions thereafter, in terms of recipient cell responses.

The chapter, therefore, seeks to address the following main objectives:

- To define a range of cytokines and chemokines that are tethered to EVs through association with HSPGs and HS-GAG chains, using a high sensitivity protein array technology.
- To explore the putative biological functions of the HS-associated factors, through gene enrichment approaches.
- Utilise traditional assay approaches to validate some of the identified factors.
- Use this information to predict the relevance of EV related HS-chains in terms of cancer microenvironment modulation.

4.2 Exploring the profile of vesicular HSPG-associated proteins

4.2.1 *Discovery of HS-associated factors in DU145 extracellular vesicles*

As previously discussed, HS-GAG chains are likely to play an important role in tethering growth factors at the surface of EVs. In section 3.3 (Chapter 3) of this thesis, the successful removal of HS-GAG chains from vesicles was demonstrated, without disruption of the vesicle morphology. Using an active HEP111 enzyme compared to a heat-inactivated HEP111 enzyme, purified EVs were treated, GAG chains and associated factors that were enzymatically cleaved were washed away, and EVs recovered. This system provided a tractable approach to identify what is lost from the EVs due to HS-GAG digestion by HEP111.

For this experiment, specimens were sent to Olink for protein profiling. Three panels of analytes, encompassing well-recognised factors involved in the regulation of tissue responses, were employed for exploration. These are pre-defined sets provided by Olink, and specifically named the Proseek Multiplex Cardiovascular III Panel, Inflammation Panel and Oncology II Panel, respectively (**Appendix 4.1**). These panels, in combination, provide a good coverage of growth factors present across a spectrum of likely cancer-relevant biological processes and, therefore, may provide useful information on potential functions that are attributable to HS-GAG chains present on the vesicle surface. Although many other analyte sets are available, these three panels maintain minimal overlap of analytes between the panels, providing data on a total of 268 unique analytes (**Appendix 4.2**). The relative levels of the 92 analytes in each panel were measured to sub picogram sensitivity, in technical triplicates, for each sample.

Several proteins were reported as below the limit of detection (LOD) across all conditions and were excluded from the analysis. In total, 184 individual proteins were measurable (8 analytes were detected within multiple panels). If a protein was detectable in one of the experimental conditions, but below the LOD on the other, it was still included in the analysis. This is because the observed change suggests the protein might have been lost completely to levels no longer detectable by the assay, or alternately, it was not detectable, but the experimental modification made its detection possible. The overall distribution of proteins included in the analysis is shown in **Table 4.1**.

Table 4.1. Summary of the number of proteins included in the Olink analysis from the three panels. *Proteins not included in the analysis due to signal below limit of detection across all samples.

	Excluded from analysis*	Total Analysed	Above LOD	Below LOD	
				HEPIII treated	Control
Cardiovascular III	41	51	45	3	3
Inflammation	30	62	50	9	3
Oncology II	17	75	67	8	0

Fold change (FC) between active HEPIII-treated and inactive HEPIII-treated (control) vesicles was calculated, and p-value assessed (t-test, adjusted for multiple testing using Benjamini-Hochberg adjustment). The threshold taken for an identification of interest was based on a ± 2 -FC ($\log_2(2) = 1$; $-\log_2(2) = -1$) in HEPIII-treated vesicles compared to the control EVs condition and a p-value <0.05 . This was purely arbitrary and was our criterion for defining an analyte of interest.

Overall, 48 analytes, matching our selection criteria, were identified across the three panels (9 from the cardiovascular III, 18 from the inflammation and 22 from the oncology II panels). Stem cell factor (SCF) was a hit in both the inflammation and oncology II panels. These data are represented as volcano plots in **Figure 4.1 (A, B, C)**. The experiment highlights the loss of these 48 analytes following digestion, suggesting that a HEPIII-mediated loss of HS-GAG chains is accompanied by a concomitant removal of these factors from the EVs. Some examples include cystatin-B (CSTB), cathepsin L2 (CTSV), and IL-8, exhibiting a large fold decrease of 10, 20, and 20, respectively ($p < 0.001$) (**Figure 4.1**). There are other more subtle changes present, however, such as growth/differentiation factor 15 (GDF-15), C-C motif chemokine 20 (CCL20) and CY561 (also known as CCN family member 1), that show decreases of 5, 2.2 and 2.3-fold, respectively ($p < 0.001$). The majority of detected proteins did not fulfil the threshold criteria of ± 2 -FC. This is encouraging and indicates that the HEPIII enzymatic treatment does not comprehensively remove all detectable proteins. Instead, it appears restricted to a specific subset of analytes within each panel, and this demonstrates a selective HS-GAG tethering function is involved for these specific analytes

When considering the potential biological impact that can result from the removal of HS-GAG associated proteins from the surface of EVs, it is also useful to consider their abundance within the sample. Relying on fold change alone may be misleading,

especially in instances where analytes are scarcely present in one sample. Fold change will provide useful information, but it is also helpful to take into consideration the abundance, and thereafter ease of detection of individual analytes, here translated by signal strength for the altered analytes of interest in the assay. As Olink is a semi-quantitative assay, it does not provide absolute quantitative measures of the analytes in the sample. Therefore, the signal strength on control vesicles was assessed as an estimation of absolute abundance and taken into consideration when selecting protein targets for downstream validation. (**Figure 4.1 D, E, F**). This estimation is dependent on analyte abundance but also antibody performance and efficiencies of oligo-hybridisation; hence, this is an imperfect estimate of the abundance of varied analytes in the system.

The volcano plot from cardiovascular III panel shows myoglobin (MB) as having a signal strength 40 times lower than CSTB ($21 \cdot 2^{\text{NPX}}$ vs $840 \cdot 2^{\text{NPX}}$), which suggests that CSTB is more easily detectable in control EVs, and potentially more abundant than MB (**Figure 4.1 D**). Other examples include MCP-1 ($34 \cdot 2^{\text{NPX}}$) and C-X-C motif chemokine 10 (CXCL10) ($117 \cdot 2^{\text{NPX}}$), which are lower than IL-8 and CCL20, with $4366 \cdot 2^{\text{NPX}}$ and $2990 \cdot 2^{\text{NPX}}$, respectively (**Figure 4.1 E**). Similarly, analytes with a high signal intensity in control vesicles include IL-6 ($860 \cdot 2^{\text{NPX}}$), CYR61 ($565 \cdot 2^{\text{NPX}}$), and midkine (MK) ($478 \cdot 2^{\text{NPX}}$) (**Figure 4.1 F**).

In summary, these data indicate that specific removal of heparan sulphate from EVs alters the protein profile of vesicles. The treatment did not affect about 85% of the analytes tested, and therefore, the observed changes indicate specificity, where the downregulated/lost analytes are associated with the HS-GAG chains on the surface of EVs. Thus, altered proteins that were likely to be more abundant offer a good rationale for target selection in subsequent validation experiments.

Chapter 4 - Results

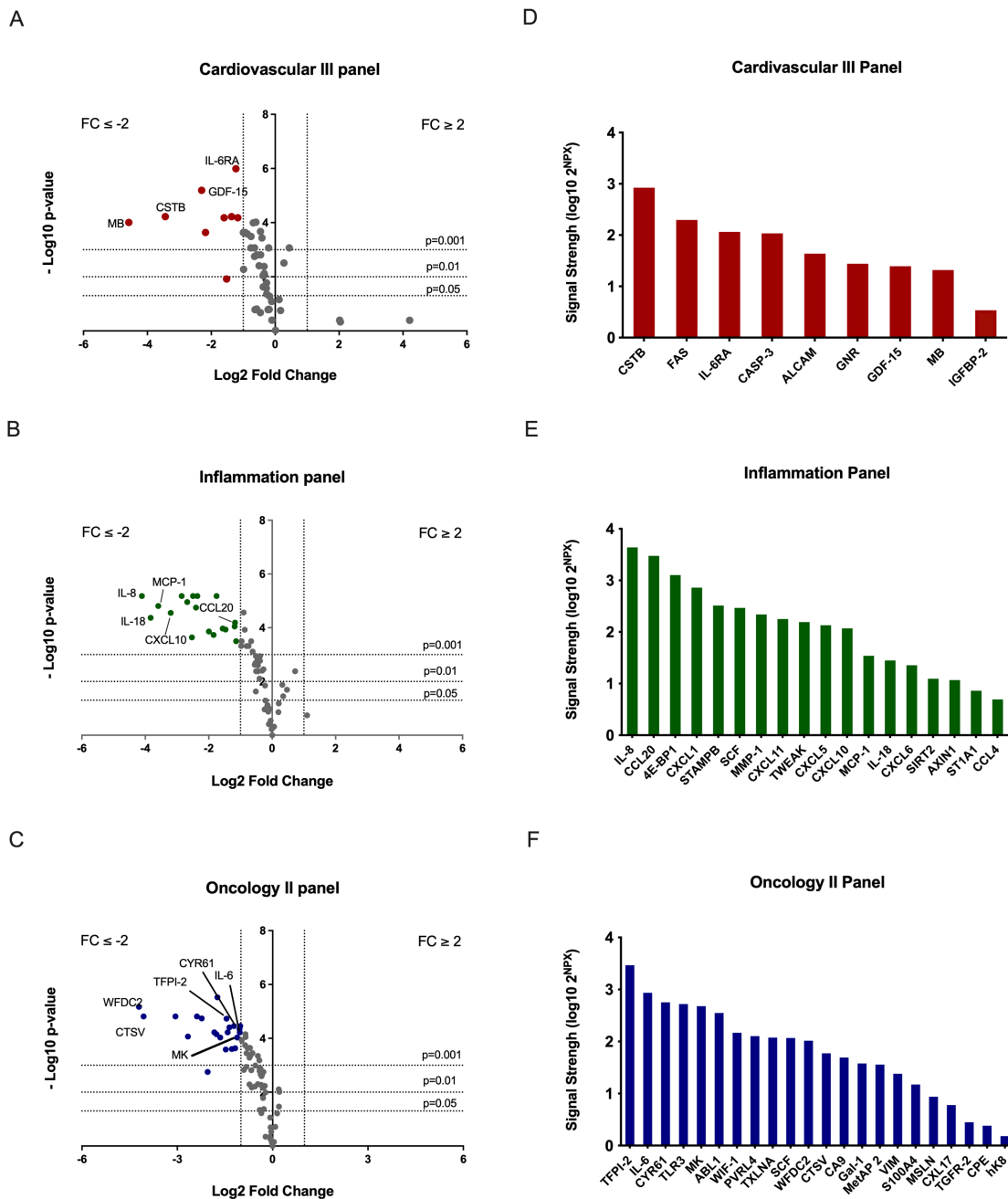


Figure 4.1. Enzymatic removal of HS side chains alters the protein profile of DU145 vesicles. A proximity extension assay by Olink was used to detect proteins on DU145 derived vesicles treated with active HEP111 compared to control EVs treated with heat-inactivated HEP111. Volcano plots for the cardiovascular III panel (A), inflammation panel (B) and oncology II panel (C), identify differentially expressed proteins with $FC \leq -2$; analytes decreased following HEP111-digestion and $FC \geq 2$; analytes increased following HEP111 digestion. Lines demark the statistical significance for proteins with $p < 0.05$, $p < 0.01$ and $p < 0.001$ (t-test, corrected for multiple testing using Benjamini-Hochberg adjustment). Red (A), green (B) and blue (C) dots show proteins which have significant decreases. Grey dots symbolize proteins below specified threshold criterion. (D, E, F) Bar graph shows the suggested relative abundance in control vesicles, conferred by signal strength, of the significantly altered analytes. Data shown represents the mean of $n=3$ replicates. NPX= Normalised Protein eXpression.

4.2.2 Functional enrichment analysis of HEPIII-digested vesicles

To further understand the underlying biological pathways that may be regulated by proteins attached to EV-associated HS-GAG chains, functional enrichment analysis, using FunRich software (<http://www.funrich.org>), was performed on the list of differentially expressed proteins arising after treatment with HEPIII.

First, the 48 proteins identified in the initial analysis, with at least 2-fold change and a $p < 0.05$, were converted to the respective gene name (**Table 4.2**). The gene names were input into FunRich to perform enrichment analysis for biological pathways. The FunRich database, for biological pathway analysis, is restricted and does not encompass all 20,000 human genes. Instead, it covers a total of 6290 genes. Because of this, not all of our 48 input genes are mapped onto the restricted FunRich dataset, but the majority (33 genes) were identified within this set. The output of pathways provided by the software was extensive; thus, a top 10 of most enriched pathways was selected, ranked based on the corrected p-values (Benjamini-Hochberg method) (**Figure 4.2**).

Interleukin and chemokine signalling pathways were identified as the most significantly enriched (**Figure 4.2 A**). This is most likely due to the fact that most of the proteins in the software associated with this pathway related heavily with the proteins featured in our list. The repertoire of interleukin and chemokines that are altered due to HS-GAG chain digestion certainly implicates HS-binding factors as drivers of these intercellular signalling pathways. Association with the “Glypican pathway” is also in the top 10 and is notable as well as reassuring, given that glypicans are amongst the HSPG present on DU145 EVs. Several of the genes mapped that are associated with the “Glypican pathway” also seem to be associated with the “Tumour necrosis factor (TNF)-related apoptosis-inducing ligand (TRAIL) pathway”. However, WNT Inhibitory Factor 1 (WIF-1) and midkine are specific to the glypican-dependent pathway, and vimentin (VIM) only shows associations with TRAIL (**Figure 4.2 B**). Additionally, the list of pathways generated by FunRich includes a number of other statistically significant associations that sit outside the top 10 (with a lower enrichment score). Some of these are depicted in **Figure 4.3 A** and include elements related to HSPGs, such as glypican-1 and syndecans, angiogenesis (“VEGF and VEGF receptor (VEGFR) signalling”), stromal differentiation (“EGF receptor (ErbB1) signalling” and “Hepatocyte growth factor receptor (c-met) signalling”), and immune modulation (“Granulocyte-macrophage

Chapter 4 - Results

colony-stimulating factor (GM-CSF) -mediated signalling events”). These pathways have all the same 16 genes associated with them (**Figure 4.3 B**). Despite the more biased approach of including these elements here, it shows that the results are consistent with current expectations of the varied roles of EVs in cancer. This suggests that many of these processes may be regulated, at least in part, by EV-associated HSPGs.

Table 4.2. List of protein and corresponding gene names input in FunRich software for enrichment analysis.

Protein name	Gene name	Protein name	Gene name
ALCAM	<i>ALCAM</i>	CCL20	<i>CCL20</i>
CSTB	<i>CSTB</i>	ST1A1	<i>SULT1A1</i>
GRN	<i>GRN</i>	STAMBP	<i>STAMBP</i>
GDF-15	<i>GDF15</i>	TXLNA	<i>TXLNA</i>
IL6-RA	<i>IL6RA</i>	CPE	<i>CPE</i>
FAS	<i>FAS</i>	MSLN	<i>MSLN</i>
MB	<i>MB</i>	TGFR-2	<i>TGFBR2</i>
SHPS-1	<i>SIRPA</i>	IL-6	<i>IL6</i>
IGFBP-2	<i>IGFBP2</i>	TFPI-2	<i>TFPI2</i>
IL-8	<i>CXCL8</i>	hK8	<i>KLK8</i>
MCP-1	<i>CCL2</i>	S100A4	<i>S100A4</i>
CXCL11	<i>CXCL11</i>	CYR61	<i>CYR61</i>
AXIN1	<i>AXIN1</i>	MetAP2	<i>METAP2</i>
CXCL1	<i>CXCL1</i>	PVRL4	<i>PVRL4</i>
CCL4	<i>CCL4</i>	Gal-1	<i>LGALS1</i>
SCF	<i>KITLG</i>	CA9	<i>CA9</i>
IL-18	<i>IL18</i>	CTSV	<i>CTSV</i>
MMP-1	<i>MMP1</i>	MK	<i>MDK</i>
CXCL5	<i>CXCL5</i>	ABL1	<i>ABL1</i>
CXCL6	<i>CXCL6</i>	TLR3	<i>TLR3</i>
CXCL10	<i>CXCL10</i>	VIM	<i>VIM</i>
4E-BP1	<i>EIF4EBP1</i>	CXCL17	<i>CXCL17</i>
SIRT2	<i>SIRT2</i>	WFDC2	<i>WFDC2</i>
TWEAK	<i>TNFSF12</i>	WIF-1	<i>WIF1</i>

Table 4.3. List of 33 genes identified in the biological pathways database from FunRich.

Genes identified in biological pathway dataset						
<i>GDF15</i>	<i>AXIN1</i>	<i>TGFBR2</i>	<i>MDK</i>	<i>CXCL10</i>	<i>KITLG</i>	<i>ALCAM</i>
<i>IL6R</i>	<i>MMP1</i>	<i>IL6</i>	<i>ABL1</i>	<i>CCL20</i>	<i>IGFBP2</i>	<i>SIRT2</i>
<i>FAS</i>	<i>EIF4EBP1</i>	<i>CYR61</i>	<i>WIF1</i>	<i>VIM;</i>	<i>SULT1A1</i>	<i>TXLNA</i>
<i>CXCL8</i>	<i>STAMBP</i>	<i>LGALS1</i>	<i>CXCL11</i>	<i>CXCL1</i>	<i>TLR3</i>	
<i>CCL2</i>	<i>CPE</i>	<i>CA9</i>	<i>CCL4</i>	<i>IL18</i>	<i>PVRL4</i>	

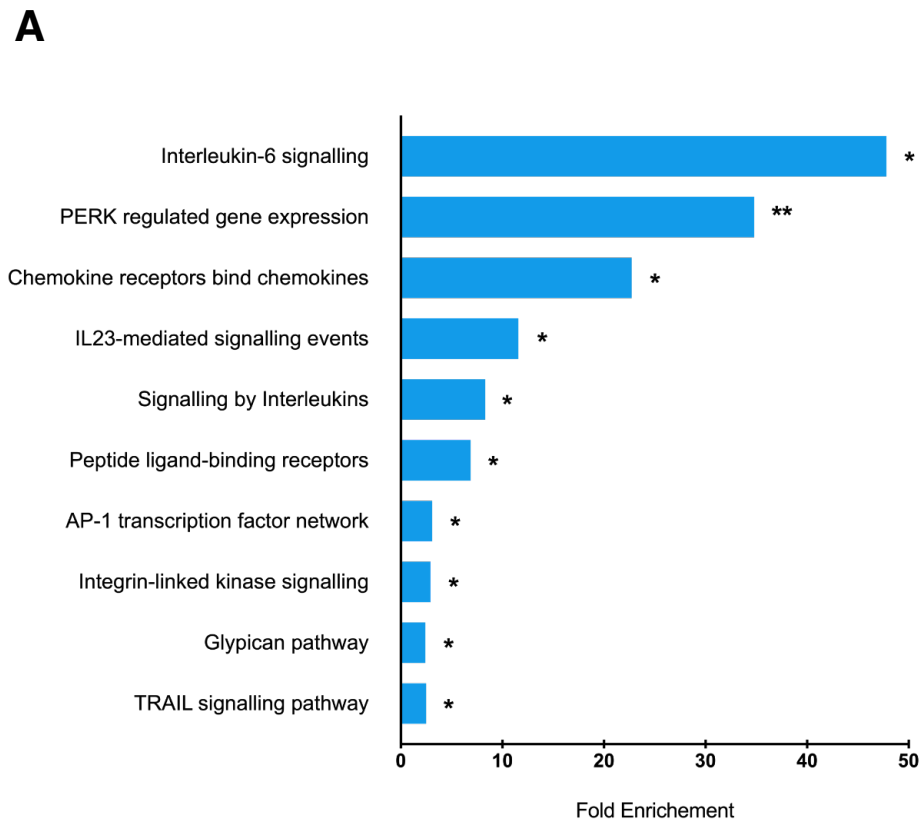
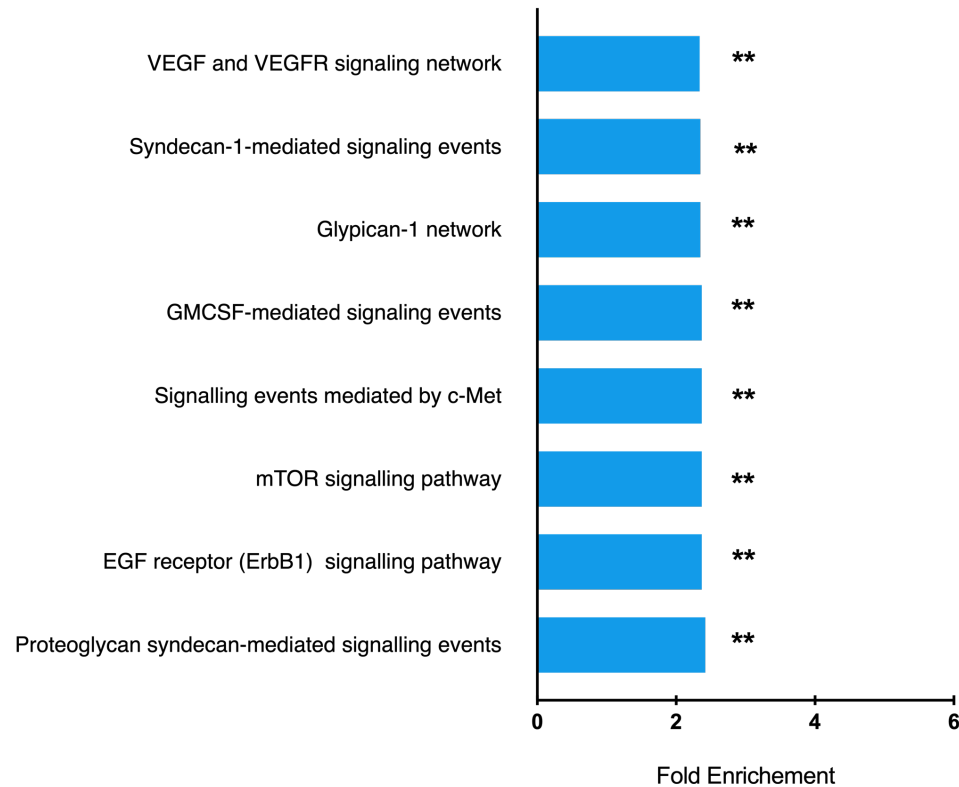


Figure 4.2. Top 10 biological pathways provided by FunRich for proteins associated with HS-GAG chains in HEP111 treated vesicles. (A) Bars indicate the possible biological pathways regulated by proteins lost following HEP111-treatment of DU145 EVs (proteins ≤ 2 -fold change; $p < 0.05$). Analysis was performed in FunRich, corrected p-values were used (BH method). * $p < 0.05$, ** $p < 0.01$; (B) List of proteins associated with each individual biological pathway.

B

Biological pathway	Genes Mapped (from input data set)
Interleukin-6 signalling	<i>IL6R</i> ; <i>IL6</i>
PERK regulated gene expression	<i>CXCL8</i> ; <i>CCL2</i>
Chemokine receptors bind chemokines	<i>CCL2</i> ; <i>CXCL11</i> ; <i>CCL4</i> ; <i>CXCL10</i> ; <i>CCL20</i>
IL23-mediated signalling events	<i>CCL2</i> ; <i>CXCL1</i> ; <i>IL18</i> ; <i>IL6</i>
Signalling by Interleukins	<i>IL6R</i> ; <i>KITLG</i> ; <i>IL18</i> ; <i>IL6</i>
Peptide ligand-binding receptors	<i>CXCL8</i> ; <i>CCL2</i> ; <i>CXCL11</i> ; <i>CCL4</i> ; <i>CXCL10</i> ; <i>CCL20</i>
AP-1 transcription factor network	<i>IL6R</i> ; <i>CXCL8</i> ; <i>CCL2</i> ; <i>AXIN1</i> ; <i>MMP1</i> ; <i>EIF4EBP1</i> ; <i>TGFBR2</i> ; <i>IL6</i> ; <i>CYR61</i> ; <i>CA9</i>
Integrin-linked kinase signalling	<i>IL6R</i> ; <i>CXCL8</i> ; <i>CCL2</i> ; <i>AXIN1</i> ; <i>MMP1</i> ; <i>EIF4EBP1</i> ; <i>TGFBR2</i> ; <i>IL6</i> ; <i>CYR61</i> ; <i>CA9</i>
Glypican pathway	<i>GDF15</i> ; <i>IL6R</i> ; <i>FAS</i> ; <i>CXCL8</i> ; <i>CCL2</i> ; <i>AXIN1</i> ; <i>MMP1</i> ; <i>EIF4EBP1</i> ; <i>STAMPB</i> ; <i>CPE</i> ; <i>TGFBR2</i> ; <i>IL6</i> ; <i>CYR61</i> ; <i>LGALS1</i> ; <i>CA9</i> ; <i>MDK</i> ; <i>ABL1</i> ; <i>WIF1</i>
TRAIL signalling pathway	<i>GDF15</i> ; <i>IL6R</i> ; <i>FAS</i> ; <i>CXCL8</i> ; <i>CCL2</i> ; <i>AXIN1</i> ; <i>MMP1</i> ; <i>EIF4EBP1</i> ; <i>STAMPB</i> ; <i>CPE</i> ; <i>TGFBR2</i> ; <i>IL6</i> ; <i>CYR61</i> ; <i>LGALS1</i> ; <i>CA9</i> ; <i>ABL1</i> ; <i>VIM</i>

A



B

Biological Pathway	Genes mapped (from input data set)
Proteoglycan syndecan-mediated signalling events	
EGF receptor (ErbB1) signalling pathway	
mTOR signalling pathway	<i>GDF15; IL6R; FAS; CXCL8; CCL2; AXIN1; MMP1; EIF4EBP1;</i>
Signalling events mediated by c-Met	<i>STAMBP; CPE; TGFBR2; IL6; CYR61; LGALS1; CA9; ABL1</i>
GMCSF-mediated signalling events	
Glypican-1 network	
Syndecan-1-mediated signalling events	
VEGF and VEGFR signalling network	

Figure 4.3. Additional significantly enriched associations (not in the top 10). (A) Figure shows additional biological pathways provided by FunRich data analysis not included in the previous top 10. Fold enrichment and statistical significance are also shown. (B) List of genes associated with each individual biological pathway.

Considering the nature of the three chosen panels provided by Olink to screen the vesicles, it was to be expected that the enrichment analysis would generate pathways that would be highly biased towards pathways related to angiogenesis, inflammation, and oncology overall. For this reason, performing such analysis on arrays that do not provide proteome-wide coverage is open to criticism. To show that the list of differentially expressed proteins obtained from the experiment is identifying genuine biological pathways that are specimen related, and not array related, we tested the functional enrichment analysis using a random protein list. To do this, a randomised list of proteins was put together from across all three Olink panels. For this, the 92 proteins of the three independent panels were merged in one list, with repeated proteins removed, which generated a list of 267 unique analytes. The list was randomised, and the first 48 proteins of this randomly generated list constituted the identifications that were input into FunRich (**Table 4.4**). If the proteins from the original list were genuinely associated with the pathways obtained during functional enrichment analysis, the randomised list of proteins should provide different overall results with a distinct ranked list of biological pathways. Naturally, due to the nature of the chosen arrays, the pathways will always be related with angiogenesis, inflammation, and oncology.

Again, the 6290 genes on the biological pathway background from FunRich were matched against the gene names of the 48 randomly selected proteins, and 32 of these were available in the database (**Table 4.5**). The results provided by the software identify biological pathways that are very different from the ones associated with the original list of targets, with only the TRAIL pathway being commonly shared (**Figure 4.4 A**). However, most of the proteins enriched for the TRAIL pathway are different between the two lists (original and random), which might indicate that this is a pathway regulated by a high number of proteins encompassed within the selected arrays (**Figure 4.4 B**). Overall, this shows that bias imposed by the nature of the arrays is not a significant concern here, increasing our confidence that the biological pathways identified from the previous analysis are likely strongly associated with the HS-GAG associated factors.

Table 4.4. List of randomised proteins and corresponding gene names for the randomised list input in FunRich software for enrichment analysis.

Protein name	Gene name	Protein name	Gene name
TNFRSF4	<i>TNFRSF4</i>	BDNF	<i>BDNF</i>
JAM-A	<i>F11R</i>	CD48	<i>CD48</i>
AR	<i>AR</i>	SHPS-1	<i>SIRPA</i>
MIA	<i>MIA</i>	IFN-gamma	<i>IFNG</i>
GZMB	<i>GZMB</i>	PODXL	<i>PODXL</i>
CXCL10	<i>CXCL10</i>	CD160	<i>CD160</i>
MMP-1	<i>MMP1</i>	PDGF subunit A	<i>PDGFA</i>
VEGF-A	<i>VEGFA</i>	BLM hydrolase	<i>BLMH</i>
GDNF	<i>GDNF</i>	PLC	<i>HSPG2</i>
WFDC2	<i>WFDC2</i>	IL-13	<i>IL13</i>
t-PA	<i>PLAT</i>	TNFRSF14	<i>TNFRSF14</i>
TRANCE	<i>TNFSF11</i>	TGF-alpha	<i>TGFA</i>
IL-10RA	<i>IL10RA</i>	MMP-10	<i>MMP10</i>
DNER	<i>DNER</i>	ERBB4	<i>ERBB4</i>
hK14	<i>KLK14</i>	XPNPEP2	<i>XPNPEP2</i>
AZU1	<i>AZU1</i>	TNFRSF10C	<i>TNFRSF10C</i>
PAI	<i>SERPINE1</i>	IL-15RA	<i>IL15RA</i>
CXCL5	<i>CXCL5</i>	RETN	<i>RETN</i>
CD244	<i>CD244</i>	ABL1	<i>ABL1</i>
ERBB3	<i>ERBB3</i>	PECAM-1	<i>PECAM1</i>
IGFBP-2	<i>IGFBP2</i>	vWF	<i>VWF</i>
EN-RAGE	<i>S100A12</i>	LY9	<i>LY9</i>
SCGB3A2	<i>SCGB3A2</i>	FAS	<i>FAS</i>
ADAM 8	<i>ADAMTS8</i>	IL-10RB	<i>IL10RB</i>

Table 4.5. List of 32 genes identified in the biological pathways database for the randomised list input in FunRich software for enrichment analysis.

Genes identified in biological pathway dataset						
<i>SERPINE1</i>	<i>PLAT</i>	<i>F11R</i>	<i>VEGFA</i>	<i>PECAM1</i>	<i>CD48</i>	<i>IL13</i>
<i>MMP1</i>	<i>CD244</i>	<i>IL10RA</i>	<i>ABL1</i>	<i>VWF</i>	<i>PLAT</i>	<i>MMP1</i>
<i>BDNF</i>	<i>AR</i>	<i>IFNG</i>	<i>TNFRSF10C</i>	<i>GZMB</i>	<i>GDNF</i>	
<i>FAS</i>	<i>TNFSF11</i>	<i>TGFA</i>	<i>ERBB4</i>	<i>ERBB3</i>	<i>PDGFA</i>	
<i>IGFBP2</i>	<i>HSPG2</i>	<i>CD160</i>	<i>BLMH</i>	<i>CXCL10</i>	<i>TNFRSF4</i>	

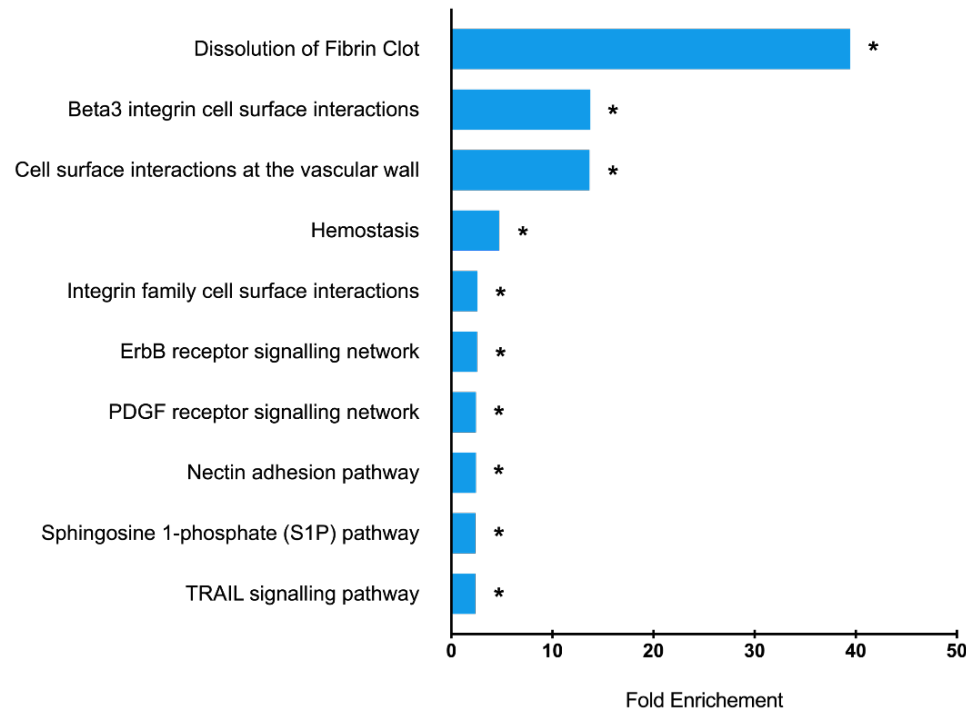
A

Figure 4.4. Functional enrichment analysis of biological pathways by FunRich for list of proteins randomly selected from the cardiovascular III, inflammation, and oncology II panels. (A) Functional enrichment analysis identified biological pathways associated with proteins randomly selected from the three Olink panels. Analysis was performed in FunRich, corrected p-values were used (BH method). * $p < 0.05$. **(B)** List of genes associated with each individual biological pathway.

B

Biological pathway	Genes Mapped (from input data set)
Dissolution of Fibrin Clot	<i>SERPINE1; PLAT</i>
Beta3 integrin cell surface interactions	<i>F11R; VEGFA; PECAM1</i>
Cell surface interactions at the vascular wall	<i>F11R; CD48; MMP1; CD244; PECAM1</i>
Haemostasis	<i>F11R; CD48; SERPINE1; MMP1; CD244; ABL1; PECAM1; VWF; PLAT</i>
Integrin family cell surface interactions	<i>TNFRSF4; BDNF; F11R; AR; IFNG; TNFRSF10C; GZMB; SERPINE1; MMP1; ABL1; VEGFA; PECAM1; GDNF; IL13; PLAT; FAS; TNFSF11; TGFA</i>
ErbB receptor signalling network	<i>TNFRSF4; BDNF; ERBB4; AR; IFNG; TNFRSF10C; GZMB; SERPINE1; MMP1; ABL1; VEGFA; ERBB3; GDNF; IL13; FAS; TNFSF11; TGFA</i>
PDGF receptor signalling network	<i>TNFRSF4; BDNF; AR; IFNG; TNFRSF10C; GZMB; SERPINE1; MMP1; PDGFA; ABL1; VEGFA; GDNF; IL13; FAS; TNFSF11; TGFA</i>
Nectin adhesion pathway	<i>TNFRSF4; BDNF; F11R; AR; IFNG; TNFRSF10C; GZMB; SERPINE1; MMP1; ABL1; VEGFA; GDNF; IL13; FAS; TNFSF11; TGFA</i>
Sphingosine 1-phosphate (S1P) pathway	<i>TNFRSF4; BDNF; AR; IFNG; TNFRSF10C; GZMB; SERPINE1; MMP1; PDGFA; ABL1; VEGFA; GDNF; IL13; FAS; TNFSF11; TGFA</i>
TRAIL signalling pathway	<i>GDNF; IL13; FAS; TNFSF11; TGFA</i>

4.2.3 Selecting protein candidates for validation

Data arising from protein arrays are mostly believed to be reliable, as their development involves extensive testing and validation before being made commercially available. However, given the multiplex nature of the analyses, there is always a possibility for cross-interaction across antibodies leading to false-positive signals. An independent validation of at least some of the identified proteins is warranted.

Different attributes were considered when choosing which of the 48 protein targets should be tested using other methods (**Table 4.6**). The Olink array reports parameters including statistical significance, fold-change and signal strength, which were used when selecting targets for further investigation. Signal strength was considered important as a stronger signal would likely increase the probability of detecting the analyte within EV isolations (**Appendix 4.4**). Additionally, very low abundance analytes may be below the detection sensitivities of traditional plate-based ELISA-like systems. For this reason, proteins with high NPX, such as IL-8 (4366 2^{NPX}) and CCL20 (2990 2^{NPX}), were chosen to be validated, and their role in immune-modulating functions also made them interesting targets. MCP-1 and IL-18, despite their low 2^{NPX} values (34 and 28, respectively), had high fold-change between treatment and control conditions (-12.19-fold for MCP-1 and -14.28-fold for IL-18), and together with their role monocyte/macrophage recruitment (MCP-1) and prostate cancer association (IL-18) were considered for further validation. Functional enrichment analysis of biological pathways was also considered, and the association of midkine and CYR61 with the glypican pathway (**Figure 4.2**) made them interesting targets to pursue. 2^{NPX} values of 478 for midkine and 565 for CYR61 suggest that they could potentially be easily detectable on vesicles. Overall, the following proteins were chosen for validation, using commercially available quantitative ELISA kits: IL-18, MCP-1, CXCL10, midkine, CYR61, CSTB, IL-6, CCL20, and IL-8.

Table 4.6. Proteins chosen for further validation by ELISA. Signal strength, p-value, fold-change, and main known function are featured in the table. BH (Benjamini-Hochberg)

Protein	Signal Strength (2^{NPX})	Adjusted p-value (BH method)	Fold Change	Main known function/Role in disease
IL-18	28	<0.0001	-14.28	Pro-inflammatory cytokine. Produced by prostate cancer and secreted in response to interferons (Lebel-Binay et al., 2003).
MCP-1	34	<0.0001	-12.19	One of the key chemokines that regulate migration and infiltration of monocytes/macrophages. Also involved in angiogenesis and tumour progression (Gschwandtner et al., 2019, Salcedo et al., 2000, Loberg et al., 2006).
CXCL10	117	<0.0001	-9.17	Small cytokine belonging to the CXC chemokine family. Involved in chemotaxis of T cells, NK cells, and dendritic cells (Romagnani et al., 2001).
Midkine	478	<0.0001	-2.17	Heparin-binding growth factor. Involved in cancer cell growth, migration, metastasis, and angiogenesis (Kadomatsu et al., 2013, Filippou et al., 2020, Sumi et al., 2002).
CYR61	565	<0.0001	-2.33	It is a secreted extracellular matrix associated protein, also found on cell surface. In prostate cancer, can promote growth, migration, and metastasis, but also contribute to TRAIL-induced cell death (Sun et al., 2008, Franzen et al., 2009).
CSTB	840	<0.0001	-10.86	Cystatin B is an intracellular thiol proteinase inhibitor, and is a tightly binding reversible inhibitor of cathepsins L, H and B. Cathepsins B and L are involved in matrix degradation and cell invasion (Nomura and Katunuma, 2005).
IL-6	860	<0.0001	-2.06	Pro-inflammatory cytokine and an anti-inflammatory myokine. One of the major cytokines in the tumour microenvironment, which reflects strong association with cancer and inflammation (Kumari et al., 2016).
CCL20	2990	<0.0001	-2.25	CCL20 is a key player in the recruitment of inflammatory cells. CCL20 and its receptor CCR6 have been implied in promotion of cancer progression by enhancing cell migration and proliferation (Marsigliante et al., 2013), as well as remodelling of tumour microenvironment by recruiting of immune cells (Beider et al., 2009).
IL-8	4366	<0.0001	-17.24	Pro-inflammatory chemokine. In tumour microenvironment enhances cancer cells proliferation and survival (Lee et al., 2004) and activates endothelial cells to promote angiogenesis (Martin et al., 2009, Li et al., 2003).

4.2.4 ELISA validation of selected proteins in DU145 EVs

DU145 EV isolates were analysed using commercial ELISA kits, in a modified fashion as detailed in Chapter 2 (section 2.5.4). EVs, at doses shown, were added to wells coated with the corresponding capture antibody. After binding and washing, the presence of the analyte was detected using a detection antibody. As EVs were not lysed at any step of these assays, the quantification obtained can be attributed to the detection of protein targets at the vesicle surface, and quantitation was compared to a recombinant analyte in parallel standard curves.

For all the representative assays shown, the ELISAs demonstrated an increase in signal that correlated with input EV dose (**Figure 4.5 A**). Linearity between input dose of EVs and readout is close to 1 for almost every analyte. IL-8, however, exhibited slightly poorer linearity ($R^2=0.8724$). Midkine and CYR61 are amongst the proteins with a higher level detected at the surface of DU145 EVs. For 8 μg of EVs per well, midkine was detected at 67 pg per μg of EVs and CYR61 at 11 pg per μg of EVs present in the sample. Other cytokines were detected at a lower concentration on the EVs surface, reading about 0.2 pg of IL-8 and 0.07 pg of IL-6 per μg of EVs, when 8 μg of EVs were added to the wells. These latter levels are extremely low and are towards the lower limits of sensitivity of these ELISAs. Testing for CXCL10, MCP1, and IL-18 was also performed, but unfortunately, it proved difficult to consistently detect any signal. For these analytes, therefore, they are either not present on the outer EV surface or, if present, are simply below the detection sensitivities of this technique (**Appendix 4.3**). The standard curves for all performed ELISAs are displayed in Chapter 2 (section 2.5.4 -Figure 2.2), indicating the dynamic range and detection limits for each protein. ELISAs were repeated using biological replicates from different batches of isolated EVs to generate data from three independent experiments (**Figure 4.5 B**). Although the absolute quantitation was variable across different batches of EVs there was, however, a consistent relationship between signal and input EV quantity. The large error bars were to be expected when we assess different EV isolates, considering the isolation process is difficult to fully standardise. Furthermore, the loading of such components onto EVs by the parent cells may be highly dynamic, and the regulatory mechanisms behind loading of such components onto EVs are not currently known. Nonetheless, it is clear that EVs display on their surface different levels of these analytes, with midkine and CYR61 appearing consistently as the more abundant of these tested.

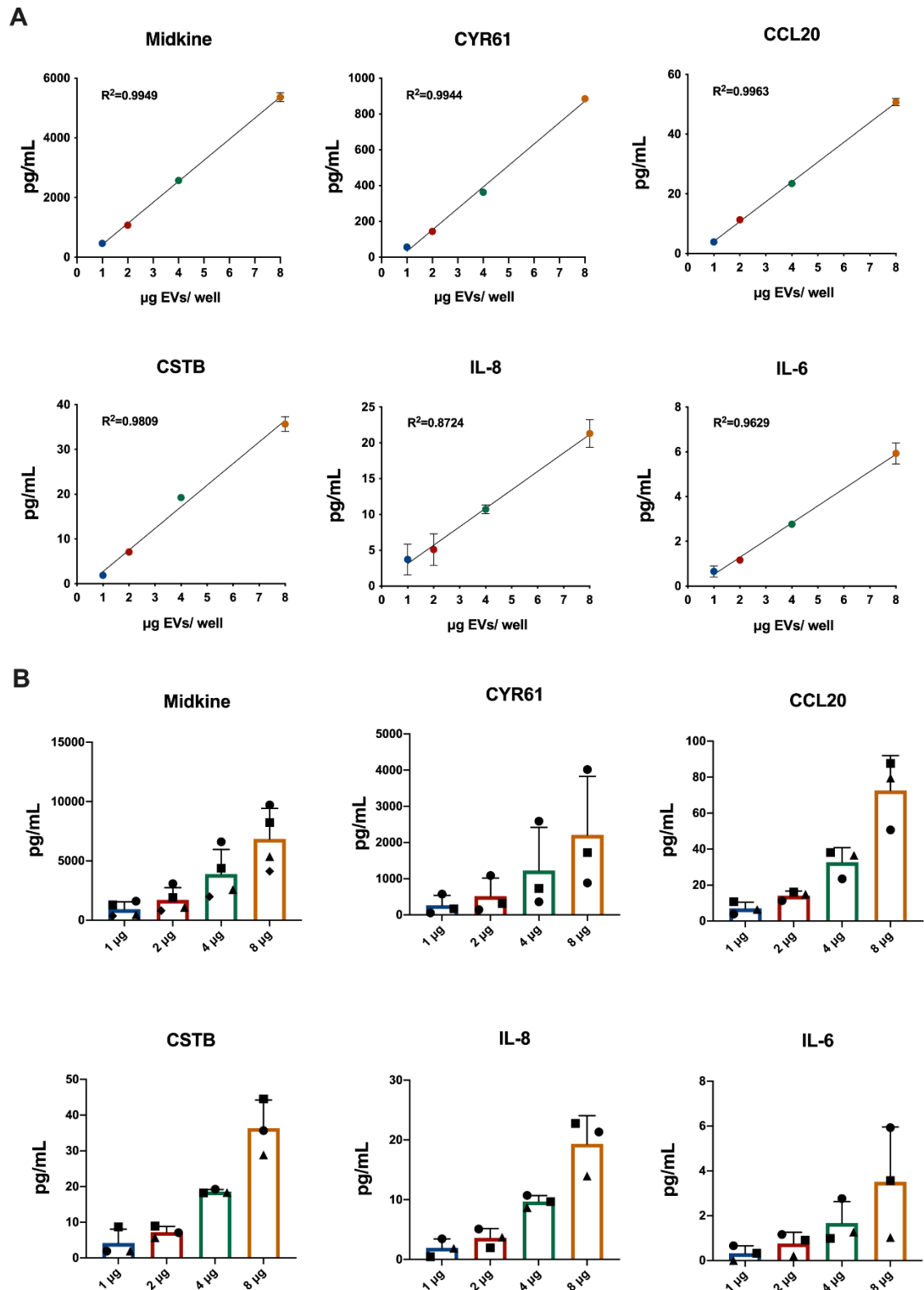


Figure 4.5. Validation of selected proteins detectable on the EV surface. (A) The graphs show best fit curve and R² values for an performed for the specified proteins on a single EV isolate. The dots correspond to mean \pm SD for concentrations (pg/mL) of protein detected at the surface of 8 μ g, 4 μ g, 2 μ g and 1 μ g of DU145 EVs per 100 μ L/well, in triplicate wells **(B)** Bar graphs show the mean \pm SEM of 3 independent experiments each based on a different EV isolation and represented by circle, square or triangle. The quantification (pg/mL) per of protein detected at the surface of DU145 EVs on 8 μ g, 4 μ g, 2 μ g and 1 μ g per 100 μ L/well is represented. Every independent experiment was performed in triplicate wells.

4.2.5 ELISA validation of selected proteins in HEP111-treated EVs

After assessing detectable protein expression by ELISA on DU145 derived EVs, the next step was to enquire whether selected growth factors were indeed tethered to the EVs surface by HS-GAGs.

For this set of experiments, control EVs (either treated with no enzyme or heat-inactivated HEP111) were compared with active HEP111-treated EVs. The heat-inactivated HEP111 control was included to account for the potential interference of having HEP111 enzyme present in the system. Production of large quantities of such samples is always problematic, and thus the input into each ELISA well was reduced slightly to accommodate these limitations. In these assays, therefore, 4 µg of vesicles were used per well for ELISA analysis. As previously, EVs were not lysed before the assay so that any detectable signal could be attributed to proteins on the surface of EVs.

A representative experiment in **Figure 4.6 A** for midkine and CYR61 shows that removal of HS-GAG chains is indeed associated with a loss of signal when compared with controls. Midkine and CYR61 were found to be strongly present at the surface of EVs, and the difference between untreated EVs and those treated with heat-inactivated HEP111 are small. Nonetheless, introducing a biologically active enzyme, in an otherwise identical system, attenuates the signal by approximately 52% for midkine and 30% for CYR61. A representative experiment for CSTB, CCL20, and IL-8 is also shown in **Figure 4.6 A**. For most of these readouts, except CYR61, there appeared to be a small but significant influence of inactive enzyme on the signal, hence this was an important control to include. Therefore, assessment of a true HEP111-mediated loss of signal is needed to account for this unexplained signal attenuation by the inactive enzyme. In this fashion midkine, CYR61, and IL-8 were lost below the level of this control, indicating they are indeed dependent on HS-GAG chains for EV attachment. Biological repeats of the ELISA assay for midkine and CYR61 on different EV isolates resulted in the variability issue as expected, where absolute concentrations between repeats were dissimilar. Nonetheless, for each individual EV batch, the trend is clearly the same, with a lower signal detected for EVs treated with the active form of HEP111 enzyme (**Figure 4.6 B**). One EV batch failed to show this trend for the IL-8 ELISA; however, this may be a technical measurement issue as the same batch was in agreement with the expected trend for the other two analytes. A reason to explain the difficulty in validating HS-GAG associations

is the comparative sensitivity of Olink in relation to the ELISA used. Olink is extremely sensitive and detects differences at sub picogram level, and such differences cannot be picked up at the same level when using a less sensitive technique such as an ELISA. For that reason, differences that were detected using the PEA technology cannot be entirely satisfactorily replicated here.

To conclude, many factors identified by the Olink array are quantifiable factors associated with purified vesicles. However, in the context of an ELISA, some analytes were below the detection sensitivity of the technique and could not be confirmed as EV-associated nor HS-GAG related factors. Nevertheless, we present here strong evidence that the novel factors midkine, CYR61 and IL-8 are located at the EV outer surface in association with HS-GAG chains.

A

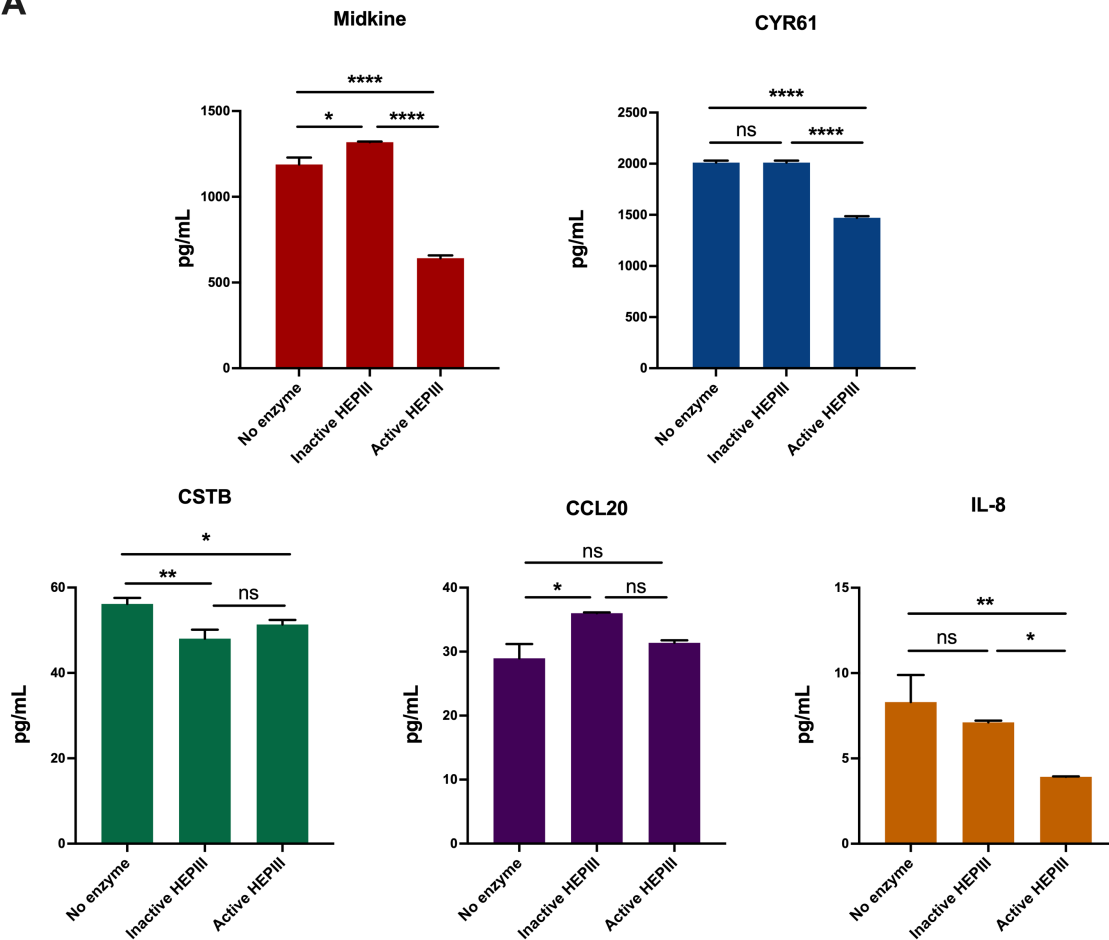


Figure 4.6 A. Impact on protein concentration upon HS-chains removal from DU145 vesicles. ELISA was performed in intact EVs to assess protein detection on vesicle surface. The bar graphs show mean \pm SD of triplicate wells for the quantification (pg/mL) of midkine (red), CYR61 (blue), CSTB (green), CCL20 (purple) and IL-8 (mustard), per 4 μ g of untreated (no enzyme), heat-inactivated HEP111 and active HEP111 treated EVs. A representative experiment is shown. **** $p < 0.001$; ** $p < 0.01$; * $p < 0.05$; ns=not significant one-way ANOVA with Tukey's multiple comparison.

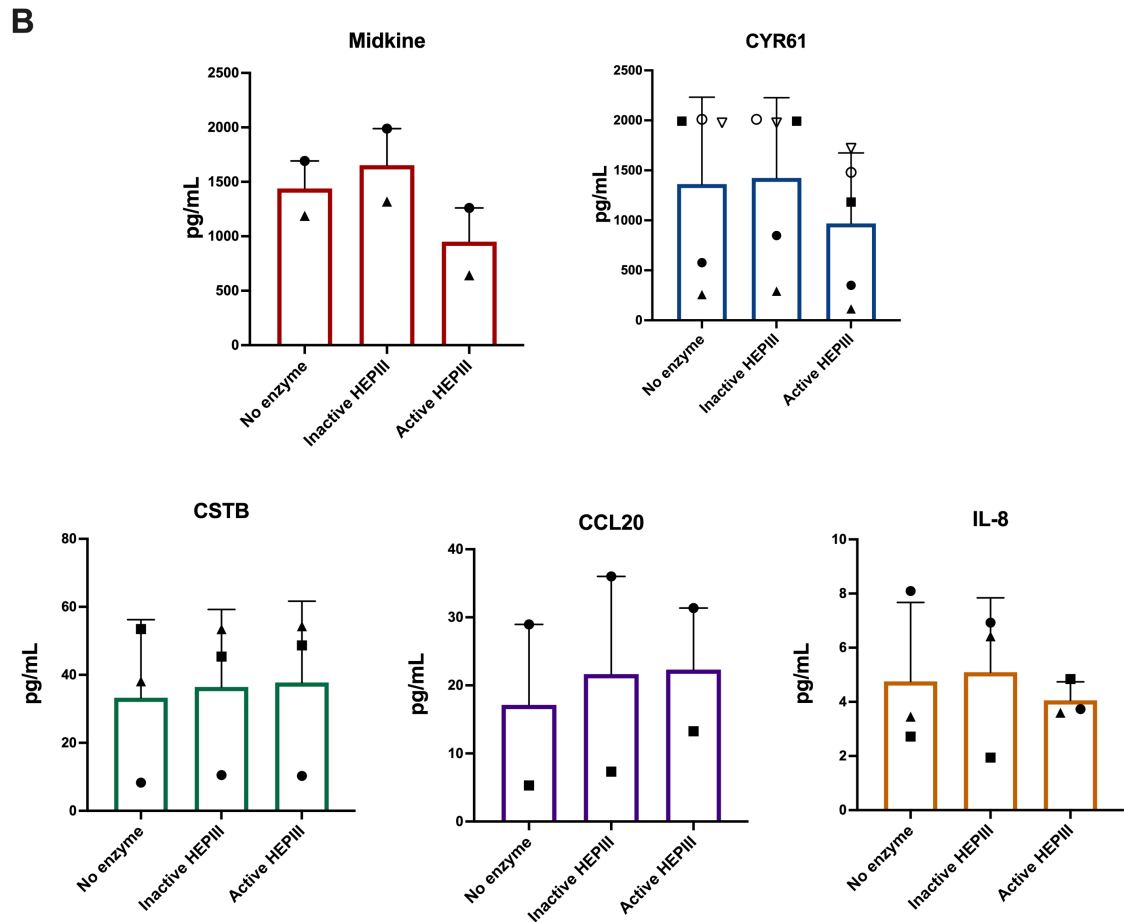


Figure 4.6 B. Impact on protein concentration upon HS-chains removal from DU145 vesicles. Bar graphs show the mean \pm SEM of at least 2 independent ELISA, performed on triplicate wells, each based on a different EV HEP111 digestion and represented by circle, triangle and square. The quantification (pg/mL) of midkine (red), CYR61 (blue), CSTB (green), CCL20 (purple) and IL-8 (mustard), per 4 μ g of untreated (no enzyme), heat-inactivated HEP111 and active HEP111 treated EVs is represented.

4.2.6 Perturbation of HSPG core proteins on vesicles and their impact on EV-associated factors

To understand if individual membrane-associated HSPGs are required for tethering specific proteins to the EV surface, we screened EVs isolated from NMC DU145 cells and from DU145 cells that had been subjected to HSPG-knockdown via shRNA-transduction. These aimed to span the relevant repertoire of membrane-associated HSPGs expressed by the cells. Relevant HSPGs included syndecan -3 (SDC3) and -4 (SDC4), glypican-1 (GPC1) and -6 (GPC6), and betaglycan (BGLY). The validation work and establishing stable HSPG knockdowns was performed by Dr Jason Webber. Isolated EVs were analysed using the Olink PEA technology and the same three panels (Proseek

Chapter 4 - Results

Multiplex Cardiovascular Panel III, Inflammation Panel and Oncology Panel II) previously mentioned. Proteins present within HSPG-deficient EV samples were compared to those present in NMC EV samples. These represent DU145 cells that had been successfully transduced by lentivirus, carrying an irrelevant shRNA sequence. The number of growth factors from each panel included in the analysis is summarised in **Tables 4.7, 4.8 and 4.9**.

Table 4.7. Number of growth factors from cardiovascular III panel included in analysis. LOD (limit of detection). NM (Non mammalian). *Proteins not included in the analysis due to low limit of detection in all samples.

Cardiovascular III panel					
HSPG-deficiency	Excluded from analysis*	Total Analysed	Above LOD	Below LOD	
				HSPG-def	NM Control
Betaglycan	43	49	40	5	4
Syndecan-3	40	52	41	4	7
Syndecan-4	42	50	40	5	5
Glypican-1	43	49	41	4	4
Glypican-6	43	49	40	5	4

Table 4.8. Number of growth factors from inflammatory II panel included in analysis. LOD (limit of detection). NM (Non mammalian). *Proteins not included in the analysis due to low limit of detection in all samples.

Inflammatory Panel					
HSPG-deficiency	Excluded from analysis*	Total Analysed	Above LOD	Below LOD	
				HSPG-def	NM Control
Betaglycan	18	74	51	13	10
Syndecan-3	17	75	55	9	11
Syndecan-4	20	72	51	13	8
Glypican-1	13	79	55	9	15
Glypican-6	21	71	51	13	7

Table 4.9. Number of growth factors from oncology II panel included in analysis. LOD (limit of detection). NM (Non mammalian). *Proteins not included in the analysis due to low limit of detection in all samples.

Oncology II Panel					
HSPG-deficiency	Excluded from analysis*	Total Analysed	Above LOD	Below LOD	
				HSPG-def	NM Control
Betaglycan	9	83	72	8	3
Syndecan-3	8	84	72	8	4
Syndecan-4	10	82	72	8	2
Glypican-1	7	85	72	8	5
Glypican-6	10	82	72	8	2

The arbitrary thresholds ($FC \pm 2$; $p < 0.05$) to identify differentially expressed proteins were applied as before. The total number of differential proteins is shown in **Table 4.10**. The specific lists of proteins increased and decreased for each HSPG-deficient core protein are represented in **Table 4.11**.

Targeting different HSPG proteins in DU145 cells results in the production of EVs with distinctive protein profiles. In section 4.2.1 of this chapter, 48 of the analysed factors were shown to be lost when HS-side chains are removed from EVs, and this is what was expected from the enzymatic digestion and wash approach. In the current experiment, and perhaps not entirely anticipated, the data revealed that whilst there are several examples of lost factors, in most cases, there was also a number of elevated factors associated with each HSPG-deficient vesicle type (**Table 4.11** and **Figure 4.7**). Overall, removing BGLY core protein from EVs was associated with the lower number of analytes increasing (13 proteins) and seems to be the modification that least affects protein changes in general. Removal of SDC3, on the other hand, seems to be associated with the greatest diversity in elevated proteins (56 proteins) (**Figure 4.7 A, B, C** and **Table 4.10**). As before, signal strength of the analytes on the differentially expressed target list was utilised as an estimate of the abundance of these proteins on the vesicles, to be later taken into consideration when selecting protein targets for downstream validation (**Appendix 4.4**).

Table 4.10. Number of proteins increased and decreased in each specific HSPG-deficiency. Arbitrary thresholds $FC \pm 2$, $p < 0.05$. BGLY-def (betaglycan-deficient EVs), SDC3-def (syndecan-3-deficient EVs), SDC4-def (syndecan-4-deficient EVs), GPC1-def (glypican-1-deficient EVs), GPC6-def (glypican-6-deficient EVs).

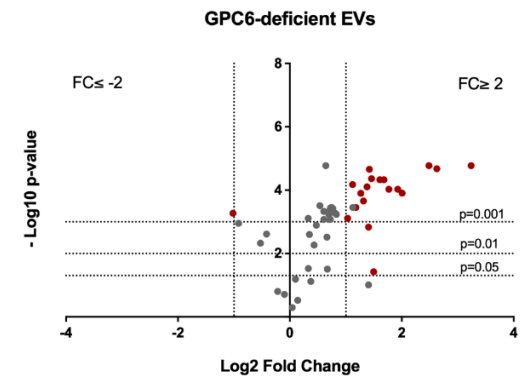
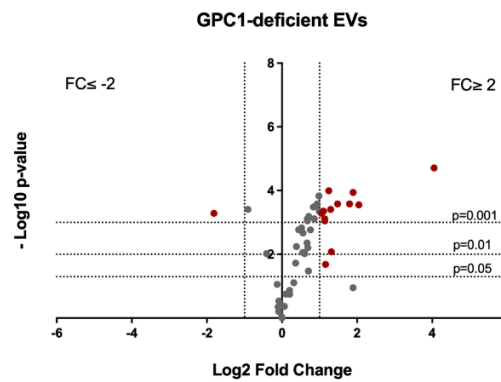
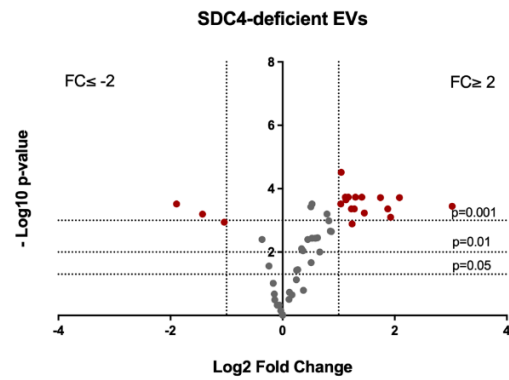
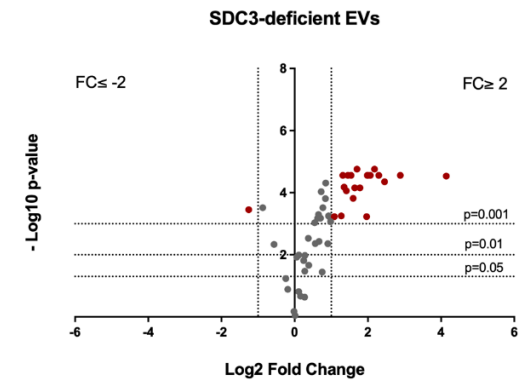
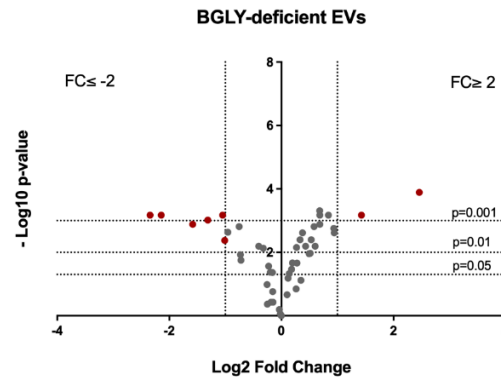
	BGLY-def	SDC3-def	SDC4-def	GPC1-def	GPC6-def
Increased	13	56	40	39	47
Decreased	14	10	8	4	8
Total	27	66	48	43	55

Table 4.11. Proteins increased and decreased for each specific HSPG-deficiency. Arbitrary thresholds $FC \pm 2$, $p < 0.05$.

HSPG-deficiency	Proteins	
	Increased	Decreased
Betaglycan	GDF-15; t-PA; TRAIL; TGF-alpha; MMP-1; Beta-NGF; IL-24; MSLN; TNFSF13; VEGFR-2; PVRL4; WFDC2; WIF-1	LDL receptor; LTBR; CNTN1; TFPI; TR; TNFR1; MCP-1; DNER; CYR61; CA9; ABL1; TNFRSF19; MIC-A; MIC-B
Syndecan-3	ITGB2; ALCAM; CSTB; Gal-3; GRN; BLM hydrolase; PLC; Notch 3; TIMP4; TNFRSF10C; GDF-15; IL-6RA; AXL; FAS; MB; SHPS-1; CASP-3; t-PA; SCGB3A2; EGFR; LAP TGF-beta-1; IL-6; TRAIL; SCF; IL-18; TGF-alpha; MMP-1; LIF-R; IL-22 RA1; PD-L1; TNF; SIRT2; CCL28; LIF; ST1A1; CSF-1; CPE; CEACAM1; MSLN; TNFSF13; EGF; TNFRSF6B; TGFR-2; hK8; PODXL; S100A4; ERBB3; PVRL4; GPNMB; DLL1; TLR3; VIM; CXL17; WFDC2; ADAM-TS 15; WIF-1	TFPI; CDCP1; AXIN1; VEGF-A; HGF; 5'-NT; LYN; TNFRSF19; MUC-16; FR-alpha
Syndecan-4	TNFRSF14; ITGB2; CSTB; Gal-3; PLC; Notch 3; TNFRSF10C; GDF-15; AXL; FAS; MB; TNFSF13B; CTSD; ST2; t-PA; EGFR; IL-6; TRAIL; TGF-alpha; TNFSF14; MMP-1; LIF-R; IL-22 RA1; PD-L1; LIF; CPE; CEACAM1; MSLN; TNFSF13; EGF; TNFRSF6B; TGFR-2; hK8; PVRL4; GPNMB; ESM-1; WFDC2; ADAM-TS 15; CD70; WIF-1	CNTN1; TFPI; MCP-1; AXIN1; HGF; CA9; ABL1; LYN
Glypican-1	ITGB2; OPG; ALCAM; MCP-1; BLM hydrolase; LTBR; GDF-15; IL-6RA; AXL; MB; CTSD; t-PA; PDGF subunit A; IL-8; GDNF; CD244; LAP; TGF-beta-1; IL-6; OSM; MMP-1; HGF; MMP-10; TNF; MIP-1 alpha; CXCL6; CXCL10; LIF; TWEAK; CCL20; TNFRSF6B; TGFR-2; VEGFR-2; PODXL; S100A4; GPNMB; DLL1; TNFRSF19; CXL17; CD70	CNTN1; DNER; GPC1; TFPI-2
Glypican-6	ITGB2; IL-17RA; TNF-R2; ALCAM; GRN; PLC; TNFRSF10C; GDF-15; IL-6RA; PI3; AXL; FAS; MB; CTSD; SHPS-1; t-PA; EGFR; CTSZ; TNF-R1; LAP TGF-beta-1; IL-6; TRAIL; TGF-alpha; MMP-1; IL-22 RA1; PD-L1; HGF; MMP-10; CPE; CEACAM1; EGF; TNFRSF6B; TGFR-2; GPC1; VEGFR-2; PODXL; S100A4; PVRL4; Gal-1; GPNMB; DKN1A; DLL1; TNFRSF19; ESM-1; WFDC2; CD70; WIF-1	TFPI; CDCP1; DNER; VEGF-A; 5'-NT; ABL1; LYN; FR-alpha

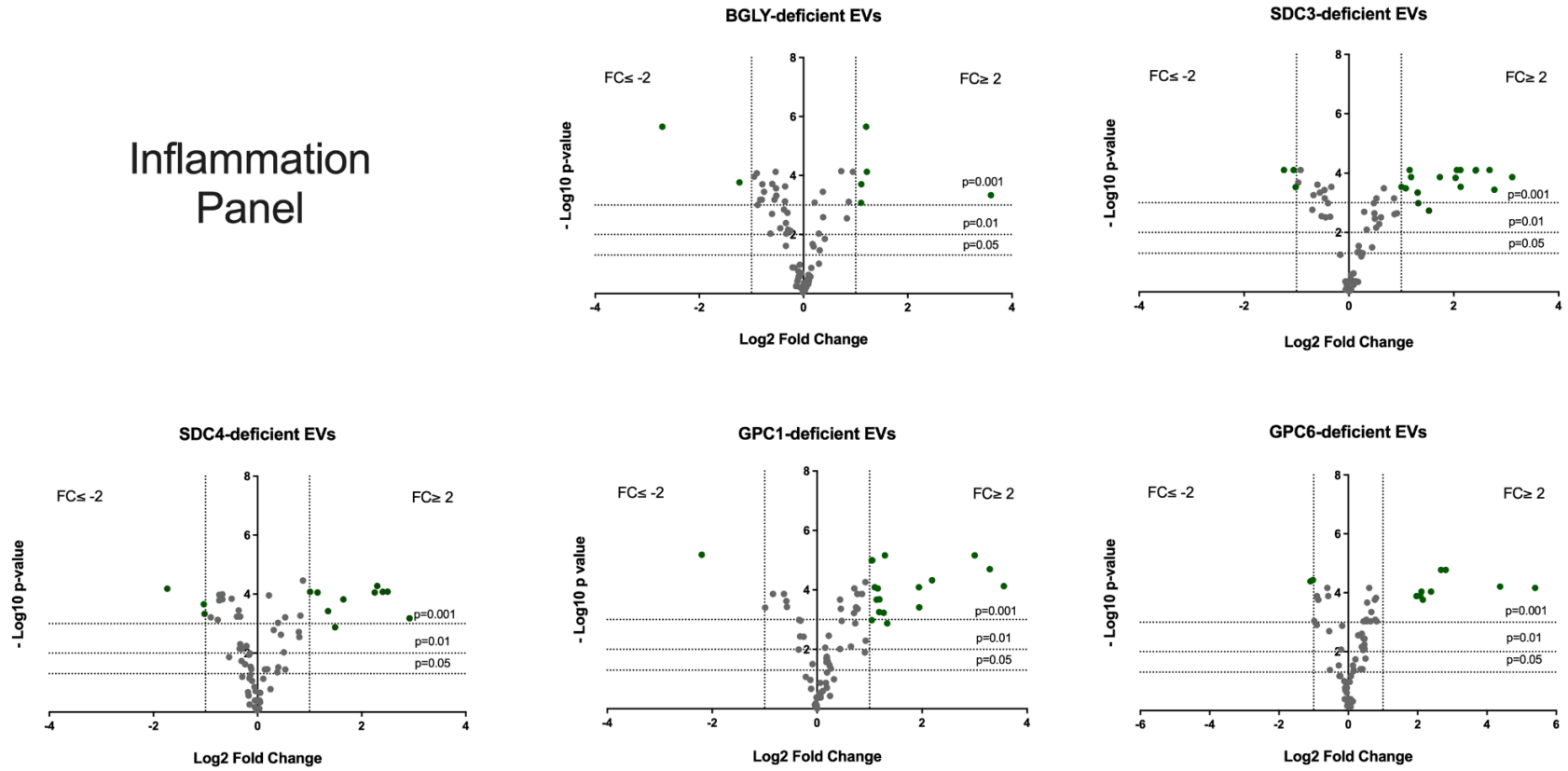
A

Cardiovascular III
Panel



B

Inflammation Panel



C

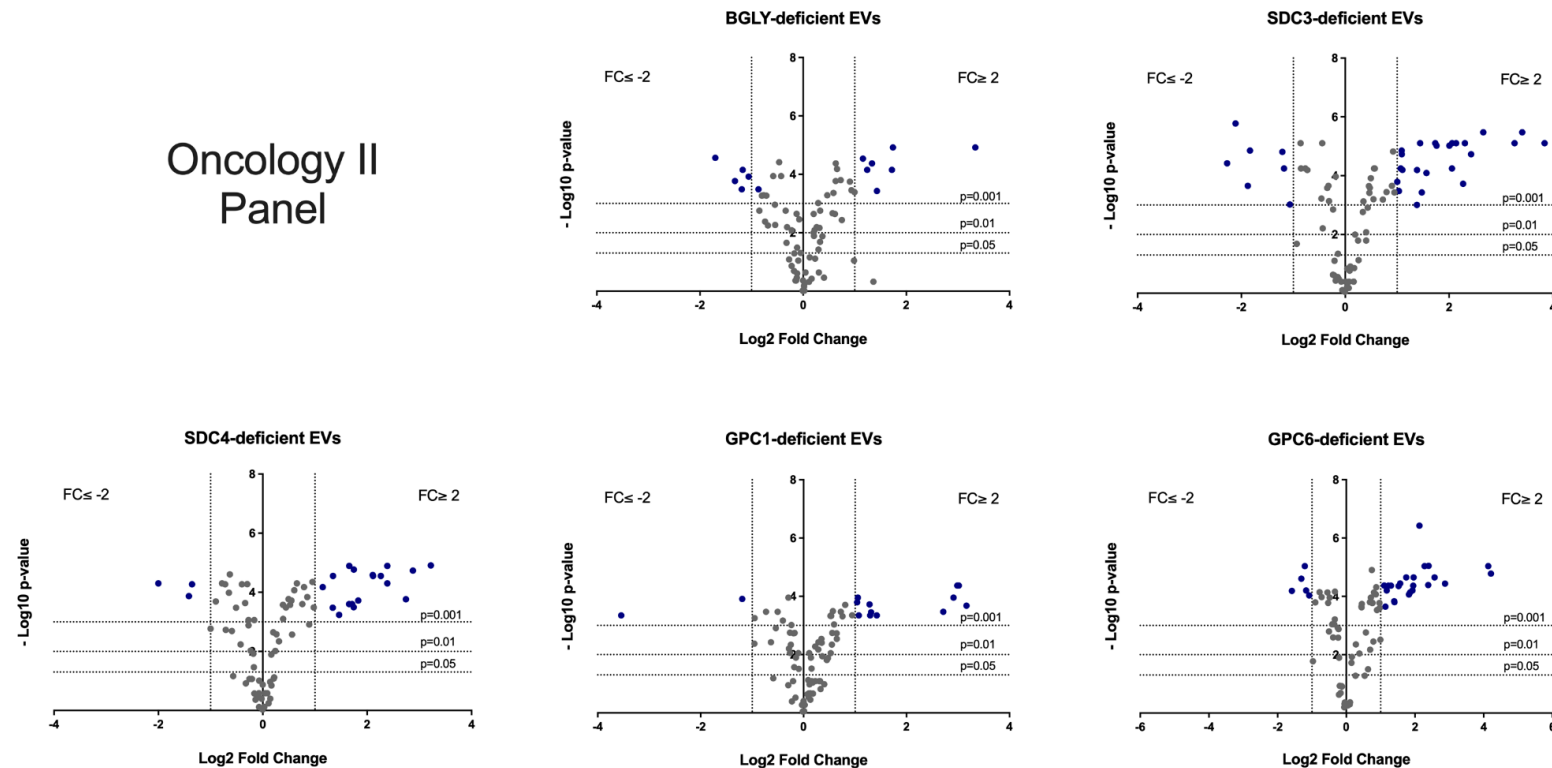
Oncology II
Panel

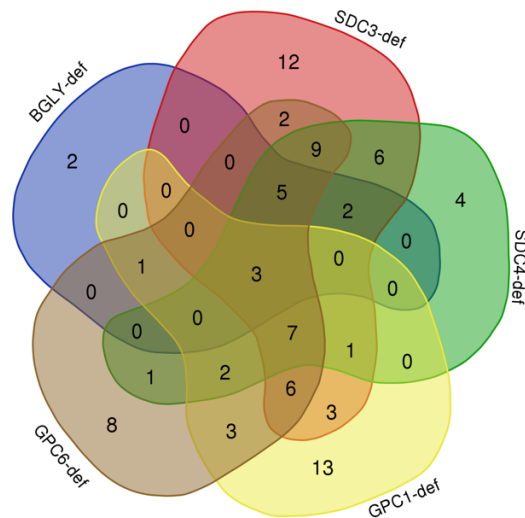
Figure 4.7. Removal of specific HSPGs from DU145 vesicles produces vesicles with distinct protein profiles. A proximity extension assay by Olink was used to detect proteins on DU145 derived vesicles treated with active HEP1III compared to control EVs treated with heat-inactivated HEP1III. Volcano plots for the cardiovascular III panel (A), inflammation panel (B) and oncology II panel (C), identify differentially expressed proteins with $\text{FC} \leq -2$; analytes decreased following HEP1III-digestion and $\text{FC} \geq 2$; analytes increased following HEP1III digestion. Lines demark the statistical significance for proteins with $p < 0.05$, $p < 0.01$ and $p < 0.001$ (t-test, corrected for multiple testing using Benjamini-Hochberg adjustment). Red (A), green (B) and blue (C) dots show proteins which have significant decreases. Grey dots symbolize proteins below specified threshold criterion. (D, E, F) Bar graph shows the suggested relative abundance, conferred by signal strength, of the significantly altered analytes. Data shown represents the mean of $n=3$ replicates. NPX= Normalised Protein eXpression. BGLY (betaglycan), SDC3 (syndecan-3), SDC4 (syndecan-4), GPC1 (glypican-1), GPC6 (glypican-6).

4.2.7 Analysis of EV changes due to HSPG core protein loss

The loss of specific HSPGs correlates with an alteration of EV-associated protein cargo. To illustrate the similarities and differences between the different lists of proteins associated with particular HSPGs, Venn diagrams were generated. These identify the overlap in elevated factors (**Figure 4.8**) and factors decreased (**Figure 4.9**) following loss of specific EV-associated HSPGs. This helps to determine the association of certain proteins with specific HSPGs and may help us understand how the removal of individual HSPGs might impact EV function.

Figure 4.8 shows a Venn diagram displaying the relations between the sets of proteins increased in the different HSPG-deficient vesicles. While some proteins, such as GDF-15, MMP-1, and tissue plasminogen activator (t-PA) seem to be increased in all vesicles, irrespective of HSPG-deficiency, others appear to be increased in response to loss of a specific HSPG, such as IL-18 for vesicles lacking SDC3, and CCL20 for those lacking GPC1 (**Figure 4.8 B**).

The relative magnitude of change was also briefly considered for three analytes GDF-15, MMP-1, and t-PA (**Table 4.12**), depicting the fold elevation associated with loss of specified HSPGs. Although there is currently incomplete understanding here, these three analytes were increased following loss of any of the five HSPGs tested, to varying magnitudes. The data suggest that GPC1 is a strong negative regulator of GDF-15 inclusion into EVs, and for MMP-1 there is a strong negative regulator by GPC6 (remind the reader that GPC6 knockdown also attenuated GPC1 expression, and this might not be a GPC6-specific association). Inclusion of t-PA seems to be similarly affected, independent of HSPG, with a stronger effect in vesicles lacking SDC4. Such preliminary observations will, of course, require some substantive follow up to assess whether or not these statements hold true. Still, the data highlight the complexity of the experimental findings and the challenge ahead in addressing the roles of HSPG in dictating the EV-proteome.

A**B**

HSPG-modification in EVs	Associated increased proteins
BGLY-def GPC1-def GPC6-def SDC3-def SDC4-def	GDF-15; MMP-1; t-PA
GPC1-def GPC6-def SDC3-def SDC4-def	GNPMB; TGFR-2; IL-6; ITGB2; TNFRSF6B; MB; AXL
BGLY-def GPC6-def SDC3-def SDC4-def	PVRL4; WIF-1; TRAIL; WFDC2; TGF-alpha
GPC1-def SDC3-def SDC4-def	LIF
GPC6-def SDC3-def SDC4-def	CEACAM1; PD-L1; PLC; TNFRSF10C; IL-22 RA1; EGFR; EGF; MB; CPE; FAS
BGLY-def SDC3-def SDC4-def	TNFSF13; MSLN;
GPC1-def GPC6-def SDC4-def	CD70; CTSD
GPC1-def GPC6-def SDC3-def	LAP TGF-beta-1; S100A4; PODXL; IL-6RA; ALCAM; DLL1
BGLY-def GPC1-def GPC6-def	VEGFR-2
SDC3-def SDC4-def	hK8; CSTB; ADAM-TS 15; LIF-R; Notch-3; Gal-3
GPC6-def SDC4-def	ESM-1
GPC1-def SDC3-def	CXL17; TNF; BLM hydrolase
GPC6-def SDC3-def	SHPS-1; GRN
GPC1-def GPC6-def	TNFRSF19; HGF; MMP-10
SDC4-def	TNFSF13B; ST2; TNFRSF14; TNFSF14
SDC3-def	SCGB3A2; CSF-1; ST1A1; TIMP4; TLR3; SIRT2; SCF; IL-18; CCL28; VIM; CASP-3; ERBB3
GPC1-def	GNDF; IL-8; CXCL10; CXCL6; MIP-1 alpha; CCL20; TWEAK; LTBR; PDGF subunit A; OSM; MCP-1; CD244; OPG
GPC6-def	PI3; CTSZ; Gal-1; TNF-R1; IL-17RA; GPC1; TNF-R2; DKN1A;
BGLY-def	Beta-NGF; IL-24

Figure 4.8. Venn diagram and list showing the associations between proteins elevated in HSPG-deficient vesicles. (A) Proteins elevated in HSPG-deficient vesicles, were combined in a Venn diagram to better demonstrate the associations between proteins and particular HSPGs. **(B)** Association between proteins and particular HSPGs can be seen in here. BGLY-def (betaglycan-deficient EVs), SDC3-def (syndecan-3-deficient EVs), SDC4-def (syndecan-4-deficient EVs), GPC1-def (glypican-1-deficient EVs), GPC6-def (glypican-6-deficient EVs).

Table 4.12. Calculated fold increase for GDF-15, MMP-1 and t-PA relative to non-mammalian control EVs. BGLY-def (betaglycan-deficient EVs), SDC3-def (syndecan-3-deficient EVs), SDC4-def (syndecan-4-deficient EVs), GPC1-def (glypican-1-deficient EVs), GPC6-def (glypican-6-deficient EVs).

	Calculated Fold Increase		
	GDF-15	MMP-1	t-PA
BGLY-def	5.50	12.09	2.69
SDC3-def	4.54	4.17	2.12
SDC4-def	2.43	7.57	8.13
GPC1-def	16.57	11.77	4.13
GPC6-def	9.45	41.89	4.02

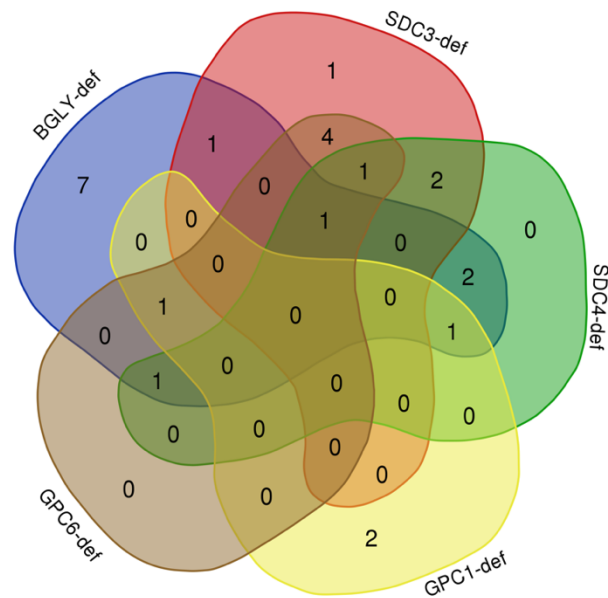
The relations between the proteins decreased across all HSPG-deficient vesicles is depicted in the Venn diagram in **Figure 4.9**. None of the proteins were decreased in all HSPG-deficient EVs. Amongst the different HSPGs-deficient vesicles, lack of GPC1 appears to be the only condition not associated with decrease of TFPI in EVs. However, GPC1 is related to a decrease in TFPI-2 (**Figure 4.9 B**), a tissue factor inhibitor, paralog of TFPI. This might point to a different function promoted by GPC1 in association with this protein or in regulating its incorporation into EVs. Overall, TFPI is one of the proteins with higher signal strength and is likely, therefore, to be a real and validatable factor (**Appendix 4.4**). Removal of betaglycan has the highest impact on decreasing TFPI association with vesicles with a 5.07-fold decrease (**Table 4.13**). Of additional note, GPC1 was part of the Olink panel coverage, and its deficiency was measured on EVs taken from GPC1-deficient cells, confirming that this knockdown is valid and as expected and that the PEA technology is able to detect known alterations to EVs.

BGLY-, GPC6-, and SDC4-deficient EVs all share a common protein, tyrosine-protein kinase ABL1 (ABL1), which is decreased following loss of any of these HSPGs (**Figure 4.9 B**). This protein is also decreased in the HEP3III-treated vesicles (**Figure 4.2 F**), however, in a much more accentuated way (almost 90% lost) (**Table 4.13**). This perhaps points to an interesting finding, whereby ABL1 binds more abundantly to HS chains of SDC4, GPC6, and BGLY, rather than binding to the HSPG core protein directly. Similarly, CYR61 is another protein decreased in vesicles after HEP3III treatment (**Figure 4.2 C, F**) as well as vesicles lacking BGLY (**Figure 4.9 B**). Considering that the magnitude of decrease, both in HEP3III-treated and BGLY-deficient vesicles, is similar (**Table 4.13**), this might suggest an important and exclusive association of CYR61 with BGLY related HS-chains, as different strategies of modifying HSPGs on vesicle surface offer a similar

result. Of course, there is an awareness that the HEP111 treatment is compared to a control different than the one used on HSPG-deficiency work. So, to make these comparisons, it is assumed that EVs treated with heat-inactivated enzyme are somewhat similar to EVs derived from NMC cells.

This data set shows that modification of HSPGs on EVs alters the protein cargo of the vesicles, and this is somewhat related with the particular HSPG that is altered on the EV. Lack of specific HSPGs can be associated with either upregulation or downregulation of distinct proteins, and surprisingly and unexpectedly, removal of HSPGs from vesicle surface is related with a higher number of upregulated proteins. This might be related with compensatory mechanisms during EV-biogenesis that we are not completely aware of, and further studies would be necessary to comprehend these findings.

A



B

HSPG-modification	Associated decreased proteins
BGLY-def GPC6-def SDC3-def SDC4-def	TFPI
GPC6-def SDC3-def SDC4-def	LYN
BGLY-def GPC1-def SDC4-def	CNTN1
BGLY-def GPC6-def SDC4-def	ABL1
BGLY-def GPC1-def GPC6-def	DNER
SDC3-def SDC4-def	HGF; AXIN1
BGLY-def SDC4-def	CA9; MCP-1
GPC6-def SDC3-def	5'-NT; VEGF-A; CDCP1; FR-alpha
BGLY-def SDC3-def	TNFRSF19
SDC3-def	MUC-16
GPC1-def	GPC1; TFPI-2
BGLY-def	TNF-R1; LDL receptor; MIC-A; MIC-B; LTBR; CYR61

Figure 4.9. Venn diagram and table showing the associations between proteins decreased in HSPG-deficient vesicles. (A) Proteins decreased in HSPG-deficient vesicles were combined in a Venn diagram to better demonstrate the associations between proteins and particular HSPGs. **(B)** Association between proteins and particular HSPGs can be seen in here. BGLY-def (betaglycan-deficient EVs), SDC3-def (syndecan-3-deficient EVs), SDC4-def (syndecan-4-deficient EVs), GPC1-def (glypican-1-deficient EVs), GPC6-def (glypican-6-deficient EVs).

Table 4.13. Calculated fold decrease for CYR61, TFPI and ABL1. BGLY-def (betaglycan-deficient EVs), SDC3-def (syndecan-3-deficient EVs), SDC4-def (syndecan-4-deficient EVs), GPC1-def (glypican-1-deficient EVs), GPC6-def (glypican-6-deficient EVs).

Calculated Fold Decrease			
	CYR61	TFPI	ABL1
BGLY-def	2.25	5.07	2.08
SDC3-def		2.38	
SDC4-def		3.71	2.56
GPC1-def			
GPC6-def		2.02	2.12
HEPIII digested	2.32		8.3

4.2.8 Functional enrichment analysis of the of HSPG-deficient EVs

Using the new data, biological pathways related to the identified differentially regulated proteins were explored as previously. However, since the lists of EV proteins attributable to individual HSPGs (**Table 4.11**) incorporate very few protein IDs, functional enrichment analysis using a program such as FunRich gives limited outputs, difficult to interpret. Therefore, a master list was generated to include all proteins, either increased or decreased across all HSPG-deficient conditions, with arbitrary thresholds of $p < 0.05$ and a ± 2 -FC. This way, unfortunately, enrichment analysis does not allow the establishment of associations between a specific individual HSPG core protein and the influence it could have in a particular biological pathway. Instead, it sheds some light into possible pathways that are associated with the EV-expressed HSPGs in a more general sense.

From this analysis, a list of 108 unique proteins was put together, and names were converted into gene names to be input into the FunRich software (**Table 4.14**). From these 108 proteins converted in the respective gene IDs, 70 genes (**Table 4.15**) were identified within the 6290 genes present in the dataset background of FunRich regarding biological pathways.

Table 4.14. List of proteins and corresponding gene name input in FunRich software for enrichment analysis.

Protein name	Gene name	Protein name	Gene name	Protein name	Gene name
TFPI	<i>TFPI</i>	IL-6RA	<i>IL6R</i>	PVRL4	<i>PVRL4</i>
CDCP	<i>CDCP</i>	AXL	<i>AXL</i>	GPNCMB	<i>GPNCMB</i>
AXIN1	<i>AXIN1</i>	FAS	<i>FAS</i>	DLL1	<i>DLL1</i>
HGF	<i>HGF</i>	MB	<i>MB</i>	TLR3	<i>TLR3</i>
VEGF-A	<i>VEGFA</i>	SHIPS-1	<i>SIRPA</i>	VIM	<i>VIM</i>
5'-NT	<i>NT5E</i>	CASP-3	<i>CASP3</i>	CXCL17	<i>CXCL17</i>
LYN	<i>LYN</i>	t-PA	<i>PLAT</i>	WFDC2	<i>WFDC2</i>
TNFRSF19	<i>TNFRSF19</i>	SCGB3A2	<i>SCGB3A2</i>	ADAM-TS 15	<i>ADAMTS15</i>
MUC-16	<i>MUC16</i>	EGFR	<i>EGFR</i>	WIF-1	<i>WIF1</i>
FR-alpha	<i>FOLR1</i>	LAP TGF-beta-1	<i>TGFB1</i>	TNFRSF14	<i>TNFRSF14</i>
CNTN1	<i>CNTN1</i>	IL-6	<i>IL6</i>	TNFSF13B	<i>TNFSF13B</i>
MCP-1	<i>CCL2</i>	TRAIL	<i>TNFSF10</i>	CTSD	<i>CTSD</i>
CA9	<i>CA9</i>	SCF	<i>KITLG</i>	TNF-R2	<i>TNFRSF1B</i>
ABL1	<i>ABL1</i>	IL-18	<i>IL18</i>	IL-1 RL1	<i>IL1RL1</i>
DNER	<i>DNER</i>	TGF-alpha	<i>TGFA</i>	TNFSF14	<i>TNFSF14</i>
GPC1	<i>GPC1</i>	MMP-1	<i>MMP1</i>	ESM-1	<i>ESM1</i>
TFPI-2	<i>TFPI2</i>	LIF-R	<i>LIFR</i>	CD70	<i>CD70</i>
LDL receptor	<i>LDLR</i>	IL-22 RA1	<i>IL22RA1</i>	TNFRSF11B	<i>TNFRSF11B</i>
TNF-R1	<i>TNFRSF1A</i>	PD-L1	<i>CD274</i>	PDGF subunit A	<i>PDGFA</i>
CYR61	<i>CYR61</i>	TNF	<i>TNF</i>	IL-8	<i>CXCL8</i>
MIC-A	<i>MICA</i>	SIRT2	<i>SIRT2</i>	GDNF	<i>GDNF</i>
MIC-B	<i>MICB</i>	CCL28	<i>CCL28</i>	CD244	<i>CD244</i>
IGFBP-2	<i>IGFBP7</i>	LIF	<i>LIF</i>	OSM	<i>OSM</i>
LTBR	<i>LTBR</i>	ST1A1	<i>SULT1A1</i>	MMP-10	<i>MMP10</i>
TR	<i>TFRC</i>	CSF-1	<i>CSF1</i>	MIP-1 Alpha	<i>CCL3</i>
ITGB2	<i>ITGB2</i>	CPE	<i>CPE</i>	CXCL6	<i>CXCL6</i>
ALCAM	<i>ALCAM</i>	CEACAM1	<i>CEACAM1</i>	CXCL10	<i>CXCL10</i>
CSTB	<i>CSTB</i>	MSLN	<i>MSLN</i>	TWEAK	<i>TNFSF12</i>
Gal-3	<i>LGALS3</i>	TNFSF13	<i>TNFSF13</i>	VEGFR-2	<i>KDR</i>
GRN	<i>GRN</i>	EGF	<i>EGF</i>	IL-17RA	<i>IL17RA</i>
BLM hydrolase	<i>BLMH</i>	TNFRSF6B	<i>TNFRSF6B</i>	PI3	<i>PI3</i>
PLC	<i>HSPG2</i>	TGFR-2	<i>TGFR2</i>	CTSZ	<i>CTSZ</i>
Notch-3	<i>NOTCH3</i>	hK8	<i>KLK8</i>	Gal-1	<i>LGALS1</i>
TIMP4	<i>TIMP4</i>	PODXL	<i>PODXL</i>	DKN1A	<i>CDKN1A</i>
TNFRSF10C	<i>TNFRSF10C</i>	S100A4	<i>S100A4</i>	Beta - NGF	<i>NGF</i>
GDF-15	<i>GDF15</i>	ERBB3	<i>ERBB3</i>	IL-24	<i>IL24</i>

Table 4.15. List of 70 genes identified in the biological pathways database for the randomize list input in FunRich software for enrichment analysis.

Genes identified in biological pathway dataset						
<i>TFPI</i>	<i>CYR61</i>	<i>IL6</i>	<i>CXCL8</i>	<i>PDGFA</i>	<i>CCL3</i>	<i>CD274</i>
<i>AXIN1</i>	<i>TFRC</i>	<i>TGFA</i>	<i>GDNF</i>	<i>ERBB3</i>	<i>CXCL10</i>	<i>TLR3</i>
<i>HGF</i>	<i>ITGB2</i>	<i>MMP1</i>	<i>KDR</i>	<i>PLAT</i>	<i>TNFRSF1B</i>	<i>TNFRSF14</i>
<i>VEGFA</i>	<i>TNFRSF10C</i>	<i>TNF</i>	<i>LGALS1</i>	<i>IL18</i>	<i>ALCAM</i>	<i>SULT1A1</i>
<i>NT5E</i>	<i>GDF15</i>	<i>LIF</i>	<i>CDKN1A</i>	<i>IL-24</i>	<i>LDLR</i>	<i>CNTN1</i>
<i>LYN</i>	<i>IL6R</i>	<i>CSF1</i>	<i>OSM</i>	<i>NOTCH3</i>	<i>HSPG2</i>	<i>SIRT2</i>
<i>CCL2</i>	<i>FAS</i>	<i>CPE</i>	<i>GPC1</i>	<i>TGFBR2</i>	<i>NGF</i>	<i>PVRL4</i>
<i>CA9</i>	<i>CASP3</i>	<i>EGF</i>	<i>WIF1</i>	<i>DLL1</i>	<i>LGALS3</i>	<i>TNFSF13</i>
<i>ABL1</i>	<i>EGFR</i>	<i>TGFBR2</i>	<i>VIM</i>	<i>DNER</i>	<i>BLMH</i>	<i>CD244</i>
<i>TNFRSF1A</i>	<i>TGFB1</i>	<i>CTSD</i>	<i>TNFSF10</i>	<i>AXL</i>	<i>KITLG</i>	<i>CCL28</i>

The top 10 pathways most enriched for this list, ranked based on the corrected p-values (Benjamini-Hochberg method), is shown in **Figure 4.10 A**. The list identifies that vesicular HSPG-associated proteins are likely to have roles in regulating apoptosis and cell survival, as several related apoptosis pathways can be identified, such as “Death receptor signalling”, “Extrinsic pathway for apoptosis”, “Fas ligand signalling pathway” and “p53 (tumour protein P53) related pathways”. Proteins associated with HSPGs also appear relevant for lipid signalling, involving pathways such as “Phospholipase A (PLA) receptor” and “Ceramide signalling”. Similar to the enrichment analysis performed previously for the proteins altered with the removal of HS-GAG chains from vesicles, cytokine related pathways are also present in this top 10. “IL-23 mediated events” are again featured here, associated with IL-6 and IL-18 (**Figure 4.10 B**), on par with **Figure 4.2 B**. This indicates a possible role of HS-chains attached to HSPGs in regulating inflammatory status in the tumour microenvironment.

As before, on the pathway list generated by FunRich, there are several other statistically significant associations but with a lower enrichment score, and hence sit outside the top 10 (**Figure 4.11**). Nevertheless, these pathways were comparable with the data obtained from HEP III-digested EVs and are highlighted in **Figure 4.11**. Whilst many genes mapped may overlap between pathways, as seen in **Figure 4.3 B**, there are some genes that are unique to a specific pathway. TFPI, as an example, is associated exclusively with “Proteoglycan-syndecan mediated signalling events”. Similarly, and not surprisingly, GPC1 is associated exclusively with the “Glypican pathway” (**Figure 4.11 B**). Several proteins were common between the two data sets in **Figures 4.3 and 4.11**, such as

Chapter 4 - Results

GDF-15, IL-6RA, IL-6, CYR61, MMP-1, ABL1, AXIN1, and more. The association of these proteins with the same biological pathways, both in the analysis of HEP1III-digested and HSPG-deficient vesicles strengthens their association with HS-GAG chains present on the specific HSPG under study here.

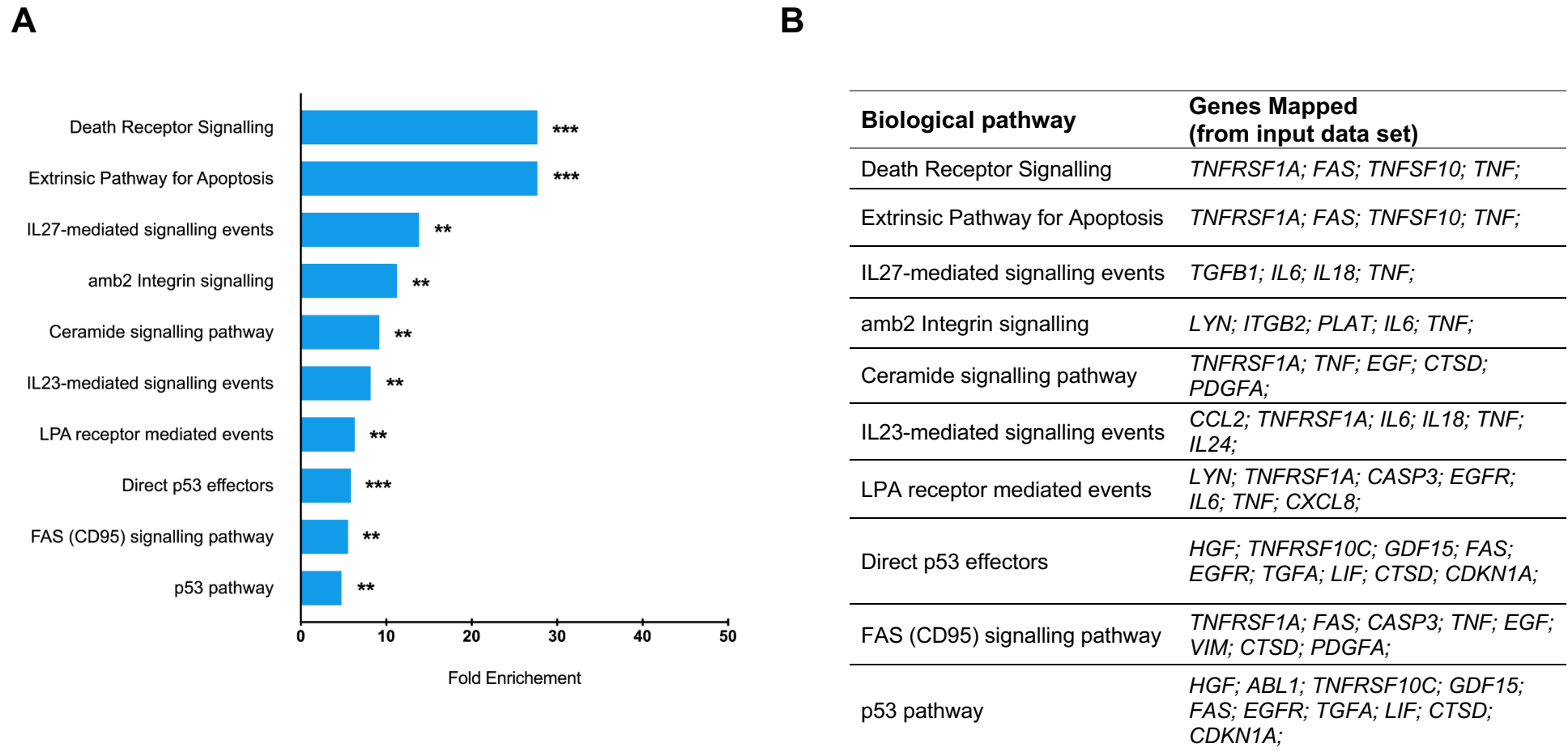


Figure 4.10. Top 10 biological pathways provided by FunRich for the differently expressed proteins associated with vesicular HSPGs. (A) Bar graph shows the biological pathways for proteins associated with HSPG-deficient vesicles. List of proteins combines proteins increased and decreased ± 2 -fold vs control and with $p < 0.05$. Functional enrichment was performed on the resultant list of 108 proteins, from which results were obtained for 70. Analysis was performed in FunRich, corrected p-values were used (BH method). *** $p < 0.001$; ** $p < 0.01$. **(B)** List of proteins associated with each individual biological pathway.

A

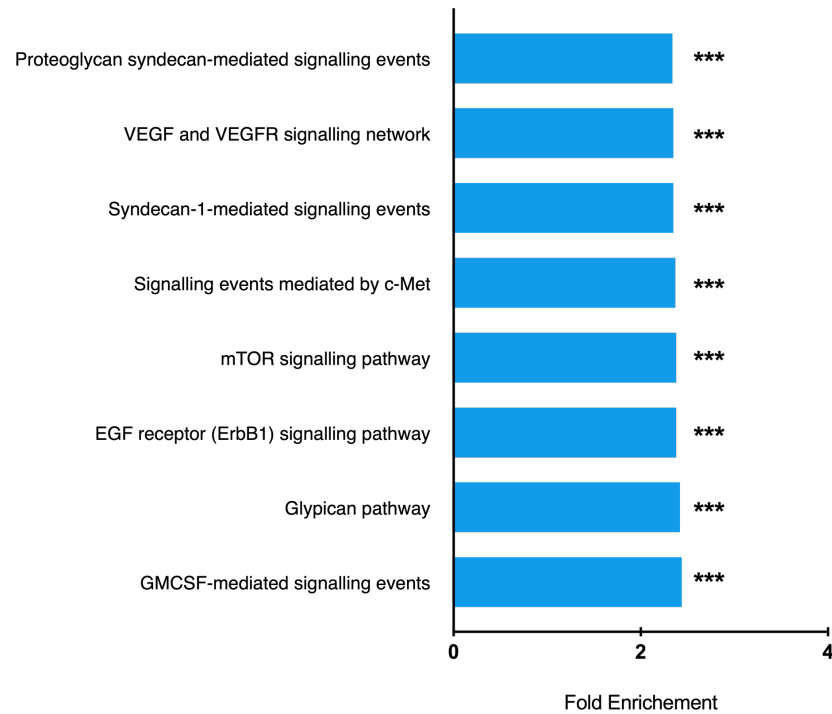


Figure 4.11. Common pathways attributable to both HSPG-deficient and HEPIII-digested EVs (not in the top 10). (A) Figure shows additional biological pathways provided by FunRich data analysis, not included in the previous top 10. These are pathways selected by us as considered relevant. *** $p < 0.001$ (B) List of genes associated with each individual biological pathway.

B

Biological Pathway	Genes mapped (from input data set)
Proteoglycan syndecan-mediated signalling events	<i>TFPI; AXIN1; HGF; VEGFA; NT5E; LYN; CCL2; CA9; ABL1; TNFRSF1A; CYR61; TFRC; ITGB2; TNFRSF10C; GDF15; IL6R; FAS; CASP3; EGFR; TGFB1; IL6; TGFA; MMP1; TNF; LIF; CSF1; CPE; EGF; TGFB2; CTSD; CXCL8; GDNF; KDR; LGALS1; CDKN1A;</i>
GMCSF-mediated signalling events	<i>AXIN1; HGF; VEGFA; NT5E; LYN; CCL2; CA9; ABL1; TNFRSF1A; CYR61; TFRC; ITGB2; TNFRSF10C; GDF15; IL6R; FAS; CASP3; EGFR; TGFB1; IL6; TGFA; MMP1; TNF; LIF; CSF1; CPE; EGF; TGFB2; CTSD; CXCL8; GDNF; OSM; KDR; LGALS1; CDKN1A;</i>
EGF receptor (ErbB1) signalling pathway	
mTOR signalling pathway	<i>AXIN1; HGF; VEGFA; NT5E; LYN; CCL2; CA9; ABL1; TNFRSF1A; CYR61; TFRC; ITGB2; TNFRSF10C; GDF15; IL6R; FAS; CASP3; EGFR; TGFB1; IL6; TGFA; MMP1; TNF; LIF; CSF1; CPE; EGF; TGFB2; CTSD; CXCL8; GDNF; KDR; LGALS1; CDKN1A;</i>
Signalling events mediated by c-Met	<i>AXIN1; HGF; VEGFA; NT5E; LYN; CCL2; CA9; ABL1; TNFRSF1A; CYR61; TFRC; ITGB2; TNFRSF10C; GDF15; IL6R; FAS; CASP3; EGFR; TGFB1; IL6; TGFA; MMP1; TNF; LIF; CSF1; CPE; EGF; TGFB2; CTSD; CXCL8; GDNF; KDR; LGALS1; CDKN1A;</i>
Syndecan-1-mediated signalling events	<i>AXIN1; HGF; VEGFA; NT5E; LYN; CCL2; CA9; ABL1; TNFRSF1A; CYR61; TFRC; ITGB2; TNFRSF10C; GDF15; IL6R; FAS; CASP3; EGFR; TGFB1; IL6; TGFA; MMP1; TNF; LIF; CSF1; CPE; EGF; TGFB2; CTSD; CXCL8; GDNF; KDR; LGALS1; CDKN1A;</i>
VEGF and VEGFR signalling network	
Glypican pathway	<i>AXIN1; HGF; VEGFA; NT5E; LYN; CCL2; CA9; ABL1; GPC1; TNFRSF1A; CYR61; TFRC; ITGB2; TNFRSF10C; GDF15; IL6R; FAS; CASP3; EGFR; TGFB1; IL6; TGFA; MMP1; TNF; LIF; CSF1; CPE; EGF; TGFB2; WIF1; CTSD; CXCL8; GDNF; KDR; LGALS1; CDKN1A;</i>

To demonstrate that the functional enrichment analysis is not biased because of the limited coverage of the Olink panels, the functional enrichment analysis was repeated on a randomised list of 108 proteins (**Table 4.16**). Of the random list, 76 genes (**Table 4.17**) were identified on the biological pathway database.

Table 4.16. List of proteins and corresponding gene name for the randomize list input in FunRich software for enrichment analysis.

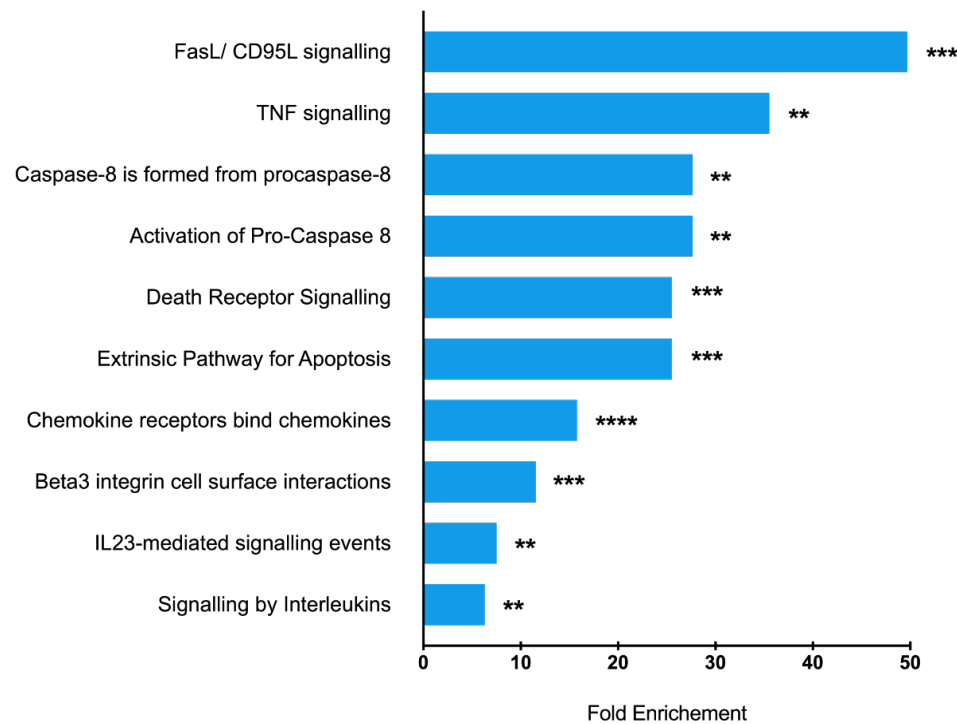
Protein name	Gene name	Protein name	Gene name	Protein name	Gene name
ST1A1	<i>SULT1A1</i>	CD207	<i>CD207</i>	CCL22	<i>CCL22</i>
CDCP1	<i>CDCP1</i>	LTBR	<i>LTBR</i>	GDF-15	<i>GDF15</i>
PLC	<i>HSPG2</i>	AXIN1	<i>AXIN1</i>	NT-3	<i>NTF3</i>
MSLN	<i>MSLN</i>	MAD homolog 5	<i>SMAD5</i>	CEACAM1	<i>CEACAM1</i>
IL-1RT1	<i>IL1R1</i>	TNF-R2	<i>TNFRSF1B</i>	TFPI	<i>TFPI</i>
CXCL5	<i>CXCL5</i>	CASP-8	<i>CASP8</i>	VEGFR-3	<i>FLT4</i>
IL-1RT2	<i>IL1R2</i>	CXCL13	<i>CXCL13</i>	MPO	<i>MPO</i>
IL-6	<i>IL6</i>	ARTN	<i>ARTN</i>	DLL1	<i>DLL1</i>
LIF-R	<i>LIFR</i>	VEGFR-2	<i>KDR</i>	4E-BP1	<i>EIF4EBP1</i>
S100A11	<i>S100A11</i>	IL-12B	<i>IL12B</i>	CD5	<i>CD5</i>
MCP-3	<i>CCL7</i>	IL-8	<i>CXCL8</i>	IL-18	<i>IL18</i>
IL-6RA	<i>IL6R</i>	t-PA	<i>PLAT</i>	Flt3L	<i>FLT3LG</i>
TNFRSF10C	<i>TNFRSF10C</i>	hK8	<i>KLK8</i>	IL-20	<i>IL20</i>
MUC-16	<i>MUC16</i>	CX3CL1	<i>CX3CL1</i>	CCL28	<i>CCL28</i>
SLAMF1	<i>SLAMF1</i>	MCP-2	<i>CCL8</i>	ALCAM	<i>ALCAM</i>
FADD	<i>FADD</i>	TR	<i>TFRC</i>	Gal-3	<i>LGALS3</i>
SPON1	<i>SPON1</i>	FURIN	<i>FURIN</i>	SYND1	<i>SDC1</i>
FAS	<i>FAS</i>	CXCL16	<i>CXCL16</i>	RARRES2	<i>RARRES2</i>
IL-18R1	<i>IL18R1</i>	CTSZ	<i>CTSZ</i>	KLK6	<i>KLK6</i>
TNFRSF6B	<i>TNFRSF6B</i>	PRTN3	<i>PRTN3</i>	CPB1	<i>CPB1</i>
IL-13	<i>IL13</i>	TNF-R1	<i>TNFRSF1A</i>	CCL15	<i>CCL15</i>
CD70	<i>CD70</i>	PGLYRP1	<i>PGLYRP1</i>	S100A4	<i>S100A4</i>
ABL1	<i>ABL1</i>	DKN1A	<i>CDKN1A</i>	AR	<i>AR</i>
Ep-CAM	<i>EPCAM</i>	FGF-23	<i>FGF23</i>	PI3	<i>PI3</i>
GRN	<i>GRN</i>	IL-10RB	<i>IL10RB</i>	EGFR	<i>EGFR</i>
RETN	<i>RETN</i>	LDL receptor	<i>LDLR</i>	IL-22 RA1	<i>IL22RA1</i>
PD-L1	<i>CD274</i>	MMP-3	<i>MMP3</i>	EPHA2	<i>EPHA2</i>
BDNF	<i>BDNF</i>	DLK-1	<i>DLK1</i>	CD6	<i>CD6</i>
IL-33	<i>IL33</i>	ADAM-TS 15	<i>ADAMTS15</i>	CD48	<i>CD48</i>
TRANCE	<i>TNFSF11</i>	PODXL	<i>PODXL</i>	MB	<i>MB</i>
DNER	<i>DNER</i>	TR-AP	<i>ACP5</i>	SELE	<i>SELE</i>
PECAM-1	<i>PECAM1</i>	U-PAR	<i>PLAUR</i>	NRTN	<i>NRTN</i>
BLM hydrolase	<i>BLMH</i>	TFF3	<i>TFF3</i>	OPN	<i>SPP1</i>
RET	<i>RET</i>	LIF	<i>LIF</i>	LYPD3	<i>LYPD3</i>
IL2-RA	<i>IL2RA</i>	IL-5	<i>IL5</i>	CCL19	<i>CCL19</i>
CTSV	<i>CTSV</i>	CCL25	<i>CCL25</i>	JAM-A	<i>F11R</i>

Table 4.17. List of 76 genes identified in the biological pathways database for the randomize list input in FunRich software for enrichment analysis.

Genes identified in biological pathway dataset								
<i>CASP8</i>	<i>FADD</i>	<i>FAS</i>	<i>HSPG2</i>	<i>CXCL13</i>	<i>CCL7</i>	<i>CX3CL1</i>	<i>F11R</i>	<i>AR</i>
<i>CCL19</i>	<i>CCL22</i>	<i>KDR</i>	<i>PECAM1</i>	<i>PLAUR</i>	<i>SPP1</i>	<i>SDC1</i>	<i>CDKN1A</i>	<i>EPHA2</i>
<i>IL12B</i>	<i>IL18</i>	<i>IL18R1</i>	<i>IL1R2</i>	<i>IL6R</i>	<i>IL2RA</i>	<i>IL5</i>	<i>EGFR</i>	<i>BDNF</i>
<i>DLK1</i>	<i>DNER</i>	<i>FURIN</i>	<i>IL13</i>	<i>IL1R1</i>	<i>GDF15</i>	<i>CDKN1A</i>	<i>MMP3</i>	<i>CD274</i>
<i>CX3CL1</i>	<i>TNFRSF10C</i>	<i>CXCL8</i>	<i>ABL1</i>	<i>AXIN1</i>	<i>CASP8</i>	<i>FGF23</i>	<i>FLT4</i>	<i>ARTN</i>
<i>EIF4EBP1</i>	<i>TNFRSF1A</i>	<i>ACP5</i>	<i>TFF3</i>	<i>TFRC</i>	<i>SMAD5</i>	<i>PLAT</i>	<i>NTF3</i>	<i>CCL25</i>
<i>LGALS3</i>	<i>TNFSF11</i>	<i>SELE</i>	<i>LDLR</i>	<i>KLK6</i>	<i>CD207</i>	<i>EPCAM</i>	<i>CXCL16</i>	<i>IL6</i>
<i>SULT1A1</i>	<i>CEACAM1</i>	<i>CD48</i>	<i>TFPI</i>	<i>PRTN3</i>	<i>ALCAM</i>	<i>CCL28</i>	<i>MPO</i>	<i>DLL1</i>
<i>LIF</i>	<i>RET</i>	<i>BLMH</i>	<i>NRTN</i>					

The top10 most enriched pathways are presented in **Figure 4.12** and show some similarities between pathways identified from HSPG-deficient EVs and the random list. The emphasis on, for example, cell death and apoptosis might be due to the limited coverage of the Olink panels and might not convincingly reflect HSPG functions on EVs. Further assessment is required to confirm this. Nonetheless, the lipid signalling aspects were not a part of the randomised biological pathway report, and this might suggest a potential novel relationship between HSPG composition of the EVs and lipids/lipid signalling.

Functional enrichment has identified likely relationships between HS-GAG tethered factors and inflammatory pathways, which were distinct from pathways reporting from random lists of input proteins. In relation to EVs generated from HSPG knockdown cells, the greater complexity, and the need to pool candidates irrespective of HSPG-specificity, has made this more complex and perhaps less informative - but has revealed relationships between HSPG-control of EV loading and lipid signalling functions, which is novel.

A**B**

Biological pathway	Genes Mapped (from input data set)
FasL/ CD95L signalling	<i>CASP8; FADD; FAS;</i>
TNF signalling	<i>TNFRSF1A; CASP8; FADD;</i>
Caspase-8 is formed from procaspase-8	<i>CASP8; FADD; FAS;</i>
Activation of Pro-Caspase 8	<i>CASP8; FADD; FAS;</i>
Death Receptor Signalling	<i>TNFRSF1A; CASP8; FADD; FAS;</i>
Extrinsic Pathway for Apoptosis	<i>TNFRSF1A; CASP8; FADD; FAS;</i>
Chemokine receptors bind chemokines	<i>CXCL13; CCL7; CX3CL1; CCL28; CXCL16; CCL25; CCL19; CCL22;</i>
Beta3 integrin cell surface interactions	<i>KDR; PECAM1; PLAUR; SPP1; SDC1; F11R;</i>
Signalling by Interleukins	<i>IL1R1; IL1R2; IL6; IL18; IL6R; IL2RA; IL5;</i>
p53 pathway	<i>HGF; ABL1; TNFRSF10C; GDF15; FAS; EGFR; TGFA; LIF; CTSD; CDKN1A;</i>

Figure 4.12. Functional enrichment analysis of biological pathways by FunRich for list of proteins randomly selected from the cardiovascular III, inflammation, and oncology II panels. (A) Bar graph represents the possible biological pathways enriched for proteins randomly selected from the three Olink panels. Functional enrichment was performed on the resultant list of 108 proteins, from which results were obtained for 76. Analysis was performed in FunRich, corrected p-values were used (BH method). *** $p < 0.001$; ** $p < 0.05$. **(B)** List of proteins associated with each individual biological pathway.

4.2.9 ELISA validation of proteins in HSPG-deficient extracellular vesicles

Following identification of interesting HSPG-associated proteins by Olink, several targets were selected for validation. The selection looked to encompass a mixture of targets that were either common across the different HSPG-deficient vesicles or had a particular association with an individual HSPG, as well as being a target previously identified in HS-deficient EVs. Their known relevance to microenvironment remodelling was also considered (**Table 4.18**).

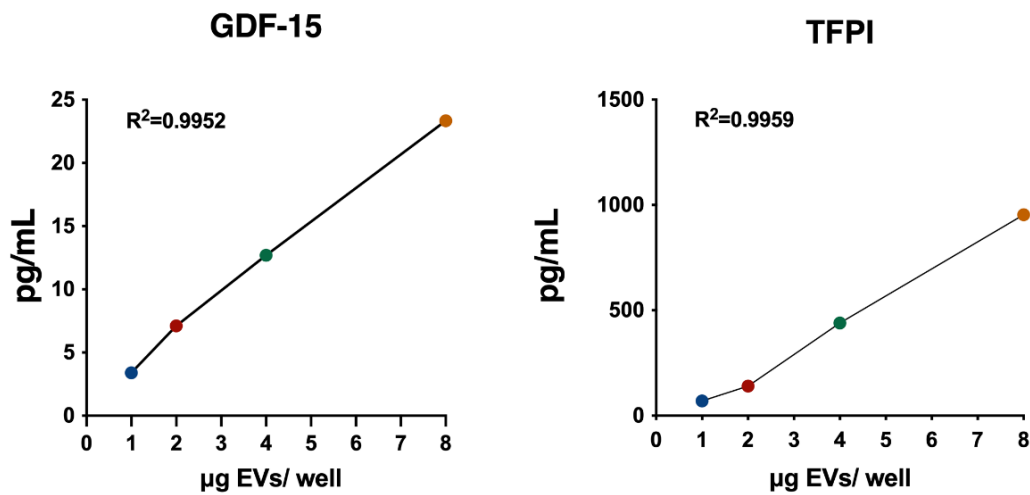
Table 4.18. Proteins from the Olink analysis of HSPG-deficient vesicles selected for further validation by ELISA. HSPG-deficiency, HEP111-treated vesicles association, as well as main function and role in diseases are featured in the table.

	Associated HSPG-deficiency	HEP111 treated EVs	Main function/Role in Disease
GDF-15	BGLY SDC3 SDC4 GPC1 GPC6	Yes	First identified as a member of the transforming growth factor beta superfamily (Bootcov et al., 1997). GDF-15 levels are increased in various diseases and It is one of the biomarkers most expressed in cancer (Welsh et al., 2003).
MMP-1		Yes	Involved in the degradation of extracellular matrix in both normal physiological and disease conditions. It has collagenase activity, breaking down the interstitial collagens, types I, II, and III (Pardo and Selman, 2005).
TFPI	BGLY SDC3 SDC4 GPC6	Yes	Supresses coagulation by binding directly and inhibiting the TF–FVII/FVIIa complex. High levels are found in patients with advanced solid tumours (Iversen et al., 1998)
ABL1	BGLY SDC4 GPC6	Yes	Functions as a non-receptor kinase and is involved in a variety of cellular processes such as proliferation and survival. Interacts with proteins involved in the actin cytoskeleton, controlling cell migration and with integrins, influencing attachment(Colicelli, 2010). In humans is encoded by the <i>ABL1</i> gene, a known oncogene. In cancer, it is most relevant in its role in the BCR-ABL fusion protein, a signature of chronic myeloid leukaemia. In solid tumours, ABL1 activation is related with hyperactivated RTKs and chemokine receptors (Greuber et al., 2013)

GDF-15, MMP-1, TFPI, and ABL1 were interesting targets to validate, as GDF-15 and MMP-1 were increased in all knockdown vesicles and TFPI and ABL1 were decreased across several HSPG-deficient conditions (**Figures 4.8 and 4.9**). These proteins were targeted in this analysis and have not been previously considered. CYR61, CSTB, CCL20, and IL-6 prompted particular interest on account of being targets identified in the analysis of HEPIII-treated vesicles, which made their validation on HSPG-deficient EVs even more appealing. Midkine was not identified as associated with vesicles from any of the HSPG-deficient conditions under study. However, it is highly detected in DU145 native vesicles, and removal of HS-GAG affected the concentration on the vesicle surface, therefore, making it an interesting target to investigate here in HSPG-deficient vesicles. Overall, ELISAs for GDF-15, MMP-1, TFPI, ABL1, CYR61, CSTB, CCL20, IL-6 and midkine were performed in intact vesicles derived from cell lines lacking specific HSPGs.

Firstly, investigation of the new proteins arising from this analysis was undertaken on DU145 intact vesicles. GDF-15, MMP-1, ABL1 and TFPI were assayed by ELISA. MMP-1 and ABL1 proved very difficult to consistently detect on DU145 vesicles, with values read being very close to the bottom of the standard curve (**Appendix 4.5. A and D**). Nonetheless, it is possible to observe some degree of detection above background for 4 μ g and 8 μ g of EVs on MMP-1 ELISA (**Appendix 4.5. B**). This indicates that, maybe, these proteins are very scarcely present on EVs, and they only start to be marginally detected on high concentrations of vesicles in the wells. GDF-15 and TFPI detection on intact DU145 vesicles was consistent, and ELISA values increased with the amount of input sample in the study, with a linearity of 0.9952 and 0.9959, respectively (**Figure 4.13 A**). GDF-15 is detected at much lower levels than TFPI, with 0.29 pg per μ g of EVs detected when 8 μ g of EVs are input in the wells, versus 12 pg of TFPI detected per μ g of EV in the same conditions. For both proteins, technical variability was very low (**Figure 4.13 B**).

A



B

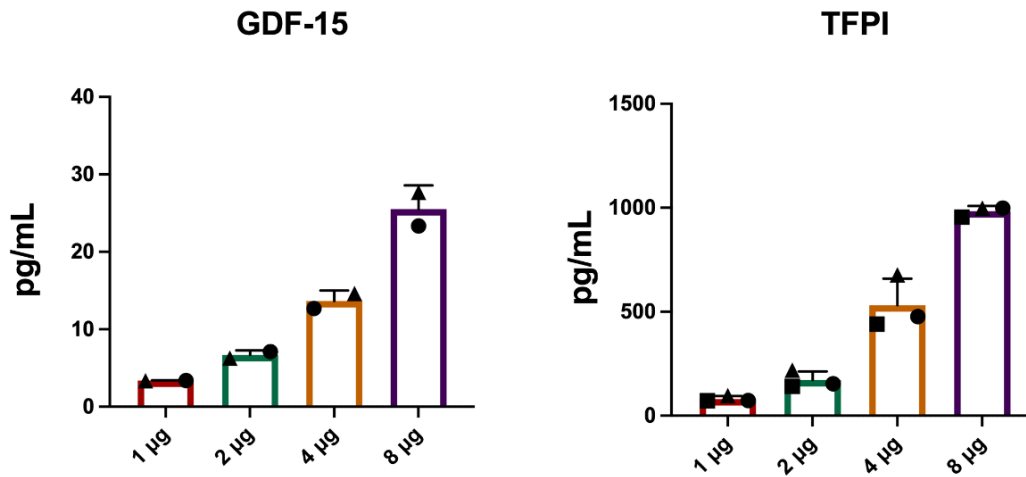


Figure 4.13. Validation of targets identified in HSPG-deficient vesicles on DU145 EVs. **(A)** The graphs show best fit curve and R^2 values for an ELISA performed in triplicate wells for the specified proteins on a single EV isolate. The dots correspond to mean \pm SD for concentrations (pg/mL) of protein detected at the surface of DU145 EVs on 8 μ g, 4 μ g, 2 μ g and 1 μ g per 100 μ L/well. **(B)** Bar graphs show the mean \pm SEM of at least 2 independent experiments each based on a different EV isolate and represented by circle, square or triangle. Every independent experiment was performed in triplicate wells.

For the assaying of HSPG-deficient vesicles, 4 µg of vesicles were used per well, and signal strength was detected and converted to pg/mL for each of the analysed proteins. As previously, EVs were not lysed before the assay so that any detectable signal could be attributed to proteins on the surface of EVs. Protein expression was normalised against the NMC condition, to allow for a better understanding of the magnitude of change of protein detection. The data represented in **Figure 4.14** demonstrates some variability in levels of proteins detected on EVs from different isolations.

Overall, consistently detecting the proteins on the HSPG-deficient EV surface proved difficult, with different samples providing different quantifications for a given analyte (**Figure 4.14**). This variability makes it difficult to draw conclusions from the data. However, it was possible to detect most of the proteins selected, with the exception of ABL1 and MMP-1. Similar to what was seen for DU145 native vesicles, both analytes were very difficult to consistently detect, with values below the limit of detection on the standard curve (**Appendix 4.5. C and E**).

In the previous Olink analysis, TFPI decrease was associated with all the HSPG-deficient conditions, except GPC1 (**Figure 4.9 B**). Here, there seems to be no change in detection of this protein; however, there is a trend to an increase in detection in GPC1- and GPC6-deficient vesicles (**Figure 4.14 B**). CCL20 seems to trend towards a decrease in detection in SDC3- and GPC1-deficient vesicles, which is in disagreement with the previous Olink analysis, where only GPC1 showed association with increased CCL20 (**Figure 4.8 B**). Here, the absence of GPC1 on the vesicles actually relates to decreased detection of CCL20 (**Figure 4.14 C**). Another protein with compelling associations was CYR61. This protein seemed to have a particular association with BGLY, only showing up as decreased when this HSPG was removed from vesicles (**Figure 4.9 B**). Removal of HS-chains from the vesicle surface had previously been associated with a decrease in the detection of CYR61 as well (**Figure 4.6**). **Figure 4.14 D** shows a trend towards a decrease in detection of CYR61 for SDC3-, SDC4-, and BGLY-deficient vesicles when compared with NMC vesicles but results for GPC1- and GPC6-deficiency are not conclusive. Detection of CSTB and IL-6 was decreased across all HSPG-deficient vesicles (**Figure 4.14 E, F**). This is in disparity with previous analysis (**Figure 4.8 B**). SDC3, SDC4, GPC1, and GPC6 had all been associated with increase in IL-6, and SDC3 and SDC4 were associated with increased CSTB. The results obtained for CCL20, CSTB and IL-6 were unexpected and quite puzzling and will no doubt require further

Chapter 4 - Results

investigation. Biological variability between EV samples, the input of EV sample in the assay, or even protein topology in the vesicle, can all be possible contributions towards the results seen here. By topology, our meaning relates to the location of the analyte either present at the outer surface of intact EVs or perhaps located within the lumen and therefore hidden from antibodies in our validation assays. This once again highlights the complexity of this data set and how difficult it is to draw any concrete conclusions. Lastly, midkine was detected in all HSPG-deficient vesicles, showing an increase in relation to the NMC for SDC3-, GPC1-, and GPC6-deficient vesicles and a decrease for BGLY-deficient EVs (**Figure 4.14 G**). Detection levels did not seem to differ with removal of SDC4 from vesicles. GPC1-deficient EVs show low variability for midkine detection between assayed samples. This consistent result points to a probable association between GPC1 and midkine loading to the vesicles, considering removal of this HSPG translates in an increase of detected protein.

Altogether, we document variability between assayed samples, and the principal sources of variability are not defined. This makes it difficult to make clear cut associations between a particular analyte and a specific HSPG. Nevertheless, these data show that it is possible to detect most of the proteins selected using the ELISA technique and that modifying the HS-GAG chains available on the vesicle surface, or the HSPGs of the cells producing EVs, exerts a drastic effect on the analyte repertoire of EVs.

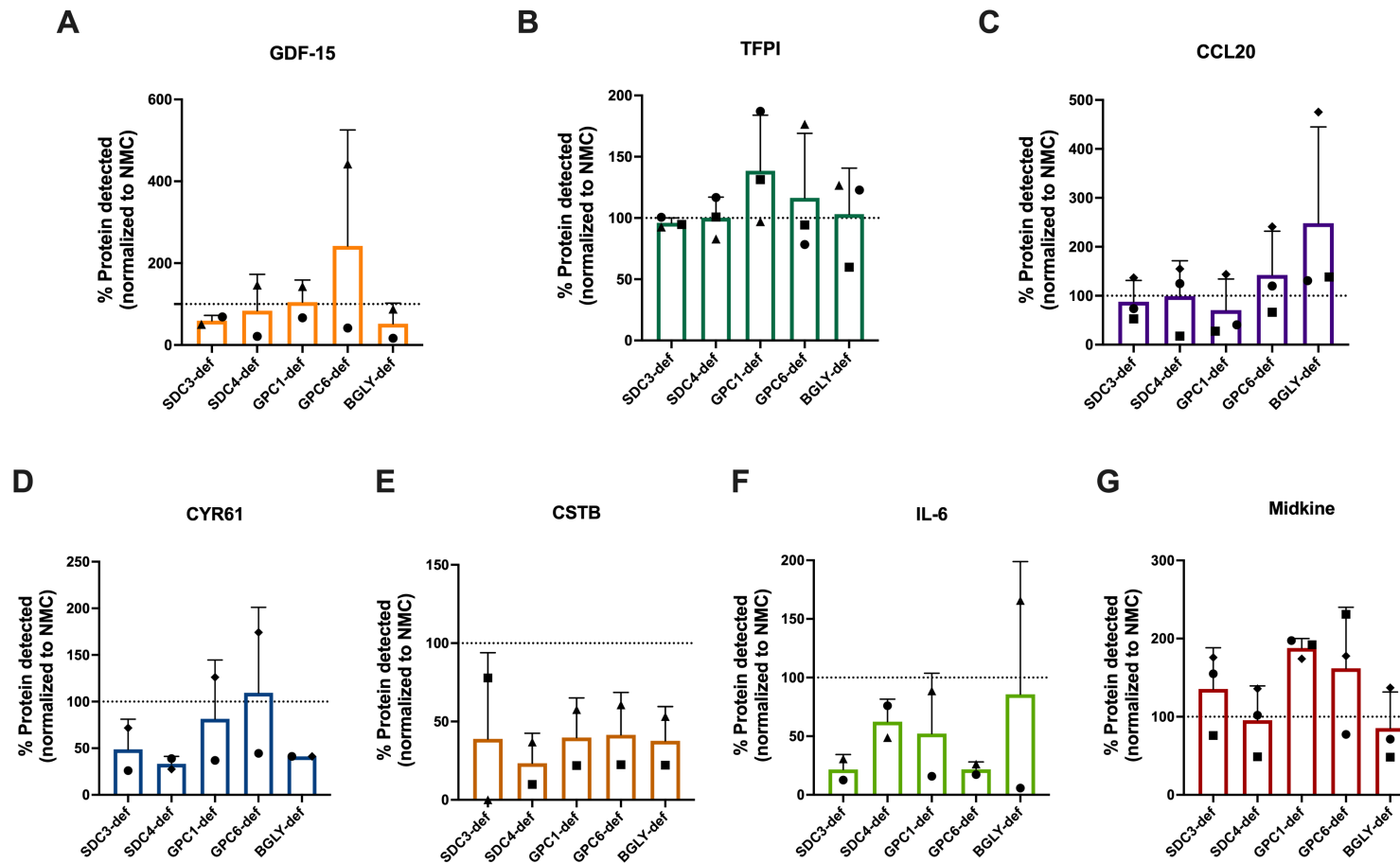


Figure 4.14. Quantification of proteins at the surface of HSPGs-deficient vesicles. (A), GDF-15 (B) TFPI (C) CCL20 (D) CYR61 (E) CSTB (F) IL-6 and (G) Midkine were assessed by ELISA on 4 μ g of each of the HSPG-deficient vesicles. The bar graphs show the % of protein detected at the surface of EVs, in relation to the NMC (Non-Mammalian Control), represented by the dotted line. Graph shows mean \pm SEM of at least 2 independent experiments, each based on a different EV isolation, represented by circle, triangle and square. Every independent experiment was performed in triplicate wells. BGLY-def (betaglycan-deficient EVs), SDC3-def (syndecan-3-deficient EVs), SDC4-def (syndecan-4-deficient EVs), GPC1-def (glypican-1-deficient EVs), GPC6-def (glypican-6-deficient EVs).

4.2.10 Comparison of proteins with altered expression following either HEP-III treatment or attenuation of specific HSPGs

Proteins that were explored in HSPG-deficient vesicles but had not been previously explored in HEP-III-digested EVs were investigated here, to try to ascertain their association with HS-side chains on HSPGs. As proteins can bind both to HS-GAG chains and core proteins of proteoglycans, this distinction can be interesting to assess which structure could potentially be responsible for the transport and delivery of growth factors.

HEP-III-treated vesicles were assayed for GDF-15, MMP-1, and TFPI. Detection of ABL1 was again unsuccessful (**Appendix 4.5. E**). This might indicate that this protein is below the detection sensitivity of the ELISA assay in use, or it is not present on the EV surface. Consistent detection of GDF-15 was difficult between different HEP-III-digested EVs preparations, and removal of HS does not seem to significantly affect protein detection between the different treatments (**Figure 4.15. A and D**), which also seems to be true for MMP-1 (**Figure 4.15. C and F**). Here, detection of MMP-1 was possible, but only just within the limit of detection, again highlighting the difficulty of detecting MMP-1 on these vesicles. TFPI shows a consistent trend that agrees with an effect promoted by removing HS-GAG chains from the EVs (**Figure 4.15. B and E**), while differences between untreated EVs and those treated with heat deactivated HEP-III are minimal (**Figure 4.15 B**). This result places TFPI as another protein associated with HS-GAG chains at the EV surface.

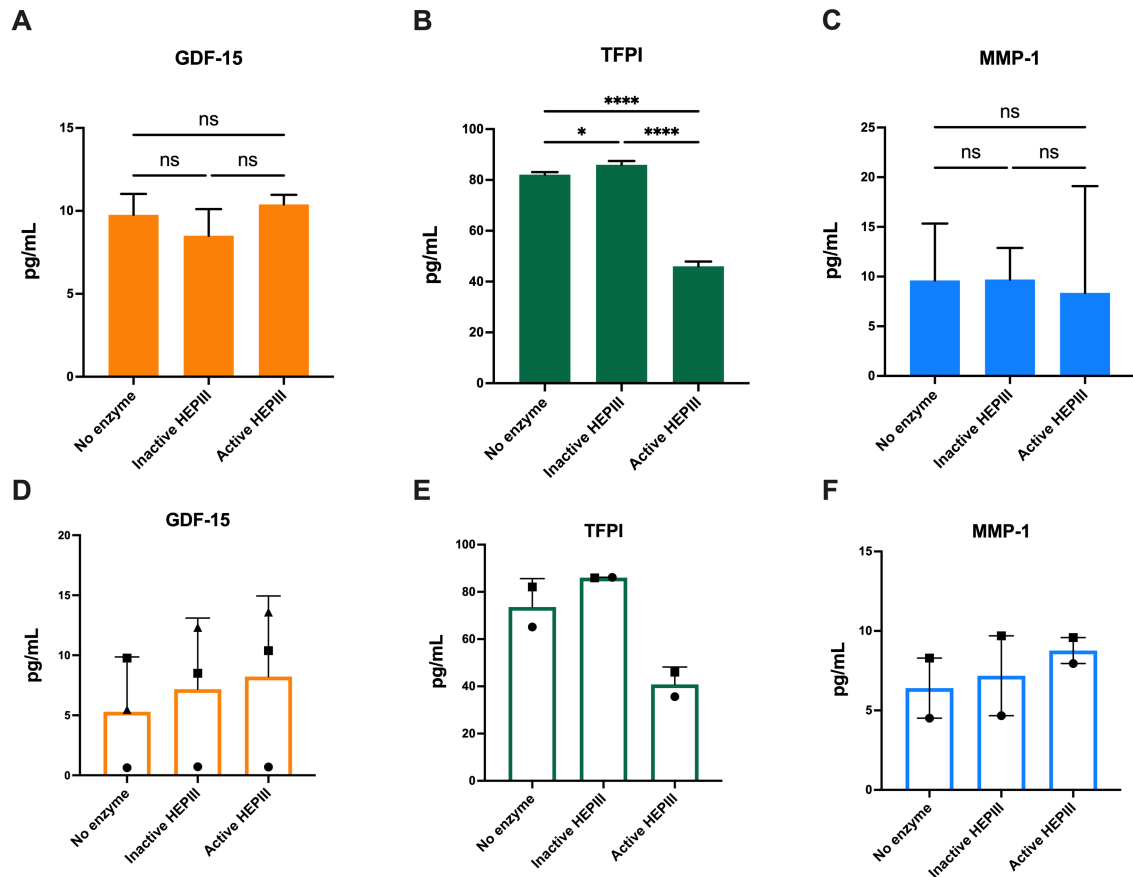


Figure 4.15. Validation of targets identified in HSPG-deficient vesicles on HEP111-treated DU145 EVs. ELISA was performed in intact EVs to assess protein detection on vesicle surface. The bar graphs show \pm SD of triplicate wells for the quantification (pg/mL) of GDF-15 (A), TFPI (B) and MMP-1 (C) per 4 μ g of untreated (no enzyme), heat-inactivated HEP111 and active HEP111 treated EVs. A representative experiment is shown. **** p <0.001; * p <0.05; ns=not significant one-way ANOVA with Tukey's multiple comparison test. (D, E, F) The bar graphs show \pm SEM of at least 2 independent experiments each based on a different EV HEP111 digestion and represented by circle, square or triangle. Every independent experiment was performed in triplicate wells.

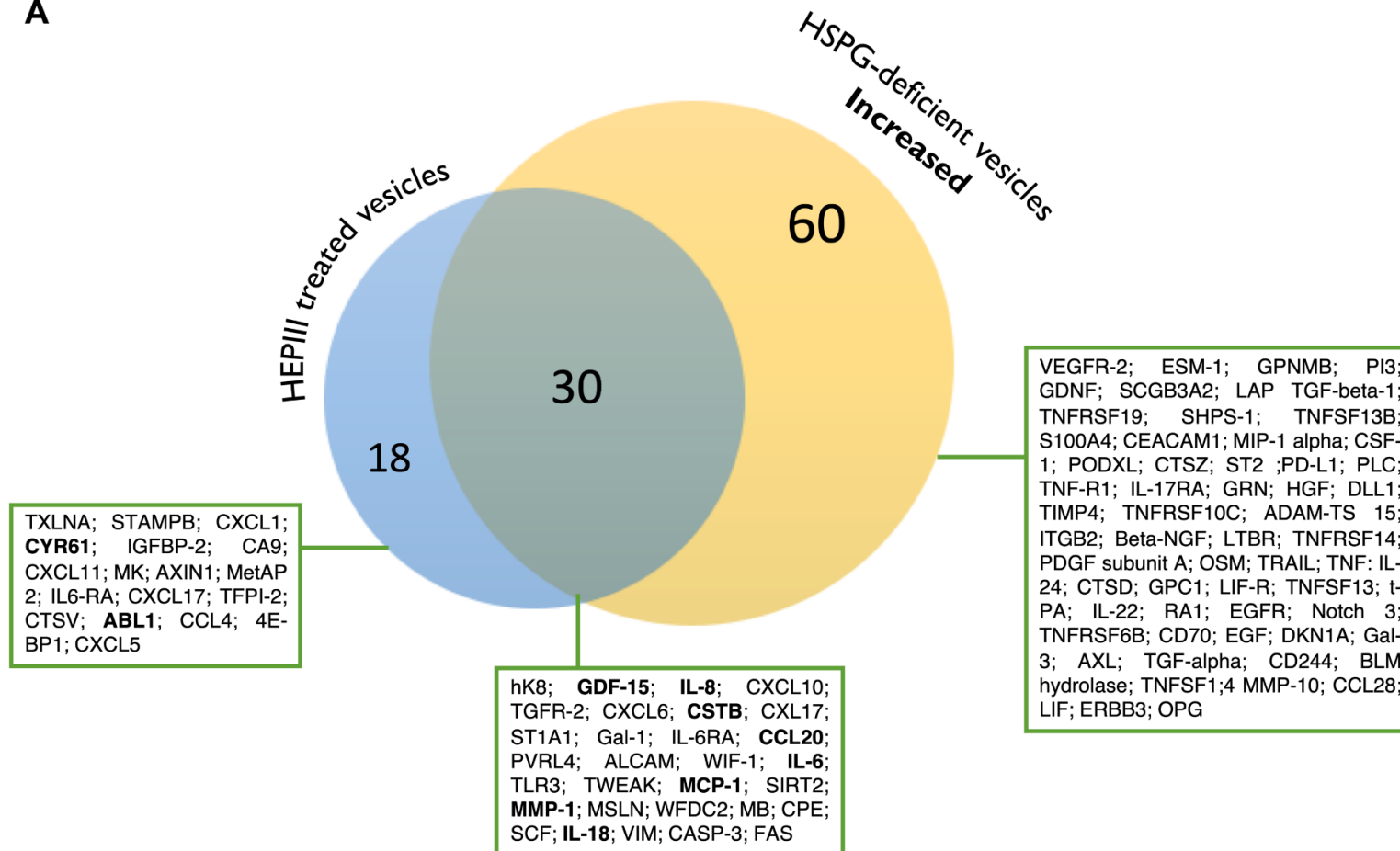
Chapter 4 - Results

In the previous section, one of the most interesting observations was the existence of proteins that were decreased in HEP1III-treated vesicles but increased in vesicles with distinct HSPGs profiles. To have a broader perception of juxtapositions between the different lists of proteins obtained from the experimental conditions, Venn diagrams were used. The 48 proteins found to decrease with HEP1III treatment (**Table 4.2**) were compared to those 108 proteins that had altered expression (increased (90 proteins) or decreased (22 proteins)) in HSPG-deficient EVs.

Interestingly, and unexpectedly, removal of HS-GAG chains leads to the decrease of 30 proteins that are upregulated in HSPG-deficient EVs (**Figure 4.16 A**). Some of the proteins in the list have previously been described within this chapter, such as GDF-15, MMP-1, IL-8, IL-6, CCL20 and CSTB. For the analysis of proteins decreased in both digested and HSPG-deficient vesicles, six proteins were common to both conditions. (**Figure 4.16 B**). CYR61, ABL1 and MCP-1 were under study in this chapter, but only CYR61 could be validated, as both ABL1 and MCP-1 failed detection within vesicles analysed in this study. The observed reduction in CYR61 detection, both when HS-GAG chains or specific HSPGs, in specific betaglycan, is removed from the vesicles, could possibly indicate that this protein does not bind specifically to any one HSPG-core protein under study here, but rather to the HS-GAG chains (that are co-removed when an HSPGs is eliminated from the surface, diminishing the availability of HS-GAG chains available for CYR61 binding).

Comprehensively, this analysis shows that both HSPG-modifying approaches under study in this chapter offer different perspectives to which variety of proteins might be associated with HS-GAG chains or specific HSPGs present in vesicles. Not all proteins arising from the Olink analysis as promising targets were successfully validated, and this is most probably related to the sensitivity of the ELISA technique employed here. At the moment, we cannot explain the upregulation observed for several proteins in relation to removal of HSPGs from vesicles. This would require further studies to evaluate if other HSPGs not in study here could be involved, or if when cells are modified to produce vesicles which will lack a specific HSPG, potential compensatory mechanisms may come into play resulting in elevation of certain factors.

A



B

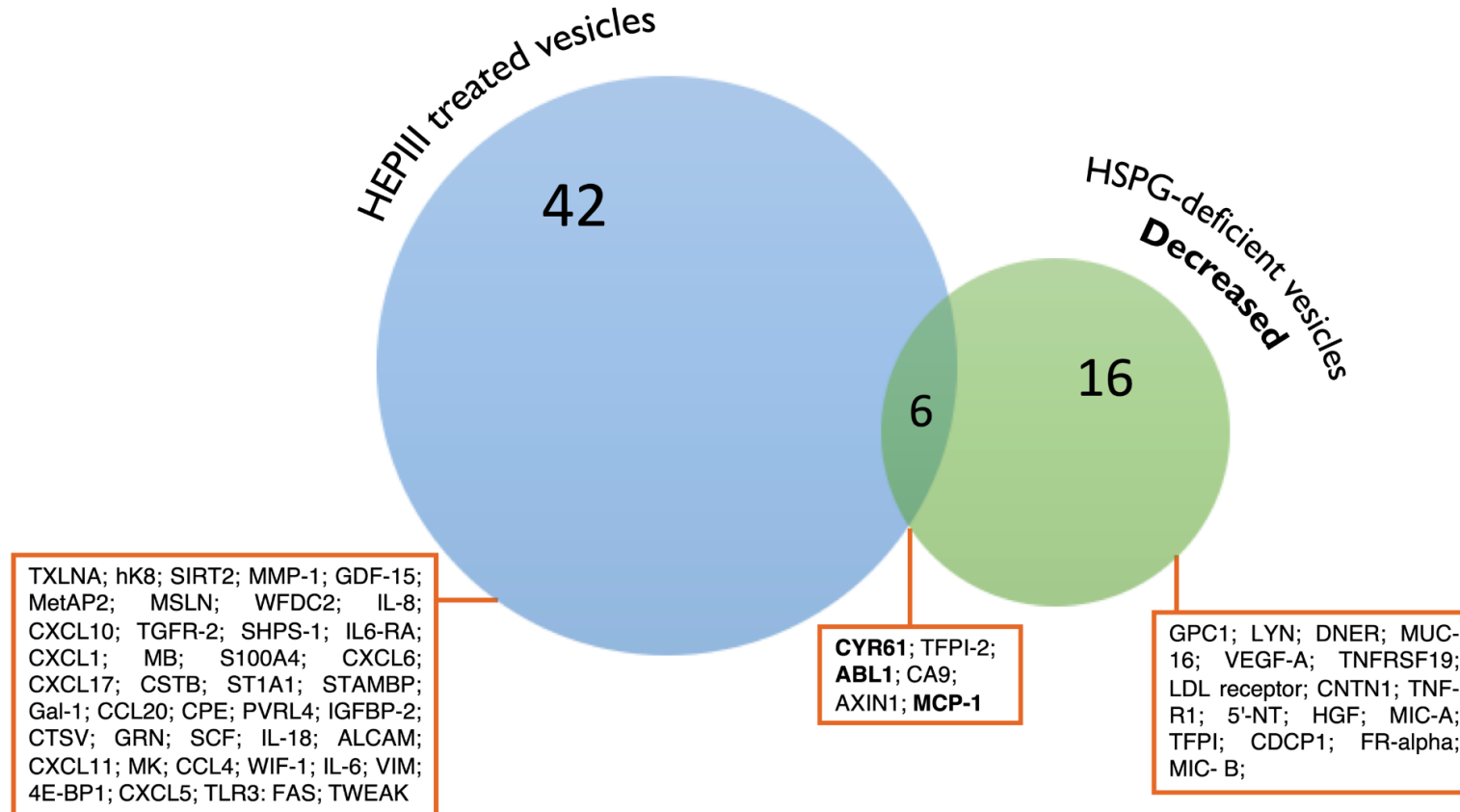


Figure 4.16. Venn diagrams show common proteins with altered expression following HEPIII-treatment of EVs or modification of EV-associated HSPGs. Venn diagrams were generated from a list of 48 unique proteins, decreased in HEPIII-treated vesicles, compared against a list of 90 proteins increased (A) and 22 proteins decreased (B) in HSPG-deficient vesicles. Proteins associated with each of the conditions are shown in the boxes.

4.3 Discussion

In this chapter, the variety of growth factors and cytokines associated with HSPGs on extracellular vesicles was explored for the first time. A high sensitivity multiplex assay was employed for this purpose, and we report a number of factors related to cancer-derived EVs that are associated to HS-GAG chains or rely on HSPG core proteins for their incorporation into, or exclusion from, EVs.

As previously mentioned, mass spectrometry, while being a system-wide and unbiased tool, is less sensitive in detecting or quantifying low abundance elements, when compared with a highly sensitive targeted immunoassay such as PEA. The PEA technology (Olink), allows for detection of relevant low molecular weight and low concentration molecules, that could otherwise be masked by high abundance protein and not detected by mass spectrometry. A recent study analyzing the complementarity of both approaches, showed that Olink was able to detect 25 proteins present in plasma, among them cytokines and interleukins, and 5 peptide hormones, none of which were detected by MS (Petrera et al., 2021). Additionally, compared with other multiplex antibody-based platforms, the PEA technology provides high specificity due to its matched pairs of antibodies linked to unique DNA oligonucleotides that are detected by real time quantitative PCR. Therefore, this approach was chosen to evaluate the proteome of the vesicles under study here.

Studies within our group have already shown that HS-GAG chains present on betaglycan on the EV-surface are essential for functional delivery of TGF- β 1 (Webber et al., 2015b) and essential to drive fibroblast differentiation towards a disease-associated phenotype not seen with soluble TGF- β 1. Furthermore, the delivery of growth factors by HSPGs had been previously reported in relation to FGF-2 and syndecans (Filla et al., 1998). Therefore, it is hypothesized that HSPGs, known to bind a plethora of ligands, may be involved in the co-delivery of multiple factors simultaneously, resulting in the unique capability of EVs in generating the cancer-associated stromal phenotype mentioned above (Sarrazin et al., 2011, Bishop et al., 2007). The exploration of such a concept of co-delivery of a cocktail of factors by EVs is in its infancy, and part of the current study has focused on defining the repertoire of growth factors bound to the EVs surface by betaglycan and other principal membrane-associated HSPGs. The initial and direct approach explored here compared undigested DU145 EVs with HS-deficient EVs,

Chapter 4 - Results

relying on the specificity of the HS-GAG chain digesting enzyme (HEP1III). Thereafter a complementary strategy was employed targeting individual core proteins in the EV-producer cell, using shRNA technologies. This less direct method was expected to present greater complexity due to unpredictable alterations in the cell, and therefore in EV biogenesis and secretion in general, that may arise from these latter manipulations.

The first strategy, through removal of HS-GAG chains, provided very clear and dramatic results. It was possible to demonstrate an association of CYR61, midkine, and TFPI with HS-GAG chains at the surface of DU145 EVs, as removal of these moieties promoted a decrease in signal detection for the aforementioned proteins when compared with undigested DU145 EVs. Past studies have described these proteins as heparin-binding proteins (Sumi et al., 2002, Kadomatsu et al., 2013, Chen et al., 2000, Grzeszkiewicz et al., 2002, Ho et al., 1997), and are associated with several processes in cancer, including angiogenesis. These heparin-binding proteins are also known as heparin/HS-binding proteins, due to the fact that heparin is very closely related in structure with heparan sulphate and is many times used as an experimental proxy to HS due to being more easily available for studies (Ori et al., 2011). However, considering heparin is secreted by basophils and mast cells, while HS is present in proteoglycans at the surface of most cells and in the ECM, it is much more likely that proteins bound to HS play a relevant role in a cancer environment. This work is the first to demonstrate an association between CYR61, midkine, and TFPI with HS-GAG chains on HSPGs present at the vesicle surface. The implication is, of course, that their location allows these factors to encounter their cognate receptors during EV to cell surface encounters. Furthermore, whilst in association with HS-GAG, there is a possible advantageous “hand-over” to such signalling receptors, as this was certainly essential for the vesicle delivery of TGF- β 1 (Webber et al., 2015b).

HSPG regulation of FGF signalling by association with FGF and its tyrosine kinase receptor, FGFR (Yayon et al., 1991, Filla et al., 1998), is one of the most explored roles of HSPGs. The HS-GAG chains serve as a template that bridges FGF and FGFR, and this complex lowers the concentration of FGF necessary to initiate signalling whilst also extending the duration of the response (Forsten-Williams et al., 2005). In addition to this, a model proposed by C. Zehe *et al.* for FGF-2 secretion places cell surface HSPGs as essential for unconventional secretion of FGF-2 by forming a molecular trap that exports FGF-2 from the cell (Zehe et al., 2006). The FGF-2 is then available on the HS-GAG

chains of HSPGs to bind to its high-affinity receptor. FGF-2 secretion was also found to involve exosomes (Ceccarelli et al., 2007). However, later studies showed that neither membrane blebbing inhibition affected FGF-2 secretion or was detection of this protein possible in plasma membrane-derived EVs (Seelenmeyer et al., 2008). In this instance, the authors do not provide enough evidence to claim that what they are studying are indeed EVs from MBV origin, and therefore, their conclusion of no association of these with FGF-2 should be taken with caution. Contrary to their claims that no FGF-2 was detectable on EVs, studies from our group showed detectable amounts of FGF-2 (0.076 pg per μg of EVs) at the surface of DU145 vesicles (Webber et al., 2015b). These levels, even if low, show a vesicular association of FGF-2. Nonetheless, how EV-associated HSPGs could be involved remains unknown. MIF is another protein secreted by unconventional means that might be related to a vesicular secretion route (Schäfer et al., 2004, Flieger et al., 2003). Association of MIF with HS-GAG chains of syndecan-1 in epithelial cells (Pasqualon et al., 2016) places HSPGs once again in the secretory route of leaderless proteins. Galectin (Gal)-1 and Gal-3 are another set of proteins secreted through unconventional means by an export mechanism that appears to involve membrane-bound vesicles (Cooper and Barondes, 1990, Mehul and Hughes, 1997). In the analysis presented in this chapter, both Gal-1 and Gal-3 were associated with HS-GAG chains and HSPG deficiency. All of these examples place HSPGs as important potential players in vesicular unconventional secretion of proteins by serving an association point between protein and vesicle.

Interestingly, as well as considering classical soluble factors, PD-L1, a protein already described to be present at the surface of EVs released by melanoma cells (Chen et al., 2018b), is featured in this analysis as increased in association with vesicular-deficiency of syndecan-3, syndecan-4 and glypican-6. No previous relation of this protein with heparin/HS or HSPGs has been described in literature, and therefore, this novel association might place HSPGs as important players in the loading of transmembrane proteins onto the secreted EVs. In this instance, HSPG would be relevant for presenting PD-L1 to PD-1 on T cells, suppressing the local immune response. Validation of association with HS/HSPGs is required to sustain this hypothesis, but such a scheme may offer therapeutic opportunities to modulate EV cargo in dramatic ways in order to abrogate their varied tumour-promoting activities.

Chapter 4 - Results

According to our current, albeit limited, knowledge of EV biogenesis and incorporation of HSPGs in small vesicles through the endosomal route (Figure 1.7– Chapter 1), it is to be expected that any proteins bound to HSPGs within the endosomal compartment may be present on the outside surface of the secreted vesicle. This would make them readily available to signal at distance and interact with recipient cells in the microenvironment. As previously mentioned, HSPGs constitute promiscuous binding platforms for positively charged proteins. The electrostatic interactions between HS-binding proteins and HS-GAG chains allow fast absorption of proteins from the soluble phase. Secreted ligands, freely available in the extracellular space, could therefore be tethered to the EV surface by HSPGs, either during EV circulation to distant places or in the interstitial space of microenvironments. This would, therefore, provide a more stable way to transport factors and additionally increase the circulating half-life of these proteins by protecting them from proteolytic degradations. The binding of several proteins to the HS-GAG chains also makes them more readily available and allows for co-deliver of factors, which is an advantage compared to proteins secreted in a soluble form. It is possible that EVs loaded with HSPG-bound ligands can be recruited to particular sections within the tumour microenvironment and exert their activity there. Therefore, EVs may enable a more orchestrated cellular response, providing responses that would not otherwise occur through the random diffusion of mixtures of soluble factors.

Furthermore, the shedding of HS-GAG chains by heparanase and the extracellular domain of HSPGs, such as syndecans, by MMPs (Purushothaman et al., 2010, Purushothaman et al., 2008) can further facilitate growth factor availability in the microenvironment, and the distribution and signalling of HS-GAG bound ligands. It is important to note that in this thesis, the bacterial HEP III was used to remove HS from the vesicles, and whereas human heparanase only partially degrades HS, HEP III degrades HS more extensively. Heparanase is able to modulate secretion, cargo and function of EVs, and cells expressing higher levels of heparanase secrete EVs with higher levels of syndecan-1, VEGF and HGF (Thompson et al., 2013). Furthermore, myeloma cells exposed to bortezomib caused increase in heparanase expression and exosome secretion. These exosomes, referred to as chemoexosomes, were loaded with high levels of heparanase that was released from the exosome surface by bacterial HEP III treatment (Bandari et al., 2018). This indicated that heparanase could be bound to HS-GAG chains present on the exosome surface, and this association could be a means for its delivery to distal places. One could also speculate that this heparanase

could contribute to trimming of the vesicular-HS, releasing its associated ligands into the extracellular matrix. On the same note, analysis in this chapter showed an association of MMP-1 and MMP-10 with HS-GAG and HSPGs. Even if MMP-1 detection was inconsistent and somewhat difficult, we have already addressed that the sensitivity of ELISA compared with PEA technology might not be enough to demonstrate these subtle differences. However, the presence of these metalloproteinases associated with HSPGs could indicate a similar role for these proteins to the one described above for heparanase.

Additionally, heparanase has been involved in EV biogenesis, with higher levels of heparanase related with higher EV secretion (Thompson et al., 2013). In EV biogenesis, upon internalization into endosomes, the cytoplasmatic domain of syndecan is able to interact with the PDZ domains of the cytoplasmatic protein syntenin. The other PDZ domain interacts with ALIX that associates with ESCRT through interactions with TSG101 and CHMP4. It is this syndecan-syntenin-ALIX complex that leads to membrane budding and generation of ILV within multivesicular endosomes (Baietti et al., 2012). In turn, it is the heparanase shedding of HS-GAG chains present in endocytosed syndecans that is responsible for promoting syndecan-1 clustering and subsequent association to more syntenin and enhancing EV secretion (Roucourt et al., 2015). This syndecan-syntenin-ALIX mechanism could also have an important role in the cargo that is loaded into EVs, associated with HS-GAG chains of syndecan-1, but further research is necessary to elucidate to what extent this is related with the different pathways taking part in the biogenesis. Additionally, due to HS highly plastic structure, in constant modification by enzymes and the surrounding environment, these can be questions quite difficult to address. Recently, the role of another syndecan in EV biogenesis was elucidated. Tetraspanin-6 (TSPN6) was just recently described as a negative regulator of EV biogenesis by restricting SDC4 shedding, and inhibiting SDC4-syntenin related EV release, as well as addressing SDC4-syntenin complex to lysosomal degradation (Ghossoub et al., 2020). Ultimately these collective studies identify significant complexities of HSPGs and their roles during EV biogenesis, and therefore, it is not surprising that manipulating these elements results in some reductions and elevations in the proteins loaded as we describe.

The putative functions of EV-associated proteins were explored using functional enrichment performed by FunRich. Functional enrichment programs are usually

Chapter 4 - Results

designed to analyse great sets of proteins against big datasets. In this case, despite having small sets of proteins, it was still considered useful to use an enrichment tool, such as FunRich to have a better understanding of the potential pathways regulated by prostate cancer EV-associated HSPGs. Moreover, syndecan and glypican mediating signalling events were featured in the analysis, strengthening the possibility of an affinity between the analysed proteins and HSPGs at the surface of EVs-

A study by Ori A. *et al.*, analysed from 435 collected human proteins interacting with HS or the structurally related heparin, looked into identifying pathways that have an over-representation of heparin/HS-binding proteins using the KEGG collection of pathways (Ori *et al.*, 2011). Similarities can be found between their results and the ones presented here. Both studies highlight enriched pathways for mechanisms related with regulation of cell response to external stimuli, as well as interactions between soluble ligands and cell surface receptors (“cytokine-cytokine receptor interaction”), and several signalling pathways promoted by interleukins, such as IL-6, IL-23, IL-27, and IL-18. “Chemokine associated interactions” are again features of both studies, as well as processes related to cytoskeleton reorganization, such as focal adhesion. Integrin related signalling was also described. The relationship between integrins and EVs in cancer has already been described (Hurwitz and Meckes, 2019). Either by carrying integrins or relying on integrins to deliver their cargo into the cells, these proteins are important for the adhesive and signalling functions promoted by EVs on the tumour microenvironment. HSPGs might have an essential role in the anchoring function related with integrins at the cell surface, that is further supported by studies showing an involvement of EV-associated HS in EV binding to the surface of recipient cells (Purushothaman *et al.*, 2016). CYR61 actually exerts its functions through binding to multiple integrins present in many different cell types (Emre and Imhof, 2014), and a study showed that both integrin $\alpha_6\beta_1$ and cell surface HSPGs are indispensable for the adhesion of normal human skin fibroblasts to CYR61 (Chen *et al.*, 2000). Therefore, proteins associated to EVs through HS-GAG chains can be relevant in these functional events and mediate information exchange between the extracellular space and intracellular signalling pathways.

In conclusion, this chapter highlights several proteins with a likely association to EV-associated HSPGs, particularly to their HS-GAG chains. The demonstrated association of CYR61, midkine, and TFPI with HS-GAG chains present at the surface of DU145 EVs is novel and expands on the current knowledge of HSPG roles in EVs. Additionally,

functional enrichment analysis provides insight into potential biological functions regulated by these proteins. Much is still unknown about loading of proteins into EVs, but the work demonstrated in this thesis provides more information about the likely functional relevance of this axis in the biological processes underpinning cancer.

Summary of objectives met:

- Analysis of Olink data highlighted several proteins with a likely association to EV-associated HSPGs, particularly to their HS-GAG chains.
- Functional enrichment analysis identified several proteins linked with inflammatory and angiogenesis-related pathways.
- Several analytes were detected on DU145 vesicles, such as midkine, CYR61, CCL20, CSTB, IL-8, IL-6, GDF-15 and TFPI. In this thesis it was demonstrated for the first time that CYR61, midkine and TFPI are associated with HS-GAG chains present at the surface of prostate cancer EVs.

Chapter 5
Exploring the impact of
heparan sulphate-deficiency on
extracellular vesicle function

5.1 Introduction

In order to exert their cell signalling role, EVs released from the parent cell can interact with the recipient cell surface and are often internalised, facilitating the release of the EV cargo into the recipient cell. The molecular mechanisms by which EVs are taken up into cells remain unclear. Suggested uptake routes are principally through endocytosis, which encompasses an assortment of mechanisms for macromolecules to traverse the plasma membrane barrier. These include macropinocytosis, phagocytosis, lipid raft-mediated internalisation, clathrin-dependent, and caveolin-mediated mechanisms. Membrane fusion, and subsequent direct release of intraluminal content into the cell, is also proposed, but strong evidence of this is lacking (Mulcahy et al., 2014, van Niel et al., 2018).

Recently, several studies have shed light on the important role of HSPGs on processes leading to both EV biogenesis and uptake into recipient cells. Internalisation of syndecan from the cell surface, has been implicated in the biogenesis of EVs, by mediating interactions between syntenin and ALIX, promoting the formation of multivesicular endosomes (Baietti et al., 2012). Moreover, EV-associated HSPGs also appear to play a role in EV binding, and therefore potentially uptake, in recipient cells. Following release, vesicular syndecan-1 interacts with fibronectin, which acts as a molecular bridge, facilitating the binding to HSPGs on the surface of the target cell (Figure 1.7 – Chapter 1) (Purushothaman et al., 2016). The levels of heparan sulphate and fibronectin present also seem to be important, as EVs with low levels of these molecules do not bind as avidly to target cells. Thus, the phenotype of vesicles and recipient cells appears to dictate the nature of binding and uptake interactions that occur, as might be expected. Another study suggests that HSPGs present on the surface of glioblastoma cells, rather than those on vesicle membranes, are required for facilitating vesicular uptake, since removal of HS from EVs had no effect in their internalisation (Christianson et al., 2013). However, saturating the system with exogenous heparin, which is molecularly similar to HS, appears to compete with cell surface HS to bind EVs, and this was an effective means of blocking subsequent cellular entry of EVs in this system.

HSPGs, as shown in this thesis, mediate the tethering of a range of factors to the EV surface. Previous studies from our group, focussing on vesicular delivery of TGF- β 1 to fibroblasts, have indicated the qualitative importance of this form of growth factor delivery in determining the biological response which occurs. Although TGF- β 1 is known to be

Chapter 5 - Results

involved in myofibroblast differentiation, soluble TGF- β 1 fails to generate the myofibroblast phenotype associated with tumour supporting characteristics. In contrast, betaglycan was shown to be important for tethering TGF- β 1 to the EV surface and for effective functional delivery to fibroblasts (Webber et al., 2010). This distinctive feature requires the HS-GAG chains of EVs, as digestion of these moieties attenuated the EV-induced SMAD3-dependent TGF- β signalling, and consequently impaired generation of a myofibroblast phenotype capable of tumour supportive functions (Webber et al., 2015b). EV-activated fibroblasts also secrete heightened levels of cytokines, such as urokinase (uPA), VEGF-A, FGF-2 and particularly HGF, compared with myofibroblasts differentiated through soluble TGF- β 1 (Webber et al., 2015b). This altered secretome is attenuated by removal of HS on vesicles, underlying the importance of HSPG in supporting differentiation to a disease supporting phenotype.

In the tumour microenvironment, extracellular matrix remodelling, angiogenesis and accumulation of immune cells are orchestrated by many growth factors, cytokines and chemokines, such as VEGF, PDGF, EGF, CXCL12, IL-8 and others. Activated fibroblasts are a source of many of these components, actively recruiting different cells to the tumour site and potentially exerting immunomodulatory functions (Kalluri, 2016). Therefore, it is possible to speculate that activation of fibroblasts by EVs can modulate tumour immunity in an indirect fashion, through the actions of fibroblasts/myofibroblasts. This indirect effect of EVs in immune modulation has not been as widely studied as the direct effect of EVs in immune cells (Maia et al., 2018).

One of the earliest roles attributed to EVs was their function as antigen-presenting vesicles, able to activate T cells in an MHC and peptide restricted manner (Raposo et al., 1996). Since then, many mechanisms have been described for EV modulation of T cells. EVs have been shown to express the immune checkpoint ligand PD-L1 at their surface, which has the potential to bind to T-cell inhibitor receptor programmed death-1 (PD-1) and block T-cell activation and proliferation (Poggio et al., 2019, Ricklefs et al., 2018). Tumour-derived EVs were also shown to suppress immune responses by inhibiting cytotoxic effector cells while at the same time supporting IL-2 induced Treg activation, an effect mediated in part by EV delivery of TGF- β 1 to lymphocytes (Clayton et al., 2007). NKG2D-dependent cytotoxicity of NK cells and CD8⁺ T cells is blocked by tumour-derived EVs carrying TGF- β 1 and NKG2D ligands (Clayton et al., 2008b), and microvesicles may also drive downregulation of CD3- ζ chain expression in T cells by carrying FAS ligand. This attenuates signalling through the T cell receptor, as well as

inducing T cell apoptosis (Taylor et al., 2003). However, these immune cell-focused studies have not probed the importance of EV-associated HSPGs in the delivery of factors that might modulate such receptors.

Tumour-derived EVs also have been attributed with the ability to support a pro-tumour microenvironment by polarising macrophages to an M2-like subset. One study showed that tumour-EVs are necessary to programme macrophages to an M2-state by activating of TLR2 and TLR3, leading to the secretion of cytokines that further drive tumour invasion and metastasis, as well as reprogramme the tumour microenvironment (Rabe et al., 2018). Similarly, polarisation of macrophages towards an M2 immuno-suppressive phenotype and induction of IL-6 secretion is promoted by activation of the STAT3 pathway in bone marrow-derived macrophages by breast cancer-derived exosomes enriched in glycoprotein 130 (Ham et al., 2018). In fact, Gabrusiewicz *et al.* showed that exosomes derived from glioblastoma stem cells seem to be preferentially taken up by monocytes leading to an M2 phenotype that is marked by upregulation of PD-L1 (Gabrusiewicz et al., 2018). Besides polarisation, EVs can also affect macrophage migration and their contribution towards pre-metastatic niche formation in several cancers, such as myeloma (Bandari et al., 2018) and liver (Costa-Silva et al., 2015), has been described. Due to their ability to promote a microenvironment suitable for cancer progression, macrophages became an interesting focus to study EV roles in immune modulation.

The interaction of HSPGs with cytokines and growth factors, resulting in modulation of the immune system, have been described previously (Proudfoot et al., 2003, Simon Davis and Parish, 2013). These studies, however, did not explore the involvement of EVs. Many factors implicated in immunological modulation have been highlighted as EV-associated in the previous chapter. For this reason, HSPGs on the EV surface may act as mobile reservoirs, involved in growth factor presentation to immune cells, contributing towards regulation of tumour immunity. Whether or not this potential influence on macrophage function is promoted directly and/or indirectly by EV-driven modifications to stromal function is the subject of this chapter.

5.1.1 Aims & Objectives

This chapter aims to explore the impact that disruption of the HS-GAG chains enacts in fibroblast function, as well as direct and indirect effects in differentiation and polarisation of macrophages.

The main goals of this chapter were to:

- Assess the impact of HS-GAG chain removal on the capacity for EV to gain cellular entry into fibroblasts.
- Explore the capacity of HSPG-deficient EVs to drive fibroblast differentiation towards a disease associated phenotype.
- Evaluate how receptor activation and cytokine secretion in fibroblasts are impacted by removal of vesicular HS.
- Explore the indirect and direct effects of EVs on myeloid cells and the consequences of HS-removal in these effects.

5.2 The impact of HS removal on vesicle uptake by fibroblast cells

5.2.1 *Imaging of EV uptake by fluorescent microscopy*

Due to the reported significance of HS-GAG chains on the uptake of EVs by cells (Purushothaman et al., 2016, Christianson et al., 2013), the impact of HEP1III treatment on fibroblast uptake of EVs was evaluated. A protocol for fluorescently labelling purified DU145 EVs was previously developed in the laboratory (Roberts-Dalton et al., 2017). This involves the addition of maleimide-Alexa Fluor 594, to form chemically stable thioether bonds between maleimide and sulfhydryl groups of EV surface proteins. It is, therefore, a surface-labelling approach, delivering sufficient fluorophore onto the EVs to allow optical tracking and analysis of cells incubated with EVs by flow cytometry. Details of the approach are found in section 2.6.2.1 (Chapter 2). EVs treated with active and heat-inactivated forms of HEP1III, as well as untreated (no enzyme) EVs, were labelled with maleimide-Alexa Fluor 594. Native control EVs were used in this experiment as there was uncertainty if the enzymatic incubations and additional ultra-centrifugation step could affect EV-labelling efficiency. In addition, a control for “free dye” was included. This represents a potential scenario where during the dye-labelling protocol, a chromatographic spin column is used to trap non-incorporated Alexa 594-maleimide, and this control reports on the efficacy of dye removal. Fibroblasts were treated with 25 µg/mL of labelled EVs in DMEM/12 for 1 hour. The dosing and timepoint chosen were informed by a previous PhD project in the laboratory and allow for optimal visualisation of EV uptake (Cocks, 2019). Cells were fixated with 4% PFA and stained with Actin Green (AlexaFluor™ 488 phalloidin) and NucBlue™ for the nuclei and imaged by fluorescence microscopy.

Images identify labelled EVs inside the fibroblasts across all EV-treatment conditions (**Figure 5.1**), observed as clear individual red puncta. These puncta, representing endocytosed EVs, appear within the cytosol in most cases, with occasional examples of distribution on, or close to, the plasma membrane. There was no evidence that the spatial distribution of EVs within the cells was altered as a consequence of HEP1III digestion, neither was there obvious attenuation of the extent of uptake. Distribution of EVs across individual cells within the microscopic field was heterogeneous, however (**Figure 5.1, regions 1 and 2**), and as such flow cytometry was employed to aid quantitative assessments.

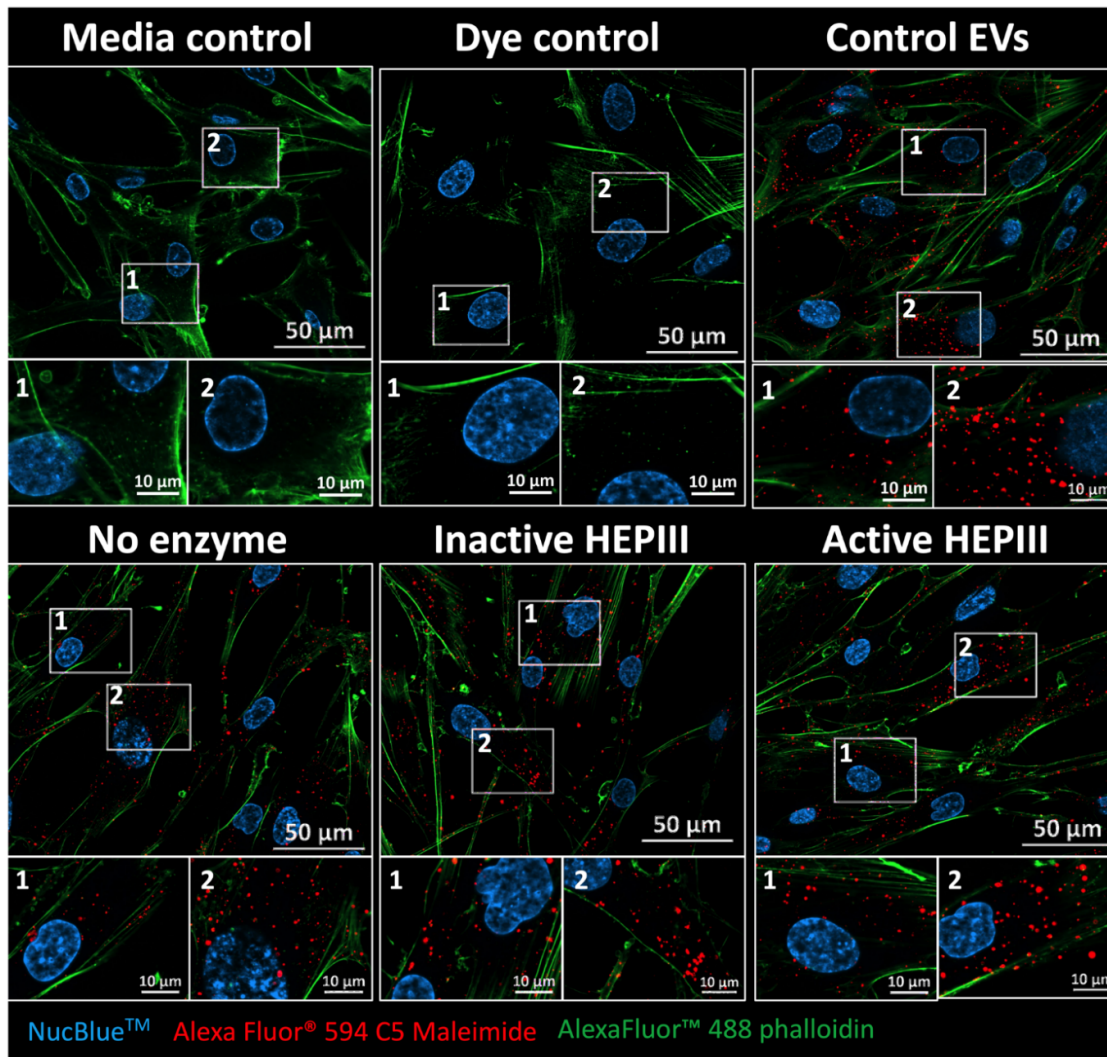


Figure 5.1. Uptake of Alexa-594 labelled EVs by fibroblasts. Fibroblasts were treated for 1 hour with 25 µg/mL of Alexa-594 labelled EVs (red), control media or a control for free dye. EVs had been previously treated with heat-inactivated HEP111, active HEP111, or no enzyme. Control EVs are DU145 native EVs not exposed to HEP111 and serve as a control of the digestion protocol. Cells were fixed with 4% PFA and actin stained with AlexaFluor™ 488 phalloidin (green), and nuclei with NucBlue™ (blue). Cells were visualised by fluorescence microscopy and images captured by Axio Observer Z1 microscope with a ZEISS Plan Apochromat 63x/ 1.4 Oil objective. Representative microscopic fields of single Z stacks are shown (scale bar = 50 µm) and also represented are regions of interest at higher magnification showing areas of lower (1) or higher (2) EV-incorporation (scale bar = 10 µm). Images are representative from an experiment of 9 fields of view across 3 wells.

5.2.2 Semi-quantitative analysis of EV uptake by flow cytometry

To obtain a quantitative measure of potential differences in uptake within the fibroblast population, detection of Alexa Fluor 633-labelled EVs in fibroblasts was assessed by flow cytometry. As previously, fibroblasts were treated with 25 µg/mL of labelled EVs in DMEM/12 for 1 hour and then trypsinised and resuspended in PBS, to be used in the flow cytometer. Trypsinisation acts to liberate EVs that have not yet gained cell entry, allowing these to be washed away (personal communication Dr Alex Cocks and Prof Aled Clayton). Gating was performed based on forward and side scatter, to eliminate cell debris and larger particles from the analysis. The gating strategy used to analyse these experiments is shown in Figure 2.3, Chapter 2.

Detection of fibroblast-associated Alexa-labelled EVs is demonstrated by the histograms, showing significant fluorescent signal consistent with uptake of EVs incorporated into the cell, when comparing cells treated with the control for free dye (**Figure 5.2 A**). There is a small percentage of the cells that are negative in the histogram, meaning they have not taken up EVs. This is roughly 1.8% for no enzyme, 3.2% for inactive HEP111 and 3.5% for active HEP111 populations. It is apparent that the histograms broadly overlap when comparing the three conditions (**Figure 5.2 B**), indicating that incorporation of labelled EVs by the cells is similar between the different conditions under study. This is also asserted by the MFI (**Figure 5.2 C**).

Removal of HS-GAG chains from EVs does not grossly affect its uptake, as shown by the EV signal detected in fibroblasts incubated with active HEP111-treated EVs compared to those incubated with untreated EVs. When comparing these conditions, the difference in fluorescence intensity is small and not significant. However, the presence of the heat-inactivated enzyme in the system seems to negatively impact EV uptake. The reasons for this are unclear and are likely related to the technical challenges of these experiments, in terms of quantifying and normalising the EV concentration added to the cells, in an absolutely uniform fashion, across the treatments. Alternatively, the denatured HEP111 protein may have a direct effect on the endocytic processes involved or the capacity of EVs to bind to the fibroblasts, in ways we do not understand. Overall, despite the experimental difficulties, the removal of HS chains from EVs is limited in terms of the interaction between EVs and fibroblasts and enzyme-treated EVs remain competent in gaining cell entry.

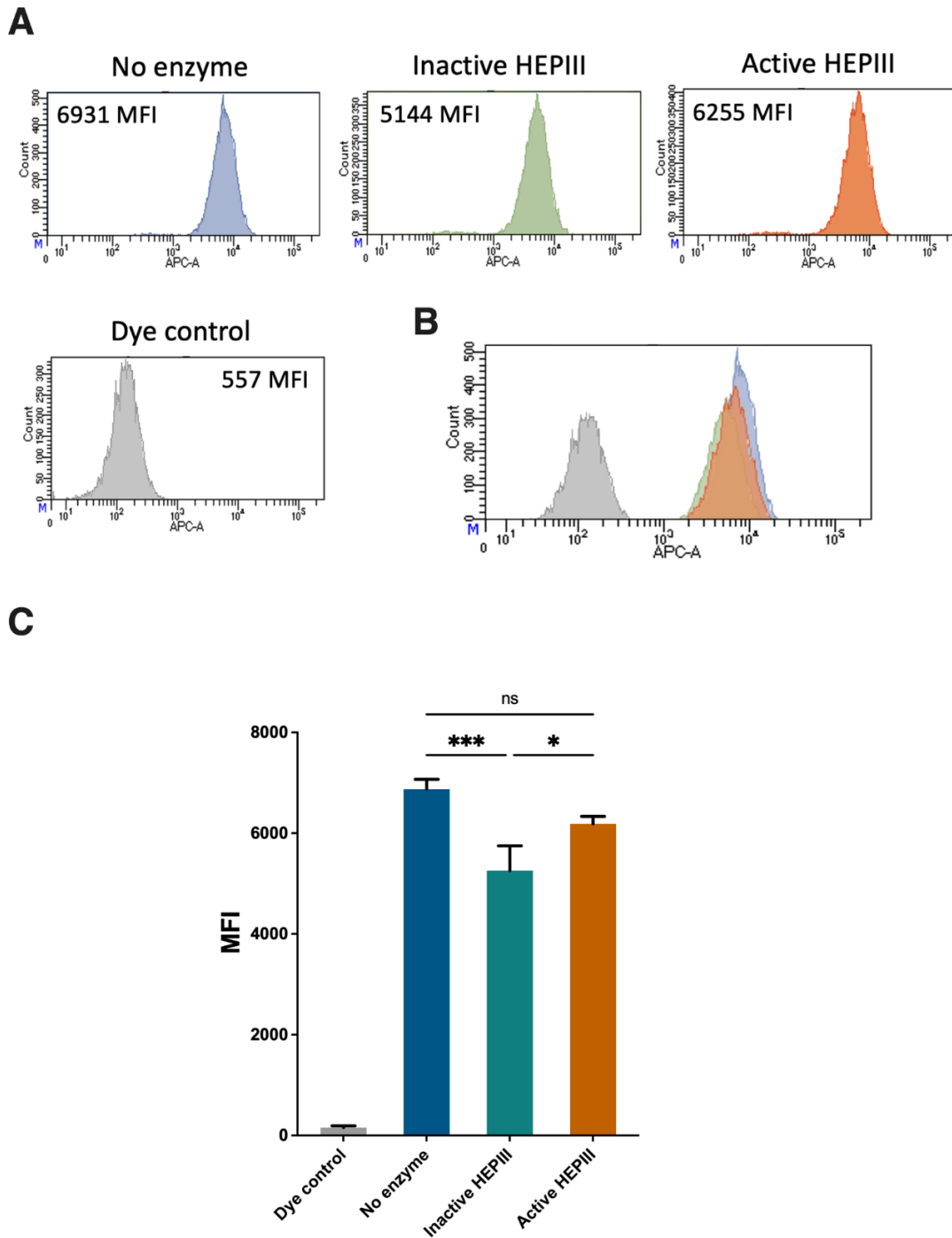


Figure 5.2. Quantification by flow cytometry of the uptake of Alexa-633 labelled EVs by fibroblasts. Fibroblasts were treated for 1 hour with 25 µg/mL of Alexa-594 labelled EVs or a control for free dye. EVs had been previously treated with heat-inactivated HEP111, active HEP111, or no enzyme. **(A)** Detection of Alexa-633 labelled EVs uptake by fibroblasts is represented by histograms for no enzyme (blue), inactive HEP111 (green), active HEP111 (orange) treated EVs and control for free dye (grey). **(B)** Comparison of signal between the study conditions by histogram overlays. **(C)** Bar graph represents the median fluorescent intensity (MFI) values. Graph shows mean ± SD of technical triplicates, and similar results were obtained in a total of 5 experiments. *p<0.05; ***p<0.001, one-way ANOVA with Tukey's multiple comparison test.

5.3 HS-mediated regulation of EV-related functions

5.3.1 Fibroblast differentiation

5.3.1.1 Induction of an α SMA-positive myofibroblast-like phenotype

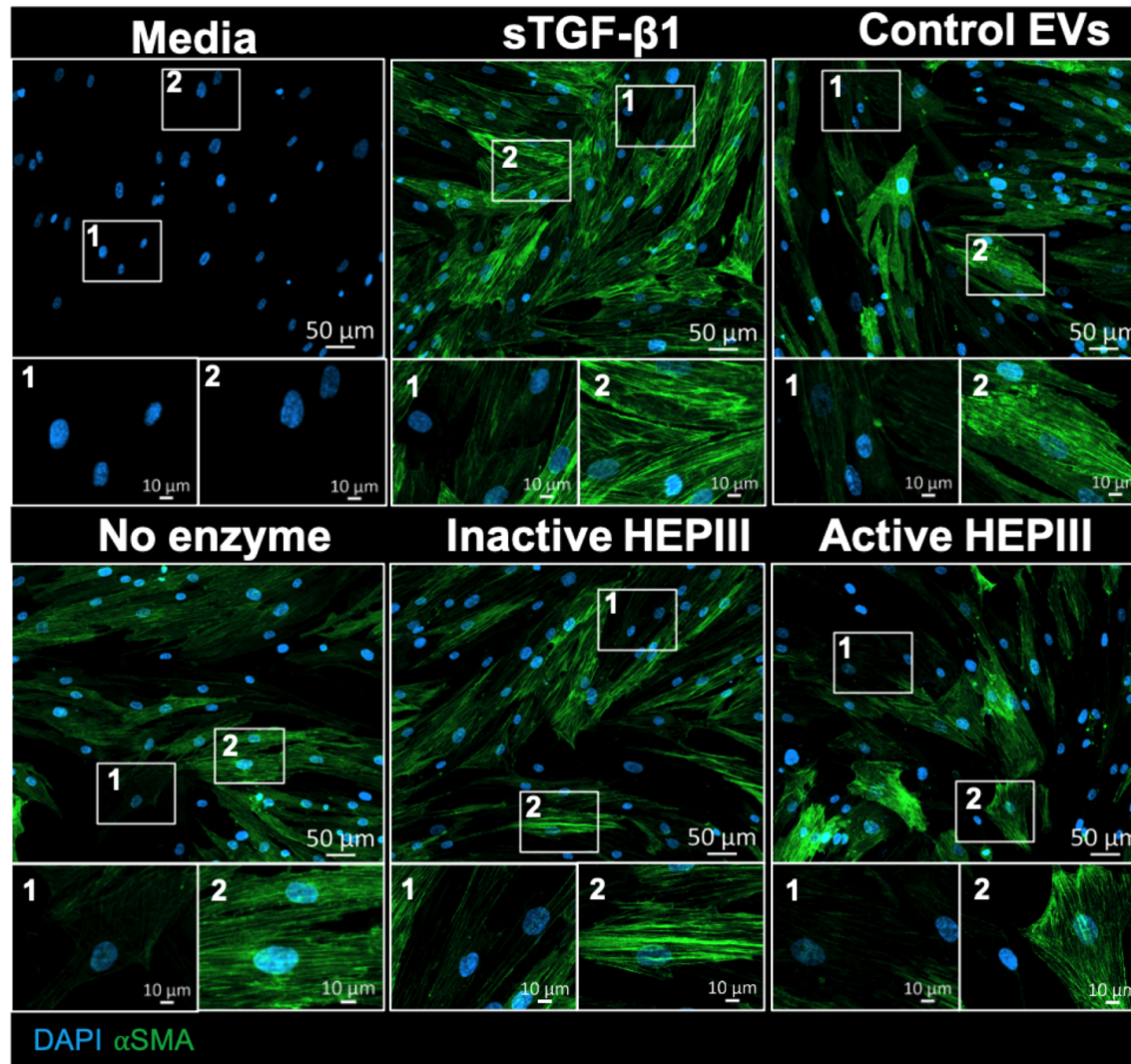
The onset of α SMA stress fibres is among the critical defining features of myofibroblast differentiation (Rønnov-Jessen and Petersen, 1993), and the capacity of DU145 EVs to drive this process is well documented (Webber et al., 2010, Chowdhury et al., 2015, Webber et al., 2015b). To explore if HS-modified EVs remain capable of triggering myofibroblast differentiation, an evaluation of α SMA expression on primary fibroblasts treated with HS-GAG chains modified EVs was undertaken.

Fibroblasts were cultured as described in section 2.1 (Chapter 2), in microscopy plates, and treated for 72 hours with pre-determined EV doses of 200 μ g/mL. Assuming the EV-associated TGF- β 1 is consistent across individual preparations, this would equate to 1.5 ng/ml of EV TGF- β 1, as we have previously reported (Webber et al., 2010). A positive control using this equivalent dose of 1.5 ng/mL soluble TGF- β 1 (sTGF- β 1) was used to compare the EV and sTGF- β 1 mediated effects, as well as a media control. Native control EVs were used in this experiment as a control of the enzymatic digestion process. Cells were fixed and then stained for α SMA and visualised by fluorescent microscopy (**Figure 5.3**). Growth arrested fibroblasts, cultured in FBS-free media, do not express α SMA. DU145 control EVs and sTGF- β 1 are both able to strongly trigger the onset of α SMA expression, translated into stress fibres, indicative of an acquired contractile myofibroblastic phenotype (**Figure 5.3 A**). The EV-induced response is more heterogeneous than that of sTGF- β 1, and this is consistent with previous reports from the group (Webber et al., 2010). Various fibroblasts treated with active HEP111-digested EVs appear to lack the expression of α SMA, which is demonstrated by the higher number of nuclei (blue) not surrounded by α SMA fibres. Additionally, the staining is at times much weaker, with a fainter expression of α SMA than the cells treated with the undigested control conditions. EV conditions where vesicles were not treated with enzyme or were treated with heat-inactivated HEP111 show a similar outcome compared to control EVs. An estimation of the reduced differentiation is presented (**Figure 5.3 B**), where the proportion of α SMA-positive cells across several microscopic fields were assessed. These data confirm that vesicular HS-GAG chains are relevant for fibroblasts to

Chapter 5 - Results

differentiate into myofibroblasts, as their removal partly attenuates the efficacy in stimulating the response, as previously demonstrated (Webber et al., 2015b).

A



B

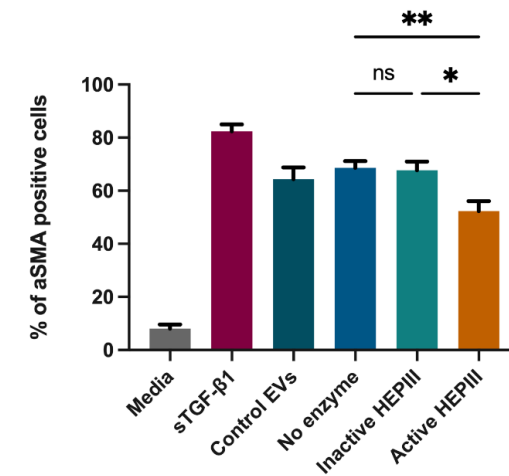


Figure 5.3. Myofibroblast differentiation induced by EVs. (A) Fibroblasts were treated for 72 hours with 200 μg/mL EVs, 1.5 ng/mL sTGF-β1 or control media. EVs had been previously treated with heat-inactivated HEP111, active HEP111, or no enzyme. Control EVs are DU145 native EVs and serve as a control of the digestion protocol. Cells were fixed and stained for αSMA (green), and nuclei were stained with DAPI (blue), and visualised by fluorescence microscopy. Representative fields show examples of zones with stress fibre structures less (1) or more (2) accentuated. (B) The proportion of positive fluorescent cells was normalised to total cell number and bar graph shows mean ± SD of a representative experiment, based on at least 9 fields of view from triplicate wells per condition. **p<0.01, one-way ANOVA with Tukey's multiple comparison test.

5.3.2 The impact on fibroblast function

5.3.2.1 Impact of vesicles on common signalling pathways

After confirming that removal of HS-GAG chains from EVs was able to modestly impact myofibroblastic differentiation, the potential consequence of HS-attenuation on EV-mediated intracellular signalling events was explored. A low-density protein array (R&D Systems) was used to explore functional differences in terms of receptor activation.

Fibroblasts were cultured as previously described and stimulated with 200 µg/mL of EVs (untreated, inactive HEP1III and active HEP1III treated) for 2 hours. A control condition of untreated fibroblasts, incubated in media only, was also included. Cell lysates were collected, corrected for protein differences, and 100 µg of lysate was incubated with the array membranes. The chosen array covers the phosphorylation of 49 human receptor tyrosine kinases (RTKs), and this system has revealed several differences arising depending on the EV-treatment condition.

Untreated fibroblasts displayed some receptors that were constitutively active. Comparing no enzyme, or inactive HEP1III treated EV conditions, to untreated fibroblasts shows an elevation in the levels of several of these RTKs, and importantly, that the fibroblast response is extremely and reassuringly similar, across these EV treatments (**Figure 5.4 A and B**). Despite minor differences in ranking position and density measures, the list of activated receptors with at least 1.5-fold change is the same for both conditions

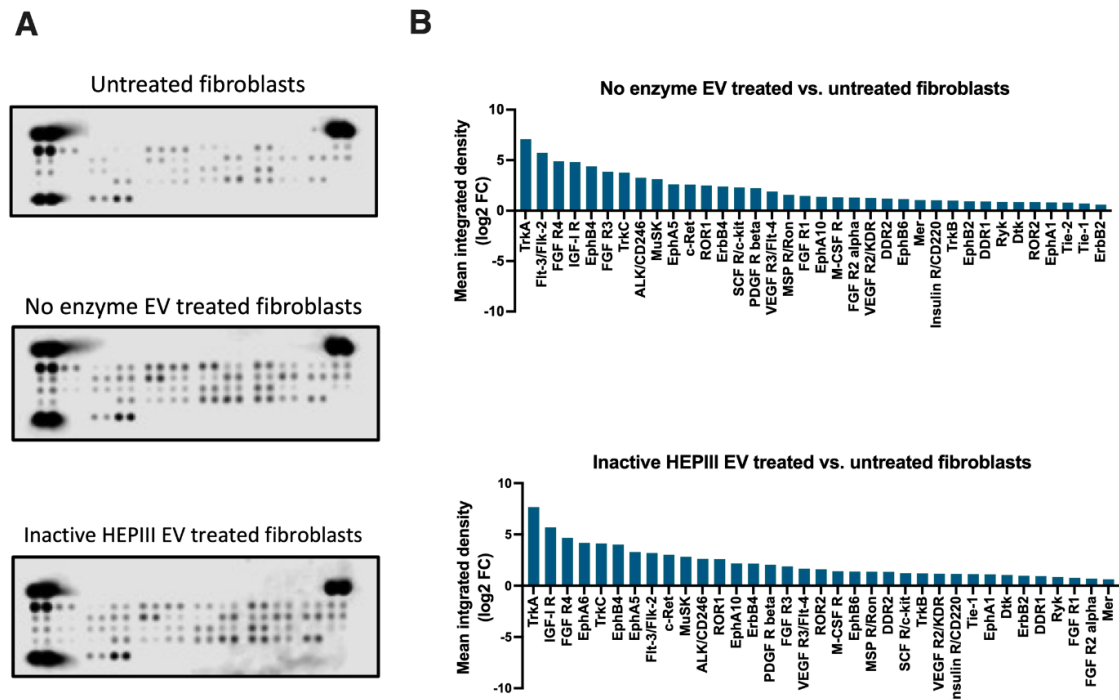
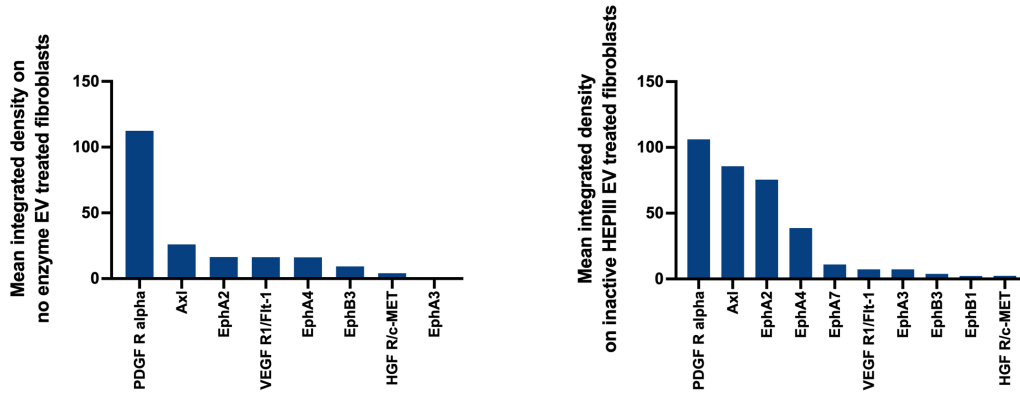


Figure 5.4. Tyrosine kinase receptors activation in fibroblasts treated with prostate cancer EVs, compared with untreated cells. (A) Scanned images from the phospho-RTK array performed on fibroblasts cell lysates incubated for 2 hours with media only (untreated fibroblasts) or EVs treated with either inactive HEPIII enzyme or no enzyme. **(B)** Bars represent the log₂ of at least 1.5-fold change of the densitometry-based analysis of duplicate dots for the receptors differently phosphorylated following incubation with EVs treated with no enzyme or inactive HEPIII enzyme compared to untreated fibroblasts. The coordinates identifying the target proteins represented by each pair of dots on the array are shown in Appendix 5.1.

Both digestion control conditions, untreated and inactive HEPIII-treated EVs, were able to promote phosphorylation of receptors that were not constitutively activated in untreated fibroblasts. Calculation of fold-change was not possible for some of the identified receptors due to lack of activation detectable on the untreated fibroblasts; hence the mean integrated density (MID) from the densitometry-based analysis is shown (**Figure 5.5 A**). MID for most of these receptors sits at the lower end of the values detected on the membranes, indicating that activation is not strongly promoted by either of the EVs conditions (**Figure 5.5 B, heat map**), with the exception of PDGF R alpha that is strongly detected in both membranes. However, it is important to remember that the biological relevance of this activation cannot be defined by the magnitude of signal measured, and these data can only indicate those receptors that are most strongly activated by these EV conditions.

A



B

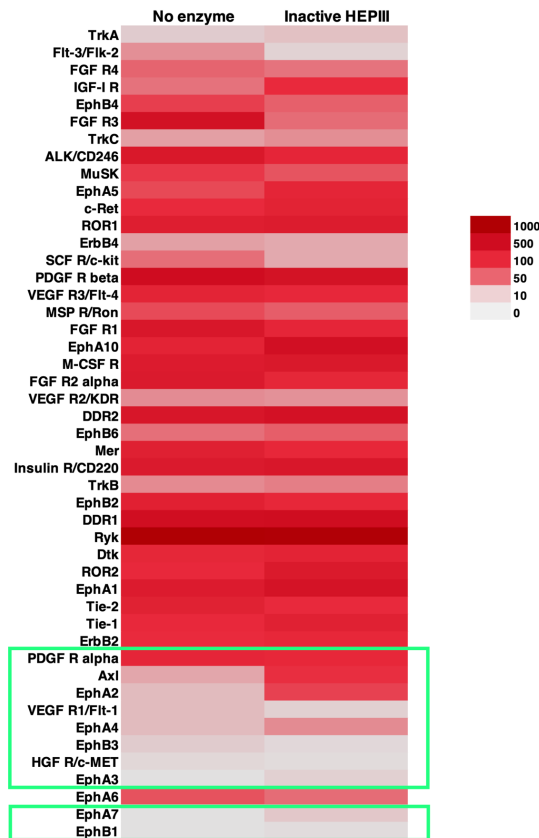


Figure 5.5. EVs promote phosphorylation of proteins not constitutively active in fibroblast cells. (A) Graphs showing mean integrated density (MID) from the densitometry-based analysis for receptors activated by EVs treated with no enzyme or inactive HEP3III, but null in untreated fibroblasts. **(B)** Heatmap of the MID values detected for receptors with 1.5-fold change activation on fibroblasts incubated with EVs treated with inactive HEP3III or no enzyme compared to untreated fibroblasts. Receptors that were below detection limits in untreated fibroblasts yet were detected following stimulation with EVs are indicated by the green box.

To explore the impact of HS-GAG chain removal on the ability of EVs to activate receptors in fibroblasts, fold change was calculated comparing cells treated with active HEP111 and inactive HEP111 EVs and receptors with a difference of at least 1.5-fold change were plotted in **Figure 5.6**. Most receptors are preferably activated by EVs with intact HS-GAG chains when compared with EVs lacking these moieties. FGF R4 and IGF-I R (insulin-like growth factor 1 receptor) have the most pronounced changes, with the VEGF receptors affected as well as c-ret, c-kit, and ALK/CD246 receptors. Ligands for these receptors, Glial cell-derived neurotrophic factor (GDNF) (c-ret), SCF (c-kit) Insulin Like Growth Factor Binding Protein 2 (IGFBP2) (IGF-I R) and midkine (ALK/CD246), have been identified in the Olink analysis explored in Chapter 4, where digestion leads to a reduction in these EV-associated ligands. Particularly, the decrease of midkine detection at the surface of HS-deficient vesicles is shown in the previous chapter of this thesis (**Chapter 4, Figure 4.10 A and B**). Ephrin type A receptor (EphA)2, EphA3 and EphA4, previously identified as de novo activated in fibroblasts after EV stimulation (**Figure 5.5**), here have their phosphorylation completely abolished when fibroblasts are stimulated with EVs lacking HS-GAG chains (**Figure 5.6 C**). This can be indicative of the importance that HS-GAG chains might have in transporting ligands for these fibroblast receptors. Additionally, of notable interest is that some receptors exhibit heightened phosphorylation following treatment with digested EVs. The loss of vesicular HS seems to increase phosphorylation by HGF R/c-Met, EphB1 and EphB3. This might be explained by the possible delivery of HS-associated factors that negatively regulate these receptors under usual situations, and the loss of these negative influences by HS-digestion allows receptor activation to occur.

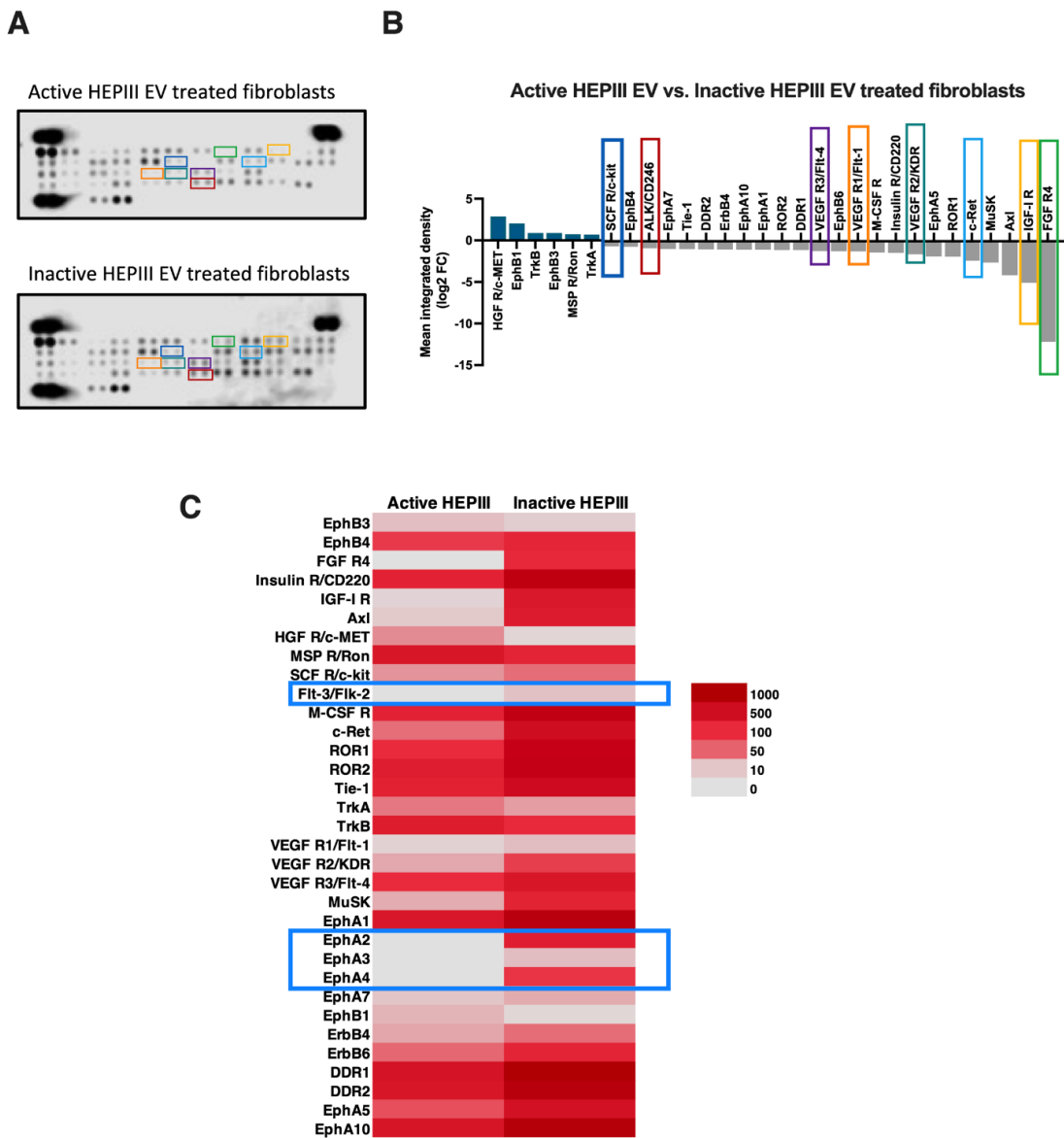


Figure 5.6. Removal of HS-GAG chains alters receptor activation promoted by EVs. (A) Scanned images from the phospho-RTK array on cell lysates from fibroblasts incubated for 2 hours with EVs treated with either active or inactive HEP1III enzyme. **(B)** Fold change of the densitometry-based analysis for the receptors differently phosphorylated following incubation with active HEP1III compared with inactive HEP1III EVs. Colour boxes reveal some HS-GAG chains driven changes, identifying the position of the analyte on the membranes and correspondingly on the bar graph. **(C)** Heatmap of the MID values detected for receptors with 1.5-fold change activation for active HEP1III EVs compared to inactive HEP1III EVs. Receptors only detected for the inactive HEP1III condition are also included and indicated by the blue boxes.

Previous work published from the lab had investigated the detection of HGF, FGF-2, and VEGF at the surface of EVs. While HGF was not detectable, at the tested dose of 1.5 ng/ml, it was possible to detect FGF-2 and VEGF on the vesicles (Webber et al., 2015b). Here, detection of VEGF in HS-deficient EVs was lower when compared to the controls (**Figure 5.7 A**). HGF detection was not possible, most likely because it sits below the detection sensitivity of this assay (**Appendix 5.3**), and FGF detection, despite a trend towards a HS-dependency, was not statistically significant (**Figure 5.7 B**). The reduction of detectable VEGF at the surface of active HEP1III-treated EVs is consistent with the loss of phosphorylation of VEGF receptors, observed in **Figure 5.6 B**.

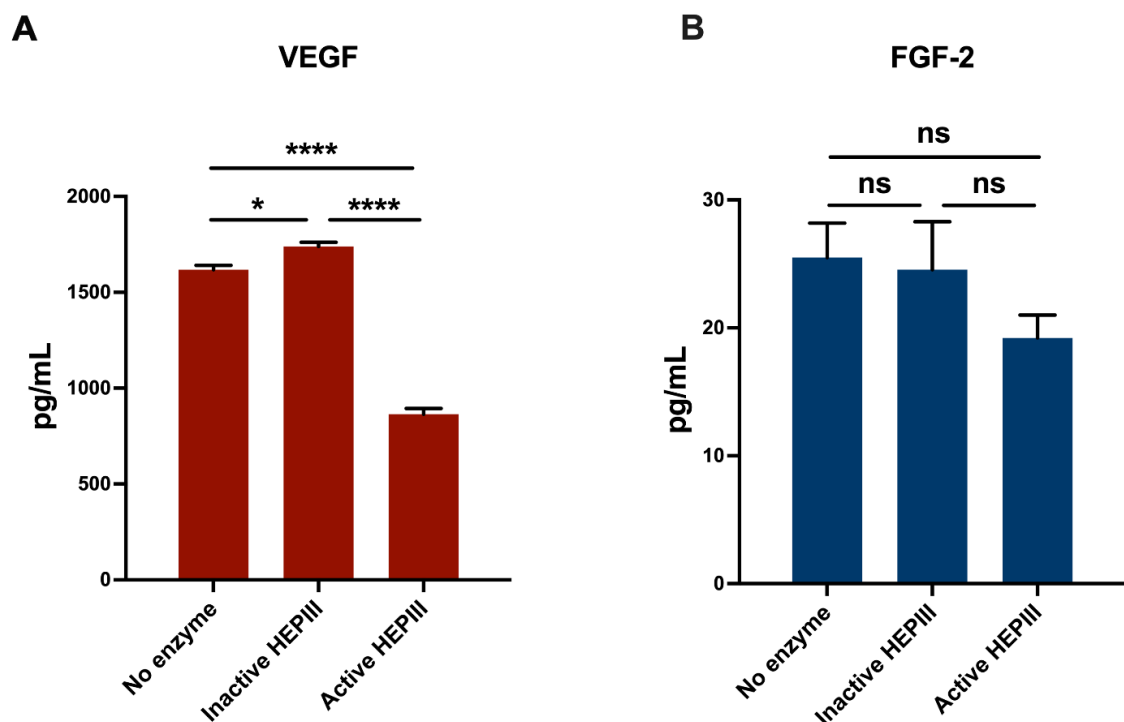


Figure 5.7. Detection of VEGF and FGF on vesicle surface. ELISA was performed in intact EVs to assess protein detection on vesicle surface. The bar graphs show \pm SD of triplicate wells for the quantification (pg/mL) of VEGF (**A**) and FGF (**B**) per 4 μ g of untreated (no enzyme), inactive HEP1III and active HEP1III treated EVs. A representative experiment is shown. **** p <0.001; * p <0.05; ns=non-significant, one-way ANOVA with Tukey's multiple comparison test.

5.3.2.2 Impact of vesicles on fibroblast cytokine secretion

Next, to evaluate the repertoire of cytokines produced by EV-stimulated fibroblasts, a human cytokine array was used. This comprises 105 protein analytes, encompassing a range of inflammatory and angiogenesis-related factors (**as detailed in Appendix 5.2**). Fibroblasts were cultured as previously described and stimulated with 200 µg/mL of EVs untreated (no enzyme) or pre-treated with either active or heat-inactivated HEP III enzyme for 72 hours. Stimulated cells were incubated with Golgi-Stop and Golgi-Plug 18 hours before lysis, to prevent cytokine secretion, and hence trap these factors inside the cell. Cell lysates were collected, assessed for protein quantity and 100 µg of lysate was incubated with the array membranes to detect the cytokines present.

In this assay, most of the proteins featured in the array did not produce any detectable readout, with very few analytes identifiable in the membranes. Again, comparing untreated fibroblasts with fibroblasts stimulated with untreated or inactive HEP III pre-treated EVs shows that the presence of HEP III enzyme in the system does not drastically affect the EV-induced production of cytokines by fibroblasts. Analysis of fold-change found six proteins with at least a 1.5-fold change between untreated fibroblasts and fibroblasts stimulated with control EVs (**Figure 5.8 A and B**). Interesting, IL-8 seems to be produced constitutively by unstimulated fibroblasts, and EV stimulation decreases its production by these cells.

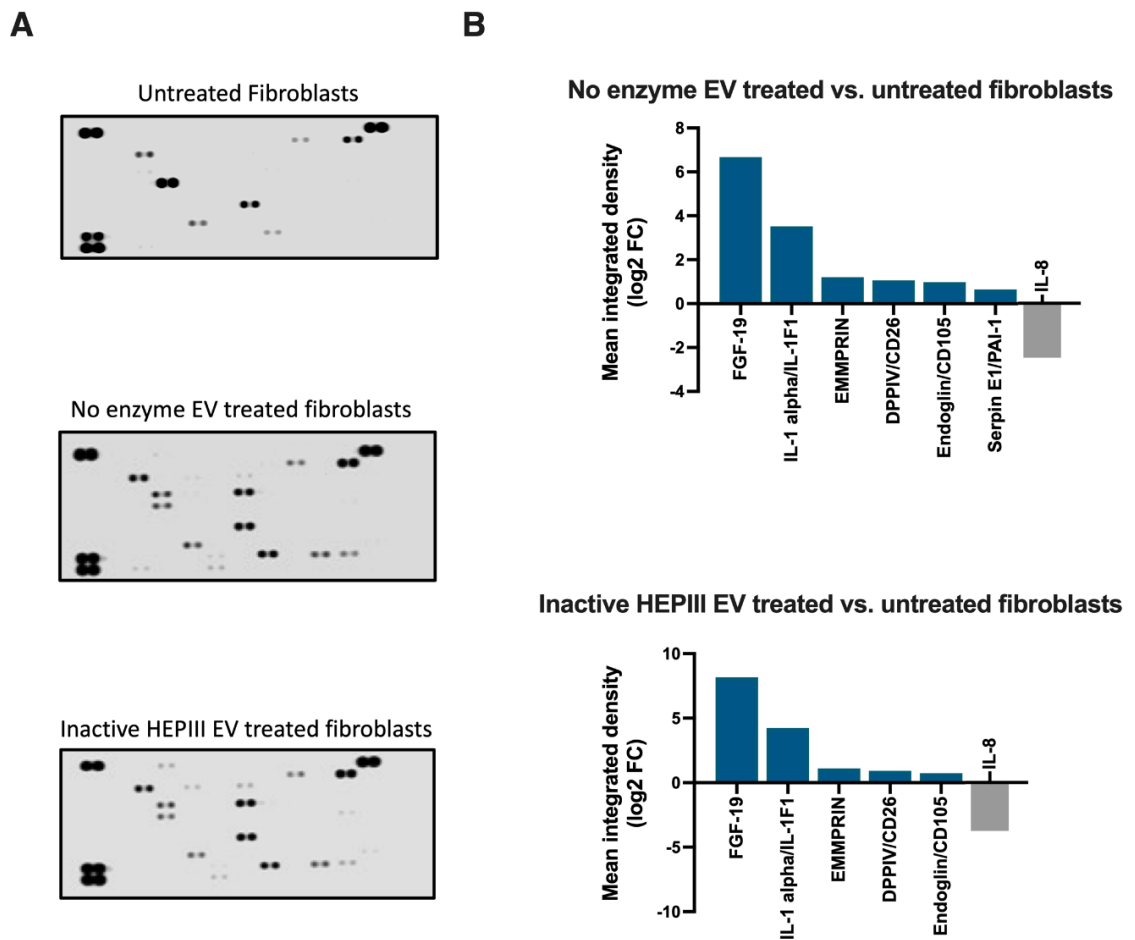


Figure 5.8. Proteins produced by fibroblasts treated with prostate cancer EVs, compared with untreated cells. (A) Scanned images from the cytokine array performed on fibroblasts cell lysates incubated for 72 hours with media only (untreated fibroblasts) or EVs treated with either inactive HEPIII enzyme or no enzyme. **(B)** Bars represent the log₂ of at least 1.5-fold change of the densitometry-based analysis of duplicate dots for the receptors differently phosphorylated following incubation with EVs treated with no enzyme or inactive HEPIII enzyme compared to untreated fibroblasts. The coordinates identifying the target-proteins represented by each pair of dots on the array are shown in Appendix 5.2.

Chapter 5 - Results

Most cytokines detectable in fibroblasts stimulated with EV were not produced by fibroblasts in a growth-arrested state. These cytokines were detectable at very different intensities, with proteins like ICAM-1 being strongly induced by EVs, while others, such as GDF-15 and IL-6, were detected with very low signal (**Figure 5.9 A and B**). More than half of the proteins that are stimulated by EVs have a very low signal intensity in the arrayed sample. In some cases, like IFN-gamma, detection is possible for fibroblasts activated by untreated EVs but not for inactive HEPIII EVs. However, the signal is very low in both samples, and it raises the question of it being a technique-related artefact. FGF-2, IL-17A, (SDF1)/CXCL12 and angiogenin are particularly relevant when active and inactive HEPIII EVs are compared. However, these seem to be markedly less produced by EVs treated with no enzyme than those treated with inactive HEPIII (**Figure 5.9 B**).

The reason for this is unknown to us, considering that other proteins such as VEGF and VCAM-1 show similar results for both EV control conditions in the same array. One possible explanation is that inactive enzyme is not completely inactivated by the elected process, and some residual activity remains. These EVs would therefore carry a different heparome compared with EVs treated with no enzyme and would distinctively influence the cell secretome, explaining the differences observed in secretion of these factors in particular. The presence of residual enzyme in the system could also influence the ability of EVs to interact with the cell, as reported in the uptake data.

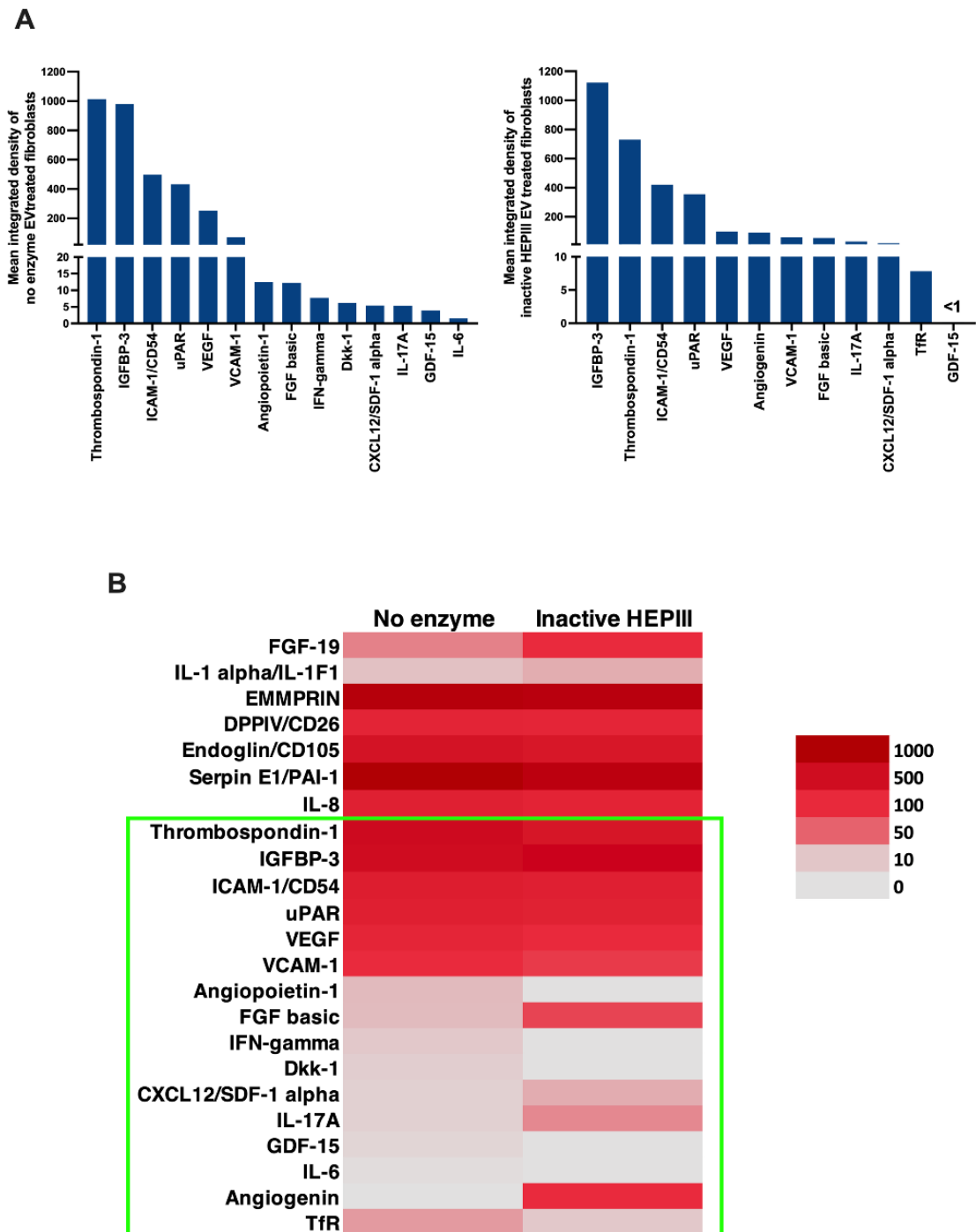


Figure 5.9. EVs promote production of different cytokines by fibroblast cells. (A) Graphs with mean integrated density (MID) from the densitometry-based analysis show the values detected for cytokines produced by fibroblasts stimulated with EVs treated with no enzyme and inactive HEP111 enzyme. **(B)** Heatmap of the MID values detected for cytokines with 1.5-fold change for activation for fibroblasts incubated with EVs treated with no enzyme or inactive HEP111 enzyme compared to untreated fibroblasts. Cytokines that were below detection limits in untreated fibroblasts yet were detected following stimulation with EVs are indicated by the green box.

Chapter 5 - Results

Removal of vesicular-HS results in EVs less capable of inducing angiogenesis-promoting factors in fibroblasts but increases production of inflammatory cytokines (**Figure 5.10**). This agrees with previous studies from the group that show that removal of HS-GAG chains from the EVs results in a decrease of secretion of angiogenic promoting factors such as VEGF, as well as making fibroblasts fail in their support of angiogenesis using in vitro assays (Webber et al., 2015b). Thus, these data strengthen the association between HS-GAG chains present on the surface of EVs and the delivery of factors able to drive pro-angiogenic fibroblasts.

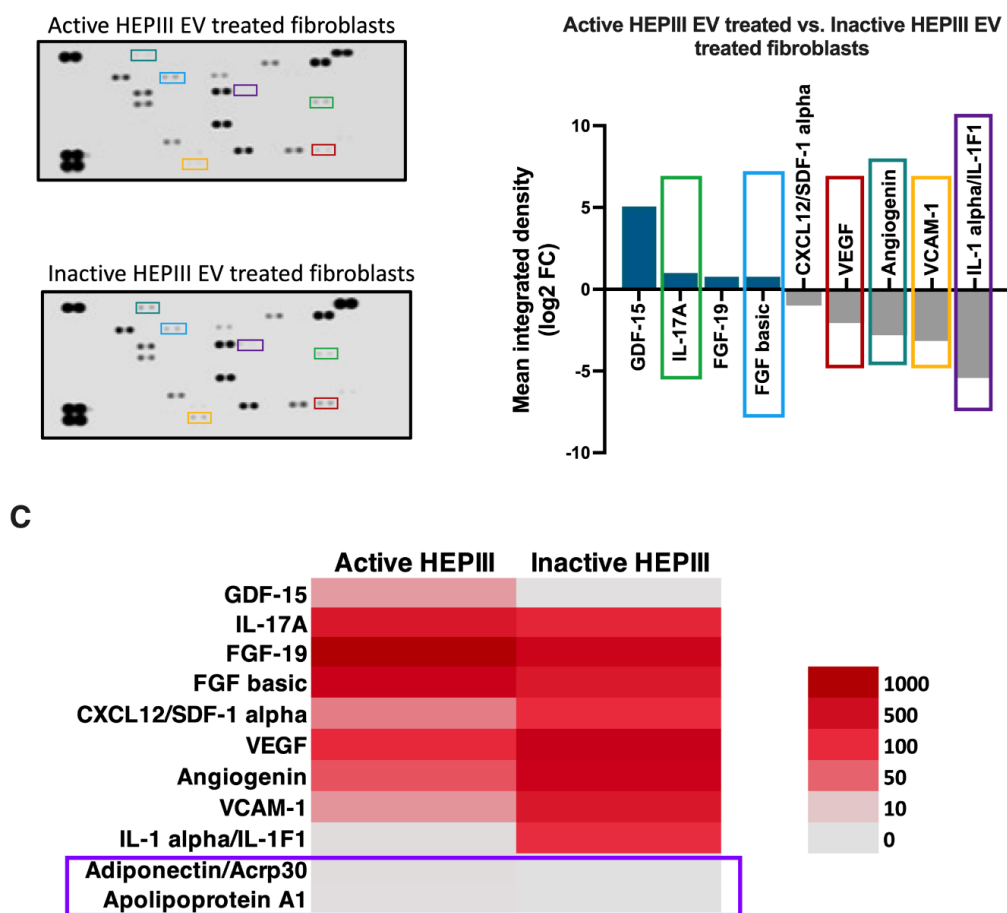


Figure 5.10. Removal of HS-GAG chains alters cytokine production promoted by EVs. (A) Scanned images from the cytokine array performed on fibroblasts cell lysates incubated for 72 hours with EVs treated with either active or inactive HEP111 enzyme. (B) Fold change of the densitometry-based analysis for the cytokines produced following treatment with active HEP111 compared with inactive HEP111. Colour boxes reveal some HS-GAG chains driven changes, identifying the position of the analyte on the membranes and correspondingly on the bar graph. (C) Heatmap of the MID values detected for cytokines with 1.5-fold change in fibroblasts treated with active HEP111 EVs compared to inactive HEP111 EVs. Cytokines that were below detection limits in untreated fibroblasts yet were detected only following stimulation with active HEP111 EVs (but at very low levels) are indicated by the purple box.

5.3.2.3 Secretion of growth factors by EV-activated fibroblasts

In order to try and validate some of the protein-profiler data, a quantitative ELISA approach was used to explore the presence of selected factors in fibroblast conditioned media (CM). These included FGF-2 (FGF basic), VEGF, HGF, IL-17A and IL-1 α . Detection was compared between growth-arrested fibroblasts and the various EV treatments at two time points to provide ample opportunity to detect a signal, as the rate of secretion is unlikely to be entirely uniform for distinct analytes. It was not possible to accomplish the detection of IL-17A and IL-1 α on the fibroblast CM collected at either 24 hours or 72 hours (**Appendix 5.4. A and B**), likely due to assay sensitivity issues. FGF-2, VEGF, and HGF were detectable at both time points in fibroblast CM, and the presence or absence of HS-GAG chains on the vesicles did have an impact on the detection of these proteins. At both 24 hours and 72 hours, levels of FGF were reduced by active HEPIII EVs to approximately the untreated level. While untreated and inactive enzyme EVs resulted in around double the quantity of FGF detected in comparison with active HEPIII EVs, these changes were not statistically significant (**Figure 5.11 A**). For VEGF, EV treatment induced a substantial secretion of VEGF by fibroblasts. Amongst EV conditions, active enzyme shows a profound attenuation of signal at 24 hours, whilst at 72 hours, this attenuation is more modest, with EVs treated with no enzyme showing levels 24% higher than active HEPIII condition (vs. 46% at 24 hours). Of note that fibroblasts barely secrete any VEGF when stimulated with sTGF- β 1, a marked difference when compared with EV conditions. Interestingly, for HGF, the trend is inverted. Here, active enzyme EVs leads to an increase of HGF secretion at 24 hours, which is even more significantly pronounced at a later time point, with levels 89% higher than EVs treated with no enzyme (and 66% than inactive enzyme) at 72 hours. Despite being a classic inducer of myofibroblastic differentiation, sTGF- β 1 was very poor at inducing the release of VEGF and HGF factors, and it seems to be an inhibitor of HGF secretion. This once again highlights how important it is, the delivery of TGF- β by vesicles to dictate the myofibroblast phenotype observed (**Figure 5.6**).

Overall, analysis of RTK phosphorylation and cytokine secretome of fibroblasts after stimulation with HS-deficient EVs revealed that vesicular HS is important to elicit receptor activation and a particular secretome in fibroblastic cells. Lack of HS-GAG chains on DU145-derived EVs seems to decrease phosphorylation of receptors whose ligands had

Chapter 5 - Results

previously been identified in this thesis as associated with EVs, as well as conferring a less pro-angiogenic and perhaps more inflammatory secretome to stimulated fibroblasts.

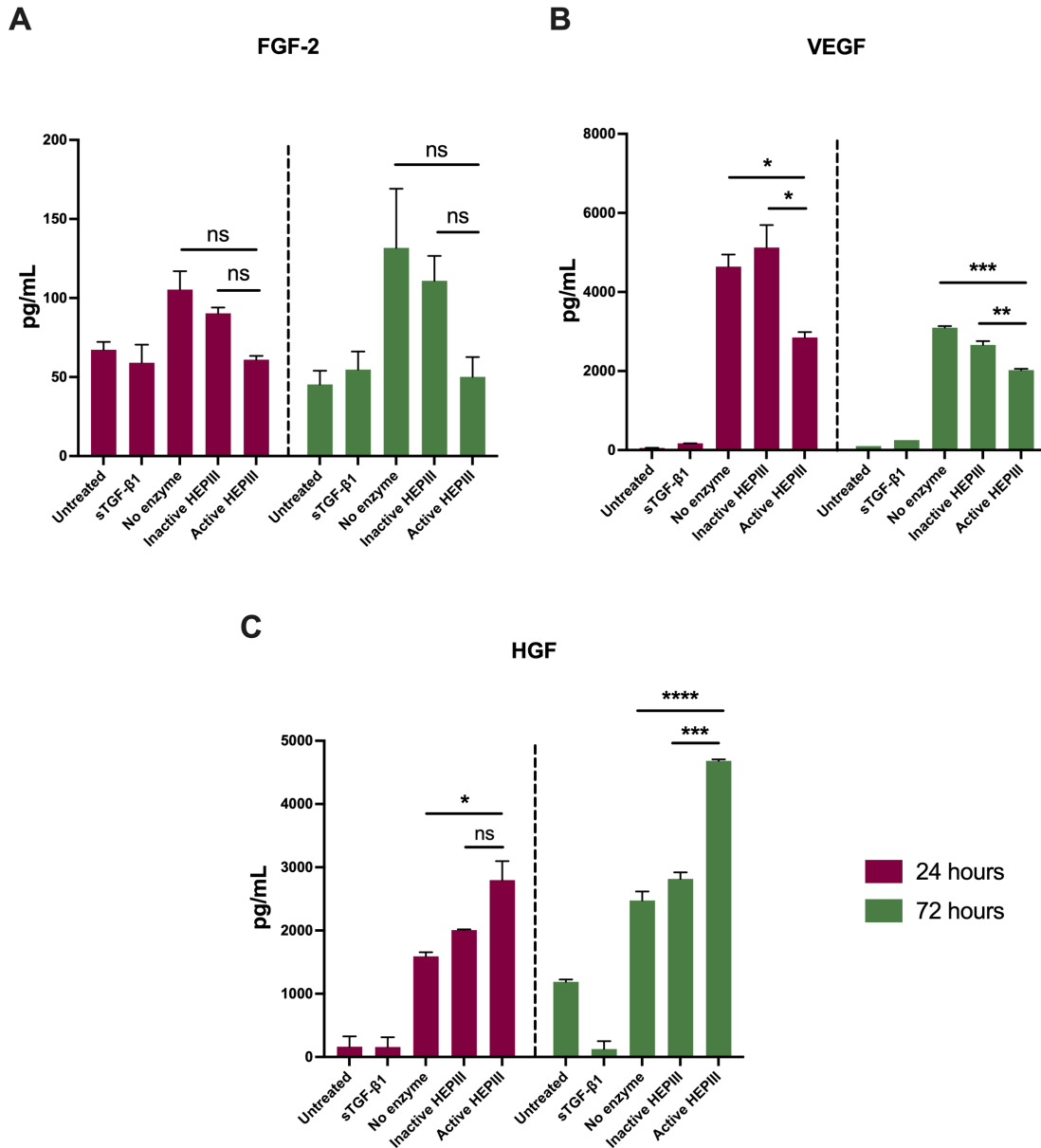


Figure 5.11. Secretion of FGF, VEGF and HGF by EV activated fibroblasts. Fibroblasts were treated for 24 hours and 72 hours with 200 µg/mL EVs, 1.5 ng/mL sTGF-β1 or control media. EVs had been previously treated with heat-inactivated HEP111, active HEP111, or no enzyme. Conditioned media was collected and assayed by ELISA. The bar graphs show ± SD of triplicate wells for the quantification (pg/mL) of FGF (A) VEGF (B) and HGF (C) at 24 hours (purple) and 72 hours (green) time-points. ****p<0.0001; ***p<0.001; **p<0.01; *p<0.05; ns=non-significant control EVs vs. active HEP111 EVs, one-way ANOVA with Tukey's multiple comparison test.

5.3.3 *The conversation between EV-activated stroma and immune cells*

The different functions that EVs have in activating the immune system are well documented, nonetheless, the importance of vesicular HS in these roles is yet to be defined. Considering the previous studies showing that CM from fibroblasts stimulated with EVs contains angiogenic and inflammatory factors, it was hypothesised that such fibroblasts may have a role in controlling immune cells, in the context of a tumour microenvironment.

To explore this, macrophages were of particular interest, as they are strongly implicated as negative regulators or positive regulators of infiltrating cells, dependant on their differentiation and phenotype. The THP-1 monocytic immortalised cell line was used in this study as it is a well-documented model used in macrophage work and has been previously used in similar studies (Sawa-Wejksza et al., 2018, Genin et al., 2015). We appreciate, however, that this is an inferior model compared to the manipulation of primary macrophages or primary blood monocytes as a macrophage precursor. THP-1 cells require a stimulus to differentiate into a macrophage phenotype. Usually, PMA is used to induce THP-1 monocytic differentiation into a resting macrophage-like state, which is primarily characterised by an increase in CD14 marker expression (Aldo et al., 2013, Starr et al., 2018, Schwende et al., 1996), as well as increase in cell adherence and morphological and physiological changes (Daigneault et al., 2010). After an adequate stimulus, macrophages can polarise towards an M1 or M2 subset characterised by expression markers such as CD80, CD86 (M1) or CD163 and CD206 (M2), as well as secretion of inflammatory cytokines such as IL-1 β and TNF- α (M1), TGF- β and VEGF (M2) (Genin et al., 2015, Sawa-Wejksza et al., 2018, Daigneault et al., 2010, Jetten et al., 2014). The following sets of experiments explore how EV-activated fibroblasts influence monocytic and macrophage-like cells phenotype.

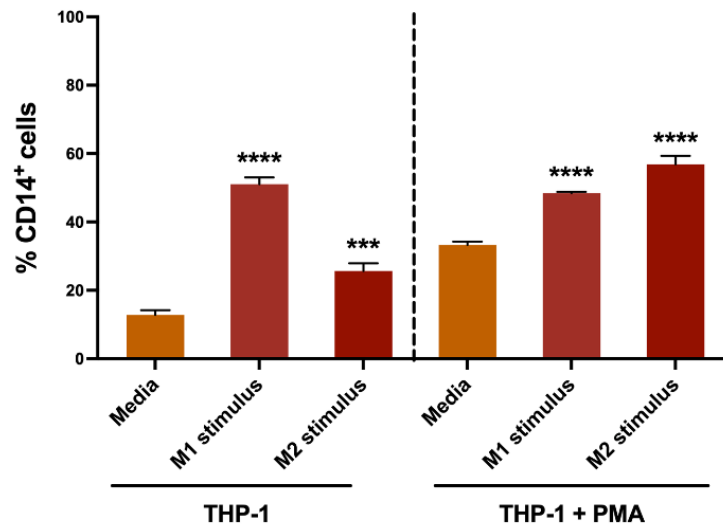
5.3.3.1 Characterisation of macrophage subsets in THP-1 cells

First, cytokines known to induce M1 and M2 polarisation states in PBMCs were used to evaluate how these cells would respond to the stimulus. M1-like macrophages were generated using 20 ng/mL IFN γ and 10 pg/mL LPS, and M2-like macrophages through treatment with 20 ng/mL IL-4, 10 ng/mL IL-10 and 20 ng/mL IL-13 (Evans et al., 2021). THP-1 were cultured without cytokines to explore the generation of unpolarised macrophages. Both THP-1 cells and THP-1 cells after priming with PMA (THP-1+PMA) were studied under these conditions (**Figure 5.12**). In both approaches, expression of typical macrophage polarisation markers (CD80, CD86, CD163 and CD206) was assessed by flow cytometry, as well as the expression of CD14. An additional marker for monocyte-macrophage differentiation, CD68, a pan-macrophage marker, was also explored (Genin et al., 2015).

The gating strategy used to analyse these experiments is shown in Figure 2.6, Chapter 2. The M1 cytokine mix employed in this study is effective at inducing strong CD14 positivity in THP-1 cells, with almost 40% more achieved compared with control. The M2 cytokines also support an increase in CD14⁺, although to a less extent. Priming the cells with PMA promotes a higher CD14⁺ baseline and increase in CD14 positivity by either M1 or M2 cytokine stimulus is more limited when compared with media control. Nonetheless, the M2 phenotype inducing cytokine mix is able to trigger higher levels of CD14⁺ cells with PMA priming (**Figure 5.12**).

Assessment of CD68⁺ cells within the live population showed that the different experimental conditions did not seem to affect the expression of this marker. PMA primed cells incubated with M2 inducing cytokines did show a significant difference in relation to the media control (**Figure 5.13 A**), but these differences were not so apparent without priming. This indicates that a combination of priming and M2 cytokine stimulus is required for decreased expression of this marker.

A



B

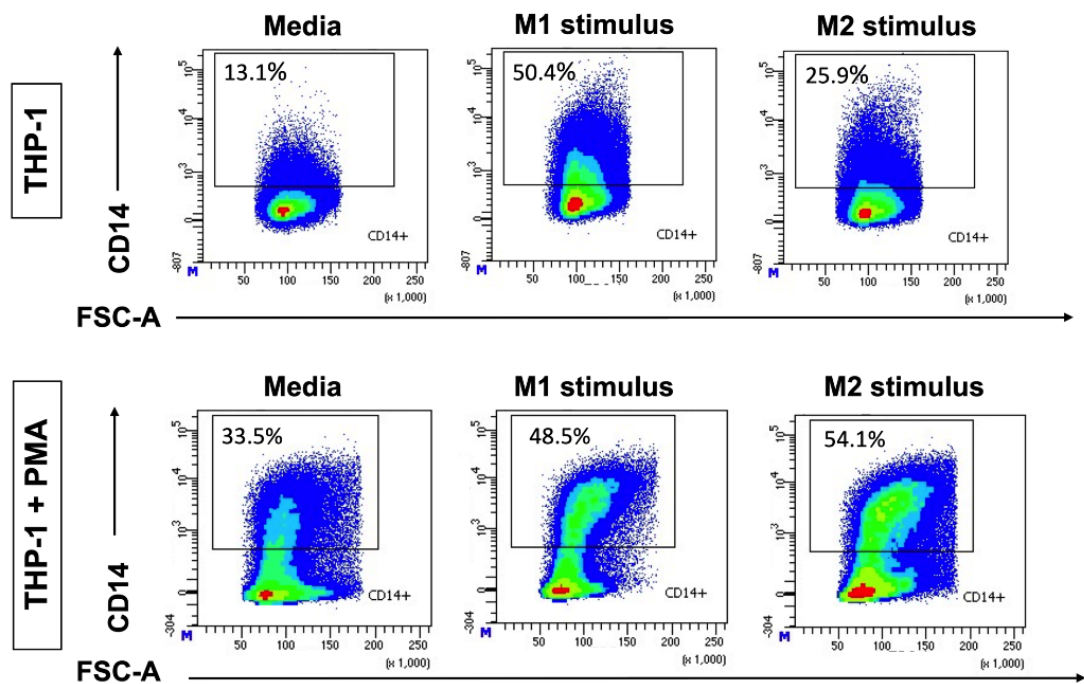
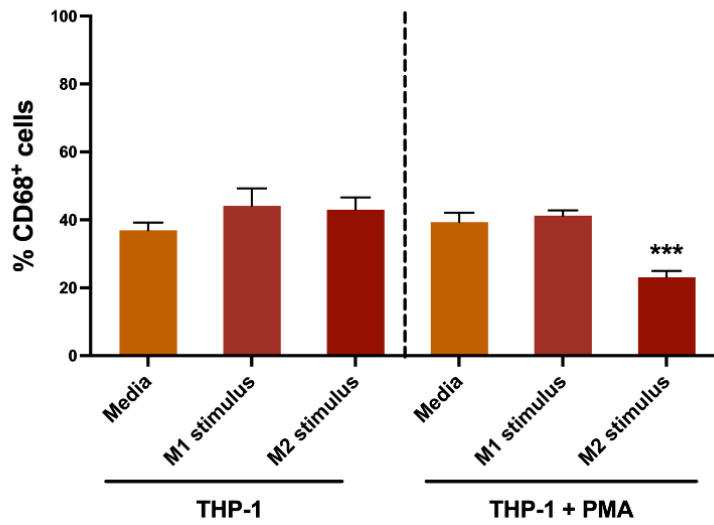


Figure 5.12. Characterisation of CD14⁺ population in THP-1 cells by flow cytometry.

(A) Bar graph shows the effect of no stimulus (media), and M1 or M2 stimulus by polarising cytokines on CD14 marker expression on THP-1 and THP-1 cells previously primed with PMA (THP-1+PMA). Data given as the % of CD14⁺ cells from the live population of cells (parent population) for each of the experimental conditions. Data represents mean \pm SD of an independent experiment based on triplicate wells. **** $p < 0.0001$; *** $p < 0.001$; one-way ANOVA with Tukey's multiple comparison test. **(B)** Representative dot plots showing the expression of CD14 marker on THP-1 and THP-1+PMA cells, treated with polarising M1 or M2 cytokines.

A



B

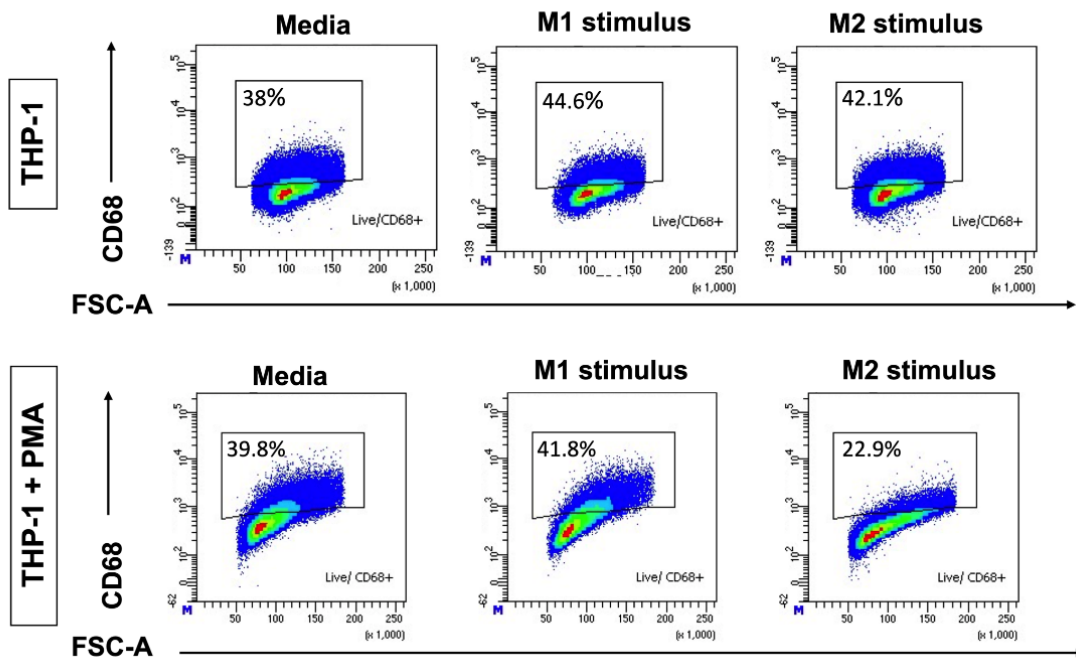
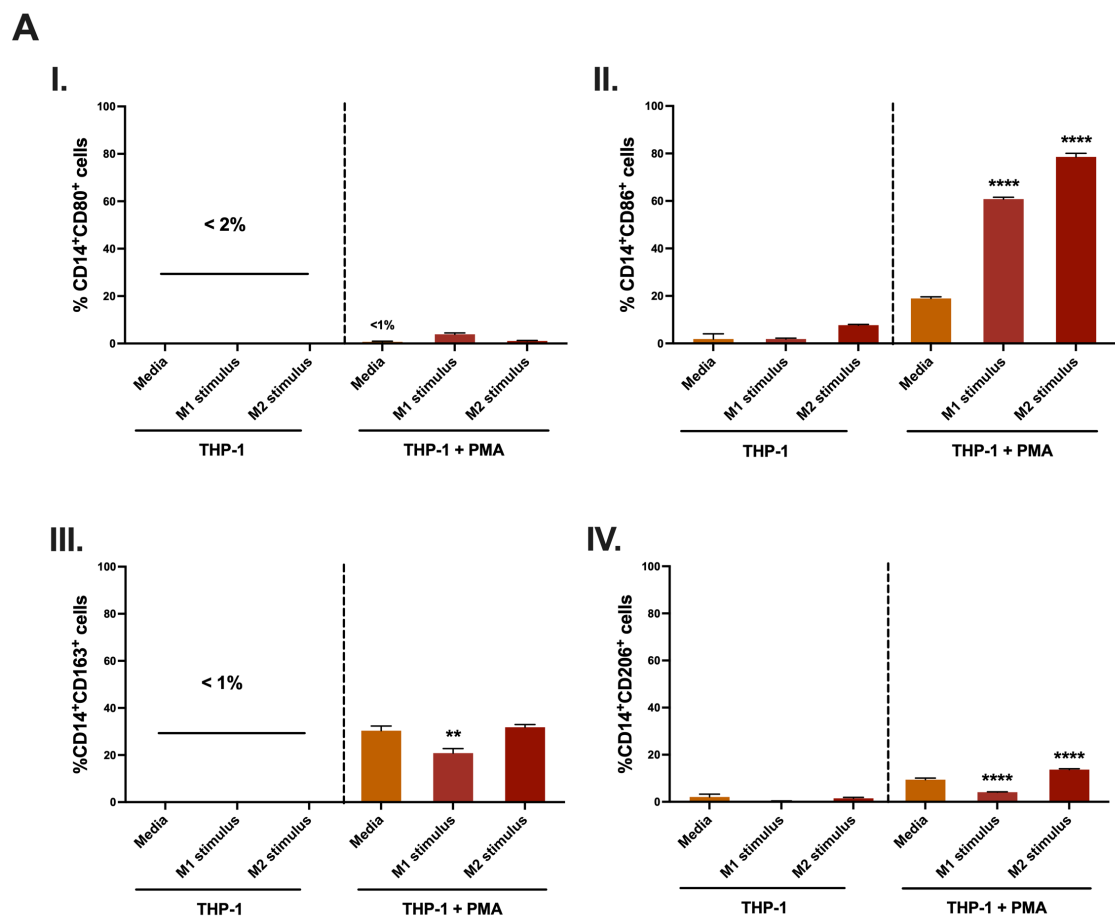


Figure 5.13. Characterisation of CD68+ cells in the THP-1 population by flow cytometry. (A) Bar graph shows the effect of no stimulus (media), and M1 or M2 stimulus by polarising cytokines on CD14 marker expression on THP-1 and THP-1 cells previously primed with PMA (THP-1+PMA). Data given as the % of CD68+ cells from the from the live population of cells (parent population) for each of the experimental conditions. Data represents mean \pm SD of an independent experiment based on triplicate wells. *** $p < 0.001$; one-way ANOVA with Tukey's multiple comparison test. (B) Representative dot plots showing the expression of CD68 marker on THP-1 and THP-1+PMA cells, treated with polarising M1 or M2 cytokines.

Overall, markers that should aid in defining polarisation, CD80, CD86, CD163, and CD206, proved difficult to detect within the CD14⁺ population of THP-1 cells. PMA priming was somewhat helpful in this regard. CD86 is the marker with the highest expression, with values close to 20% for media control and with M1 and M2 cytokine stimulus close to 60% and 80%, respectively (**Figure 5.14 A II.**). For the remaining markers, CD80 expression is higher for M1 than M2, agreeing with CD80 being an M1 marker, and CD163 and CD206 are higher in M2 stimulus, in accordance with expectations for M2-defining markers (**Figure 5.14 A I., III., IV.**). However, with this model system, assigning a strict and clear-cut definition of an M1 or an M2 differentiation based solely on these markers retains some uncertainty as to the nature of the macrophage-like cell being studied.



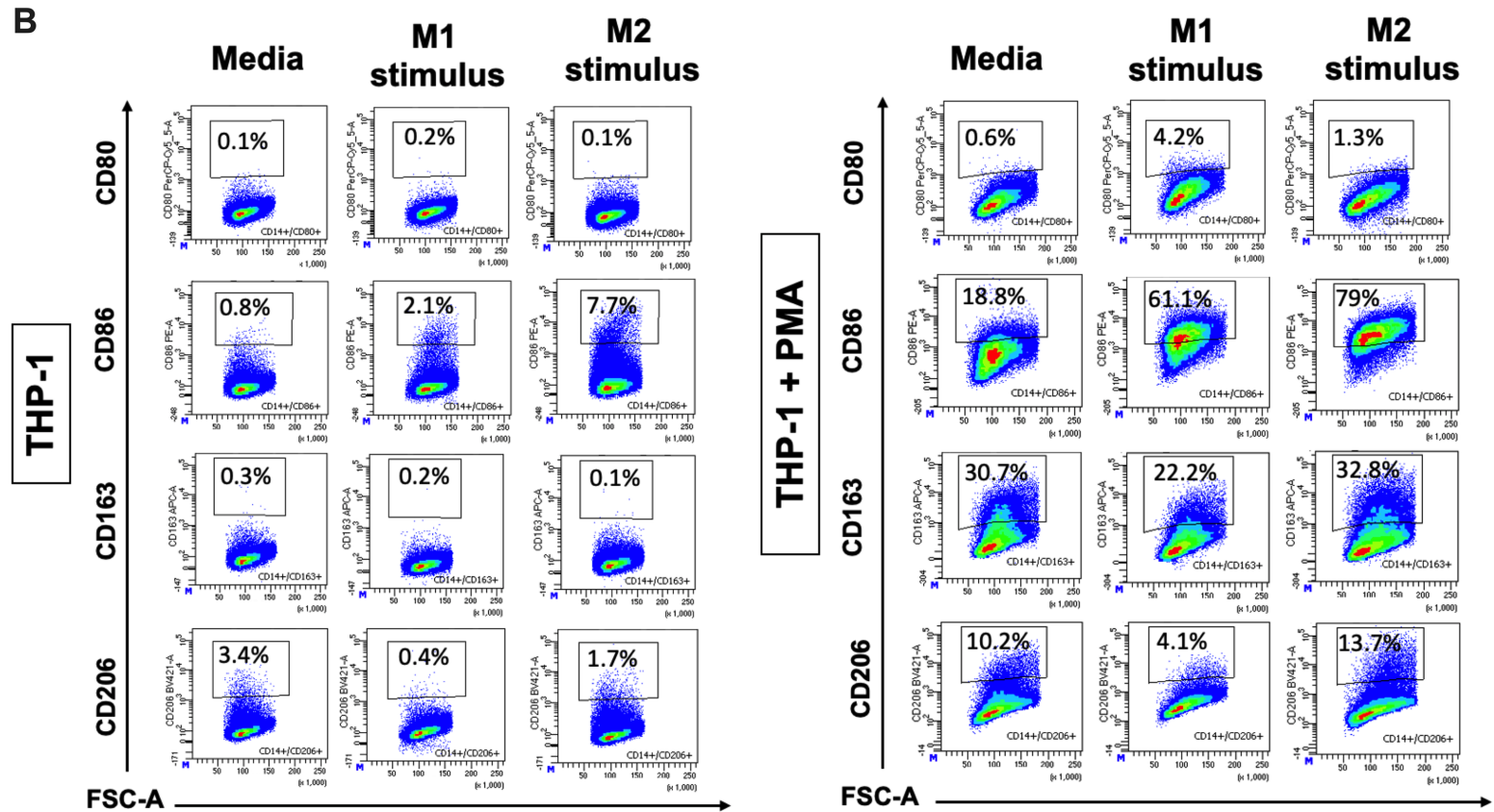


Figure 5.14. Characterisation of CD14⁺CD80⁺, CD14⁺CD86⁺, CD14⁺CD163⁺ and CD14⁺CD206⁺ population in THP-1 cells by flow cytometry. (A) Bar graph shows the effect of no stimulus (media), and M1 or M2 stimulus by polarising cytokines on CD14⁺ THP-1 and THP-1 cells previously primed with PMA (THP-1+PMA). Data given as the % of CD80⁺ (I.), CD86⁺ (II.), CD163⁺ (III.) and CD206⁺ (IV.) cells from the CD14⁺ population of cells (parent population) for each of the experimental conditions. Data represents mean \pm SD of an independent experiment based on triplicate wells. **** p <0.0001; ** p <0.01, one-way ANOVA with Tukey's multiple comparison test. **(B)** Representative dot plots showing marker expression on THP-1 and THP-1+PMA cells, treated with polarising M1 or M2 cytokines.

5.3.3.2 Differentiation and polarisation responses induced by EV activated fibroblasts

Next, to explore the effect that EV-activated fibroblasts have on THP-1 monocytic cells, two different approaches were undertaken. One looks into the effects of EV-activated fibroblast CM added to THP-1 cells in their monocytic state (**Figure 5.15 A**), while in the other, the THP-1 cells are subject to PMA-priming prior to exposure to fibroblast CM. (**Figure 5.15 B**). Fibroblasts were cultured as previously described and stimulated with 200 $\mu\text{g}/\text{mL}$ of untreated (no enzyme), inactive HEPIII, or active HEPIII-treated EVs for 72 hours. Fibroblasts CM was collected and THP-1 monocytes, or primed THP-1 cells, were incubated with 50% fibroblast CM for a further 72 hours.

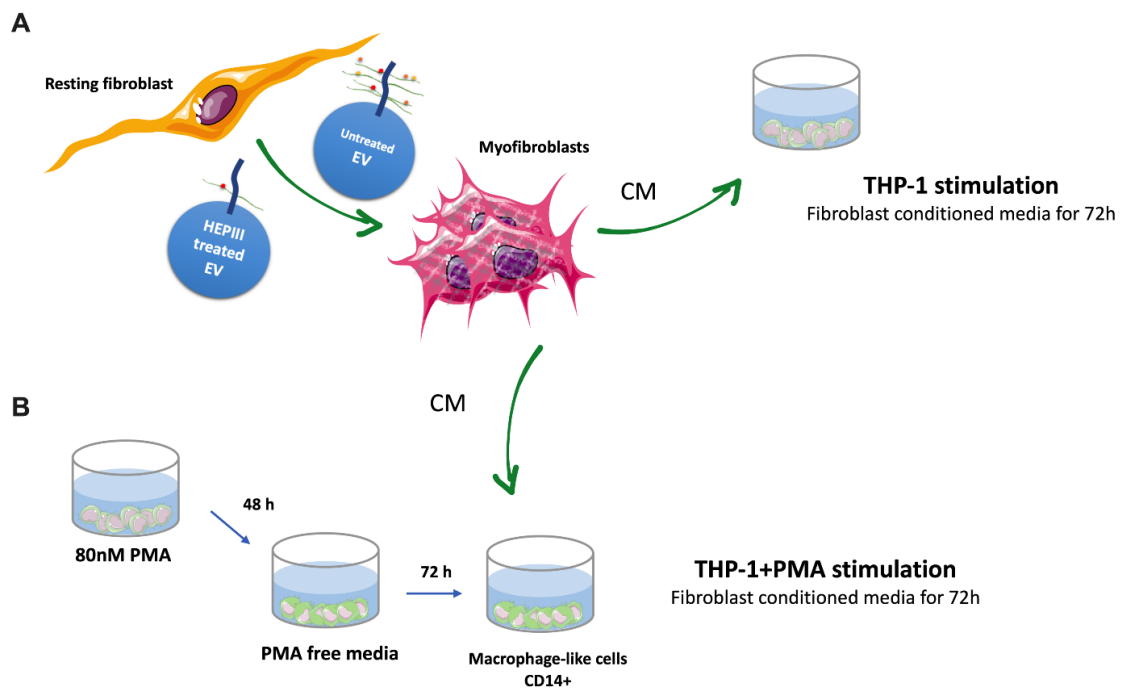


Figure 5.15. Schematic representation of indirect EV-stimulation of THP-1 cells and THP-1 cells previously primed with PMA. Figure shows experimental set up for indirect EV-stimulation of immune cells. Fibroblasts are incubated with 200 $\mu\text{g}/\text{mL}$ of different EV conditions for 72 hours, and fibroblast conditioned media (CM) is collected. EVs had been previously treated with heat-inactivated HEPIII, active HEPIII, or no enzyme. THP-1 cells are either directly incubated with 50% fibroblast CM for 72 (h)ours (**A**) or are stimulated with PMA previously to incubation (**B**). For PMA differentiation, THP-1 cells are treated with 80nM PMA for 48 (h)ours, and then left to rest for 72 hours in PMA free media. By this point cells should present an adherent morphology and increase in CD14⁺ expression and are then incubated with 50% fibroblast conditioned media for 72 (h)ours.

Chapter 5 - Results

After setting up the experiments as described, THP-1 cells were phenotyped by flow cytometry for CD14, CD68, CD80, CD86, CD163, and CD206 markers. In terms of CD14-positivity, THP-1 cells that are previously primed with PMA see a small but significant increase in the %CD14⁺ population above the basal levels promoted by the PMA stimulus. Without PMA priming, CM from EV-activated fibroblasts has the ability to at least treble the proportion of CD14⁺ cells compared to control media treatment (~ 55% vs. 13%). CM from unstimulated fibroblasts has a minimal effect (**Figure 5.16 A and B**). Nonetheless, these EV-mediated effects are independent of vesicular-HS, as CM from fibroblasts stimulated with the HS modified EVs were not different from the respective controls.

CD68 marker expression on THP-1 cells does not seem to be affected by any of the conditions under study, in the context of no PMA priming, with all cells expressing similar levels of CD68 within the live population. In the context of PMA priming of THP-1 cells, there was a general PMA-mediated drop in CD68⁺ cells, but the varied fibroblast treatments were not different. Fibroblasts treated with active HEPIII-EVs hinted at a weak further reduction in CD68 (**Figure 5.17 A and B**). However, there is no significant difference between the EV conditions under study, which points to an unlikely HS-related effect.

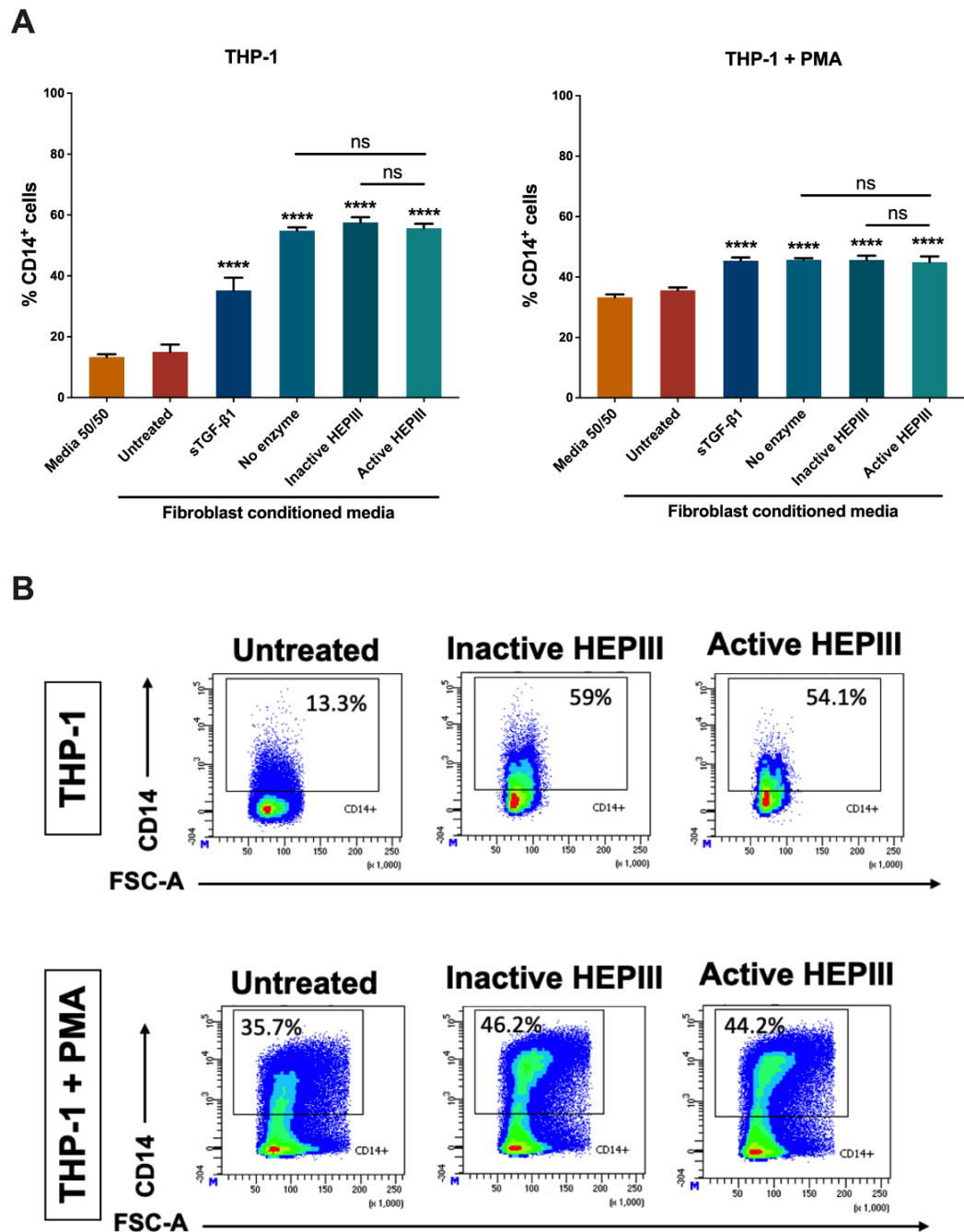


Figure 5.16. Characterisation of CD14⁺ population in THP-1 and THP-1+PMA cells after indirect EV-stimulation through fibroblast conditioned media. Fibroblasts were treated for 72 hours with 200 $\mu\text{g}/\text{mL}$ of EVs, 1.5 ng/mL sTGF- β 1 or media only (untreated). EVs had been previously treated with heat-inactivated HEPIII, active HEPIII, or no enzyme. THP-1 and THP-1+PMA cells were stimulated with 50% of fibroblast CM or 50% DMEM/RPMI media for 72 hours and analysed by flow. **(A)** Bar graph shows the effect of these stimulus on CD14 marker expression on THP-1 and THP-1+PMA cells. Data given as the % of CD14⁺ cells from the live population of cells (parent population) for each of the experimental conditions. Data represents mean \pm SD of an independent experiment based on triplicate wells. **** $p < 0.0001$ study conditions vs. media 50/50; ns = non-significant control EVs vs. active HEPIII EVs; one-way ANOVA with Tukey's multiple comparison test. **(B)** Representative dot plots showing the expression of CD14 marker on THP-1 and THP-1+PMA cells, that are either untreated or incubated with EVs pre-treated with inactive HEPIII or active HEPIII.

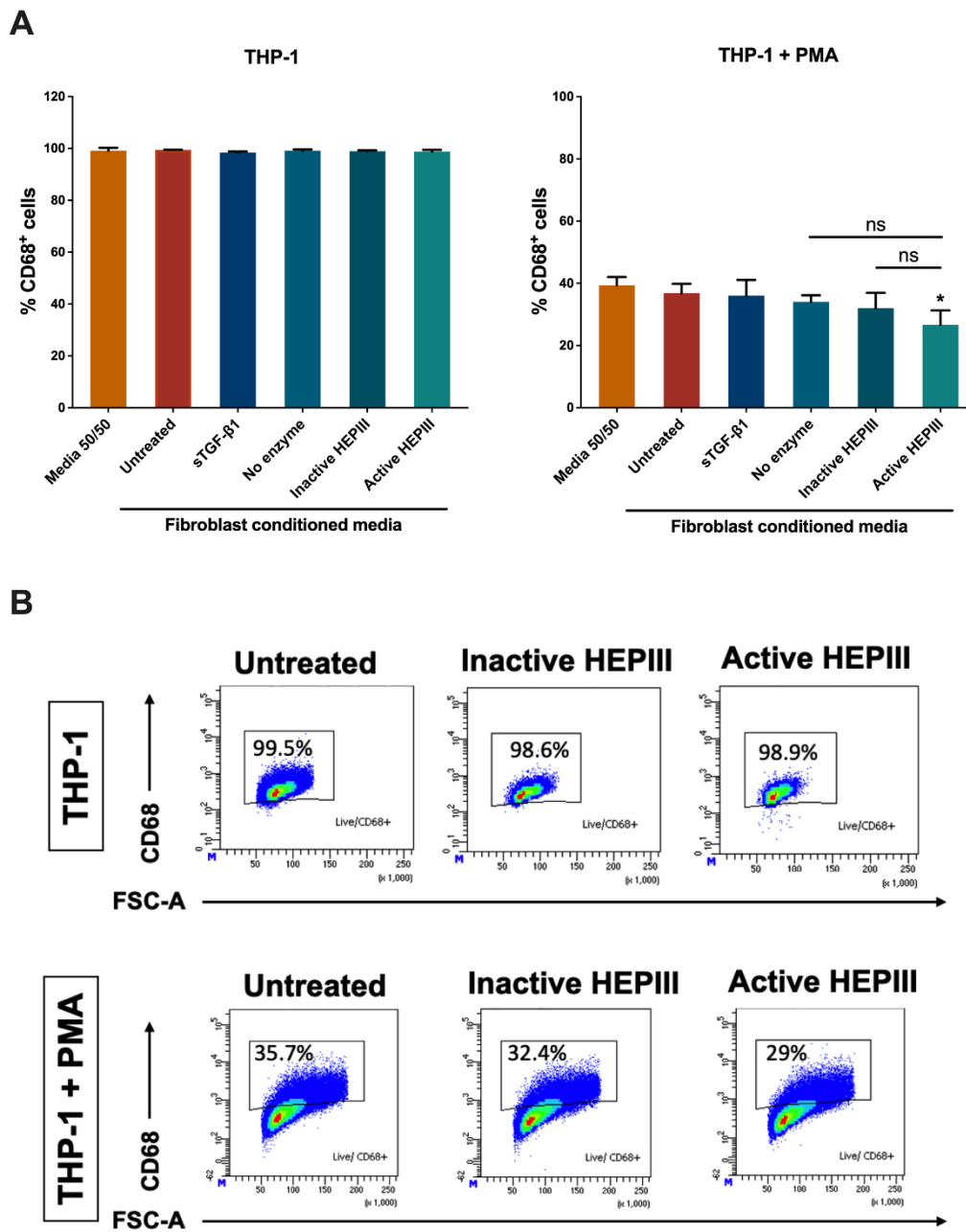
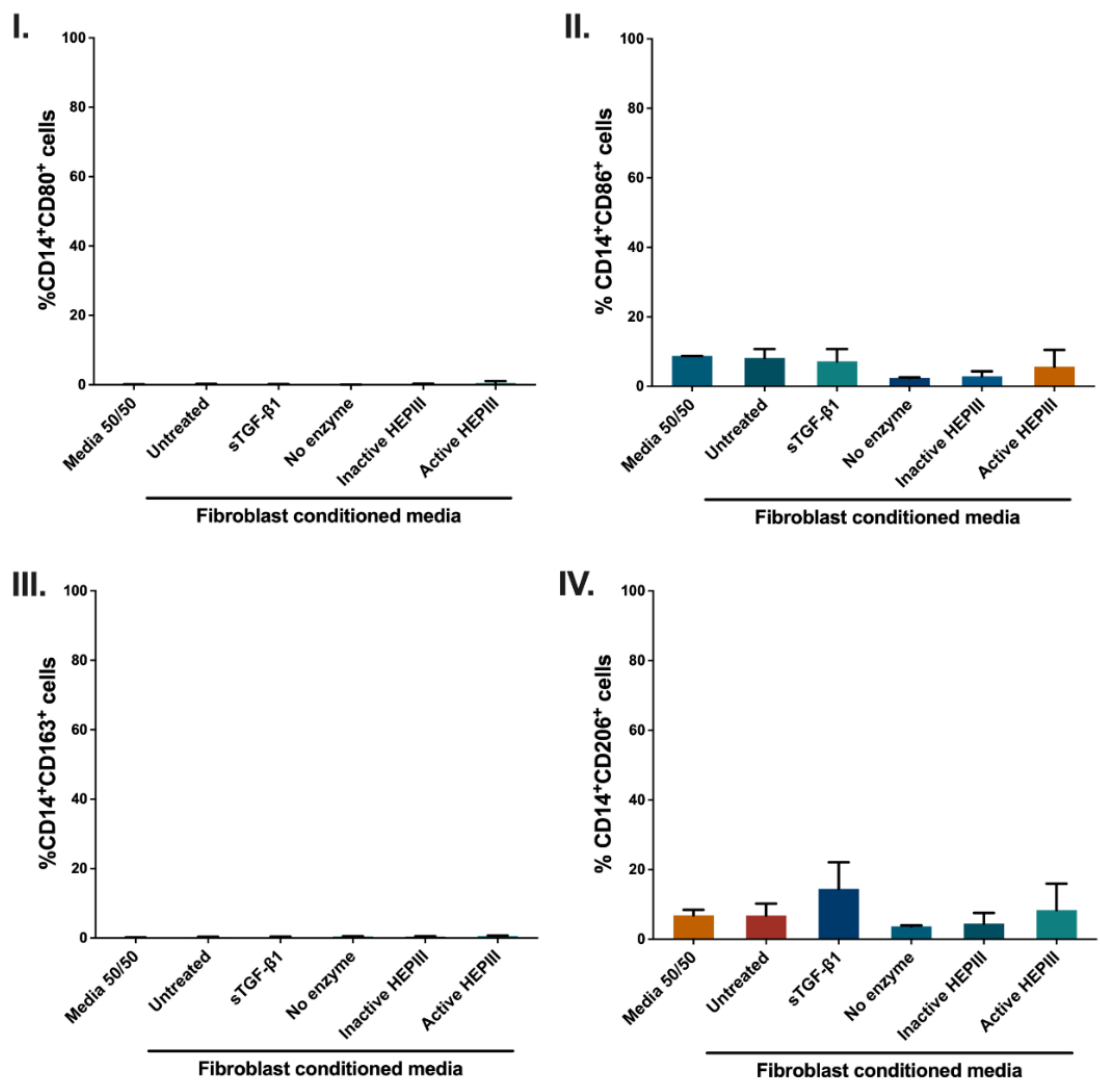


Figure 5.17. Characterisation of CD68⁺ population in THP-1 and THP-1+PMA cells after indirect EV-stimulation through fibroblast cell conditioned media. Fibroblasts were treated for 72 hours with 200 µg/mL of EVs, 1.5 ng/mL sTGF-β1 or media only (untreated). EVs had been previously treated with heat-inactivated HEPIII, active HEPIII, or no enzyme. THP-1 and THP-1+PMA cells were stimulated with 50% of fibroblast CM or 50% DMEM/RPMI media for 72 hours and analysed by flow. **(A)** Bar graph shows the effect of these stimulus on CD68 marker expression on THP-1 and THP-1+PMA cells. Data given as the % of CD68⁺ cells from the live population of cells (parent population) for each of the experimental conditions. Data represents mean ± SD of an independent experiment based on triplicate wells. *p<0.05 study conditions vs. media 50/50; ns= non-significant control EVs vs. active HEPIII EVs; one-way ANOVA with Tukey's multiple comparison test. **(B)** Representative dot plots showing the expression of CD68 marker on THP-1 and THP-1+PMA cells, that are either untreated or incubated with EVs pre-treated with inactive HEPIII or active HEPIII.

Fibroblast CM does not seem to affect the expression of markers CD80, CD86, CD163, or CD206, within the parent population of CD14⁺ THP-1 cells. CD80 and CD163 expression represents less than 2% of the CD14⁺ population (**Figure 5.18 A I., III.**). These values are negligible and may be due to background associated with the assay, and hence making firm conclusions on such low-frequency events is difficult. CD163 and CD206 are more detectable on THP-1 cells (**Figure 5.18 A II., IV.**), but the proportion of positive cells is below 20%, and no EV-associated changes between fibroblast conditions were observed (**Figure 5.18 B**).

A

THP-1



B

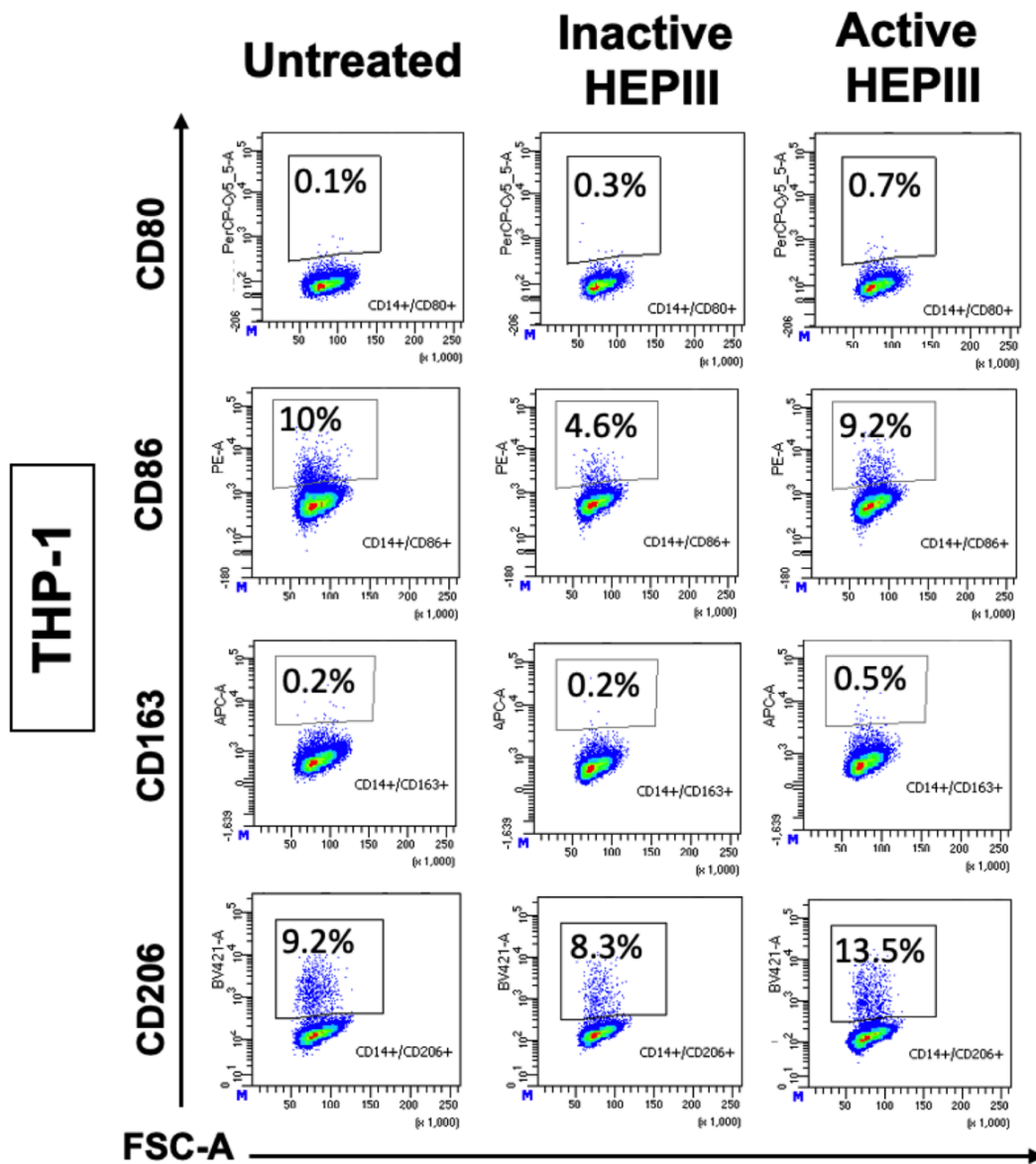
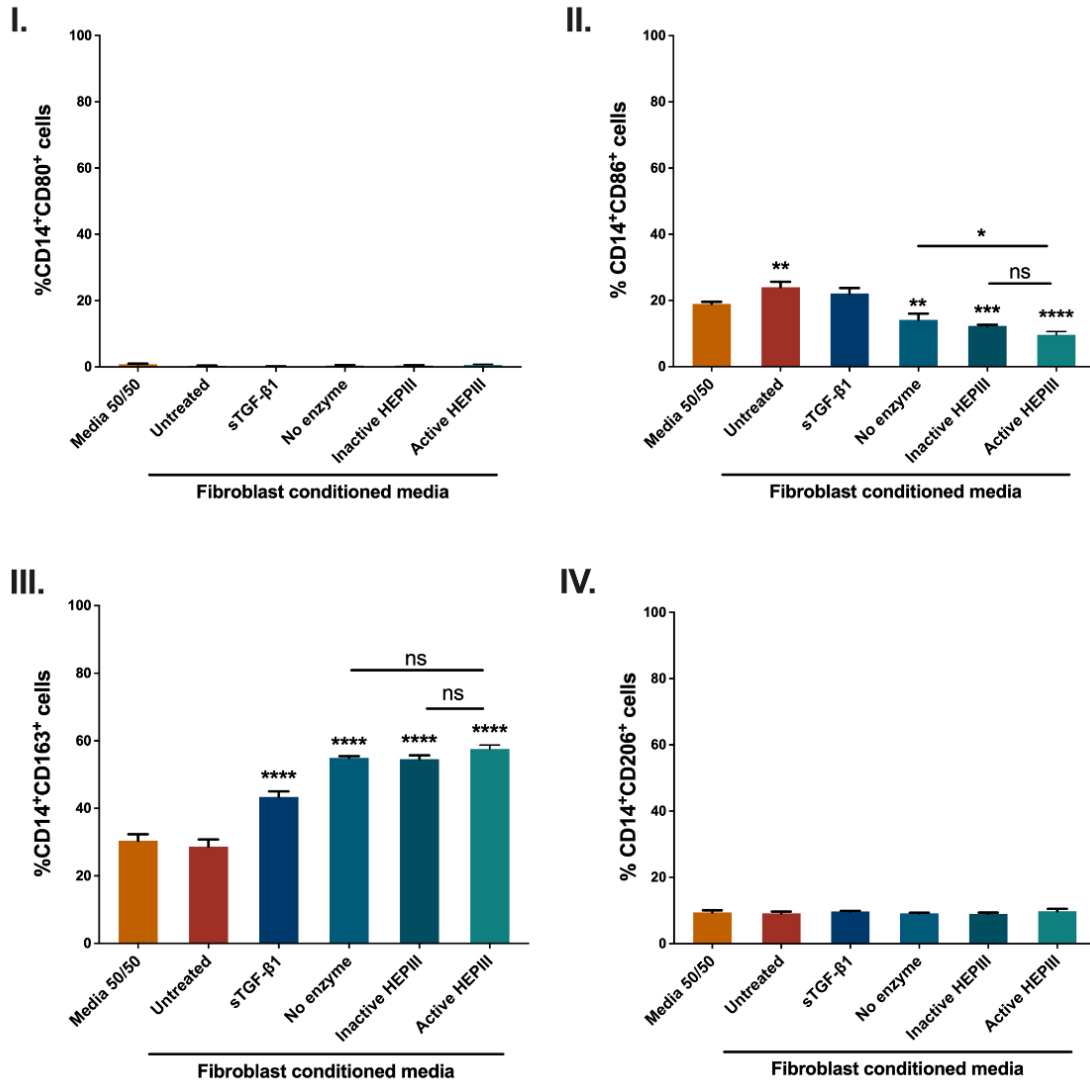


Figure 5.18. Characterisation of CD14⁺CD80⁺, CD14⁺CD86⁺, CD14⁺CD163⁺ and CD14⁺CD206⁺ population in THP-1 cells after indirect EV-stimulation through fibroblast conditioned media. Fibroblasts were treated for 72 hours with 200 µg/mL of EVs, 1.5 ng/mL sTGF-β1 or media only (untreated). EVs had been previously treated with heat-inactivated HEPIII, active HEPIII, or no enzyme. THP-1 cells were stimulated with 50% of fibroblast CM or 50% DMEM/RPMI media for 72 hours and analysed by flow. **(A)** Bar graph shows the % of CD80⁺ (I.), CD86⁺ (II.), CD163⁺ (III.) and CD206⁺ (IV.) cells from the CD14⁺ population of cells (parent population) for each of the experimental conditions. Data represents mean ± SD of an independent experiment based on triplicate wells. **(B)** Representative dot plots showing marker expression on THP-1 cells that are either untreated or incubated with EVs pre-treated with inactive HEPIII or active HEPIII.

In THP-1+PMA cells, CM of untreated fibroblasts seems to promote expression of CD86 while EV-activated fibroblasts significantly impair CD86 expression on cells (**Figure 5.19 A II. and B**). Removal of vesicular HS seems to promote alterations in fibroblasts that do not support CD86 expression by CD14⁺ THP-1+PMA cells, as a significant difference is observed between active HEP13 treated fibroblasts and the untreated (no enzyme) EV condition. However, compared with inactive HEP13 EVs, this difference is non-significant (**Figure 5.19 A II. and B**). Since CD86 is a marker of a pro-inflammatory M1 subset, and therefore an indicator of M1 polarisation, this result reflects a possibly less inflammatory secretome produced by fibroblasts when stimulated with HS-deficient vesicles. Conditioned media from EV-activated fibroblasts is able to promote accentuated CD163 positivity on THP-1+PMA cells (**Figure 5.19 A III and B**), while unstimulated fibroblasts induce a similar expression of CD163⁺ as to untreated cells (**Figure 5.20 A III.**). This expression seems to be independent of vesicular-HS, as there is no difference observed between EV conditions. CD80 expression was barely detected during flow cytometry-based analysis of these cells, and CD206 marker expression it is not affected by any of the experimental conditions under study here (**Figure 5.19 A I. and IV.**)

Overall, these data show that EV-activated fibroblasts are able to differentiate THP-1 cells, in a similar manner as the PMA compound used in these studies, by increasing the CD14⁺ population within live cells. Despite this monocytic differentiation effect, fibroblast CM only seems to be able to polarise cells towards an M1 or M2 phenotype after PMA treatment and not when cells are still in a monocytic state. Conditioned media from EV-activated fibroblasts seems to abrogate marker expression for CD86 in a HS-dependent manner but also seems to promote an increase in expression for CD163, independently of HS. This might indicate that EVs have a potential lower capacity to instil fibroblasts to induce a pro-inflammatory response in immune cells and instead direct towards a more anti-inflammatory phenotype.

A THP-1+ PMA



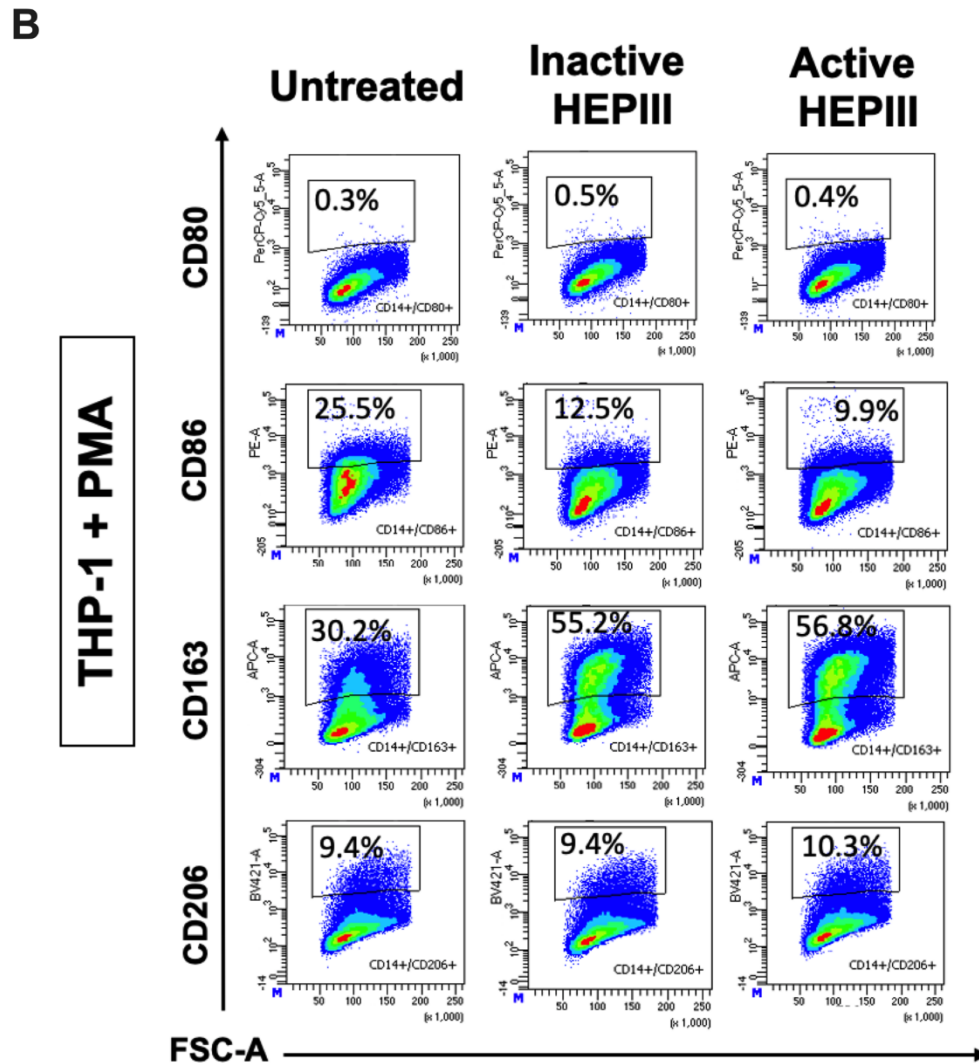


Figure 5.19. Characterisation of CD14+CD80+, CD14+CD86+, CD14+CD163+ and CD14+CD206+ population in THP-1+PMA cells after indirect EV-stimulation through fibroblast conditioned media. Fibroblasts were treated for 72 hours with 200 $\mu\text{g}/\text{mL}$ of EVs, 1.5 ng/mL sTGF- β 1 or media only (untreated). EVs had been previously treated with heat-inactivated HEP1III, active HEP1III, or no enzyme. THP-1 cells were primed with PMA, previous to stimulation with 50% of fibroblast CM or 50% DMEM/RPMI media for 72 hours and analysed by flow. **(A)** Bar graph shows the % of CD80+ (I.), CD86+ (II.), CD163+ (III.) and CD206+ (IV.) cells from the CD14+ population of cells (parent population) for each of the experimental conditions. Data represents mean \pm SD of an independent experiment based on triplicate wells. **** $p < 0.0001$; *** $p < 0.001$; ** $p < 0.01$ study conditions vs. media 50/50; * $p < 0.05$; ns=non-significant control EVs vs. active HEP1III EVs; one-way ANOVA with Tukey's multiple comparison test. **(B)** Representative dot plots showing marker expression on THP-1+PMA cells that are either untreated or incubated with EVs pre-treated with inactive HEP1III or active HEP1III.

5.3.3.3 Differentiation and polarisation responses induced directly by EVs

The direct effect that HS-modified EVs would have in differentiation and polarisation of THP-1 cells was assessed next. Again, two different approaches were tested to evaluate the vesicle effect on cells previously primed, or not, with PMA. To be consistent with EV concentration used in fibroblast differentiation studies, 200 µg/mL of EVs were used. One approach investigates the direct effect of EVs on THP-1 cells (**Figure 5.20 A**), while in the other, the THP-1 cells are subject to PMA-priming prior to adding EV stimulus for 72 hours (**Figure 5.20 B**).

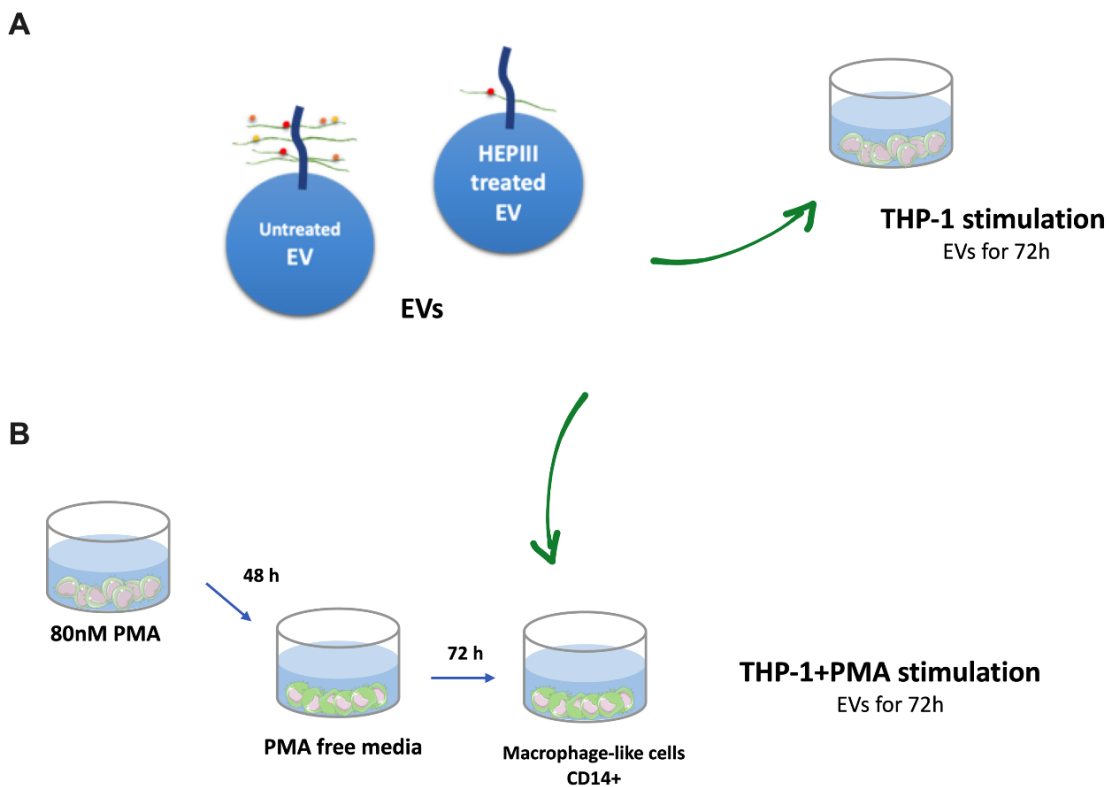
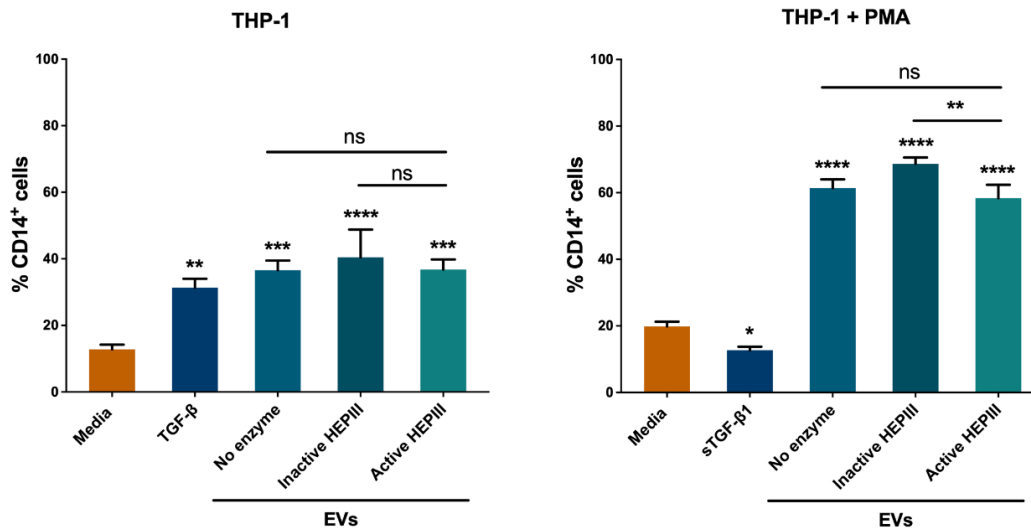


Figure 5.20. Schematic representation of direct EV-stimulation of THP-1 cells and THP-1 cells previously primed with PMA. Figure shows experimental set up for direct EV-stimulation of immune cells. THP-1 cells are either directly incubated with 200 µg/mL of different EV conditions for 72 (h)ours (**A**) or are stimulated with PMA previously to incubation (**B**). EVs had been previously treated with heat-inactivated HEPIII, active HEPIII, or no enzyme. For PMA differentiation, cells are treated with 80nM PMA for 48 (h)ours, and then leave to rest for 72 (h)ours in PMA free media. By this point cells should present an adherent morphology and increase in CD14⁺ expression and are then incubated with EVs for 72 (h)ours.

Stimulating THP-1 cells with HS-modified EVs and corresponding controls for 72 hours significantly increased CD14⁺ population in a HS-independent way. When compared with unstimulated cells, CD14 positivity was more accentuated after PMA priming of THP-1, and EVs lacking HS are less able to promote CD14⁺ cells (**Figure 5.21**). However, basal CD14 positivity is not as accentuated between PMA-primed and non-primed conditions. This can perhaps be explained by daily variability or higher passage numbers of cells used for this experiment. Soluble TGF- β 1 seems to promote CD14 positivity in THP-1 cells, but the opposite effect is observed for THP-1 primed cells (**Figure 5.21 A**). Soluble TGF- β 1 also seems to increase CD68 positivity in THP-1 cells, but no such effect is observed for EV conditions (**Figure 5.22 A**). However, THP1+PMA cells show a decrease in the expression of CD68 in a HS-independent fashion (**Figure 5.22 B**).

A



B

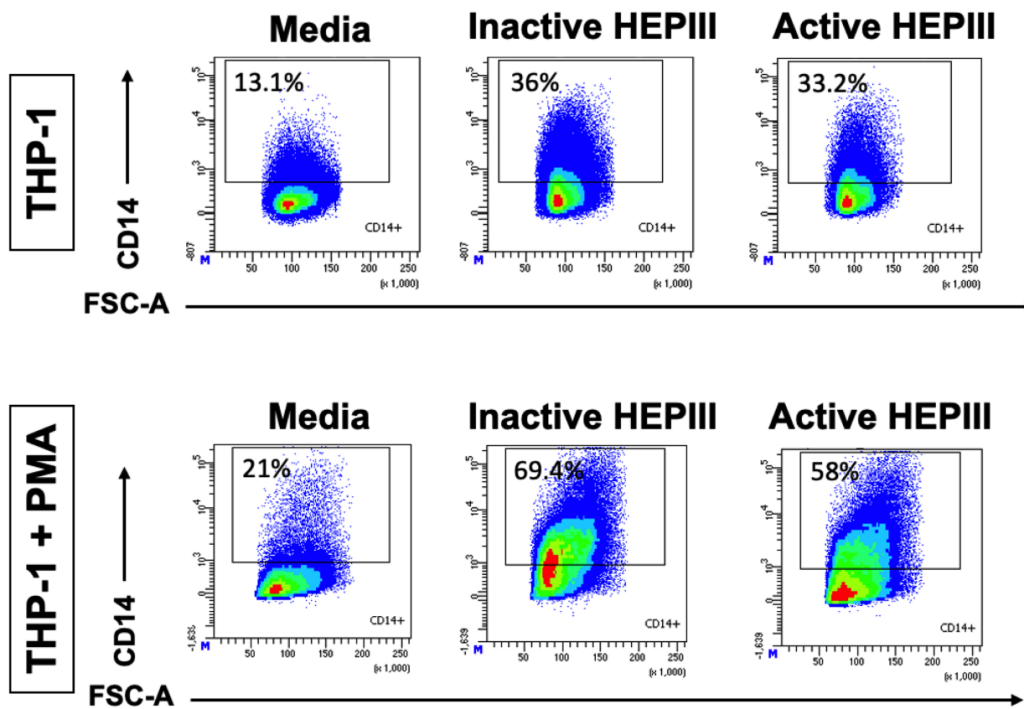
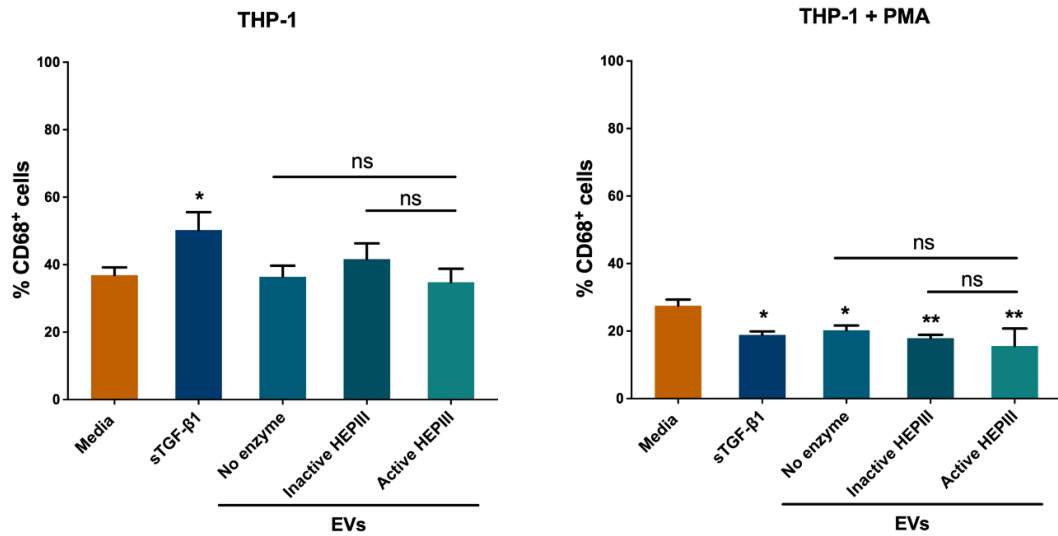


Figure 5.21. Characterisation of CD14⁺ population in THP-1 and THP-1+PMA cells after direct EV-stimulation. THP-1 and THP-1+PMA cells were treated for 72 hours with 200 μ g/mL of EVs, 1.5 ng/mL sTGF- β 1 or media only (untreated). EVs had been previously treated with heat-inactivated HEP111, active HEP111, or no enzyme. **(A)** Bar graph shows the effect of the stimulus on CD14 marker expression on THP-1 cells with and without PMA priming. Data given as the % of CD14⁺ cells from the from the live population of cells (parent population) for each of the experimental conditions. Data represents mean \pm SD of an independent experiment based on triplicate wells. *** p <0.001; ** p <0.01; * p <0.05 study conditions vs. media; ns=non-significant, ** p <0.01 control EVs vs. active HEP111 EVs; one-way ANOVA with Tukey's multiple comparison test. **(B)** Representative dot plots showing the % expression of CD14 marker on THP-1 and THP-1+PMA cells that are either untreated or incubated with EVs pre-treated with inactive HEP111 or active HEP111.

A



B

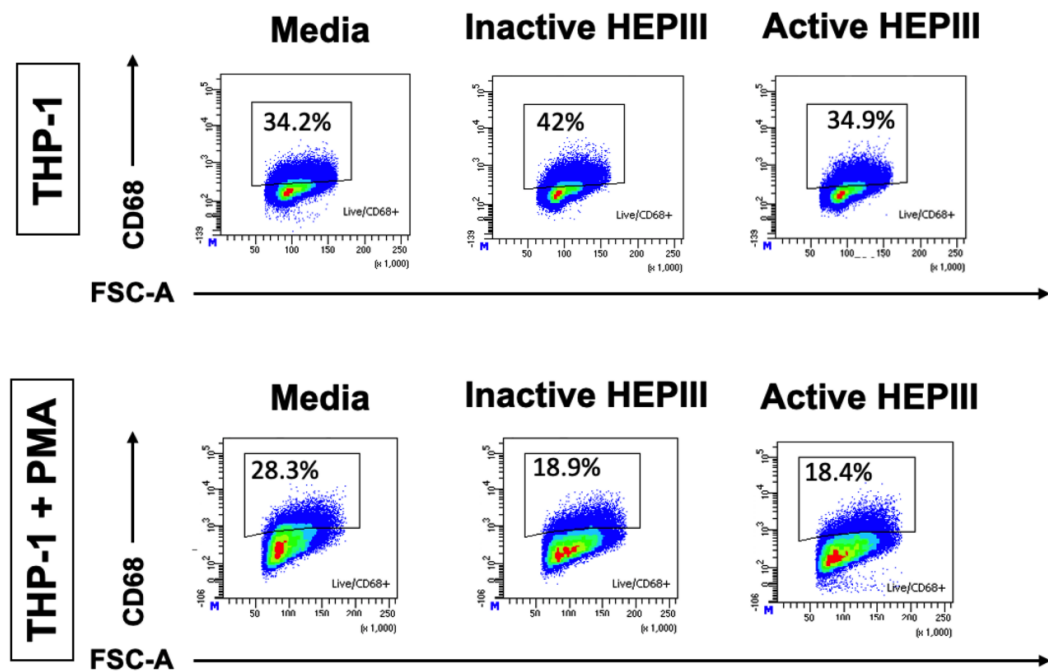
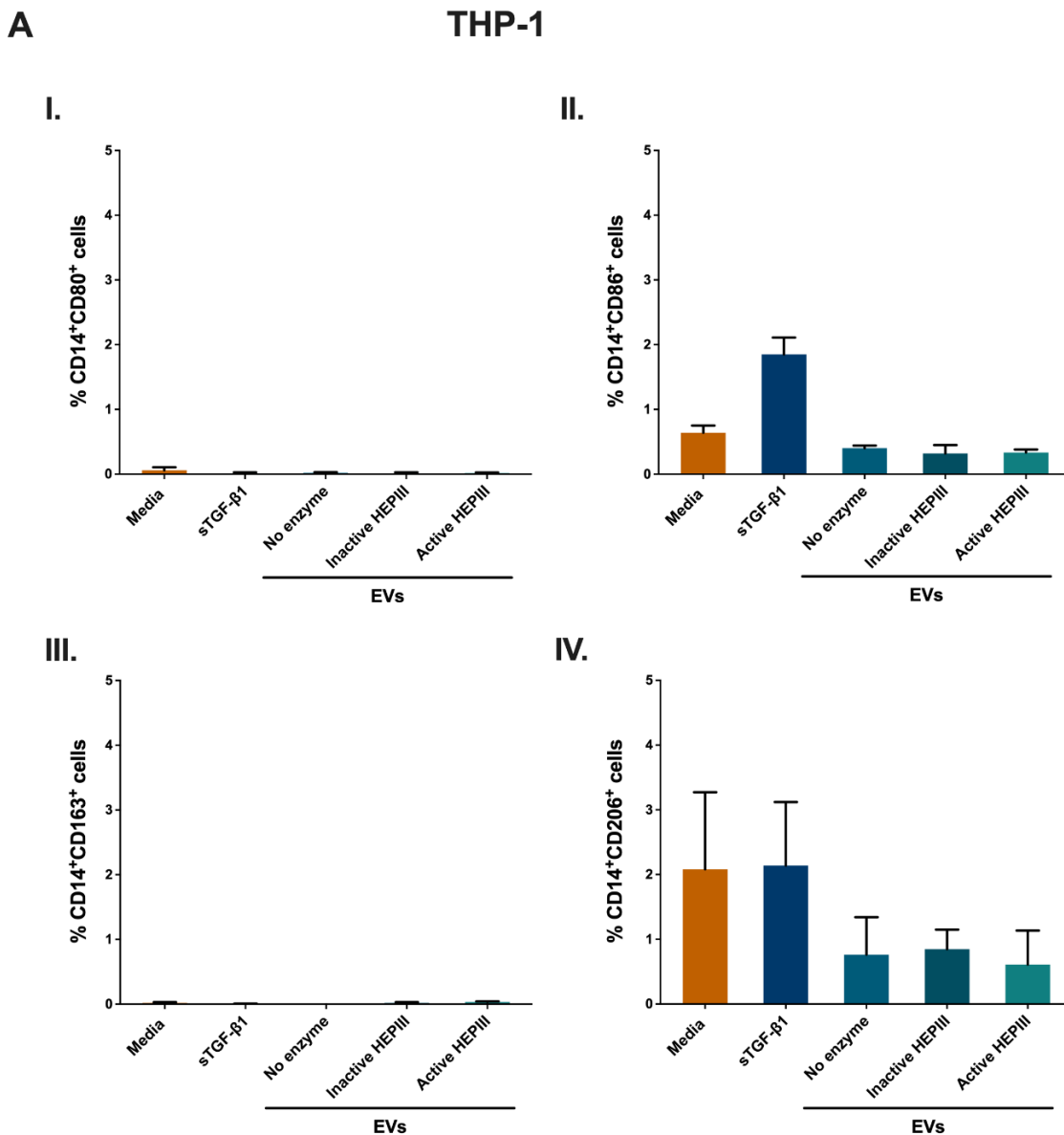


Figure 5.22. Characterisation of CD68⁺ population in THP-1 and THP-1+PMA cells after direct EV-stimulation. THP-1 and THP-1+PMA cells were treated for 72 hours with 200 $\mu\text{g}/\text{mL}$ of EVs, 1.5 ng/mL sTGF- β 1 or media only (untreated). EVs had been previously treated with heat-inactivated HEP111, active HEP111, or no enzyme. **(A)** Bar graph shows the effect of the stimulus on CD68 marker expression on THP-1 cells with and without PMA priming. Data given as the % of CD68⁺ cells from the live population of cells (parent population) for each of the experimental conditions. Data represents mean \pm SD of an independent experiment based on triplicate wells. ** $p < 0.01$; * $p < 0.05$ study conditions vs. media; ns=non-significant control EVs vs. active HEP111 EVs; one-way ANOVA with Tukey's multiple comparison test. **(B)** Representative dot plots showing the % expression of CD68 marker on THP-1 and THP-1+PMA cells that are either untreated or incubated with EVs pre-treated with inactive HEP111 or active HEP111.

Chapter 5 - Results

Detection of polarisation markers was barely achieved for primed and non-primed THP-1 cells treated with different EV conditions, with detection below 1% for CD80 and CD163 and below 5% for CD86 and CD206 (**Figure 5.23 A**). There is an exception observed for CD206 on THP-1+PMA cells, where media and sTGF- β 1 were able to increase CD206 positivity above 10% (**Figure 5.24 A**). However, this % is based on a cell number below 1000 events, so confidence in the importance of this result and its biological relevance is low. The same can be assumed for CD14⁺CD86⁺ cells increased with sTGF- β 1, as this increase corresponds a less than 2% of the CD14⁺ population. Contrary to the fibroblast CM effect observed before, where priming of THP-1 cells contributed to differences in the expression of CD86 and CD163, here EVs do not seem to be able to promote the same polarising effect (**Figure 5.24**).



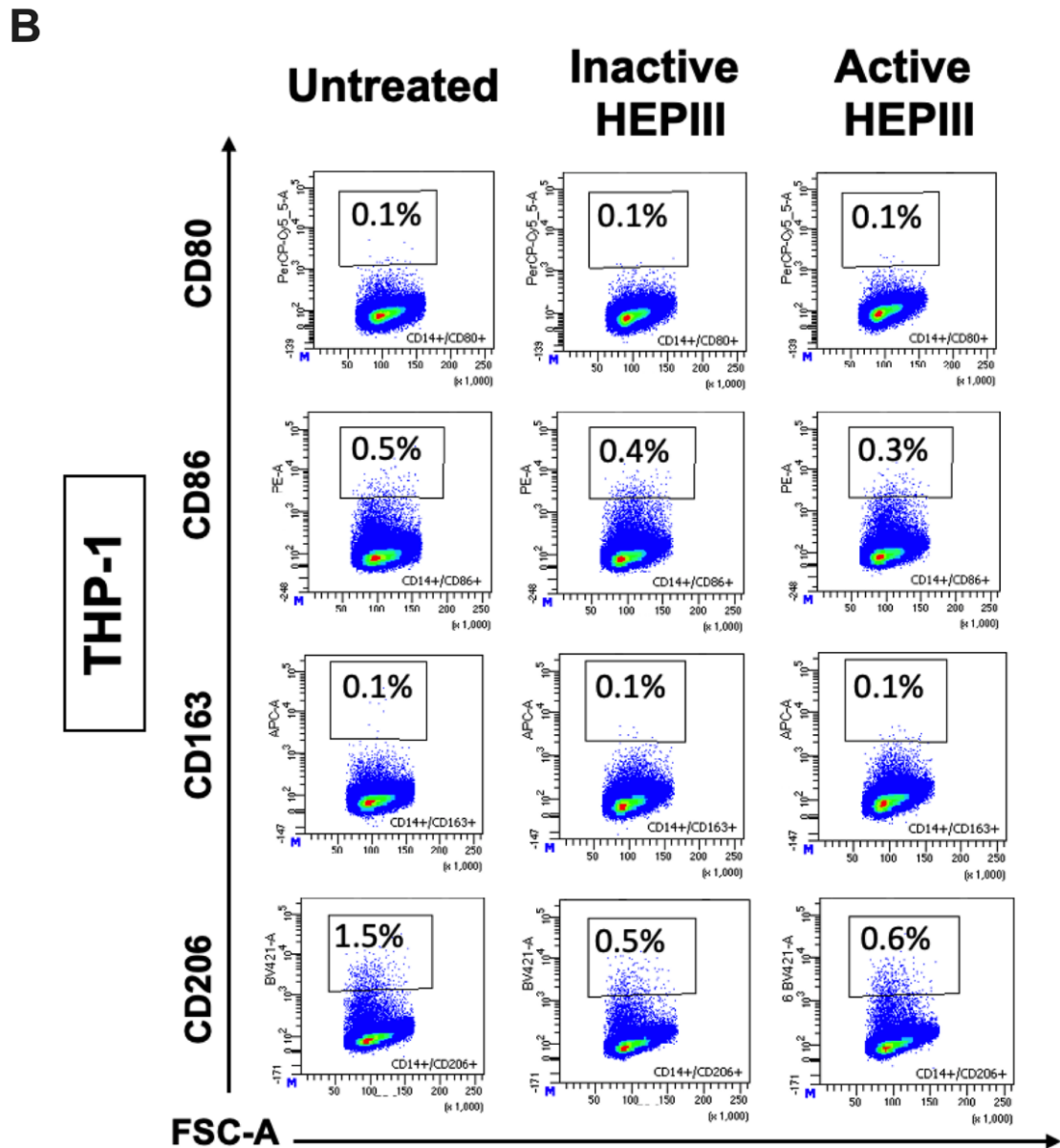
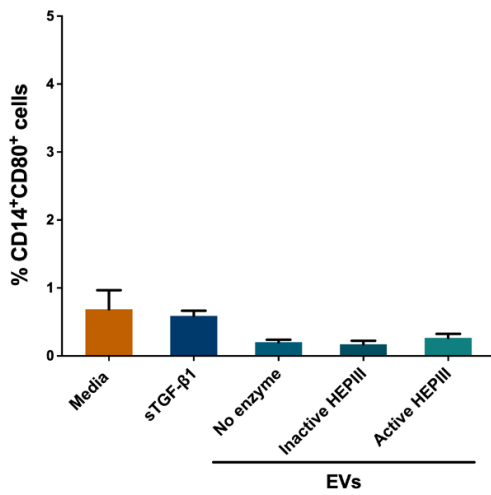


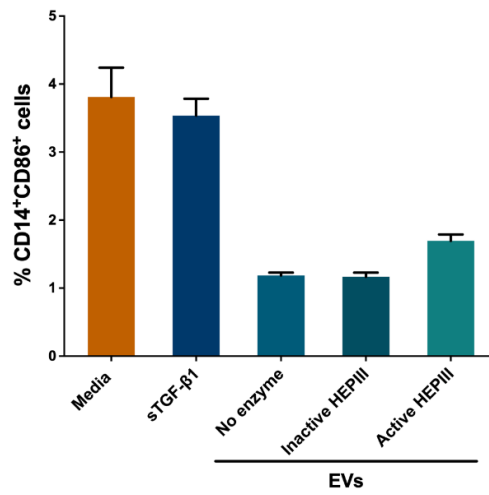
Figure 5.23. Characterisation of CD14⁺CD80⁺, CD14⁺CD86⁺, CD14⁺CD163⁺ and CD14⁺CD206⁺ population in THP-1 cells after direct EV-stimulation. THP-1 cells were treated for 72 hours with 200 μ g/mL of EVs, 1.5 ng/mL sTGF- β 1 or media only (untreated). EVs had been previously treated with heat-inactivated HEPIII, active HEPIII, or no enzyme. **(A)** Bar graph shows the % of CD80⁺ (I.), CD86⁺ (II.), CD163⁺ (III.) and CD206⁺ (IV.) cells from the CD14⁺ population of cells (parent population) for each of the experimental conditions. Data represents mean \pm SD of an independent experiment based on triplicate wells **(B)** Representative dot plots showing marker expression on THP-1 cells that are either untreated or incubated with EVs pre-treated with inactive HEPIII or active HEPIII.

A THP-1+PMA

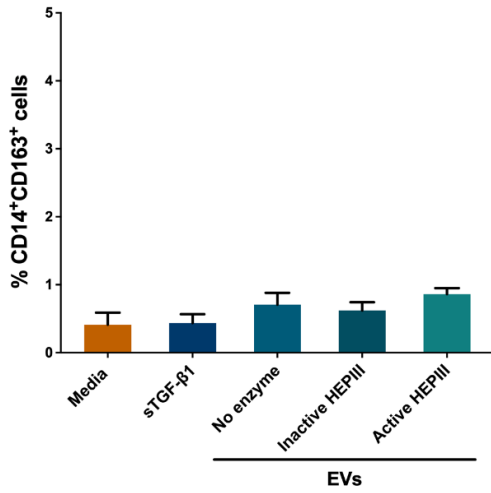
I.



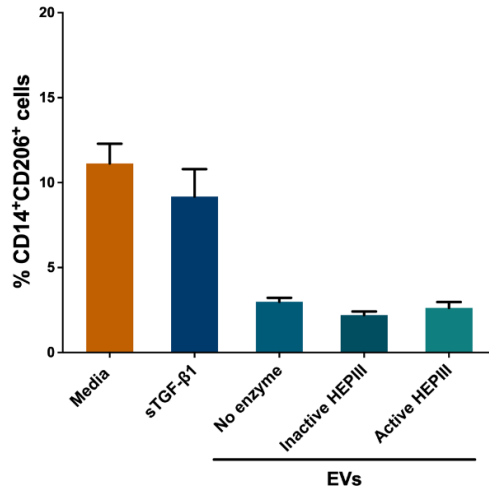
II.



III.



IV.



B

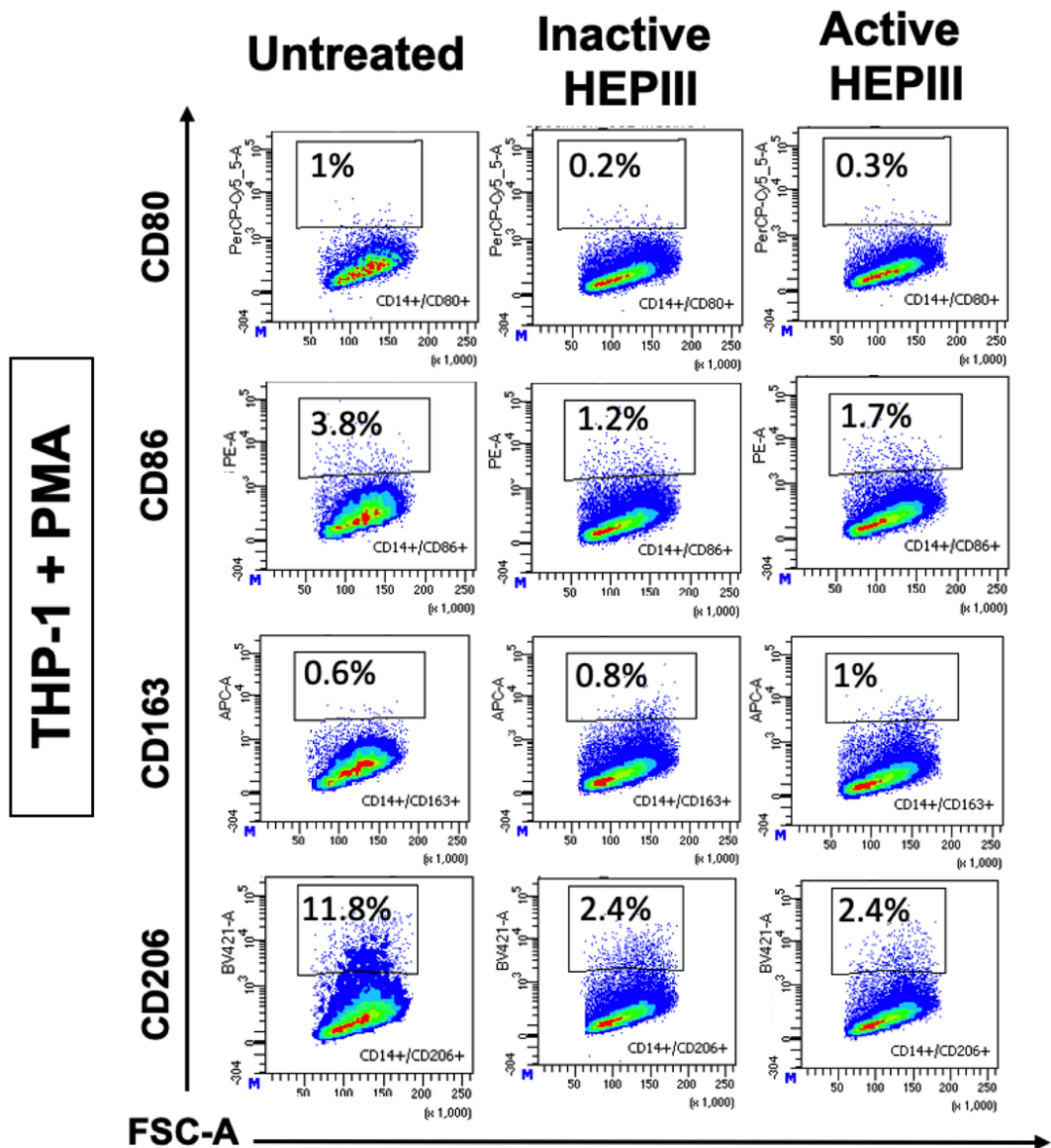


Figure 5.24. Characterisation of CD14+CD80+, CD14+CD86+, CD14+CD163+ and CD14+CD206+ population in THP-1+PMA cells after direct EV-stimulation. THP-1+PMA cells were treated for 72 hours with 200 μ g/mL of EVs, 1.5 ng/mL sTGF- β 1 or media only (untreated). EVs had been previously treated with heat-inactivated HEPIII, active HEPIII, or no enzyme. **(A)** Bar graph shows the % of CD80+ (I.), CD86+ (II.), CD163+ (III.) and CD206+ (IV.) cells from the CD14+ population of cells (parent population) for each of the experimental conditions. Data represents mean \pm SD of an independent experiment based on triplicate wells **(B)** Representative dot plots showing marker expression on THP-1+PMA cells that are either untreated or incubated with EVs pre-treated with inactive HEPIII or active HEPIII.

5.3.4 Assessment of cytokine secretion by stimulated THP-1 cells

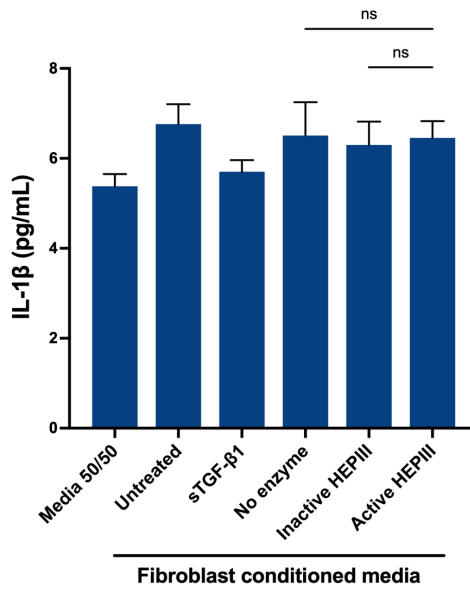
The production of cytokines and chemokines characteristic of both M1 and M2 subsets was explored in THP-1 and THP-1+PMA cells, as the cytokine release repertoire can shed light on the true nature of the subsets, where phenotyping data alone is inconclusive.

Treatment of THP-1 cells with fibroblast CM appears to induce the secretion of IL-1 β and TNF- α , but only in THP-1 primed cells (**Figure 5.25 B I. and II.**). For IL-1 β , this fibroblast mediated influence seems to be dependent on the HS status of EVs used to pre-treat the fibroblasts. Here, pre-treatment of fibroblasts with HS-deficient EVs resulted in a reduced capability of fibroblast CM to induce IL-1 β secretion from THP-1 cells, compared to fibroblasts treated with EVs that had not been digested with HEP1III (**Figure 5.25 B I.**). EV stimulus did not seem to majorly affect the secretion of IL-1 β and TNF- α (**Figure 5.25 C and D, I. and II.**). VEGF and the anti-inflammatory cytokine TGF- β 1 have elevated expression in monocytic and macrophage-like cells co-cultured with fibroblast CM or EVs (**Figure 5.25 A, B, C, D**). While TGF- β 1 secretion is HS-independent, once again, vesicular HS shows to be relevant for an angiogenic effect associated with VEGF. (**Figure 5.25 A, B, C, D III. and IV.**) Active HEP1III enzyme greatly reduced VEGF across all conditions, with the exception of PMA primed cells treated with fibroblast CM (**Figure 5.25 A, B, C, D III.**). The secretion of IL-1 β and TNF- α , even if low, was mostly detected when THP-1 cells exhibited a macrophage-like state, which indicates the necessity of polarising effect previous to detection of these cytokines. VEGF and TGF- β 1, on the other hand, are steadily detected across all experimental conditions and at much higher levels. While one cannot exclude some carryover of these cytokines from fibroblast CM, EV stimulus points to a genuine increase in secretion of these factors and promotion of an anti-inflammatory environment (**Figure 5.25. C and D III.**). Statistical analysis only performed on experiments in triplicate wells.

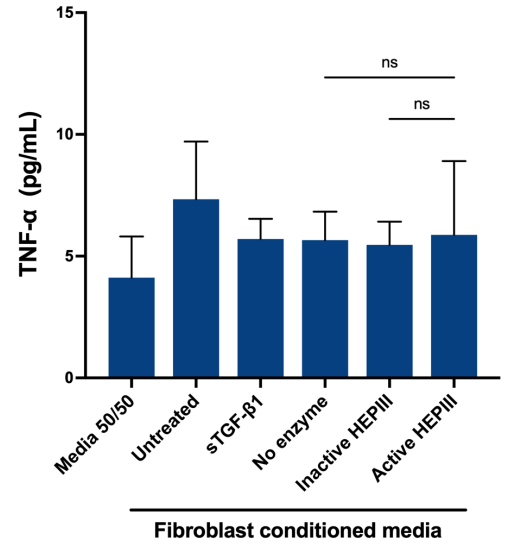
A

THP-1

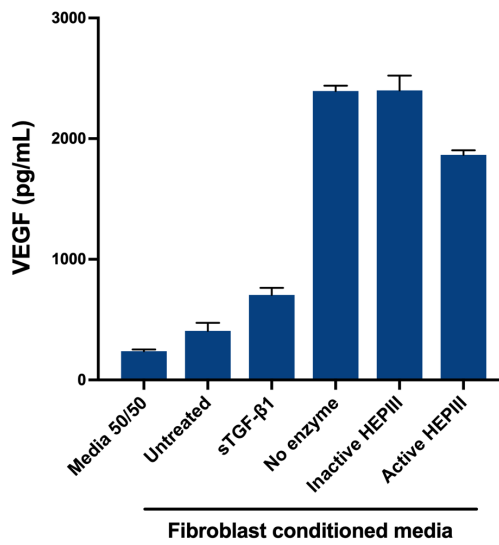
I.



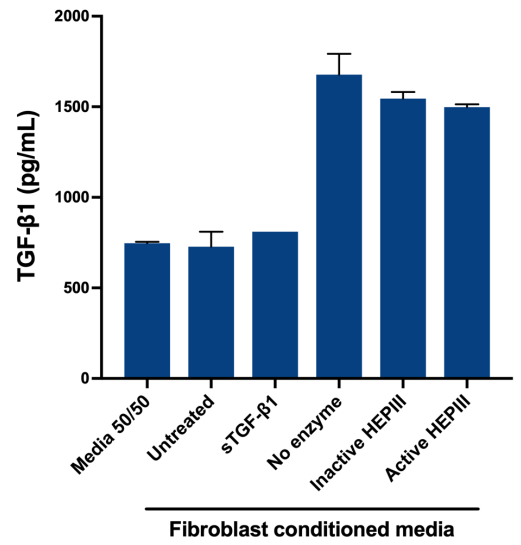
II.



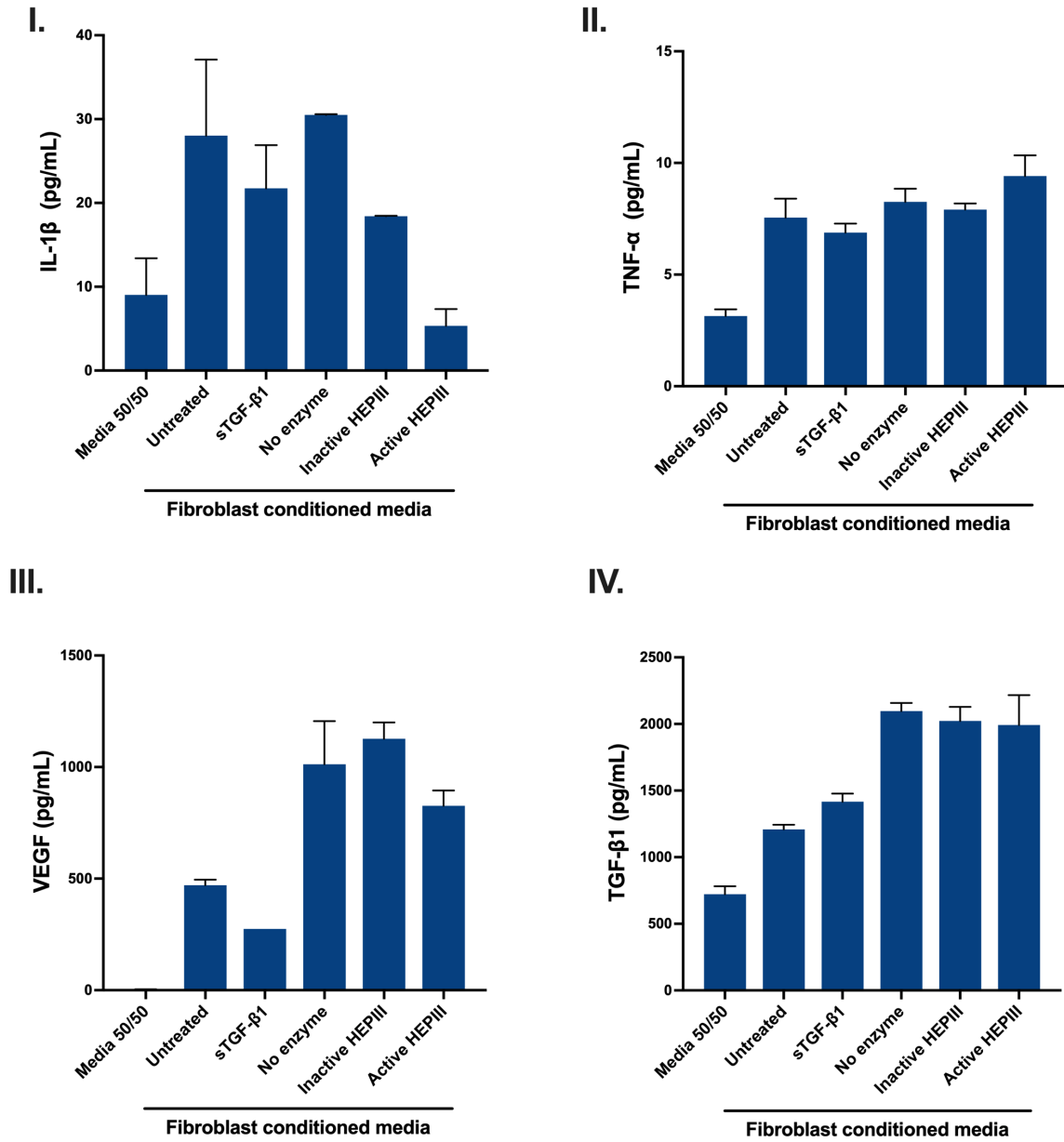
III.

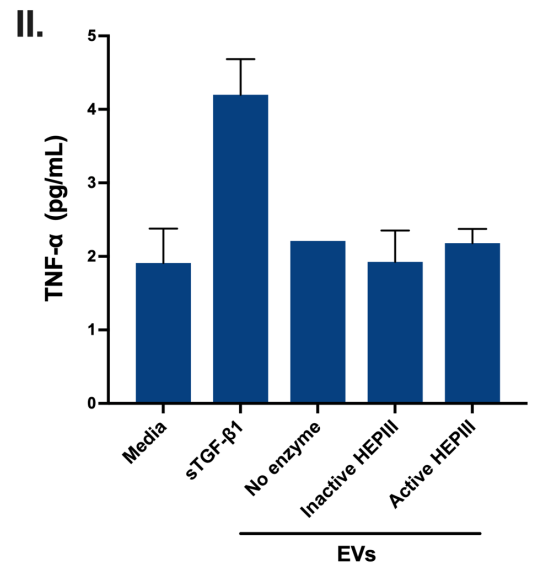
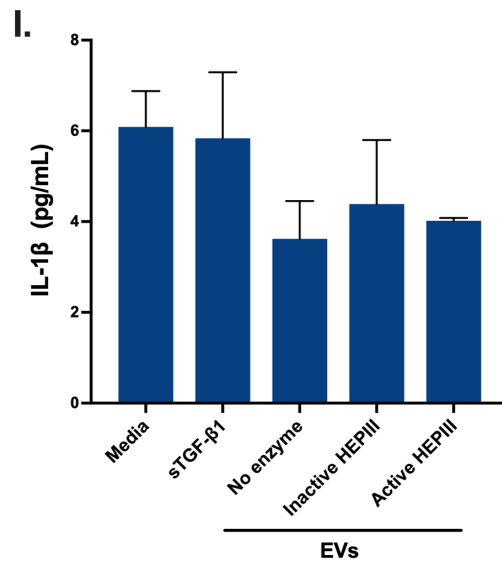
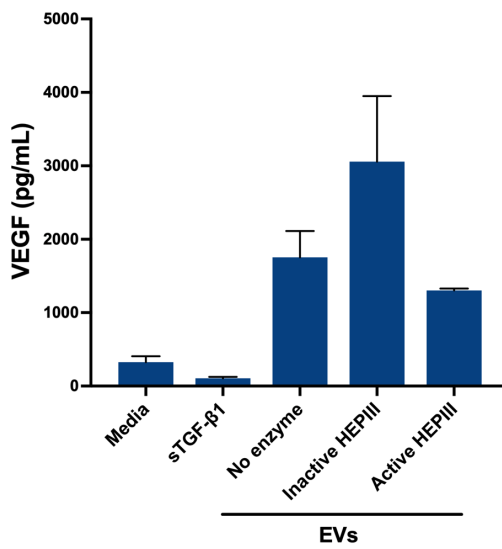
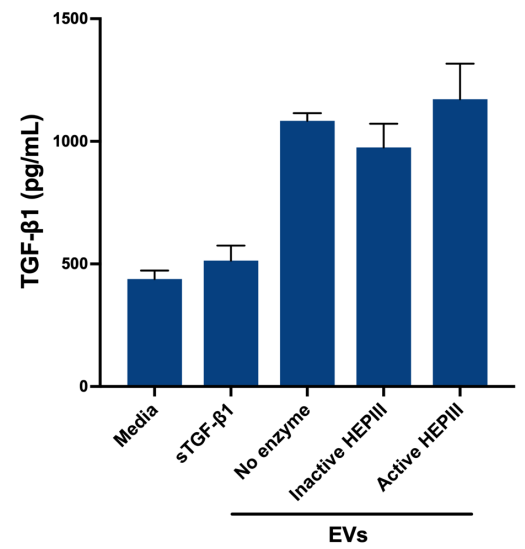


IV.



B THP-1+PMA



C**THP-1****III.****IV.**

D THP-1+PMA

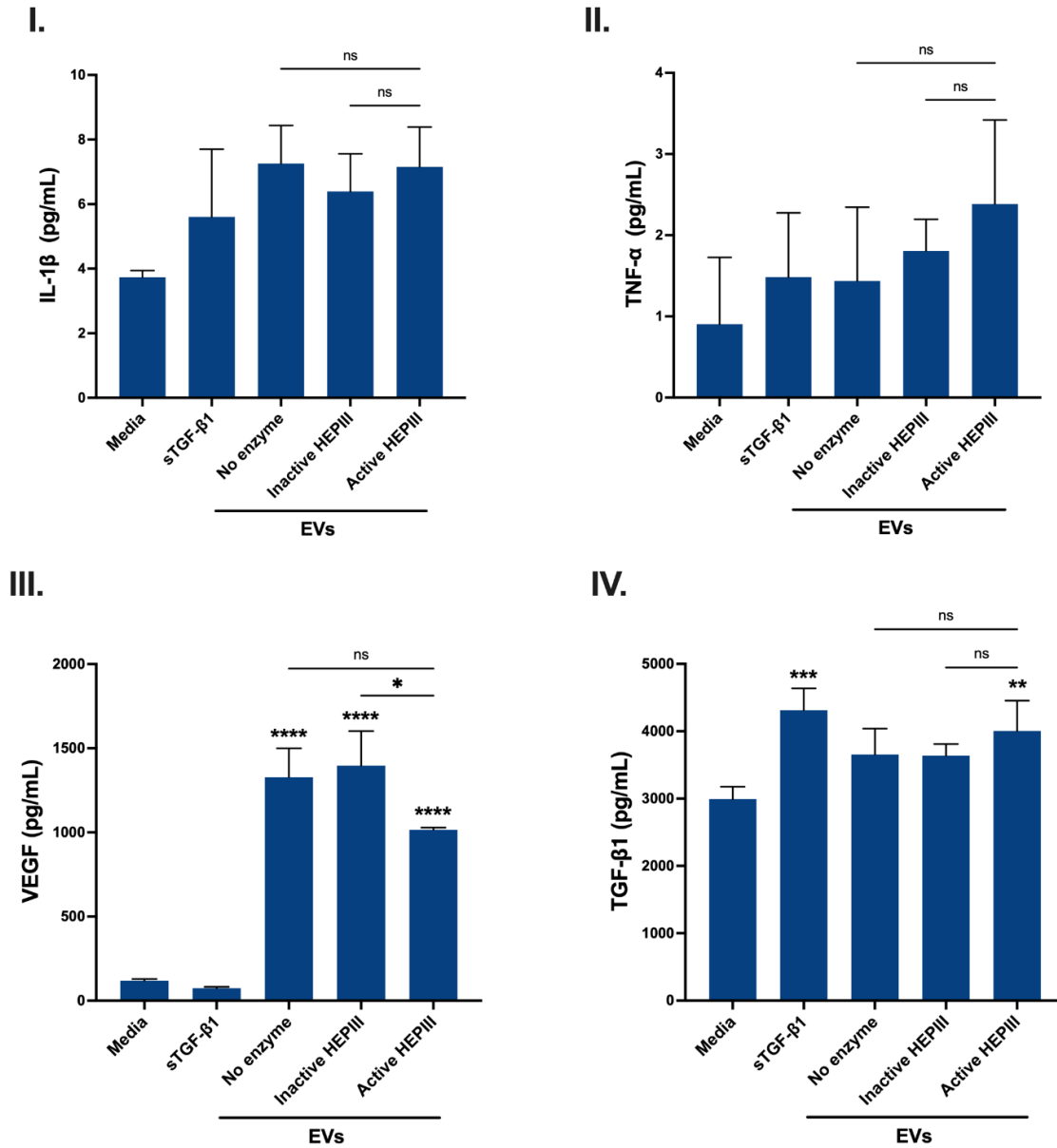


Figure 5.25. Secretion of IL-1 β , TNF- α , VEGF and TGF- β by THP-1 and THP-1+PMA cells directly or indirectly stimulated by EVs. Conditioned media from THP-1 and THP-1+PMA cells stimulated with fibroblast CM (A and B) or directly by EVs (C and D) for 72 hours, was collected and assayed by ELISA. EVs had been previously treated with heat-inactivated HEP111, active HEP111, or no enzyme. The bar graphs show \pm SD of at least two wells for the quantification (pg/mL) of IL-1 β (I.), TNF- α (II.), VEGF (III.) and TGF- β 1 (IV.) secreted by the cells. ****p<0.0001; **p<0.001; *p<0.01; *p<0.05 study conditions vs. media control and **p<0.01; *p<0.0; ns = non-significant control EVs vs. active HEP111 EVs; one-way ANOVA with Tukey's multiple comparison test.

5.4 Discussion

In this chapter, the impact of removing HS moieties from the vesicle surface on uptake and function was explored.

This study showed that vesicular HS does not seem to affect fibroblast uptake to a great extent. This suggests that EV uptake might not be necessary for promotion of phenotypic changes observed in EV-differentiated fibroblasts. Instead, the functional changes might be principally attributed to the co-delivery of factors and activation of receptors at the recipient cell surface. Previous studies from our lab (Cocks, 2019) showed that heparin, a heparan sulphate like molecule, was able to inhibit the uptake of DU145 EVs by fibroblast cells by 45%. However, the onset of α SMA expression was unaffected when fibroblasts were stimulated with EVs in the presence of heparin. Again, these observations support the hypothesis that uptake might not be an essential requirement for EV-mediated myofibroblast differentiation. Classically, myofibroblast differentiation is dependent on TGF- β 1 but considering that EVs are highly complex nanostructures, that bring an assortment of other factors to the recipient cell, it is perhaps not surprising the cellular response arising is complex, and not identical to the response to soluble TGF- β 1. However, our suggestion that co-delivery actually occurs has not been well documented if at all in the literature; hence the experiments depicted in this chapter are of considerable importance in understanding how EVs operate in cell-to-cell communication.

Stimulating growth-arrested fibroblasts with EVs triggered the activation of several receptors, measured through phospho-specific antibodies in an array. Removal of HS from vesicles also proved to be impactful for multiple receptor phosphorylation events, with fibroblasts incubated with such deficient vesicles demonstrating attenuated phosphorylation compared to control conditions. The most interesting observation is that ligands for several of these receptors were already identified in Chapter 4 as being associated with HS on vesicles. These include, for example, midkine, a ligand for ALK/CD246 receptor (Stoica et al., 2002), which was confirmed as an HS-associated factor on EVs (**Figure 4.10 A and B, Chapter 4**). Other ligands include SCF, a ligand of c-kit receptor, IGFBP2 ligand for IGF-I receptor, and GDNF ligand for c-ret receptor, all identified in previous protein profiling analyses (Chapter 4). Therefore, the stimulation of fibroblasts with EVs carrying these and other ligands leads to co-activation of multiple

Chapter 5 - Results

receptors. The kinetics of this effect, as well as minimum EV dosing requirements needed to elicit multi-receptor signalling events and its effects on recipient cells would require further studies. Nonetheless, the data certainly identify the original concept as true, with co-delivery being among the unique functional advantages of EVs as physiological carriers of cytokines and growth factors.

This phenomenon may explain the unique form of differentiation driven by EVs. In fact, the functional consequences of EVs were explored further in terms of their influence on the fibroblast secretome. EVs are able to induce the *de novo* production of several pro-angiogenic cytokines such as ICAM, uPA, VEGF, VCAM-1, and angiogenin. For the last three factors, this influence is diminished in fibroblasts treated with HS-deficient EVs. This is another indicator of the importance of vesicular HS, where the loss of this element seems to have a negative impact, as seen in previous angiogenesis and tumour growth assays (Webber et al., 2015b).

EV-mediated IL-1 α production by fibroblasts is another example of regulation implicating HS-GAG chains on the EV surface. However, despite the high fold-change difference observed, this protein had very low-intensity levels detected on the proteome profiler array membrane and attempts to detect its secretion through ELISA were unmet. IL-1 α is a unique pro-inflammatory cytokine that can be present in the cells as a membrane-associated or secretable form, and this defines its role. In its membrane form has important immune roles, while when secreted into the tumour microenvironment, it induces angiogenesis and other pro-inflammatory cytokines. (Fettelschoss et al., 2011, Rider et al., 2013). GDF-15 production by fibroblasts also seems to be stimulated by HS-deficient EVs compared with control EV conditions. However, due to the very low intensity detected in the profiler array, further confirmatory experiments are required.

Interestingly, the assessment of whole-cell lysates, used for the proteome profile array, shows an increase in production of angiogenic factor FGF-2 associated with EV-lacking HS-GAG chains. However, ELISA data obtained from fibroblast CM, at the corresponding time point of 72 hours, shows that active HEP III EVs associate with lower levels of this protein detected in the secretome. This, however, was not statistically sound and, together with the small change observed in the array data, might indicate that FGF-2 production and secretion is not extremely dependent on vesicular HS-GAG chains. Furthermore, when exploring secretion of FGF-2, VEGF and HGF, HS-deficient EVs

seem to promote higher secretion levels of HGF at both 24 hours and 72 hours, a clear contrast with the other two cytokines that have their levels decreased in relation to EV control conditions. Such data indicates specificity; rather than global effects regulated by HS-GAG and shows both positive and negative influences. Additionally, this could also explain why an increase in the phosphorylation of HGF-receptor is seen in fibroblasts treated under the same EV conditions due to the higher availability of secreted HGF (Figure 5.6).

In this chapter, it was also of interest to explore the conversation between stromal fibroblasts, EVs, and infiltrating cells such as macrophages. Here, I addressed the question of whether EVs are able to directly or indirectly affect monocytic cell differentiation/polarisation using THP-1 cells as a model. The initial idea was to use primary PBMC cells as a model; however, inaccessibility to fresh peripheral blood monocytes for these experiments meant a reliance on a less perfect model to explore this and obtain some of the preliminary data shown. However, THP-1 have been widely used in studies of assessing the effect of tumour conditioned media in macrophage differentiation (Sawa-Wejksza et al., 2018, Wu et al., 2014), which is why they were a reasonable model in this instance.

Conditioned media from EV-activated fibroblasts, as well as direct stimulation of THP-1 monocytes with EVs, can promote differentiation to a macrophage-like cell type measured by an increase of CD14⁺ cells in the population. These were HS-independent effects, however. Notably, polarisation markers were only significantly detected in macrophage-like cells, obtained by previous priming of THP-1 cells with PMA, perhaps as might be expected. However, direct EV stimulus did not result in strong polarisation. Conditioned media from activated fibroblasts seemed to be more potent in modulating macrophage phenotypes and could, for example, impair expression of the M1 marker, CD86, and this effect seems to be stronger for fibroblasts treated with HS-deficient EVs. This indicates perhaps a lower capacity of these modified vesicles in triggering a pro-inflammatory stroma. These observations were corroborated with data obtained from ELISA. While fibroblast CM is still able to induce some expression of pro-inflammatory markers such as IL-1 β and TNF- α in macrophage-like cells, the data suggests a diminished secretion of IL-1 β with HS-deficient EVs, compared to other conditions under study. Moreover, these EV-activated fibroblasts increased CD163 marker expression, in macrophage-like cells, in a HS-independent way. Expression of this M2 subset marker

Chapter 5 - Results

was further supported by an increase in TGF- β 1 secretion, which was again a HS-independent effect. The same is not true for VEGF. In both indirect and direct stimulation, EVs have a strong pro-angiogenic effect, and VEGF secretion by monocytic and macrophage-like cells is dependent on vesicular HS. As macrophages are known to secrete VEGF to support angiogenesis (Jetten et al., 2014) once again, HS seems to be important for the pro-angiogenic functions of not only fibroblasts but also myeloid cells. Furthermore, the production of IL-17A, a cytokine produced *de novo* by fibroblasts stimulated with EVs, has a chemotactic effect on macrophages through its receptor, IL-17RA, possibly indicating a role for EV-activated fibroblasts in accumulating macrophages in the tumour microenvironment (Liu et al., 2012). To distinguish the impact of soluble factors or EVs, secreted by fibroblasts, on monocyte differentiation/polarisation, further experiments are required. This could include clearance of vesicles from fibroblast CM prior to administration to monocyte cells. This step would help to clarify if the functional features observed in the monocytes could be attributed to EVs within the CM or secreted soluble cytokines.

When THP-1 cells were chosen for this project, there was the awareness that these cells do not totally convey the characteristics of typical monocytes, and using PMA to differentiate THP-1 cells would not provide a model identical to tissue macrophages or monocyte-derived macrophages, a recognised model of differentiated tissue macrophages (Tedesco et al., 2018, Shiratori et al., 2017, Daigneault et al., 2010). Unfortunately, there is not one consensual protocol for THP-1 differentiation, and different protocols can greatly influence the characteristics of differentiated cells (Lund et al., 2016, Maeß et al., 2014, Aldo et al., 2013). THP-1 cells, as opposed to primary monocytes, express low levels of CD14 (Bosshart and Heinzelmann, 2004) that decreases with macrophage differentiation (Steinbach and Thiele, 1994). However, THP-1 cells stimulated with PMA present an increase of CD14 positivity, which is widely used as a marker of monocytic differentiation (Schwende et al., 1996, Daigneault et al., 2010). A decrease in CD14 positivity has also been reported in response to PMA priming, which indicates that these differences might mostly relate with the PMA-differentiation protocol used (Aldo et al., 2013). The current study also showed conflicting results with the pan-macrophage marker CD68. This marker is expected to be increased in macrophages (Allavena et al., 1998); however, our data show that its expression does not change between cells with different EV and fibroblast CM treatments, except in the case of THP-1+PMA cells directly treated with EVs, where the proportion of CD68

positive cells decreased. The clear lack of defined populations, as assessed by flow cytometry, brings into question the value of this marker in a THP-1 model. The results presented in this chapter highlight an interesting role of EV-mediated regulation of THP-1 cell phenotype, following priming with PMA. However, there is a clear need to repeat these studies using primary blood-derived monocytes. This will allow us to explore the capacity of EVs to regulate monocyte function, either directly or via an altered fibroblast secretome, using a system that better reflects the in vivo setting.

Overall, HS-modifications imposed on the EVs can have a functional effect on fibroblasts, by modifying receptor activation as well as leading to alterations in fibroblast secretome. The loss of receptor phosphorylation will most likely affect several signalling pathways involved in the promotion of a disease-associated phenotype, which was shown to be attenuated following HS-digestion from the EV surface. Furthermore, EVs aid stromal changes that are consistent with an immunosuppressive and pro-angiogenic microenvironment. Following EV-mediated activation fibroblasts are able to promote changes in macrophage like cells that are consistent with a pattern of anti-inflammatory effect, which is in part regulated by vesicular HS.

Summary of objectives met:

- The HS-modifications imposed on the EVs despite having no marked impact on vesicular uptake by fibroblasts, contribute to a decreased capacity of these EVs to promote a disease-associated phenotype.
- HS-modified EVs can have a functional effect on fibroblasts, by modifying receptor activation as well as the fibroblast secretome.
- EV activated fibroblasts induce changes in macrophage like cells that are consistent with an immunosuppressive effect, which is in part regulated by vesicular HS.

Chapter 6

Discussion

6.1 General discussion

The work presented in this thesis focused on the hypothesis that vesicle surface associated HSPGs are required for EV-mediated delivery of growth factors and cytokines. Alterations of these vesicular components are shown to directly alter functionally critical features of vesicles. Furthermore, this had a direct impact on EV-mediated stromal cell behaviour in terms of fibroblast to myofibroblast differentiation and myeloid cell regulation. Through examining the repertoire of factors tethered to EVs we have provided new knowledge of the EV corona, and the vital importance of these complex elements of EVs in modulating biological pathways important for cancer progression.

In the field of extracellular vesicles, it is important to report data characterizing the nature of the EV isolate to define issues such as vesicle purity. Without this, attributing research findings to vesicles, as opposed to co-isolated factors, would be open to challenge. In this study, a critical aspect was the explicit specificity of the enzymatic digestion of HS-GAG chains from EV surface in order to accurately assign factors as HS-GAG associated. Moreover, a broader approach was also investigated by knockdown of specific HSPGs in the parent cell. The data presented here shows that the EV isolates obtained through ultracentrifugation on a sucrose cushion and subsequent pelleting have the structure, size and protein expression associated with typical EVs derived from endosomal compartments. Furthermore, the HSPG-modifications imposed in these EVs did not affect EV size and protein expression but had significant impacts on the molecular composition of vesicles, highlighting the HSPGs as major and integral elements in the formation of EVs and in their functional operation in biological systems.

To define the repertoire of growth factors and cytokines tethered to the EV surface by HSPGs and HS-GAG chains, a multiplex protein array, employing PEA technology, was used. This technology has revealed factors that would likely otherwise be at such low levels to be undetectable. This approach revealed differences in proteins detected between HSPG/HS-deficient and control EVs such as midkine, CYR61 and TFPI. Validation by ELISA was often difficult yet was achieved for some of the more abundant elements, and these data supported a true association with HS-GAG chains on HSPGs at the EV surface. Despite the association of these proteins with heparin/HS being previously known (Sumi et al., 2002, Kadomatsu et al., 2013, Chen et al., 2000,

Chapter 6 - Discussion

Grzeszkiewicz et al., 2002, Ho et al., 1997), the association with HS-GAG chains at EV surface is novel. Cellular processes that regulate the inclusion of HSPG during EV biogenesis offer a modality for tethering such factors to EVs and the subsequent capacity to deliver such cytokines/growth factors in the context of vesicle-mediated intercellular communication.

Growth factors could either be incorporated into EVs while within the extracellular environment, or HSPGs could play an important role in direct loading of proteins during biogenesis prior to vesicle secretion. This issue, however, of where and how such factors become incorporated onto the EV surface has not been resolved in the current study and is an open question that requires further investigation. In a past report, exogenous incubation of EVs with excess recombinant TGF- β 1 did not result in an elevation of TGF- β 1-associated to EVs (Clayton et al., 2007). This might suggest that loading takes place during a biogenesis process, intracellularly, rather than capturing factors present extracellularly. Alternatively, the EV surface is finite, and may have a limited capacity to bind additional growth factors through passive binding in such an experiment. Determining the nature and rules governing EV loading with growth factors will be challenging and may need to be approached from a growth-factor specific perspective, as a general model in such a complex system may be beyond our current grasp. Exploring the impact of HSPG-knockdown clearly identified a huge number of changes, with a reduction as well as an elevation in several elements. The reason why this result is not entirely surprising comes from the prior knowledge that HSPGs are involved in EV biogenesis and possibly cargo loading (Baietti et al., 2012, Ghossoub et al., 2020). Such complex datasets are far from defining the processes of EV-loading; nevertheless, they demonstrate the critical importance of HSPG in the regulation of EV molecular content and suggest an intracellular loading of growth factors is at least partially involved.

Functional enrichment analysis revealed that the differently detected proteins between HSPG/HS-deficient and control EVs were often associated with proteoglycan pathways, such as the glypican pathway, which is reassuring. Also, features including integrin related signalling and inflammatory pathways were identified. Interpreting the data arising from HSPG knockdown was more difficult, given some elements were elevated and others attenuated by these parent cell manipulations. Furthermore, pooling the identified protein lists limits our ability here to assign particular biological functions to a specific HSPG core protein. Nonetheless, regardless of these limitations, these analyses

strongly support our endeavours to better understand the EV heparome and its functional relevance in pathological processes and provides rich avenues for future investigations aimed at demonstrating the diversity of EV-mediated functions that are dependent on HSPG-associated factors.

Fluorescently labelled EVs were internalised by fibroblasts, and this was observed by microscopy and flow cytometry. Removal of HS-GAG chains from the EVs appears to have a limited effect on EV uptake. Christianson *et al.* showed that cell surface HSPGs were essential for EV attachment to the cell and subsequent uptake (Christianson *et al.*, 2013). However, the study also showed that enzymatic digestion of vesicular-HS did not affect their internalisation, which is in agreement with our findings. Therefore, any functional impact of HS-GAG manipulations is more likely than not to be related to changes in EV-phenotype and less due to issues of cell dosing.

The loss of HS-GAG chains clearly had a highly significant impact on EV function, with a decreased capacity of EVs to induce fibroblast to myofibroblast differentiation. For this differentiation process, these observations suggest that vesicular uptake might not be required for promotion of the myofibroblastic phenotype, and instead, the trigger for differentiation is centred on EV-driven interactions at the cell surface. Similarly, other work from our group showed that inhibition of EV uptake did not extensively affect the onset of α SMA expression in fibroblasts, indicating that endocytosis of EV is not a requirement for fibroblast stimulation by EVs (Cocks, 2019). Theoretically, the removal of vesicular HS could affect their capacity to attach to the recipient cell, removing the connection point for ligands necessary for EV binding to the cell surface, such as fibronectin (Purushothaman *et al.*, 2016). This would then abrogate receptor activation and attenuate the promotion of the cell signalling responses. An in-depth analysis of EV tethering to the recipient cell surface would certainly be a valuable addition and provide important data to help us truly understand the role of HS-GAG chains in EV attachment to cells. However, the complexity of the system is high as it might be the factors associated with HS-GAG that are both driving the signalling responses and participating in adhesive interactions. As such, it was not possible in the current study to delve deeper into these aspects.

The detection of differently phosphorylated receptors in fibroblasts exposed to HS-GAG deficient EVs compared to control EVs is an important highlight of the current study.

Chapter 6 - Discussion

Amongst the receptors where phosphorylation was reduced are receptors for ligands that were downregulated upon enzymatic digestion of EVs. These include GDNF receptor (c-ret), SCF receptor (c-kit), IGFBP2 receptor (IGF-I), midkine receptor (ALK/CD246) and VEGF receptor (VEGFR). These findings directly link the modifications of EV phenotype to deficiencies in the intracellular signalling events, and therefore, provide strong evidence for the functional relevance of these identified HS-GAG associated EV-delivered growth factors. As well as signalling events, EVs are also able to induce the *de novo* production of pro-angiogenic cytokines such as ICAM, uPA, VEGF, VCAM, FGF-2 and angiogenin. Again, secretion of such factors was attenuated following stimulation of fibroblasts with HS deficient EVs compared to control EVs. In consequence, the biological potency of cancer cell-derived EVs becomes severely limited in terms of stromal cell activation/differentiation following HS-GAG removal, emphasising the profound importance of these features of EVs in dictating the functional outcomes. The use of techniques such as RNA-seq would allow for exploration of the cell transcriptome and provide additional information on the impact of HS-GAG modifications, and associated heparome, on downstream pathway activation and changes to transcription.

The final aim of this thesis was to briefly explore the relationship between EVs, fibroblasts, and myeloid cells in an effort to validate some of the functional enrichment results that indicated inflammation was a putative biological pathway related to the HSPG-associated identifications. The capacity of EVs to directly or indirectly affect monocytic cell differentiation and polarisation was explored. Ideally, PBMCs obtained from fresh peripheral blood would have been used here, but such material was restricted at the time of the study, and therefore a model system was employed relying on THP-1 cells (Sawa-Wejksza et al., 2018, Wu et al., 2014).

THP-1 cells were either primed into macrophage-like cells with PMA or used in their native state. EVs promoted differentiation of THP-1 monocytes towards a macrophage-like cell type, by an increase in CD14⁺ cells in the population. This is observed both in PMA primed and non-primed THP-1 cells, however, the effect is more significant in native THP-1 cells. Nonetheless, this effect was completely independent of HS-GAG chains across all tested conditions. Priming of THP-1 cells with PMA promoted a significant change in polarisation markers CD86 and CD163 of cells incubated with EV-treated fibroblast CM. These changes reflected a decrease in the M1 marker (CD86) and

increase in the M2 marker (CD163), pointing towards a tumour supporting phenotypical change in these cells. Supporting these data, detection of pro-inflammatory cytokine secretion such as IL-1 β was decreased, but anti-inflammatory cytokines such as TGF- β 1 and VEGF were increased. Interestingly, VEGF secretion in this system was HS-dependent highlighting once again the contributions of vesicular HS to promote pro-angiogenic effects on stromal cells. Still, a clear HS-GAG dependent effect on THP-1 cells was more elusive. Clearly, a physiologically more relevant follow-on study is needed on primary monocytes and tissue macrophages, to generate a more definitive understanding of EV influence on myeloid cell behaviours, and to confirm whether or not HS-GAG associated features are important in any effects imposed.

6.2 Future Directions

A key question which remains unanswered is the contribution that particular EV-associated factors, delivered either individually or in combination, have towards activation of signalling pathways within recipient cells, such as stromal fibroblasts. In the future, the use of strategies to block receptors related to some of the proteins identified with a vesicular HS association will help to elucidate the physiological implications of a particular protein in promoting the myofibroblastic phenotype. Proteins, which loss of vesicular HS was associated with a diminished detection on the EV surface, as well as abrogated phosphorylation of its receptors in fibroblasts, could provide interesting candidates to explore using this strategy. Examples of these proteins would be midkine, SCF and VEGF. In addition, exploring the role of vesicular delivery of TGF- β , a strong M2 activator factor, in macrophage polarisation would also be of interest.

Future work could also include strategies exploring the tethering and uptake of HS-deficient EVs by both fibroblast and monocytes/macrophages to evaluate the importance of HS-GAG chains in EV attachment to recipient cells, as well as the requirements for EV-uptake in driving a disease associated phenotype and differentiation/polarisation effects. Besides the HEP111 digestion employed in this thesis, other strategies can be used to inhibit/modify EV-HS. For example, establishment of cell lines with knockdown (or knockout) of enzymes involved in HS synthesis, such as exostosin proteins, EXTL2 and EXTL3, and sulfotransferases, will provide additional tools to explore the vesicular heparome and complement the findings obtained with HEP111 enzymatic digestion.

Chapter 6 - Discussion

Additionally, the use of these genetically modified cells as recipient cells would allow exploration of the importance of cellular HS in EV adhesion and uptake by recipient cells.

Finally, the use of PBMCs derived monocytes and macrophages to investigate the differentiation and polarisation effects of EVs would be of high priority, considering all the caveats associated with the THP-1 cell model, as described above. Furthermore, exploring and optimizing a different antibody panel, with additional markers, such as CD11b (pan macrophage marker), TLR2/4 (M1 markers) and arginase (M2), would provide robustness to the study and allow to better understand the functional effects that prostate cancer-EVs can promote on monocytes/macrophages.

6.3 Concluding Remarks

The new data presented in this study demonstrate that extracellular vesicles express membrane-associated HSPGs, which in turn tether a broad variety of factors to the EV surface. These factors are delivered to recipient stromal cells, instigate multiple signalling pathways, and in turn, modify the activation and differentiation status of the recipient. Removal of HS-GAG from the EV outer surface causes profound changes in the overall EV phenotype, resulting in loss of functional potency that is independent from EV-dosing. This study emphasises the critical roles of vesicular HSPG in regulating the molecular content of EVs and in dictating their biological functions. Furthermore, it identifies potential targets that could be manipulated in future studies to limit cancer cell to stromal cell cross-talk in the tumour microenvironment.

Summary of key findings:

- Extracellular vesicles express membrane-associated HSPGs, that tether a broad variety of factors to the EV surface. This thesis presents a novel association of vesicular HS with midkine, CYR61 and TFPI.
- Vesicular HS is important to deliver factors to recipient stromal cells. This activates multiple signalling pathways and influences the differentiation status of the recipient cell.
- Vesicular HSPG are critical in regulating the molecular content of EVs and in dictating their biological functions.

Appendices

Appendices

Chapter 4. APPENDIX

Cardiovascular III Panel - <https://www.olink.com/products/cvd-iii-panel/>

TNFRSF14	GRN	GDF-15	AP-N	IL-1RT2	PON3
LDL receptor	MEPE	SELE	AXL	SHPS-1	CTSZ
ITGB2	BLM hydrolase	AZU1	IL-1RT1	CCL15	MMP-3
IL-17RA	PLC	DLK-1	MMP-2	CASP-3	RARRES2
TNF-R2	LTBR	SPON1	FAS	uPA	ICAM-2
MMP-9	Notch 3	MPO	MB	CPB1	KLK6
EPHB4	TIMP4	CXCL16	TNFSF13B	CHI3L1	PDGF subunit A
IL2-RA	CNTN1	IL-6RA	PRTN3	ST2	TNF-R1
OPG	CDH5	RETN	PCSK9	t-PA	IGFBP-2
ALCAM	TLT-2	IGFBP-1	U-PAR	SCGB3A2	vWF
TFF3	FABP4	CHIT1	OPN	EGFR	PECAM-1
SELP	TFPI	TR-AP	CTSD	IGFBP-7	NT-pro BNP
CSTB	PAI	CCL22	PGLYRP1	CD93	CCL16
MCP-1	CCL24	PSP-D	CPA1	IL-18BP	
CD163	TR	PI3	JAM-A	COL1A1	
Gal-3	TNFRSF10C	Ep-CAM	Gal-4		

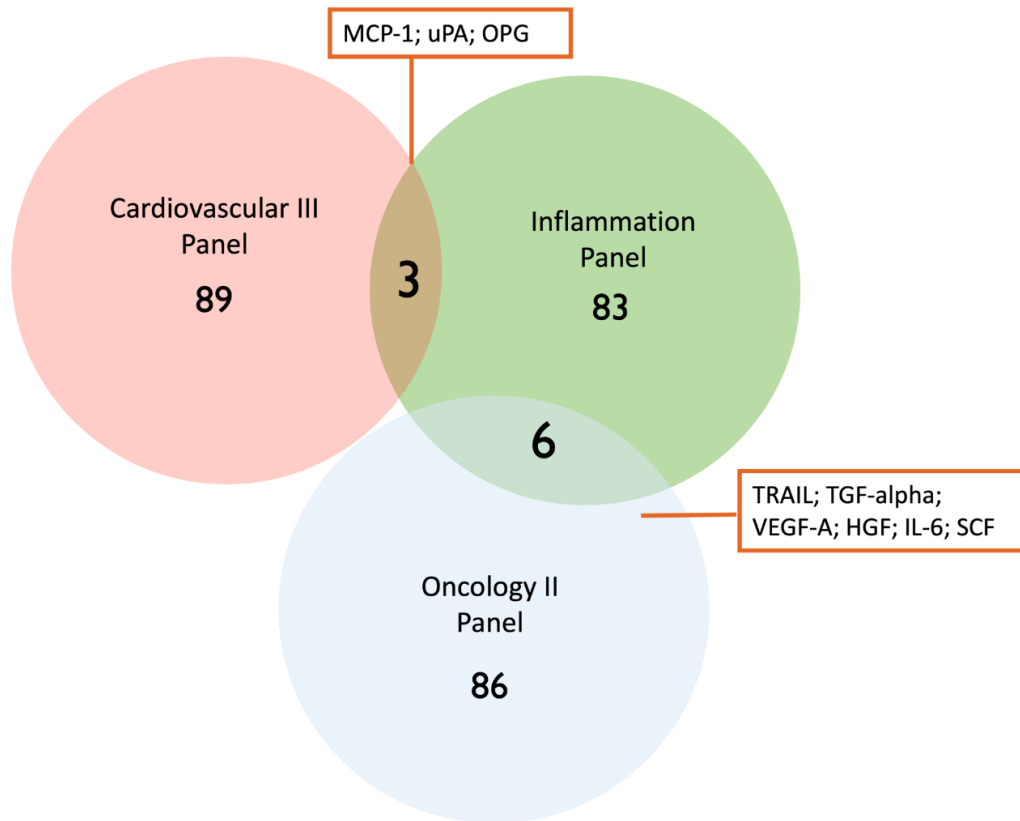
Inflammation Panel - <https://www.olink.com/products/inflammation/>

IL-8	AXIN1	TGF-alpha	Beta-NGF	CXCL10	CCL25
VEGF-A	TRAIL	MCP-4	CXCL5	4E-BP1	CX3CL1
BDNF	IL-20RA	CCL11	TRANCE	IL-20	TNFRSF9
MCP-3	CXCL9	TNFSF14	HGF	SIRT2	NT-3
GDNF	CST5	FGF-23	IL-12B	CCL28	TWEAK
CDCP1	IL-2RB	IL-10RA	IL-24	DNER	CCL20
CD244	IL-1 alpha	FGF-5	IL-13	EN-RAGE	ST1A1
IL-7	OSM	MMP-1	ARTN	CD40	STAMPB
OPG	IL-2	LIF-R	MMP-10	IL-33	IL-5
LAP TGF-beta-1	CXCL1	FGF-21	IL-10	IFN-gamma	ADA
uPA	TSLP	CCL19	TNF	FGF-19	TNFB
IL-6	CCL4	IL-15RA	CCL23	IL-4	CSF-1
IL-17C	CD6	IL-10RB	CD5	LIF	
MCP-1	SCF	IL-22 RA1	MIP-1 alpha	NRTN	
IL-17A	IL-18	IL-18R1	Fit3L	MCP-2	
CXCL11	SLAMF1	PD-L1	CXCL6	CASP-8	

Oncology II Panel - <https://www.olink.com/products/oncology/>

TXLNA	ITGAV	TGF-alpha	CD27	CRNN	ADAM-TS 15
VEGF-A	TRAIL	FURIN	XPNPEP2	TCL1A	CD70
CPE	hK11	CYR61	ERBB4	CD160	RSPO3
KLK13	GPC1	hK14	HGF	TNFRSF4	FR-gamma
CEACAM1	TFPI-2	FADD	ADAM 8	MIC-A/B	CEACAM5
MSLN	hK8	MetAP 2	5'-NT	WISP-1	VEGFR-3
TNFSF13	VEGFR-2	PVRL4	DKN1A	CXL17	MUC-16
EGF	LYPD3	FASLG	DLL1	PPY	WIF-1
TNFRSF6B	PODXL	EPHA2	MK	S100A11	GZMB
SYND1	S100A4	ITGB5	ABL1	AR	FCRLB
TGFR-2	IGF1R	Gal-1	FGF-BP1	ESM-1	ANXA1
IL-6	ERBB2	SEZ6L	TLR3	CD207	FR-alpha
CD48	ERBB3	GNPMB	LYN	ICOSLG	
SCAMP3	SCF	CA9	RET	WFDC2	
LY9	SPARC	MIA	VIM	CXCL13	
IFN-gamma-R1	GZMH	CTSV	TNFRSF19	MAD homolog 5	

Appendix 4.1. Biomarkers in Olink Panels. Complete list of 92 proteins featured in the Cardiovascular III, Inflammation and Oncology II panels. Links for protein full names are provided.



Appendix 4.2. Venn diagram showing the overlap between Cardiovascular III, Inflammation and Oncology II panels from Olink.

A

pg/mL	CXCL10 standard curve mean absorbance (337/615 A)
500	4855
250	2641.5
125	1528
62.5	929.5
31.3	679.5
15.6	602
7.8	515.5
0	539

 $R^2=0.9991$

	Mean absorbance (337/615 A)
8 μg	477.667
4 μg	482.333
2 μg	468.000
1 μg	456.667
0 μg	427.333

B

pg/mL	MCP-1 standard curve mean absorbance (337/615 A)
250	3692.5
125	2071
62.5	1171.5
31.3	818
15.6	554
7.8	496
3.9	469.5
0	443.5

 $R^2=0.9991$

	Mean absorbance (337/615 A)
8 μg	470.667
4 μg	386.667
2 μg	457.000
1 μg	454.667
0 μg	387.667

C

pg/mL	IL-18 standard curve mean absorbance (337/615 A)
750	46494
188	23104
93.8	16988.5
46.9	15578
11.7	11878.5
0	12140

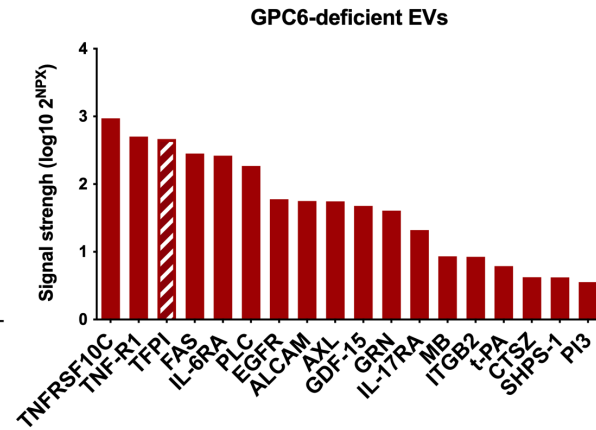
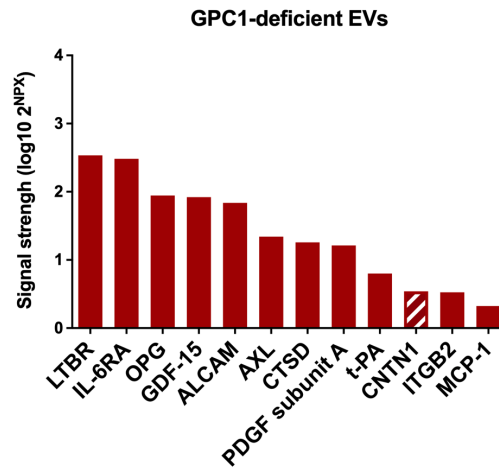
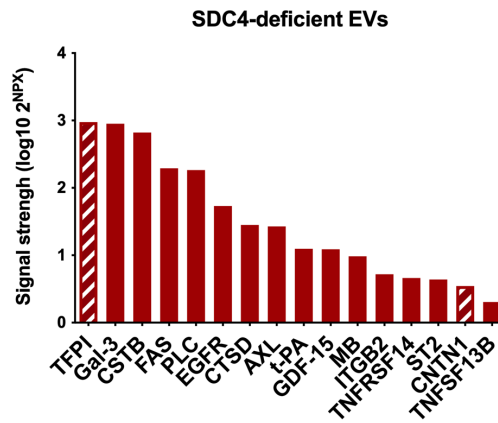
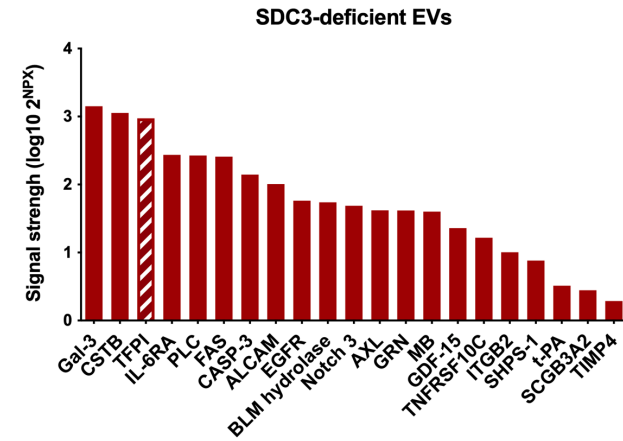
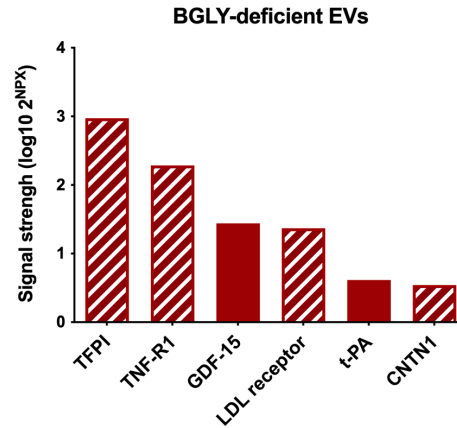
	Mean absorbance (337/615 A)
10 μg	7619
5 μg	11077
2 μg	11993
1 μg	11399
0 μg	13010

Appendix 4.3. Standard curve for **(A) CXCL10 (B) MCP-1** and **(C) IL-18** ELISA and absorbance readout detected for DU145 EVs on 8 μg , 4 μg , 2 μg and 1 μg per 100 μL /well. Each ELISA represents technical replicate of n=3 wells.

A

Cardiovascular III Panel

 Decreased in HSPG-KD EVs
 Increased in HSPG-KD EVs

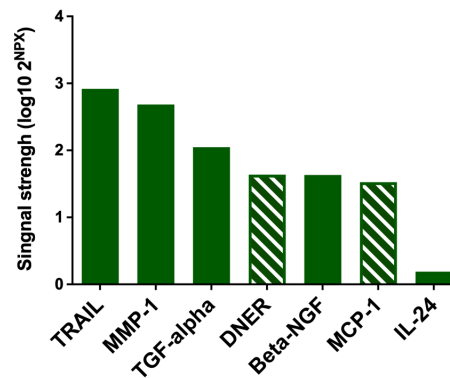


B

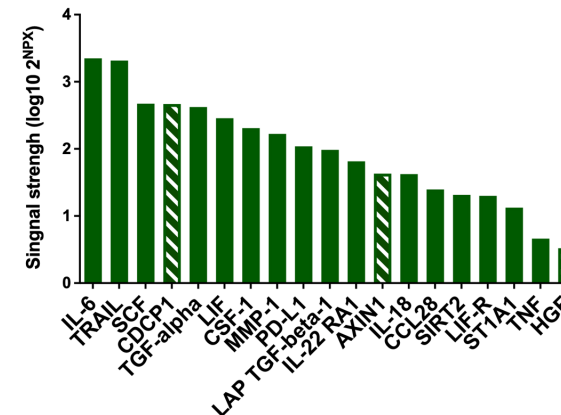
Inflammation Panel

 Decreased in HSPG-KD EVs
 Increased in HSPG-KD EVs

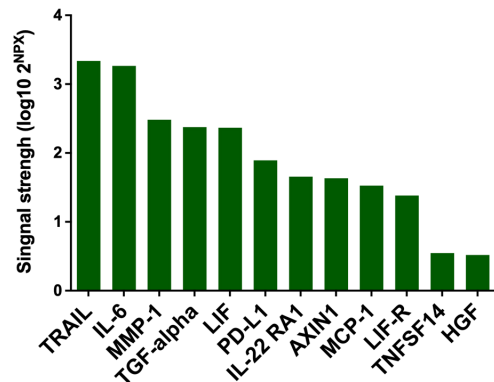
BGLY-deficient EVs



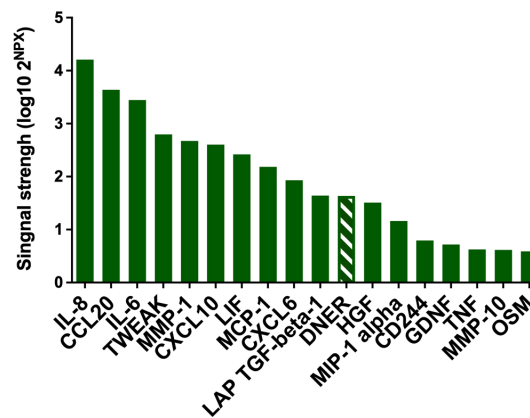
SDC3-deficient EVs



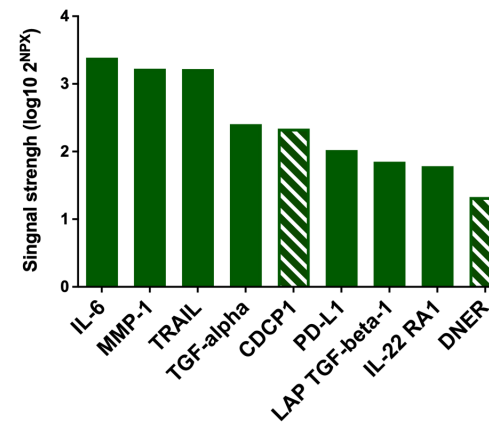
SDC4-deficient EVs



GPC1-deficient EVs



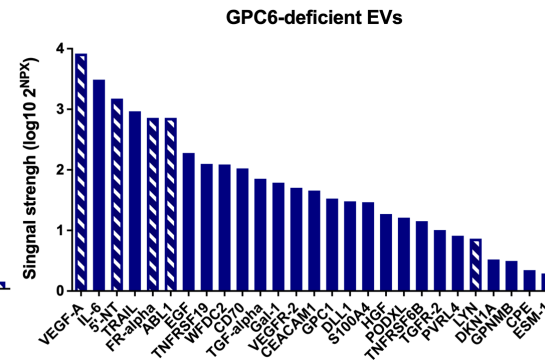
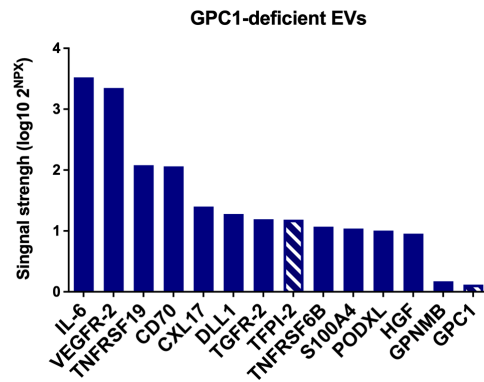
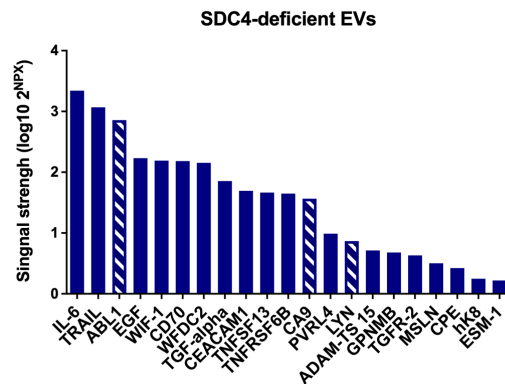
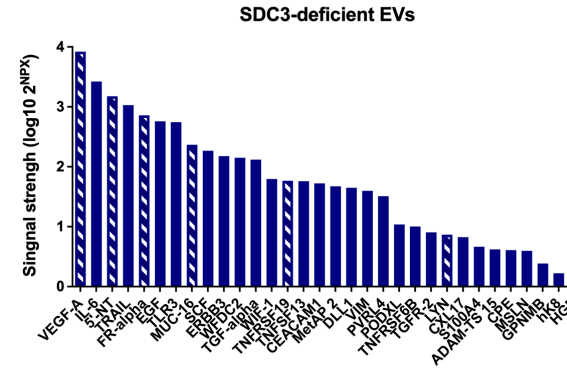
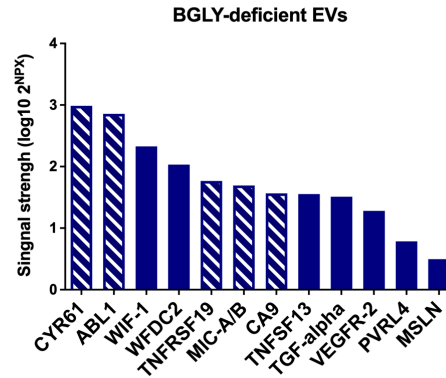
GPC6-deficient EVs



C

Oncology II Panel

▨ Decreased in HSPG-KD EVs
 ■ Increased in HSPG-KD EVs



Appendix 4.4. The abundance of proteins in control and HSPG-deficient vesicles can be translated in the strength of signal detected by the Olink assay. Bar graph shows the suggested abundance of proteins in vesicles lacking the different HSPGs core proteins, in relation to the control, in cardiovascular III panel (A), inflammation panel (B) and oncology II panel (C). Only proteins with a with a fold change (FC) ± 2 and statistical significance ≤ 0.05 (t-test, corrected for multiple testing using Benjamini-Hochberg adjustment) are displayed in the graph. Proteins elevated in HSPG-modified vesicles are showed in solid bars and proteins decreased are shown striped. Data shown represents the mean of n=3 replicates. NPX= Normalised Protein eXpression.

A

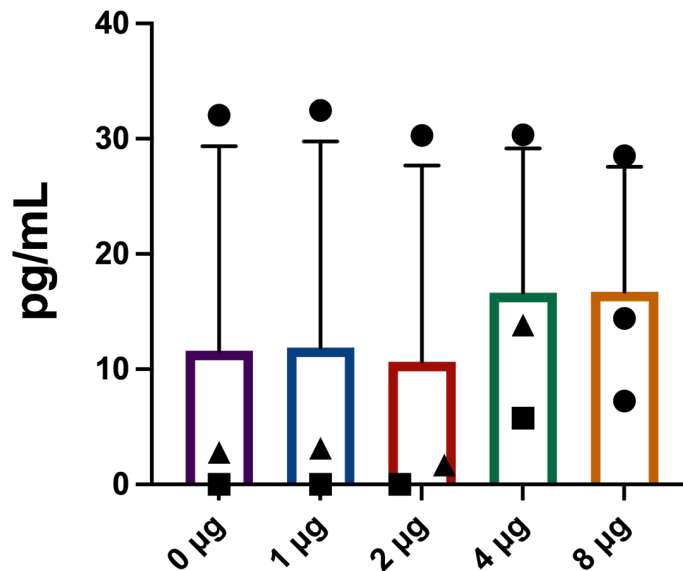
pg/mL	MMP-1 standard curve mean TRF (337/615)
1600	2.4275
800	1.8955
400	1.3495
200	0.8595
50	0.5505
25	0.464
12.5	0.654
0	0.46

	MMP-1 TRF (337/615)
8 µg	0.374
4 µg	0.445
2 µg	0.389
1 µg	0.415
0 µg	0.356

Appendix 4.5. (A) Standard curve for MMP-1 ELISA and absorbance readout detected for DU145 EVs on 8 µg, 4µg, 2 µg and 1µg per 100 µL/well.

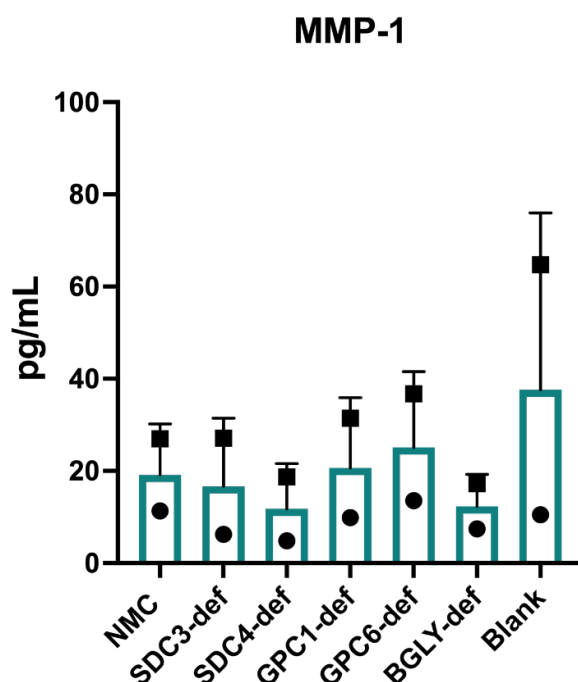
B

MMP-1



Appendix 4.5. (B) Quantification of MMP-1 on DU145 EVs. The bar graphs show the mean ± SEM of at least 2 independent experiments each based on a different EV isolate and represented by circle, square or triangle. The concentrations (pg/mL) of protein detected at the surface of DU145 EVs on 8 µg, 4 µg, 2 µg and 1 µg per 100 µL/well are represented. Every independent experiment was performed in triplicate wells.

C



4.5. (C) Quantification of MMP-1 on HSPG deficient EVs. The bar graphs show mean \pm SEM of at least 2 independent experiments, each based on a different EV isolation, represented by circle, triangle and square. The concentration of MMP-1 detected 4 μ g of HSPG-deficient EVs is shown. Every independent experiment was performed in triplicate wells. NMC (non-mammalian control) SDC3-def (syndecan-3-deficient EVs), SDC4-def (syndecan-4-deficient EVs), GPC1-def (glypican-1-deficient EVs), GPC6-def (glypican-6-deficient EVs), BGLY-def (betaglycan-deficient EVs).

D

pg/mL	ABL1 standard curve mean absorbance (337/615 A)	ABL1 absorbance (337/615 A)
1600	2.4275	8 μ g
800	1.8955	4 μ g
400	1.3495	2 μ g
200	0.8595	1 μ g
100	0.654	0 μ g
50	0.5505	
25	0.464	
0	0.46	

Appendix 4.5. (D) Standard curve for ABL1 ELISA ELISA and absorbance readout detected for DU145 EVs on 8 μ g, 4 μ g, 2 μ g and 1 μ g per 100 μ L/well.

E

pg/mL	ABL1 standard curve mean absorbance (337/615 A)
1600	2.4275
800	1.8955
400	1.3495
200	0.8595
100	0.654
50	0.5505
25	0.464
0	0.46

	ABL1 absorbance (337/615 A)
NMC	0.374
SDC3-def	0.445
SDC4-def	0.389
GPC1-def	0.415
GPC6-def	0.356
BGLY-def	0.409
Blank	0.365

Appendix 4.5. (E) Standard curve for ABL1 ELISA and absorbance readout detected for 4 µg of HSPG-deficient EVs.

F

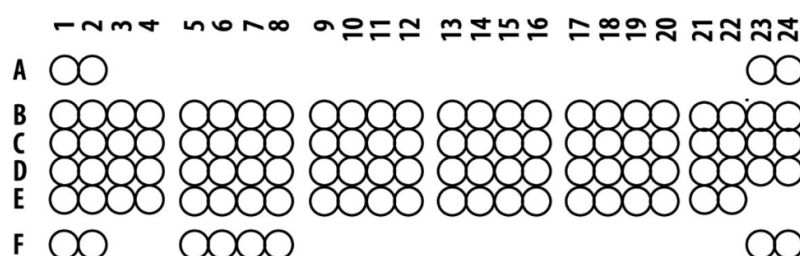
pg/mL	ABL1 standard curve mean absorbance (337/615 A)
1600	2.4275
800	1.8955
400	1.3495
200	0.8595
100	0.654
50	0.5505
25	0.464
0	0.46

	ABL1 absorbance (337/615 A)
No enzyme	0.374
Inactive HEP III	0.445
Active HEP III	0.389
Blank	0.365

Appendix 4.5. (F) Standard curve for ABL1 ELISA and absorbance readout detected for 4 µg of HEP III treated and untreated EV conditions.

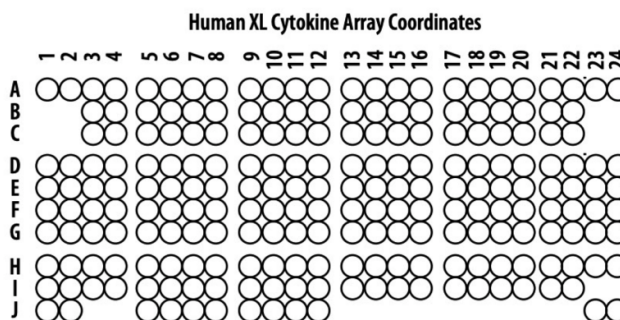
Chapter 5. APPENDIX

Human Phospho-RTK Array Coordinates



A1, A2	Reference spots	C9, C10	PDGF R β	D21, D22	EphA3
A23, A24	Reference spots	C11, C12	SCF R/c-kit	D23, D24	EphA4
B1, B2	EGF R	C13, C14	Flt-3/Flk-2	E1, E2	EphA6
B3, B4	ErbB2	C15, C16	M-CSF R	E3, E4	EphA7
B5, B6	ErbB3	C17, C18	c-Ret	E5, E6	EphB1
B7, B8	ErbB4	C19, C20	ROR1	E7, E8	EphB2
B9, B10	FGF R1	C21, C22	ROR2	E9, E10	EphB4
B11, B12	FGF R2 α	C23, C24	Tie-1	E11, E12	EphB6
B13, B14	FGF R3	D1, D2	Tie-2	E13, E14	ALK/CD246
B15, B16	FGF R4	D3, D4	TrkA	E15, E16	DDR
B17, B18	Insulin R D	D5, D6	TrkB	E17, E18	DDR2
B19, B20	IGF-I R	D7, D8	TrkC	E19, E20	EphA5
B21, B22	Axl	D9, D10	VEGF R1/Flt-1	E21, E22	EphA10
B23, B24	Dtk	D11, D12	VEGF R2/KDR	F1, F2	Reference spots
C1, C2	Mer	D13, D14	VEGF R3/Flt-4	F5, F6	EphB3
C3, C4	HGF R/c-MET	D15, D16	MuSK	F7, F8	RYK
C5, C6	MSP R/Ron	D17, D18	EphA1	F23, F24	Control (-)
C7, C8	PDGF R α	D19, D20	EphA2		

Appendix 5.1. Coordinates identifying the target-proteins represented by each pair of dots on the Human Phospho-RTK profiler array.



A1, A2	Reference spots	C15, C16	Flt-3 Ligand	F1, F2	IL-19	H9, H10	Pentraxin 3
A3, A4	Adiponectin	C17, C18	G-CSF	F3, F4	IL-22	H11, H12 P	PF4
A5, A6	Apolipoprotein A-I	C19, C20	GDF-15	F5, F6	IL-23	H13, H14	RAGE
A7, A8	Angiogenin	C21, C22	GM-CSF	F7, F8	IL-24	H15, H16	RANTES/CCL5
A9, A10	Angiopoietin-1	D1, D2	GRO α	F9, F10	IL-27	H17, H18	RBP-4
A11, A12	Angiopoietin-2	D3, D4	Growth Hormone	F11, F12	IL-31	H19, H20	Relaxin-2
A13, A14	BAFF	D5, D6	HGF	F13, F14	IL-32	H21, H22	Resistin
A15, A16	BDNF	D7, D8	ICAM-1	F15, F16	IL-33	H23, H24	SDF-1 α /CXCL12
A17, A18	Complement Component C5/C5a	D9, D10	IFN- γ	F17, F18	IL-34	I1, I2	Serpin E1
A19, A20	CD14	D11, D12	IGFBP-2	F19, F20	IP-10	I3, I4	SHBG
A21, A22	CD30	D13, D14	IGFBP-3 3	F21, F22	I-TAC	I5, I6	ST2
A23, A24	Reference Spots	D15, D16	IL-1 α	F23, F24	Kallikrein 3/PSA	I7, I8	TARC
B3, B4	CD40 ligand	D17, D18	IL-1 β	G1, G2	Leptin	I9, I10	TFF3
B5, B6	Chitinase 3-like 1	D19, D20	IL-1ra	G3, G4	LIF	I11, I12	TfR
B7, B8	Complement Factor D	D21, D22	IL-2	G5, G6	Lipocalin-2	I13, I14	TGF- α
B9, B10	C-Reactive Protein	D23, D24	IL-3	G7, G8	MCP-1	I15, I16	Thrombospondin-1
B11, B12	Cripto-1	E1, E2	IL-4	G9, G10	MCP-3	I17, I18	TNF- α
B13, B14	Cystatin C	E3, E4	IL-5	G11, G12	M-CSF	I19, I20	uPAR
B15, B16	Dkk-1	E5, E6	IL-6	G13, G14	MIF	I21, I22	VEGF
B17, B18	DPPIV	E7, E8	IL-8	G15, G16	MIG	J1, J2 R	Reference Spots
B19, B20	EGF	E9, E10	IL-10	G17, G18	MIP-1 α /MIP-1 β	J5, J6	Vitamin D BP
B21, B22	Emmprin	E11, E12	IL-11	G19, G20	MIP-3 α	J7, J8	CD31/PECAM
C3, C4	ENA-78	E13, E14	IL-12 p70	G21, G22	MIP-3 β	J9, J10	TIM-3
C5, C6	Endoglin	E15, E16	IL-13	G23, G24	MMP-9	J11, J12	VCAM-1
C7, C8	Fas Ligand	E17, E18	IL-15	H1, H2	Myeloperoxidase	J23, J24	Control (-)
C9, C10	FGF basic	E19, E20	IL-16	H3, H4	Osteopontin		
C11, C12	FGF-7	E21, E22	IL-17A	H5, H6	PDGF-AA		
C13, C14	FGF-19	E23, E24	IL-18 Bpa	H7, H8 P	PDGF-AB/BB		

Appendix 5.2. Coordinates identifying the target-proteins represented by each pair of dots on the Human XL cytokine profiler array.

Appendices

pg/mL	HGF standard curve mean absorbance (337/615 A)
8000	93897.5
4000	48261
2000	24526.5
1000	12921
500	7231
250	4253
125	2739.5
0	428.5

R²=0.9999

	Mean absorbance (337/615 A)
No enzyme	849
Inactive HEP111	812
Active HEP111	913.3
Blank	828.3

Appendix 5.3. Standard curve for HGF ELISA and absorbance readout detected for 4 µg of no enzyme, heat-inactivated HEP111 and active HEP111 treated EV conditions.

A

pg/mL	IL-1α standard curve mean absorbance (337/615 A)
250	30014.5
125	16253.5
62.5	8645
31.3	4624.5
15.6	2769
7.8	1771
0	628.5

R²=0.9999

	Mean absorbance (337/615 A)
Untreated	598
sTGF-β1	589
No enzyme	624
Inactive HEP111	673
Active HEP111	573
PBS	623

B

pg/mL	IL-17A standard curve mean absorbance (337/615 A)
125	6753.5
62.5	3980.5
31.3	2331
15.6	1570
7.8	1126
3.9	870.5
0	574

	Mean absorbance (337/615 A)
Untreated	628.3
sTGF-β1	604.3
No enzyme	527.3
Inactive HEP111	504.6
Active HEP111	551
PBS	615.6

Appendix 5.4. Standard curve for IL-1α (A) and IL-17A (B) ELISA and absorbance readout detected from assayed conditioned media of fibroblasts stimulated for 72 hours with media only (untreated), no enzyme, heat-inactivated HEP111 and active HEP111 treated EV conditions.

References

References

- ACERBI, I., CASSEREAU, L., DEAN, I., SHI, Q., AU, A., PARK, C., CHEN, Y. Y., LIPHARDT, J., HWANG, E. S. & WEAVER, V. M. 2015. Human breast cancer invasion and aggression correlates with ECM stiffening and immune cell infiltration. *Integrative Biology*, 7, 1120-1134.
- ADACHI, E., SAKAI, K., NISHIUCHI, T., IMAMURA, R., SATO, H. & MATSUMOTO, K. 2016. Different growth and metastatic phenotypes associated with a cell-intrinsic change of Met in metastatic melanoma. *Oncotarget*, 7, 70779-70793.
- AI, X., DO, A. T., LOZYNSKA, O., KUSCHE-GULLBERG, M., LINDAHL, U. & EMERSON, C. P., JR. 2003. QSulf1 remodels the 6-O sulfation states of cell surface heparan sulfate proteoglycans to promote Wnt signaling. *J Cell Biol*, 162, 341-51.
- AL-NEDAWI, K., MEEHAN, B., KERBEL, R. S., ALLISON, A. C. & RAK, J. 2009. Endothelial expression of autocrine VEGF upon the uptake of tumor-derived microvesicles containing oncogenic EGFR. *Proceedings of the National Academy of Sciences*, 106, 3794-3799.
- AL-NEDAWI, K., MEEHAN, B., MICALLEF, J., LHOTAK, V., MAY, L., GUHA, A. & RAK, J. 2008. Intercellular transfer of the oncogenic receptor EGFRvIII by microvesicles derived from tumour cells. *Nature Cell Biology*, 10, 619-624.
- ALDO, P. B., CRAVEIRO, V., GULLER, S. & MOR, G. 2013. Effect of culture conditions on the phenotype of THP-1 monocyte cell line. *American journal of reproductive immunology (New York, N.Y. : 1989)*, 70, 80-86.
- ALLAVENA, P., PIEMONTE, L., LONGONI, D., BERNASCONI, S., STOPPACCIARO, A., RUCO, L. & MANTOVANI, A. 1998. IL-10 prevents the differentiation of monocytes to dendritic cells but promotes their maturation to macrophages. *European Journal of Immunology*, 28, 359-369.
- ANDRÉ, F., SCHARTZ, N. E. C., MOVASSAGH, M., FLAMENT, C., PAUTIER, P., MORICE, P., POMEL, C., LHOMME, C., ESCUDIER, B., LE CHEVALIER, T., TURSZ, T., AMIGORENA, S., RAPOSO, G., ANGEVIN, E. & ZITVOGEL, L. 2002. Malignant effusions and immunogenic tumour-derived exosomes. *The Lancet*, 360, 295-305.
- ANDREOLA, G., RIVOLTINI, L., CASTELLI, C., HUBER, V., PEREGO, P., DEHO, P., SQUARCINA, P., ACCORNERO, P., LOZUPONE, F., LUGINI, L., STRINGARO, A., MOLINARI, A., ARANCIA, G., GENTILE, M., PARMIANI, G. & FAIS, S. 2002. Induction of Lymphocyte Apoptosis by Tumor Cell Secretion of FasL-bearing Microvesicles. *Journal of Experimental Medicine*, 195, 1303-1316.
- ANNAVAL, T., WILD, R., CRÉTINON, Y., SADIR, R., VIVÈS, R. R. & LORTAT-JACOB, H. 2020. Heparan Sulfate Proteoglycans Biosynthesis and Post Synthesis Mechanisms Combine Few Enzymes and Few Core Proteins to Generate Extensive Structural and Functional Diversity. *Molecules (Basel, Switzerland)*, 25, 4215.
- ARRAUD, N., LINARES, R., TAN, S., GOUNOU, C., PASQUET, J.-M., MORNET, S. & BRISSON, A. R. 2014. Extracellular vesicles from blood plasma: determination of their morphology, size, phenotype and concentration. *Journal of Thrombosis and Haemostasis*, 12, 614-627.
- ASSARSSON, E., LUNDBERG, M., HOLMQUIST, G., BJÖRKESTEN, J., BUCHT THORSEN, S., EKMAN, D., ERIKSSON, A., RENNEL DICKENS, E., OHLSSON, S., EDFELDT, G., ANDERSSON, A.-C., LINDSTEDT, P., STENVANG, J., GULLBERG, M. & FREDRIKSSON, S. 2014. Homogenous 96-Plex PEA Immunoassay Exhibiting High Sensitivity, Specificity, and Excellent Scalability. *PLOS ONE*, 9, e95192.

References

- ATAI, N. A., BALAJ, L., VAN VEEN, H., BREAKEFIELD, X. O., JARZYNA, P. A., VAN NOORDEN, C. J. F., SKOG, J. & MAGUIRE, C. A. 2013. Heparin blocks transfer of extracellular vesicles between donor and recipient cells. *Journal of neuro-oncology*, 115, 343-351.
- BAGHBAN, R., ROSHANGAR, L., JAHANBAN-ESFAHLAN, R., SEIDI, K., EBRAHIMI-KALAN, A., JAYMAND, M., KOLAHIAN, S., JAVAHERI, T. & ZARE, P. 2020. Tumor microenvironment complexity and therapeutic implications at a glance. *Cell Communication and Signaling*, 18, 59.
- BAIETTI, M. F., ZHANG, Z., MORTIER, E., MELCHIOR, A., DEGEEST, G., GEERAERTS, A., IVARSSON, Y., DEPOORTERE, F., COOMANS, C., VERMEIREN, E., ZIMMERMANN, P. & DAVID, G. 2012. Syndecan–syntenin–ALIX regulates the biogenesis of exosomes. *Nature Cell Biology*, 14, 677.
- BALKWILL, F. R., CAPASSO, M. & HAGEMANN, T. 2012. The tumor microenvironment at a glance. *Journal of Cell Science*, 125, 5591-5596.
- BANDARI, S. K., PURUSHOTHAMAN, A., RAMANI, V. C., BRINKLEY, G. J., CHANDRASHEKAR, D. S., VARAMBALLY, S., MOBLEY, J. A., ZHANG, Y., BROWN, E. E., VLODAVSKY, I. & SANDERSON, R. D. 2018. Chemotherapy induces secretion of exosomes loaded with heparanase that degrades extracellular matrix and impacts tumor and host cell behavior. *Matrix Biology*, 65, 104-118.
- BEAUVAIS, D. M. & RAPRAEGER, A. C. 2003. Syndecan-1-mediated cell spreading requires signaling by alpha v beta 3 integrins in human breast carcinoma cells. *Exp Cell Res*, 286, 219-32.
- BEBELMAN, M. P., SMIT, M. J., PEGTEL, D. M. & BAGLIO, S. R. 2018. Biogenesis and function of extracellular vesicles in cancer. *Pharmacology & Therapeutics*, 188, 1-11.
- BEIDER, K., ABRAHAM, M., BEGIN, M., WALD, H., WEISS, I. D., WALD, O., PIKARSKY, E., ABRAMOVITCH, R., ZEIRA, E., GALUN, E., NAGLER, A. & PELED, A. 2009. Interaction between CXCR4 and CCL20 pathways regulates tumor growth. *PLoS one*, 4, e5125-e5125.
- BELTING, M. 2003. Heparan sulfate proteoglycan as a plasma membrane carrier. *Trends in Biochemical Sciences*, 28, 145-151.
- BERGAMASCHI, A., TAGLIABUE, E., SØRLIE, T., NAUME, B., TRIULZI, T., ORLANDI, R., RUSSNES, H. G., NESLAND, J. M., TAMMI, R., AUVINEN, P., KOSMA, V. M., MÉNARD, S. & BØRRESEN-DALE, A. L. 2008. Extracellular matrix signature identifies breast cancer subgroups with different clinical outcome. *J Pathol*, 214, 357-67.
- BERGERS, G., BREKKEN, R., MCMAHON, G., VU, T. H., ITOH, T., TAMAKI, K., TANZAWA, K., THORPE, P., ITOHARA, S., WERB, Z. & HANAHAN, D. 2000. Matrix metalloproteinase-9 triggers the angiogenic switch during carcinogenesis. *Nat Cell Biol*, 2, 737-44.
- BISHOP, J. R., SCHUKSZ, M. & ESKO, J. D. 2007. Heparan sulphate proteoglycans fine-tune mammalian physiology. *Nature*, 446, 1030-7.
- BLANCHARD, N., LANKAR, D., FAURE, F., REGNAULT, A., DUMONT, C., RAPOSO, G. & HIVROZ, C. 2002. TCR Activation of Human T Cells Induces the Production of Exosomes Bearing the TCR/CD3/ζ Complex. *The Journal of Immunology*, 168, 3235.

- BOOTCOV, M. R., BAUSKIN, A. R., VALENZUELA, S. M., MOORE, A. G., BANSAL, M., HE, X. Y., ZHANG, H. P., DONNELLAN, M., MAHLER, S., PRYOR, K., WALSH, B. J., NICHOLSON, R. C., FAIRLIE, W. D., POR, S. B., ROBBINS, J. M. & BREIT, S. N. 1997. MIC-1, a novel macrophage inhibitory cytokine, is a divergent member of the TGF-beta superfamily. *Proceedings of the National Academy of Sciences of the United States of America*, 94, 11514-11519.
- BOOTH, A. M., FANG, Y., FALLON, J. K., YANG, J. M., HILDRETH, J. E. & GOULD, S. J. 2006. Exosomes and HIV Gag bud from endosome-like domains of the T cell plasma membrane. *J Cell Biol*, 172, 923-35.
- BOSSHART, H. & HEINZELMANN, M. 2004. Lipopolysaccharide-mediated cell activation without rapid mobilization of cytosolic free calcium. *Molecular Immunology*, 41, 1023-1028.
- BRENNAN, K., MARTIN, K., FITZGERALD, S. P., O'SULLIVAN, J., WU, Y., BLANCO, A., RICHARDSON, C. & MC GEE, M. M. 2020. A comparison of methods for the isolation and separation of extracellular vesicles from protein and lipid particles in human serum. *Scientific Reports*, 10, 1039.
- BRISSON, A. R., TAN, S., LINARES, R., GOUNOU, C. & ARRAUD, N. 2017. Extracellular vesicles from activated platelets: a semiquantitative cryo-electron microscopy and immuno-gold labeling study. *Platelets*, 28, 263-271.
- BROWN, L. F., GUIDI, A. J., SCHNITT, S. J., VAN DE WATER, L., IRUELA-ARISPE, M. L., YEO, T. K., TOGNAZZI, K. & DVORAK, H. F. 1999. Vascular stroma formation in carcinoma in situ, invasive carcinoma, and metastatic carcinoma of the breast. *Clin Cancer Res*, 5, 1041-56.
- BUSATTO, S., VILANILAM, G., TICER, T., LIN, W.-L., DICKSON, D. W., SHAPIRO, S., BERGESE, P. & WOLFRAM, J. 2018. Tangential Flow Filtration for Highly Efficient Concentration of Extracellular Vesicles from Large Volumes of Fluid. *Cells*, 7.
- BUSCHMANN, D., KIRCHNER, B., HERMANN, S., MÄRTE, M., WURMSER, C., BRANDES, F., KOTSCHOTE, S., BONIN, M., STEINLEIN, O. K., PFAFFL, M. W., SCHELLING, G. & REITHMAIR, M. 2018. Evaluation of serum extracellular vesicle isolation methods for profiling miRNAs by next-generation sequencing. *Journal of Extracellular Vesicles*, 7, 1481321.
- BUZÁS, E. I., TÓTH, E. Á., SÓDAR, B. W. & SZABÓ-TAYLOR, K. É. 2018. Molecular interactions at the surface of extracellular vesicles. *Seminars in Immunopathology*, 40, 453-464.
- CAMPOS-SILVA, C., SUÁREZ, H., JARA-ACEVEDO, R., LINARES-ESPINÓS, E., MARTINEZ-PIÑEIRO, L., YÁÑEZ-MÓ, M. & VALÉS-GÓMEZ, M. 2019. High sensitivity detection of extracellular vesicles immune-captured from urine by conventional flow cytometry. *Scientific Reports*, 9, 2042.
- CAPURRO, M. I., XIANG, Y. Y., LOBE, C. & FILMUS, J. 2005. Glypican-3 promotes the growth of hepatocellular carcinoma by stimulating canonical Wnt signaling. *Cancer Res*, 65, 6245-54.
- CECCARELLI, S., VISCO, V., RAFFA, S., WAKISAKA, N., PAGANO, J. S. & TORRISI, M. R. 2007. Epstein-Barr virus latent membrane protein 1 promotes concentration in multivesicular bodies of fibroblast growth factor 2 and its release through exosomes. *International Journal of Cancer*, 121, 1494-1506.

References

- CEREZO-MAGAÑA, M., BÅNG-RUDENSTAM, A. & BELTING, M. 2020. The pleiotropic role of proteoglycans in extracellular vesicle mediated communication in the tumor microenvironment. *Seminars in Cancer Biology*, 62, 99-107.
- CEREZO-MAGAÑA, M., CHRISTIANSON, H. C., VAN KUPPEVELT, T. H., FORSBERG-NILSSON, K. & BELTING, M. 2021. Hypoxic Induction of Exosome Uptake through Proteoglycan-Dependent Endocytosis Fuels the Lipid Droplet Phenotype in Glioma. *Mol Cancer Res*, 19, 528-540.
- CHARGAFF, E. & WEST, R. 1946. The biological significance of the thromboplastic protein of blood. *The Journal of biological chemistry*, 166, 189-197.
- CHEN, C., ZONG, S., WANG, Z., LU, J., ZHU, D., ZHANG, Y., ZHANG, R. & CUI, Y. 2018a. Visualization and intracellular dynamic tracking of exosomes and exosomal miRNAs using single molecule localization microscopy. *Nanoscale*, 10, 5154-5162.
- CHEN, G., HUANG, A. C., ZHANG, W., ZHANG, G., WU, M., XU, W., YU, Z., YANG, J., WANG, B., SUN, H., XIA, H., MAN, Q., ZHONG, W., ANTELO, L. F., WU, B., XIONG, X., LIU, X., GUAN, L., LI, T., LIU, S., YANG, R., LU, Y., DONG, L., MCGETTIGAN, S., SOMASUNDARAM, R., RADHAKRISHNAN, R., MILLS, G., LU, Y., KIM, J., CHEN, Y. H., DONG, H., ZHAO, Y., KARAKOUSIS, G. C., MITCHELL, T. C., SCHUCHTER, L. M., HERLYN, M., WHERRY, E. J., XU, X. & GUO, W. 2018b. Exosomal PD-L1 contributes to immunosuppression and is associated with anti-PD-1 response. *Nature*, 560, 382-386.
- CHEN, N., CHEN, C. C. & LAU, L. F. 2000. Adhesion of human skin fibroblasts to Cyr61 is mediated through integrin alpha 6beta 1 and cell surface heparan sulfate proteoglycans. *J Biol Chem*, 275, 24953-61.
- CHEN, W.-X., LIU, X.-M., LV, M.-M., CHEN, L., ZHAO, J.-H., ZHONG, S.-L., JI, M.-H., HU, Q., LUO, Z., WU, J.-Z. & TANG, J.-H. 2014. Exosomes from Drug-Resistant Breast Cancer Cells Transmit Chemoresistance by a Horizontal Transfer of MicroRNAs. *PLOS ONE*, 9, e95240.
- CHEN, X., ZHOU, J., LI, X., WANG, X., LIN, Y. & WANG, X. 2018c. Exosomes derived from hypoxic epithelial ovarian cancer cells deliver microRNAs to macrophages and elicit a tumor-promoted phenotype. *Cancer Lett*, 435, 80-91.
- CHEN, Y., SONG, Y., DU, W., GONG, L., CHANG, H. & ZOU, Z. 2019. Tumor-associated macrophages: an accomplice in solid tumor progression. *Journal of Biomedical Science*, 26, 78.
- CHERNOUSOV, M. A. & CAREY, D. J. 1993. N-syndecan (syndecan 3) from neonatal rat brain binds basic fibroblast growth factor. *J Biol Chem*, 268, 16810-4.
- CHOW, A., ZHOU, W., LIU, L., FONG, M. Y., CHAMPER, J., VAN HAUTE, D., CHIN, A. R., REN, X., GUGIU, B. G., MENG, Z., HUANG, W., NGO, V., KORTYLEWSKI, M. & WANG, S. E. 2014. Macrophage immunomodulation by breast cancer-derived exosomes requires Toll-like receptor 2-mediated activation of NF-κB. *Scientific reports*, 4, 5750-5750.
- CHOWDHURY, R., WEBBER, J. P., GURNEY, M., MASON, M. D., TABI, Z. & CLAYTON, A. 2015. Cancer exosomes trigger mesenchymal stem cell differentiation into pro-angiogenic and pro-invasive myofibroblasts. *Oncotarget*, 6, 715-31.
- CHRISTIANSON, H. C. & BELTING, M. 2014. Heparan sulfate proteoglycan as a cell-surface endocytosis receptor. *Matrix Biology*, 35, 51-55.

- CHRISTIANSON, H. C., SVENSSON, K. J., VAN KUPPEVELT, T. H., LI, J.-P. & BELTING, M. 2013. Cancer cell exosomes depend on cell-surface heparan sulfate proteoglycans for their internalization and functional activity. *Proceedings of the National Academy of Sciences*, 110, 17380-17385.
- CHUNG, J.-S., BONKOBARA, M., TOMIHARI, M., CRUZ, P. D., JR. & ARIIZUMI, K. 2009. The DC-HIL/syndecan-4 pathway inhibits human allogeneic T-cell responses. *European journal of immunology*, 39, 965-974.
- CHUNG, J.-S., DOUGHERTY, I., CRUZ, P. D. & ARIIZUMI, K. 2007. Syndecan-4 Mediates the Coinhibitory Function of DC-HIL on T Cell Activation. *The Journal of Immunology*, 179, 5778-5784.
- CHUNG, J.-S., TAMURA, K., CRUZ, P. D., JR. & ARIIZUMI, K. 2014. DC-HIL-expressing myelomonocytic cells are critical promoters of melanoma growth. *The Journal of investigative dermatology*, 134, 2784-2794.
- CLAYTON, A., AL-TAEI, S., WEBBER, J., MASON, M. D. & TABI, Z. 2011. Cancer exosomes express CD39 and CD73, which Suppress T cells through adenosine production. *The Journal of Immunology*, 187, 676.
- CLAYTON, A., COURT, J., NAVABI, H., ADAMS, M., MASON, M. D., HOBOT, J. A., NEWMAN, G. R. & JASANI, B. 2001. Analysis of antigen presenting cell derived exosomes, based on immuno-magnetic isolation and flow cytometry. *Journal of Immunological Methods*, 247, 163-174.
- CLAYTON, A., MITCHELL, J. P., COURT, J., LINNANE, S., MASON, M. D. & TABI, Z. 2008a. Human tumor-derived exosomes down-modulate NKG2D expression. *J Immunol*, 180, 7249-58.
- CLAYTON, A., MITCHELL, J. P., COURT, J., LINNANE, S., MASON, M. D. & TABI, Z. 2008b. Human Tumor-Derived Exosomes Down-Modulate NKG2D Expression. *The Journal of Immunology*, 180, 7249.
- CLAYTON, A., MITCHELL, J. P., COURT, J., MASON, M. D. & TABI, Z. 2007. Human tumor-derived exosomes selectively impair lymphocyte responses to interleukin-2. *Cancer Res*, 67, 7458-66.
- CLAYTON, A. & TABI, Z. 2005. Exosomes and the MICA-NKG2D system in cancer. *Blood Cells, Molecules, and Diseases*, 34, 206-213.
- CLAYTON, A., TURKES, A., DEWITT, S., STEADMAN, R., MASON, M. D. & HALLETT, M. B. 2004. Adhesion and signaling by B cell-derived exosomes: the role of integrins. *The FASEB Journal*, 18, 977-979.
- CLOS-GARCIA, M., LOIZAGA-IRIARTE, A., ZUÑIGA-GARCIA, P., SÁNCHEZ-MOSQUERA, P., ROSA CORTAZAR, A., GONZÁLEZ, E., TORRANO, V., ALONSO, C., PÉREZ-CORMENZANA, M., UGALDE-OLANO, A., LACASA-VISCASILLAS, I., CASTRO, A., ROYO, F., UNDA, M., CARRACEDO, A. & FALCÓN-PÉREZ, J. M. 2018. Metabolic alterations in urine extracellular vesicles are associated to prostate cancer pathogenesis and progression. *J Extracell Vesicles*, 7, 1470442.
- COCKS, A. 2019. *Fibroblast uptake of prostate cancer vesicles*. . Cardiff University.
- COHEN, N., SHANI, O., RAZ, Y., SHARON, Y., HOFFMAN, D., ABRAMOVITZ, L. & EREZ, N. 2017. Fibroblasts drive an immunosuppressive and growth-promoting microenvironment in breast cancer via secretion of Chitinase 3-like 1. *Oncogene*, 36, 4457-4468.
- COLICELLI, J. 2010. ABL tyrosine kinases: evolution of function, regulation, and specificity. *Science signaling*, 3, re6-re6.

References

- COMITO, G., GIANNONI, E., SEGURA, C. P., BARCELLOS-DE-SOUZA, P., RASPOLINI, M. R., BARONI, G., LANCIOTTI, M., SERNI, S. & CHIARUGI, P. 2014. Cancer-associated fibroblasts and M2-polarized macrophages synergize during prostate carcinoma progression. *Oncogene*, 33, 2423-2431.
- CONDE-VANCELLS, J., RODRIGUEZ-SUAREZ, E., EMBADE, N., GIL, D., MATTHIESEN, R., VALLE, M., ELORTZA, F., LU, S. C., MATO, J. M. & FALCON-PEREZ, J. M. 2008. Characterization and comprehensive proteome profiling of exosomes secreted by hepatocytes. *J Proteome Res*, 7, 5157-66.
- COOPER, D. N. & BARONDES, S. H. 1990. Evidence for export of a muscle lectin from cytosol to extracellular matrix and for a novel secretory mechanism. *J Cell Biol*, 110, 1681-91.
- CORCORAN, C., RANI, S., O'BRIEN, K., O'NEILL, A., PRENCIPE, M., SHEIKH, R., WEBB, G., MCDERMOTT, R., WATSON, W., CROWN, J. & O'DRISCOLL, L. 2012. Docetaxel-resistance in prostate cancer: evaluating associated phenotypic changes and potential for resistance transfer via exosomes. *PLoS one*, 7, e50999-e50999.
- COSSETTI, C., IRACI, N., MERCER, T. R., LEONARDI, T., ALPI, E., DRAGO, D., ALFARO-CERVELLO, C., SAINI, H. K., DAVIS, M. P., SCHAEFFER, J., VEGA, B., STEFANINI, M., ZHAO, C., MULLER, W., GARCIA-VERDUGO, J. M., MATHIVANAN, S., BACHI, A., ENRIGHT, A. J., MATTICK, J. S. & PLUCHINO, S. 2014. Extracellular vesicles from neural stem cells transfer IFN- γ via Ifngr1 to activate Stat1 signaling in target cells. *Molecular cell*, 56, 193-204.
- COSTA-SILVA, B., AIELLO, N. M., OCEAN, A. J., SINGH, S., ZHANG, H., THAKUR, B. K., BECKER, A., HOSHINO, A., MARK, M. T., MOLINA, H., XIANG, J., ZHANG, T., THEILEN, T.-M., GARCÍA-SANTOS, G., WILLIAMS, C., ARARSO, Y., HUANG, Y., RODRIGUES, G., SHEN, T.-L., LABORI, K. J., LOTHE, I. M. B., KURE, E. H., HERNANDEZ, J., DOUSSOT, A., EBBESEN, S. H., GRANDGENETT, P. M., HOLLINGSWORTH, M. A., JAIN, M., MALLYA, K., BATRA, S. K., JARNAGIN, W. R., SCHWARTZ, R. E., MATEI, I., PEINADO, H., STANGER, B. Z., BROMBERG, J. & LYDEN, D. 2015. Pancreatic cancer exosomes initiate pre-metastatic niche formation in the liver. *Nature cell biology*, 17, 816-826.
- CVJETKOVIC, A., LÖTVALL, J. & LÄSSER, C. 2014. The influence of rotor type and centrifugation time on the yield and purity of extracellular vesicles. *J Extracell Vesicles*, 3.
- DAIGNEAULT, M., PRESTON, J. A., MARRIOTT, H. M., WHYTE, M. K. B. & DOCKRELL, D. H. 2010. The Identification of Markers of Macrophage Differentiation in PMA-Stimulated THP-1 Cells and Monocyte-Derived Macrophages. *PLOS ONE*, 5, e8668.
- DE PALMA, M., BIZIATO, D. & PETROVA, T. V. 2017. Microenvironmental regulation of tumour angiogenesis. *Nature Reviews Cancer*, 17, 457-474.
- DEEPA, S. S., YAMADA, S., ZAKO, M., GOLDBERGER, O. & SUGAHARA, K. 2004. Chondroitin Sulfate Chains on Syndecan-1 and Syndecan-4 from Normal Murine Mammary Gland Epithelial Cells Are Structurally and Functionally Distinct and Cooperate with Heparan Sulfate Chains to Bind Growth Factors: A NOVEL FUNCTION TO CONTROL BINDING OF MIDKINE, PLEIOTROPHIN, AND BASIC FIBROBLAST GROWTH FACTOR*. *Journal of Biological Chemistry*, 279, 37368-37376.

- DEL CONDE, I., SHRIMPTON, C. N., THIAGARAJAN, P. & LÓPEZ, J. A. 2005. Tissue-factor-bearing microvesicles arise from lipid rafts and fuse with activated platelets to initiate coagulation. *Blood*, 106, 1604-1611.
- DERKSEN, P. W. B., KEEHNEN, R. M. J., EVERS, L. M., VAN OERS, M. H. J., SPAARGAREN, M. & PALS, S. T. 2002. Cell surface proteoglycan syndecan-1 mediates hepatocyte growth factor binding and promotes Met signaling in multiple myeloma. *Blood*, 99, 1405-1410.
- DESMOULIÈRE, A., GEINOZ, A., GABBIANI, F. & GABBIANI, G. 1993. Transforming growth factor-beta 1 induces alpha-smooth muscle actin expression in granulation tissue myofibroblasts and in quiescent and growing cultured fibroblasts. *The Journal of cell biology*, 122, 103-111.
- DESMOULIÈRE, A., REDARD, M., DARBY, I. & GABBIANI, G. 1995. Apoptosis mediates the decrease in cellularity during the transition between granulation tissue and scar. *Am J Pathol*, 146, 56-66.
- DING, K., LOPEZ-BURKS, M., SÁNCHEZ-DURAN, J. A., KORC, M. & LANDER, A. D. 2005. Growth factor-induced shedding of syndecan-1 confers glypican-1 dependence on mitogenic responses of cancer cells. *The Journal of cell biology*, 171, 729-738.
- DONG, J., GRUNSTEIN, J., TEJADA, M., PEALE, F., FRANTZ, G., LIANG, W.-C., BAI, W., YU, L., KOWALSKI, J., LIANG, X., FUH, G., GERBER, H.-P. & FERRARA, N. 2004. VEGF-null cells require PDGFR alpha signaling-mediated stromal fibroblast recruitment for tumorigenesis. *The EMBO journal*, 23, 2800-2810.
- DU, R., LU, K. V., PETRITSCH, C., LIU, P., GANSS, R., PASSEGUÉ, E., SONG, H., VANDENBERG, S., JOHNSON, R. S., WERB, Z. & BERGERS, G. 2008. HIF1alpha induces the recruitment of bone marrow-derived vascular modulatory cells to regulate tumor angiogenesis and invasion. *Cancer Cell*, 13, 206-20.
- DUCHESNE, L., OCTEAU, V., BEARON, R. N., BECKETT, A., PRIOR, I. A., LOUNIS, B. & FERNIG, D. G. 2012. Transport of fibroblast growth factor 2 in the pericellular matrix is controlled by the spatial distribution of its binding sites in heparan sulfate. *PLoS Biol*, 10, e1001361.
- DVORAK, H. F. 1986. Tumors: Wounds That Do Not Heal. *New England Journal of Medicine*, 315, 1650-1659.
- DVORAK, H. F., NAGY, J. A., BERSE, B., BROWN, L. F., YEO, K. T., YEO, T. K., DVORAK, A. M., VAN DE WATER, L., SIOUSSAT, T. M. & SENGER, D. R. 1992. Vascular permeability factor, fibrin, and the pathogenesis of tumor stroma formation. *Ann N Y Acad Sci*, 667, 101-11.
- EMRE, Y. & IMHOF, B. A. 2014. Matricellular protein CCN1/CYR61: a new player in inflammation and leukocyte trafficking. *Seminars in Immunopathology*, 36, 253-259.
- ESCREVENTE, C., KELLER, S., ALTEVOGT, P. & COSTA, J. 2011. Interaction and uptake of exosomes by ovarian cancer cells. *BMC Cancer*, 11, 108.
- EVANS, L., MILWARD, K., ATTANOOS, R., CLAYTON, A., ERRINGTON, R. & TABI, Z. 2021. Macrophage Plasticity and Function in the Lung Tumour Microenvironment Revealed in 3D Heterotypic Spheroid and Explant Models. *Biomedicines*, 9, 302.
- FABBRI, M., PAONE, A., CALORE, F., GALLI, R., GAUDIO, E., SANTHANAM, R., LOVAT, F., FADDA, P., MAO, C., NUOVO, G. J., ZANESI, N., CRAWFORD, M., OZER, G. H., WERNICKE, D., ALDER, H., CALIGIURI, M. A., NANA-SINKAM, P., PERROTTI, D. & CROCE, C. M. 2012. MicroRNAs bind to Toll-like receptors to induce

References

- prometastatic inflammatory response. *Proceedings of the National Academy of Sciences*, 109, E2110-E2116.
- FEDELE, C., SINGH, A., ZERLANKO, B. J., IOZZO, R. V. & LANGUINO, L. R. 2015. The $\alpha\beta 6$ integrin is transferred intercellularly via exosomes. *The Journal of biological chemistry*, 290, 4545-4551.
- FELICETTI, F., DE FEO, A., COSCIA, C., PUGLISI, R., PEDINI, F., PASQUINI, L., BELLENGHI, M., ERRICO, M. C., PAGANI, E. & CARÈ, A. 2016. Exosome-mediated transfer of miR-222 is sufficient to increase tumor malignancy in melanoma. *Journal of Translational Medicine*, 14, 56.
- FENG, D., ZHAO, W. L., YE, Y. Y., BAI, X. C., LIU, R. Q., CHANG, L. F., ZHOU, Q. & SUI, S. F. 2010. Cellular internalization of exosomes occurs through phagocytosis. *Traffic*, 11, 675-87.
- FETTELSCHOSS, A., KISTOWSKA, M., LEIBUNDGUT-LANDMANN, S., BEER, H.-D., JOHANSEN, P., SENTI, G., CONTASSOT, E., BACHMANN, M. F., FRENCH, L. E., OXENIUS, A. & KÜNDIG, T. M. 2011. Inflammasome activation and IL-1 β target IL-1 α for secretion as opposed to surface expression. *Proceedings of the National Academy of Sciences of the United States of America*, 108, 18055-18060.
- FIDLER, I. J. 2003. The pathogenesis of cancer metastasis: the 'seed and soil' hypothesis revisited. *Nature Reviews Cancer*, 3, 453-458.
- FILIPPOU, P. S., KARAGIANNIS, G. S. & CONSTANTINIDOU, A. 2020. Midkine (MDK) growth factor: a key player in cancer progression and a promising therapeutic target. *Oncogene*, 39, 2040-2054.
- FILLA, M. S., DAM, P. & RAPRAEGER, A. C. 1998. The cell surface proteoglycan syndecan-1 mediates fibroblast growth factor-2 binding and activity. *J Cell Physiol*, 174, 310-21.
- FITZNER, D., SCHNAARS, M., VAN ROSSUM, D., KRISHNAMOORTHY, G., DIBAJ, P., BAKHTI, M., REGEN, T., HANISCH, U.-K. & SIMONS, M. 2011. Selective transfer of exosomes from oligodendrocytes to microglia by macropinocytosis. *Journal of Cell Science*, 124, 447-458.
- FLIEGER, O., ENGLING, A., BUCALA, R., LUE, H., NICKEL, W. & BERNHAGEN, J. 2003. Regulated secretion of macrophage migration inhibitory factor is mediated by a non-classical pathway involving an ABC transporter. *FEBS Letters*, 551, 78-86.
- FOLKMAN, J. 1971. Tumor Angiogenesis: Therapeutic Implications. *New England Journal of Medicine*, 285, 1182-1186.
- FONG, M. Y., ZHOU, W., LIU, L., ALONTAGA, A. Y., CHANDRA, M., ASHBY, J., CHOW, A., O'CONNOR, S. T. F., LI, S., CHIN, A. R., SOMLO, G., PALOMARES, M., LI, Z., TREMBLAY, J. R., TSUYADA, A., SUN, G., REID, M. A., WU, X., SWIDERSKI, P., REN, X., SHI, Y., KONG, M., ZHONG, W., CHEN, Y. & WANG, S. E. 2015. Breast-cancer-secreted miR-122 reprograms glucose metabolism in premetastatic niche to promote metastasis. *Nature cell biology*, 17, 183-194.
- FORSTEN-WILLIAMS, K., CHUA, C. C. & NUGENT, M. A. 2005. The kinetics of FGF-2 binding to heparan sulfate proteoglycans and MAP kinase signaling. *Journal of Theoretical Biology*, 233, 483-499.
- FRANZEN, C. A., CHEN, C.-C., TODOROVIĆ, V., JURIC, V., MONZON, R. I. & LAU, L. F. 2009. Matrix protein CCN1 is critical for prostate carcinoma cell proliferation and TRAIL-induced apoptosis. *Molecular cancer research : MCR*, 7, 1045-1055.

- FRANZEN, C. A., SIMMS, P. E., VAN HUIS, A. F., FOREMAN, K. E., KUO, P. C. & GUPTA, G. N. 2014. Characterization of uptake and internalization of exosomes by bladder cancer cells. *BioMed research international*, 2014, 619829-619829.
- FUENTES, P., SESÉ, M., GUIJARRO, P. J., EMPERADOR, M., SÁNCHEZ-REDONDO, S., PEINADO, H., HÜMMER, S. & RAMÓN Y CAJAL, S. 2020. ITGB3-mediated uptake of small extracellular vesicles facilitates intercellular communication in breast cancer cells. *Nature Communications*, 11, 4261.
- GABBIANI, G., RYAN, G. B. & MAJNE, G. 1971. Presence of modified fibroblasts in granulation tissue and their possible role in wound contraction. *Experientia*, 27, 549-50.
- GABRUSIEWICZ, K., LI, X., WEI, J., HASHIMOTO, Y., MARISSETTY, A. L., OTT, M., WANG, F., HAWKE, D., YU, J., HEALY, L. M., HOSSAIN, A., AKERS, J. C., MAITI, S. N., YAMASHITA, S., SHIMIZU, Y., DUNNER, K., ZAL, M. A., BURKS, J. K., GUMIN, J., NWAJELI, F., REZAVANIAN, A., ZHOU, S., RAO, G., SAWAYA, R., FULLER, G. N., HUSE, J. T., ANTEL, J. P., LI, S., COOPER, L., SULMAN, E. P., CHEN, C., GEULA, C., KALLURI, R., ZAL, T. & HEIMBERGER, A. B. 2018. Glioblastoma stem cell-derived exosomes induce M2 macrophages and PD-L1 expression on human monocytes. *Oncoimmunology*, 7, e1412909-e1412909.
- GAGGIOLI, C., HOOPER, S., HIDALGO-CARCEDO, C., GROSSE, R., MARSHALL, J. F., HARRINGTON, K. & SAHAI, E. 2007. Fibroblast-led collective invasion of carcinoma cells with differing roles for RhoGTPases in leading and following cells. *Nat Cell Biol*, 9, 1392-400.
- GARDINER, C., FERREIRA, Y. J., DRAGOVIC, R. A., REDMAN, C. W. G. & SARGENT, I. L. 2013. Extracellular vesicle sizing and enumeration by nanoparticle tracking analysis. *Journal of extracellular vesicles*, 2, 10.3402/jev.v2i0.19671.
- GASTPAR, R., GEHRMANN, M., BAUSERO, M. A., ASEA, A., GROSS, C., SCHROEDER, J. A. & MULTHOFF, G. 2005. Heat shock protein 70 surface-positive tumor exosomes stimulate migratory and cytolytic activity of natural killer cells. *Cancer Res*, 65, 5238-47.
- GENIN, M., CLEMENT, F., FATTACCIOLI, A., RAES, M. & MICHIELS, C. 2015. M1 and M2 macrophages derived from THP-1 cells differentially modulate the response of cancer cells to etoposide. *BMC Cancer*, 15, 577.
- GESIERICH, S., BEREZOVSKIY, I., RYSCHICH, E. & ZÖLLER, M. 2006. Systemic Induction of the Angiogenesis Switch by the Tetraspanin D6.1A/CO-029. *Cancer Research*, 66, 7083.
- GHOSSOUB, R., CHÉRY, M., AUDEBERT, S., LEBLANC, R., EGEA-JIMENEZ, A. L., LEMBO, F., MAMMAR, S., LE DEZ, F., CAMOIN, L., BORG, J.-P., RUBINSTEIN, E., DAVID, G. & ZIMMERMANN, P. 2020. Tetraspanin-6 negatively regulates exosome production. *Proceedings of the National Academy of Sciences of the United States of America*, 117, 5913-5922.
- GHOSSOUB, R., LEMBO, F., RUBIO, A., GAILLARD, C. B., BOUCHET, J., VITALE, N., SLAVÍK, J., MACHALA, M. & ZIMMERMANN, P. 2014. Syntenin-ALIX exosome biogenesis and budding into multivesicular bodies are controlled by ARF6 and PLD2. *Nature Communications*, 5, 3477.
- GIUSTI, I., DI FRANCESCO, M., D'ASCENZO, S., PALMERINI, M. G., MACCHIARELLI, G., CARTA, G. & DOLO, V. 2018. Ovarian cancer-derived extracellular vesicles affect normal human fibroblast behavior. *Cancer biology & therapy*, 19, 722-734.

References

- GOODALL, K. J., POON, I. K. H., PHIPPS, S. & HULETT, M. D. 2014. Soluble Heparan Sulfate Fragments Generated by Heparanase Trigger the Release of Pro-Inflammatory Cytokines through TLR-4. *PLOS ONE*, 9, e109596.
- GOULD, S. J. & RAPOSO, G. 2013. As we wait: coping with an imperfect nomenclature for extracellular vesicles. *Journal of extracellular vesicles*, 2, 10.3402/jev.v2i0.20389.
- GRANGE, C., TAPPARO, M., COLLINO, F., VITILLO, L., DAMASCO, C., DEREGIBUS, M. C., TETTA, C., BUSSOLATI, B. & CAMUSSI, G. 2011. Microvesicles Released from Human Renal Cancer Stem Cells Stimulate Angiogenesis and Formation of Lung Premetastatic Niche. *Cancer Research*, 71, 5346.
- GREUBER, E. K., SMITH-PEARSON, P., WANG, J. & PENDERGAST, A. M. 2013. Role of ABL family kinases in cancer: from leukaemia to solid tumours. *Nature Reviews Cancer*, 13, 559-571.
- GRZESZKIEWICZ, T. M., LINDNER, V., CHEN, N., LAM, S. C. & LAU, L. F. 2002. The angiogenic factor cysteine-rich 61 (CYR61, CCN1) supports vascular smooth muscle cell adhesion and stimulates chemotaxis through integrin alpha(6)beta(1) and cell surface heparan sulfate proteoglycans. *Endocrinology*, 143, 1441-50.
- GSCHWANDTNER, M., DERLER, R. & MIDWOOD, K. S. 2019. More Than Just Attractive: How CCL2 Influences Myeloid Cell Behavior Beyond Chemotaxis. *Frontiers in Immunology*, 10.
- GUTKIN, A., UZIEL, O., BEERY, E., NORDENBERG, J., PINCHASI, M., GOLDBASER, H., HENICK, S., GOLDBERG, M. & LAHAV, M. 2016. Tumor cells derived exosomes contain hTERT mRNA and transform nonmalignant fibroblasts into telomerase positive cells. *Oncotarget*, 7, 59173-59188.
- HAKULINEN, J., SANKKILA, L., SUGIYAMA, N., LEHTI, K. & KESKI-OJA, J. 2008. Secretion of active membrane type 1 matrix metalloproteinase (MMP-14) into extracellular space in microvesicular exosomes. *Journal of Cellular Biochemistry*, 105, 1211-1218.
- HAM, S., LIMA, L. G., CHAI, E. P. Z., MULLER, A., LOBB, R. J., KRUMEICH, S., WEN, S. W., WIEGMANS, A. P. & MÖLLER, A. 2018. Breast Cancer-Derived Exosomes Alter Macrophage Polarization via gp130/STAT3 Signaling. *Frontiers in immunology*, 9, 871-871.
- HAMMOND, E., KHURANA, A., SHRIDHAR, V. & DREDGE, K. 2014. The Role of Heparanase and Sulfatases in the Modification of Heparan Sulfate Proteoglycans within the Tumor Microenvironment and Opportunities for Novel Cancer Therapeutics. *Frontiers in Oncology*, 4, 195.
- HANAHAH, D. & WEINBERG, R. A. 2000. The Hallmarks of Cancer. *Cell*, 100, 57-70.
- HANAHAH, D. & WEINBERG, ROBERT A. 2011. Hallmarks of Cancer: The Next Generation. *Cell*, 144, 646-674.
- HARDING, C., HEUSER, J. & STAHL, P. 1983. Receptor-mediated endocytosis of transferrin and recycling of the transferrin receptor in rat reticulocytes. *J Cell Biol*, 97, 329-39.
- HECHT, M.-L., ROSENTAL, B., HORLACHER, T., HERSHKOVITZ, O., DE PAZ, J. L., NOTI, C., SCHAUER, S., PORGADOR, A. & SEEBERGER, P. H. 2009. Natural Cytotoxicity Receptors NKp30, NKp44 and NKp46 Bind to Different Heparan Sulfate/Heparin Sequences. *Journal of Proteome Research*, 8, 712-720.

- HEIJNEN, H. F., SCHIEL, A. E., FIJNHEER, R., GEUZE, H. J. & SIXMA, J. J. 1999. Activated platelets release two types of membrane vesicles: microvesicles by surface shedding and exosomes derived from exocytosis of multivesicular bodies and alpha-granules. *Blood*, 94, 3791-9.
- HESS, C., SADALLAH, S., HEFTI, A., LANDMANN, R. & SCHIFFERLI, J. A. 1999. Ectosomes released by human neutrophils are specialized functional units. *J Immunol*, 163, 4564-73.
- HO, G., BROZE, G. J., JR. & SCHWARTZ, A. L. 1997. Role of heparan sulfate proteoglycans in the uptake and degradation of tissue factor pathway inhibitor-coagulation factor Xa complexes. *J Biol Chem*, 272, 16838-44.
- HOSHINO, A., COSTA-SILVA, B., SHEN, T.-L., RODRIGUES, G., HASHIMOTO, A., TESIC MARK, M., MOLINA, H., KOHSAKA, S., DI GIANNATALE, A., CEDER, S., SINGH, S., WILLIAMS, C., SOPLOP, N., URYU, K., PHARMER, L., KING, T., BOJMAR, L., DAVIES, A. E., ARARSO, Y., ZHANG, T., ZHANG, H., HERNANDEZ, J., WEISS, J. M., DUMONT-COLE, V. D., KRAMER, K., WEXLER, L. H., NARENDRAN, A., SCHWARTZ, G. K., HEALEY, J. H., SANDSTROM, P., JØRGEN LABORI, K., KURE, E. H., GRANDGENETT, P. M., HOLLINGSWORTH, M. A., DE SOUSA, M., KAUR, S., JAIN, M., MALLYA, K., BATRA, S. K., JARNAGIN, W. R., BRADY, M. S., FODSTAD, O., MULLER, V., PANTEL, K., MINN, A. J., BISSELL, M. J., GARCIA, B. A., KANG, Y., RAJASEKHAR, V. K., GHAJAR, C. M., MATEI, I., PEINADO, H., BROMBERG, J. & LYDEN, D. 2015. Tumour exosome integrins determine organotropic metastasis. *Nature*, 527, 329-335.
- HSU, Y.-L., HUNG, J.-Y., CHANG, W.-A., JIAN, S.-F., LIN, Y.-S., PAN, Y.-C., WU, C.-Y. & KUO, P.-L. 2018. Hypoxic Lung-Cancer-Derived Extracellular Vesicle MicroRNA-103a Increases the Oncogenic Effects of Macrophages by Targeting PTEN. *Molecular Therapy*, 26, 568-581.
- HSU, Y. L., HUNG, J. Y., CHANG, W. A., LIN, Y. S., PAN, Y. C., TSAI, P. H., WU, C. Y. & KUO, P. L. 2017. Hypoxic lung cancer-secreted exosomal miR-23a increased angiogenesis and vascular permeability by targeting prolyl hydroxylase and tight junction protein ZO-1. *Oncogene*, 36, 4929-4942.
- HURLEY, J. H. 2008. ESCRT complexes and the biogenesis of multivesicular bodies. *Current opinion in cell biology*, 20, 4-11.
- HURWITZ, S. N. & MECKES, D. G. 2019. Extracellular Vesicle Integrins Distinguish Unique Cancers. *Proteomes*, 7, 14.
- INDIRA CHANDRAN, V., WELINDER, C., MÅNSSON, A.-S., OFFER, S., FREYHULT, E., PERNEMALM, M., LUND, S. M., PEDERSEN, S., LEHTIÖ, J., MARKO-VARGA, G., JOHANSSON, M. C., ENGLUND, E., SUNDGREN, P. C. & BELTING, M. 2019. Ultrasensitive Immunoprofiling of Plasma Extracellular Vesicles Identifies Syndecan-1 as a Potential Tool for Minimally Invasive Diagnosis of Glioma. *Clinical Cancer Research*, 25, 3115.
- IOZZO, R. V. & SCHAEFER, L. 2015. Proteoglycan form and function: A comprehensive nomenclature of proteoglycans. *Matrix Biology*, 42, 11-55.
- IVERSEN, N., LINDAHL, A. K. & ABILDGAARD, U. 1998. Elevated TFPI in malignant disease: relation to cancer type and hypercoagulation. *Br J Haematol*, 102, 889-95.
- JAKOBSSON, L., KREUGER, J., HOLMBORN, K., LUNDIN, L., ERIKSSON, I., KJELLÉN, L. & CLAESON-WELSH, L. 2006. Heparan Sulfate in trans Potentiates VEGFR-Mediated Angiogenesis. *Developmental Cell*, 10, 625-634.

References

- JAYASINGAM, S. D., CITARTAN, M., THANG, T. H., MAT ZIN, A. A., ANG, K. C. & CH'NG, E. S. 2020. Evaluating the Polarization of Tumor-Associated Macrophages Into M1 and M2 Phenotypes in Human Cancer Tissue: Technicalities and Challenges in Routine Clinical Practice. *Frontiers in oncology*, 9, 1512-1512.
- JETTEN, N., VERBRUGGEN, S., GIJBELS, M. J., POST, M. J., DE WINTHER, M. P. J. & DONNERS, M. M. P. C. 2014. Anti-inflammatory M2, but not pro-inflammatory M1 macrophages promote angiogenesis in vivo. *Angiogenesis*, 17, 109-118.
- JOHNSON, G. B., BRUNN, G. J., KODAIRA, Y. & PLATT, J. L. 2002. Receptor-mediated monitoring of tissue well-being via detection of soluble heparan sulfate by Toll-like receptor 4. *J Immunol*, 168, 5233-9.
- JOHNSTONE, R. M., ADAM, M., HAMMOND, J. R., ORR, L. & TURBIDE, C. 1987. Vesicle formation during reticulocyte maturation. Association of plasma membrane activities with released vesicles (exosomes). *J Biol Chem*, 262, 9412-20.
- JUNG, O., TRAPP-STAMBORSKI, V., PURUSHOTHAMAN, A., JIN, H., WANG, H., SANDERSON, R. D. & RAPRAEGER, A. C. 2016. Heparanase-induced shedding of syndecan-1/CD138 in myeloma and endothelial cells activates VEGFR2 and an invasive phenotype: prevention by novel synstatins. *Oncogenesis*, 5, e202.
- KADOMATSU, K., KISHIDA, S. & TSUBOTA, S. 2013. The heparin-binding growth factor midkine: the biological activities and candidate receptors. *The Journal of Biochemistry*, 153, 511-521.
- KALLURI, R. 2016. The biology and function of fibroblasts in cancer. *Nat Rev Cancer*, 16, 582-98.
- KARIMI, N., CVJETKOVIC, A., JANG, S. C., CRESCITELLI, R., HOSSEINPOUR FEIZI, M. A., NIEUWLAND, R., LÖTVALL, J. & LÄSSER, C. 2018. Detailed analysis of the plasma extracellular vesicle proteome after separation from lipoproteins. *Cellular and Molecular Life Sciences*, 75, 2873-2886.
- KECK, P. J., HAUSER, S. D., KRIVI, G., SANZO, K., WARREN, T., FEDER, J. & CONNOLLY, D. T. 1989. Vascular permeability factor, an endothelial cell mitogen related to PDGF. *Science*, 246, 1309-12.
- KEERTHIKUMAR, S., CHISANGA, D., ARIYARATNE, D., AL SAFFAR, H., ANAND, S., ZHAO, K., SAMUEL, M., PATHAN, M., JOIS, M., CHILAMKURTI, N., GANGODA, L. & MATHIVANAN, S. 2016. ExoCarta: A Web-Based Compendium of Exosomal Cargo. *J Mol Biol*, 428, 688-692.
- KELLY, T., MIAO, H. Q., YANG, Y., NAVARRO, E., KUSSIE, P., HUANG, Y., MACLEOD, V., CASCIANO, J., JOSEPH, L., ZHAN, F., ZANGARI, M., BARLOGIE, B., SHAUGHNESSY, J. & SANDERSON, R. D. 2003. High heparanase activity in multiple myeloma is associated with elevated microvessel density. *Cancer Res*, 63, 8749-56.
- KIM, K. J., LI, B., WINER, J., ARMANINI, M., GILLET, N., PHILLIPS, H. S. & FERRARA, N. 1993. Inhibition of vascular endothelial growth factor-induced angiogenesis suppresses tumour growth in vivo. *Nature*, 362, 841-4.
- KITAGAWA, H., SHIMAKAWA, H. & SUGAHARA, K. 1999. The tumor suppressor EXT-like gene EXTL2 encodes an alpha1, 4-N-acetylhexosaminyltransferase that transfers N-acetylgalactosamine and N-acetylglucosamine to the common glycosaminoglycan-protein linkage region. The key enzyme for the chain initiation of heparan sulfate. *J Biol Chem*, 274, 13933-7.
- KOLIHA, N., WIENCEK, Y., HEIDER, U., JÜNGST, C., KLADT, N., KRAUTHÄUSER, S., JOHNSTON, I. C. D., BOSIO, A., SCHAUSS, A. & WILD, S. 2016. A novel multiplex

- bead-based platform highlights the diversity of extracellular vesicles. *Journal of extracellular vesicles*, 5, 29975-29975.
- KONOSHENKO, M. Y., LEKCHNOV, E. A., VLASSOV, A. V. & LAKTIONOV, P. P. 2018. Isolation of Extracellular Vesicles: General Methodologies and Latest Trends. *Biomed Res Int*, 2018, 8545347.
- KOWAL, J., ARRAS, G., COLOMBO, M., JOUVE, M., MORATH, J. P., PRIMDAL-BENGTSON, B., DINGLI, F., LOEW, D., TKACH, M. & THÉRY, C. 2016. Proteomic comparison defines novel markers to characterize heterogeneous populations of extracellular vesicle subtypes. *Proceedings of the National Academy of Sciences of the United States of America*, 113, E968-E977.
- KREUGER, J. & KJELLÉN, L. 2012. Heparan sulfate biosynthesis: regulation and variability. *The journal of histochemistry and cytochemistry : official journal of the Histochemistry Society*, 60, 898-907.
- KSIAZKIEWICZ, M., GOTTFRIED, E., KREUTZ, M., MACK, M., HOFSTAEDTER, F. & KUNZ-SCHUGHART, L. A. 2010. Importance of CCL2-CCR2A/2B signaling for monocyte migration into spheroids of breast cancer-derived fibroblasts. *Immunobiology*, 215, 737-47.
- KUCHARZEWSKA, P., CHRISTIANSON, H. C., WELCH, J. E., SVENSSON, K. J., FREDLUND, E., RINGNÉR, M., MÖRGELIN, M., BOURSEAU-GUILMAIN, E., BENZON, J. & BELTING, M. 2013. Exosomes reflect the hypoxic status of glioma cells and mediate hypoxia-dependent activation of vascular cells during tumor development. *Proceedings of the National Academy of Sciences of the United States of America*, 110, 7312-7317.
- KUGERATSKI, F. G., HODGE, K., LILLA, S., MCANDREWS, K. M., ZHOU, X., HWANG, R. F., ZANIVAN, S. & KALLURI, R. 2021. Quantitative proteomics identifies the core proteome of exosomes with syntenin-1 as the highest abundant protein and a putative universal biomarker. *Nature Cell Biology*, 23, 631-641.
- KUMARI, N., DWARAKANATH, B., DAS, A. & BHATT, A. 2016. Role of interleukin-6 in cancer progression and therapeutic resistance. *Tumor Biology*, 37.
- LAI, J., CHIEN, J., STAUB, J., AVULA, R., GREENE, E. L., MATTHEWS, T. A., SMITH, D. I., KAUFMANN, S. H., ROBERTS, L. R. & SHRIDHAR, V. 2003. Loss of HSulf-1 Up-regulates Heparin-binding Growth Factor Signaling in Cancer *. *Journal of Biological Chemistry*, 278, 23107-23117.
- LAI, J. P., SANDHU, D. S., YU, C., HAN, T., MOSER, C. D., JACKSON, K. K., GUERRERO, R. B., ADERCA, I., ISOMOTO, H., GARRITY-PARK, M. M., ZOU, H., SHIRE, A. M., NAGORNEY, D. M., SANDERSON, S. O., ADJEI, A. A., LEE, J. S., THORGEIRSSON, S. S. & ROBERTS, L. R. 2008. Sulfatase 2 up-regulates glypican 3, promotes fibroblast growth factor signaling, and decreases survival in hepatocellular carcinoma. *Hepatology*, 47, 1211-22.
- LAMORTE, S., FERRERO, S., ASCHERO, S., MONITILLO, L., BUSSOLATI, B., OMEDE, P., LADETTO, M. & CAMUSSI, G. 2012. Syndecan-1 promotes the angiogenic phenotype of multiple myeloma endothelial cells. *Leukemia*, 26, 1081-1090.
- LAMPARSKI, H. G., METHA-DAMANI, A., YAO, J. Y., PATEL, S., HSU, D. H., RUEGG, C. & LE PECQ, J. B. 2002. Production and characterization of clinical grade exosomes derived from dendritic cells. *J Immunol Methods*, 270, 211-26.
- LEBEL-BINAY, S., THIOUNN, N., DE PINIEUX, G., VIEILLEFOND, A., DEBRÉ, B., BONNEFOY, J.-Y., FRIDMAN, W.-H. & PAGÈS, F. 2003. IL-18 is produced by prostate cancer

References

- cells and secreted in response to interferons. *International Journal of Cancer*, 106, 827-835.
- LEE, L. F., LOUIE, M. C., DESAI, S. J., YANG, J., CHEN, H. W., EVANS, C. P. & KUNG, H. J. 2004. Interleukin-8 confers androgen-independent growth and migration of LNCaP: differential effects of tyrosine kinases Src and FAK. *Oncogene*, 23, 2197-205.
- LI, A., DUBEY, S., VARNEY, M. L., DAVE, B. J. & SINGH, R. K. 2003. IL-8 Directly Enhanced Endothelial Cell Survival, Proliferation, and Matrix Metalloproteinases Production and Regulated Angiogenesis. *The Journal of Immunology*, 170, 3369.
- LINARES, R., TAN, S., GOUNOU, C., ARRAUD, N. & BRISSON, A. R. 2015. High-speed centrifugation induces aggregation of extracellular vesicles. *J Extracell Vesicles*, 4, 29509.
- LINDE, N., LEDERLE, W., DEPNER, S., VAN ROOIJEN, N., GUTSCHALK, C. M. & MUELLER, M. M. 2012. Vascular endothelial growth factor-induced skin carcinogenesis depends on recruitment and alternative activation of macrophages. *J Pathol*, 227, 17-28.
- LIU, L., GE, D., MA, L., MEI, J., LIU, S., ZHANG, Q., REN, F., LIAO, H., PU, Q., WANG, T. & YOU, Z. 2012. Interleukin-17 and prostaglandin E2 are involved in formation of an M2 macrophage-dominant microenvironment in lung cancer. *Journal of thoracic oncology : official publication of the International Association for the Study of Lung Cancer*, 7, 1091-1100.
- LIU, T., HAN, C., WANG, S., FANG, P., MA, Z., XU, L. & YIN, R. 2019. Cancer-associated fibroblasts: an emerging target of anti-cancer immunotherapy. *Journal of Hematology & Oncology*, 12, 86.
- LLORENTE, A., SKOTLAND, T., SYLVÄNNE, T., KAUKANEN, D., RÓG, T., ORŁOWSKI, A., VATTULAINEN, I., EKROOS, K. & SANDVIG, K. 2013. Molecular lipidomics of exosomes released by PC-3 prostate cancer cells. *Biochim Biophys Acta*, 1831, 1302-9.
- LO CICERO, A., STAHL, P. D. & RAPOSO, G. 2015. Extracellular vesicles shuffling intercellular messages: for good or for bad. *Current Opinion in Cell Biology*, 35, 69-77.
- LOBB, R. J., BECKER, M., WEN WEN, S., WONG, C. S. F., WIEGMANS, A. P., LEIMGRUBER, A. & MÖLLER, A. 2015. Optimized exosome isolation protocol for cell culture supernatant and human plasma. *Journal of Extracellular Vesicles*, 4, 27031.
- LOBERG, R. D., DAY, L. L., HARWOOD, J., YING, C., ST JOHN, L. N., GILES, R., NEELEY, C. K. & PIENTA, K. J. 2006. CCL2 is a potent regulator of prostate cancer cell migration and proliferation. *Neoplasia (New York, N.Y.)*, 8, 578-586.
- LÓPEZ-CASILLAS, F., CHEIFETZ, S., DOODY, J., ANDRES, J. L., LANE, W. S. & MASSAGUE, J. 1991. Structure and expression of the membrane proteoglycan betaglycan, a component of the TGF- β receptor system. *Cell*, 67, 785-795.
- LOTVALL, J., HILL, A. F., HOCHBERG, F., BUZAS, E. I., DI VIZIO, D., GARDINER, C., GHO, Y. S., KUROCHKIN, I. V., MATHIVANAN, S., QUESENBERRY, P., SAHOO, S., TAHARA, H., WAUBEN, M. H., WITWER, K. W. & THERY, C. 2014. Minimal experimental requirements for definition of extracellular vesicles and their functions: a position statement from the International Society for Extracellular Vesicles. *J Extracell Vesicles*, 3, 26913.

- LUDWIG, N. & WHITESIDE, T. L. 2018. Potential roles of tumor-derived exosomes in angiogenesis. *Expert opinion on therapeutic targets*, 22, 409-417.
- LUND, M. E., TO, J., O'BRIEN, B. A. & DONNELLY, S. 2016. The choice of phorbol 12-myristate 13-acetate differentiation protocol influences the response of THP-1 macrophages to a pro-inflammatory stimulus. *Journal of Immunological Methods*, 430, 64-70.
- MACCARANA, M., CASU, B. & LINDAHL, U. 1993. Minimal sequence in heparin/heparan sulfate required for binding of basic fibroblast growth factor. *J Biol Chem*, 268, 23898-905.
- MAES, M. B., WITTIG, B., CIGNARELLA, A. & LORKOWSKI, S. 2014. Reduced PMA enhances the responsiveness of transfected THP-1 macrophages to polarizing stimuli. *Journal of Immunological Methods*, 402, 76-81.
- MAIA, J., CAJA, S., STRANO MORAES, M. C., COUTO, N. & COSTA-SILVA, B. 2018. Exosome-Based Cell-Cell Communication in the Tumor Microenvironment. *Frontiers in Cell and Developmental Biology*, 6.
- MANTOVANI, A., MARCHESI, F., MALESCI, A., LAGHI, L. & ALLAVENA, P. 2017. Tumour-associated macrophages as treatment targets in oncology. *Nature reviews. Clinical oncology*, 14, 399-416.
- MARSIGLIANTE, S., VETRUGNO, C. & MUSCELLA, A. 2013. CCL20 induces migration and proliferation on breast epithelial cells. *J Cell Physiol*, 228, 1873-83.
- MARTIN, D., GALISTEO, R. & GUTKIND, J. S. 2009. CXCL8/IL8 stimulates vascular endothelial growth factor (VEGF) expression and the autocrine activation of VEGFR2 in endothelial cells by activating NFkappaB through the CBM (Carma3/Bcl10/Malt1) complex. *The Journal of biological chemistry*, 284, 6038-6042.
- MATSUDA, K., MARUYAMA, H., GUO, F., KLEEFF, J., ITAKURA, J., MATSUMOTO, Y., LANDER, A. D. & KORC, M. 2001. Glypican-1 Is Overexpressed in Human Breast Cancer and Modulates the Mitogenic Effects of Multiple Heparin-binding Growth Factors in Breast Cancer Cells. *Cancer Research*, 61, 5562-5569.
- MEHUL, B. & HUGHES, R. C. 1997. Plasma membrane targetting, vesicular budding and release of galectin 3 from the cytoplasm of mammalian cells during secretion. *J Cell Sci*, 110 (Pt 10), 1169-78.
- MELO, S. A., LUECKE, L. B., KAHLERT, C., FERNANDEZ, A. F., GAMMON, S. T., KAYE, J., LEBLEU, V. S., MITTENDORF, E. A., WEITZ, J., RAHBARI, N., REISSFELDER, C., PILARSKY, C., FRAGA, M. F., PIWNICA-WORMS, D. & KALLURI, R. 2015. Glypican-1 identifies cancer exosomes and detects early pancreatic cancer. *Nature*, 523, 177-182.
- MINCIACCHI, V. R., YOU, S., SPINELLI, C., MORLEY, S., ZANDIAN, M., ASPURIA, P. J., CAVALLINI, L., CIARDIELLO, C., REIS SOBREIRO, M., MORELLO, M., KHARMATE, G., JANG, S. C., KIM, D. K., HOSSEINI-BEHESHTI, E., TOMLINSON GUNS, E., GLEAVE, M., GHO, Y. S., MATHIVANAN, S., YANG, W., FREEMAN, M. R. & DI VIZIO, D. 2015. Large oncosomes contain distinct protein cargo and represent a separate functional class of tumor-derived extracellular vesicles. *Oncotarget*, 6, 11327-41.
- MÖBIUS, W., VAN DONSELAAR, E., OHNO-IWASHITA, Y., SHIMADA, Y., HEIJNEN, H. F., SLOT, J. W. & GEUZE, H. J. 2003. Recycling compartments and the internal

References

- vesicles of multivesicular bodies harbor most of the cholesterol found in the endocytic pathway. *Traffic*, 4, 222-31.
- MONTECALVO, A., LARREGINA, A. T., SHUFESKY, W. J., BEER STOLZ, D., SULLIVAN, M. L. G., KARLSSON, J. M., BATY, C. J., GIBSON, G. A., ERDOS, G., WANG, Z., MILOSEVIC, J., TKACHEVA, O. A., DIVITO, S. J., JORDAN, R., LYONS-WEILER, J., WATKINS, S. C. & MORELLI, A. E. 2012. Mechanism of transfer of functional microRNAs between mouse dendritic cells via exosomes. *Blood*, 119, 756-766.
- MORALES-KASTRESANA, A., TELFORD, B., MUSICH, T. A., MCKINNON, K., CLAYBORNE, C., BRAIG, Z., ROSNER, A., DEMBERG, T., WATSON, D. C., KARPOVA, T. S., FREEMAN, G. J., DEKRUYFF, R. H., PAVLAKIS, G. N., TERABE, M., ROBERT-GUROFF, M., BERZOFKY, J. A. & JONES, J. C. 2017. Labeling Extracellular Vesicles for Nanoscale Flow Cytometry. *Scientific reports*, 7, 1878-1878.
- MORELLI, A. E., LARREGINA, A. T., SHUFESKY, W. J., SULLIVAN, M. L. G., STOLZ, D. B., PAPWORTH, G. D., ZAHORCHAK, A. F., LOGAR, A. J., WANG, Z., WATKINS, S. C., FALO, L. D. & THOMSON, A. W. 2004. Endocytosis, intracellular sorting, and processing of exosomes by dendritic cells. *Blood*, 104, 3257-3266.
- MULCAHY, L. A., PINK, R. C. & CARTER, D. R. F. 2014. Routes and mechanisms of extracellular vesicle uptake. *Journal of extracellular vesicles*, 3, 10.3402/jev.v3.24641.
- MURRAY, PETER J., ALLEN, JUDITH E., BISWAS, SUBHRA K., FISHER, EDWARD A., GILROY, DEREK W., GOERDT, S., GORDON, S., HAMILTON, JOHN A., IVASHKIV, LIONEL B., LAWRENCE, T., LOCATI, M., MANTOVANI, A., MARTINEZ, FERNANDO O., MEGE, J.-L., MOSSER, DAVID M., NATOLI, G., SAEIJ, JEROEN P., SCHULTZE, JOACHIM L., SHIREY, KARI A., SICA, A., SUTTLES, J., UDALOVA, I., VAN GINDERACHTER, JO A., VOGEL, STEFANIE N. & WYNN, THOMAS A. 2014. Macrophage Activation and Polarization: Nomenclature and Experimental Guidelines. *Immunity*, 41, 14-20.
- NABHAN, J. F., HU, R., OH, R. S., COHEN, S. N. & LU, Q. 2012. Formation and release of arrestin domain-containing protein 1-mediated microvesicles (ARMMs) at plasma membrane by recruitment of TSG101 protein. *Proc Natl Acad Sci U S A*, 109, 4146-51.
- NAITO, Y., YOSHIOKA, Y., YAMAMOTO, Y. & OCHIYA, T. 2017. How cancer cells dictate their microenvironment: present roles of extracellular vesicles. *Cellular and Molecular Life Sciences*, 74, 697-713.
- NAKAI, W., YOSHIDA, T., DIEZ, D., MIYATAKE, Y., NISHIBU, T., IMAWAKA, N., NARUSE, K., SADAMURA, Y. & HANAYAMA, R. 2016. A novel affinity-based method for the isolation of highly purified extracellular vesicles. *Scientific reports*, 6, 33935-33935.
- NANBO, A., KAWANISHI, E., YOSHIDA, R. & YOSHIYAMA, H. 2013. Exosomes derived from Epstein-Barr virus-infected cells are internalized via caveola-dependent endocytosis and promote phenotypic modulation in target cells. *J Virol*, 87, 10334-47.
- NARITA, K., STAUB, J., CHIEN, J., MEYER, K., BAUER, M., FRIEDL, A., RAMAKRISHNAN, S. & SHRIDHAR, V. 2006. HSulf-1 inhibits angiogenesis and tumorigenesis in vivo. *Cancer Res*, 66, 6025-32.
- NAZARENKO, I., RANA, S., BAUMANN, A., MCALEAR, J., HELLWIG, A., TRENDELENBURG, M., LOCHNIT, G., PREISSNER, K. T. & ZÖLLER, M. 2010. Cell Surface Tetraspanin

- Tspan8 Contributes to Molecular Pathways of Exosome-Induced Endothelial Cell Activation. *Cancer Research*, 70, 1668.
- NOLTE-'T HOEN, E. N., BUERMANS, H. P., WAASDORP, M., STOORVOGEL, W., WAUBEN, M. H. & T HOEN, P. A. 2012a. Deep sequencing of RNA from immune cell-derived vesicles uncovers the selective incorporation of small non-coding RNA biotypes with potential regulatory functions. *Nucleic Acids Res*, 40, 9272-85.
- NOLTE-'T HOEN, E. N. M., VAN DER VLIST, E. J., AALBERTS, M., MERTENS, H. C. H., BOSCH, B. J., BARTELINK, W., MASTROBATTISTA, E., VAN GAAL, E. V. B., STOORVOGEL, W., ARKESTEIJN, G. J. A. & WAUBEN, M. H. M. 2012b. Quantitative and qualitative flow cytometric analysis of nanosized cell-derived membrane vesicles. *Nanomedicine : nanotechnology, biology, and medicine*, 8, 712-720.
- NOMURA, T. & KATUNUMA, N. 2005. Involvement of cathepsins in the invasion, metastasis and proliferation of cancer cells. *J Med Invest*, 52, 1-9.
- NOY, R. & POLLARD, J. W. 2014. Tumor-associated macrophages: from mechanisms to therapy. *Immunity*, 41, 49-61.
- OLINK. <https://www.olink.com/content/uploads/2019/12/Olink-CVD-III-Validation-Data-v2.1.pdf> [Online]. [Accessed].
- OLUMI, A. F., GROSSFELD, G. D., HAYWARD, S. W., CARROLL, P. R., TLSTY, T. D. & CUNHA, G. R. 1999. Carcinoma-associated Fibroblasts Direct Tumor Progression of Initiated Human Prostatic Epithelium. *Cancer Research*, 59, 5002.
- ONÓDI, Z., PELYHE, C., TERÉZIA NAGY, C., BRENNER, G. B., ALMÁSI, L., KITTEL, Á., MANČEK-KEBER, M., FERDINANDY, P., BUZÁS, E. I. & GIRICZ, Z. 2018. Isolation of High-Purity Extracellular Vesicles by the Combination of Iodixanol Density Gradient Ultracentrifugation and Bind-Elute Chromatography From Blood Plasma. *Frontiers in Physiology*, 9.
- ORI, A., WILKINSON, M. C. & FERNIG, D. G. 2011. A systems biology approach for the investigation of the heparin/heparan sulfate interactome. *The Journal of biological chemistry*, 286, 19892-19904.
- ORIMO, A., GUPTA, P. B., SGROI, D. C., ARENZANA-SEISDEDOS, F., DELAUNAY, T., NAEEM, R., CAREY, V. J., RICHARDSON, A. L. & WEINBERG, R. A. 2005. Stromal fibroblasts present in invasive human breast carcinomas promote tumor growth and angiogenesis through elevated SDF-1/CXCL12 secretion. *Cell*, 121, 335-48.
- OSAWA, S., KURACHI, M., YAMAMOTO, H., YOSHIMOTO, Y. & ISHIZAKI, Y. 2017. Fibronectin on extracellular vesicles from microvascular endothelial cells is involved in the vesicle uptake into oligodendrocyte precursor cells. *Biochemical and Biophysical Research Communications*, 488, 232-238.
- OSTEIKOETXEA, X., BALOGH, A., SZABÓ-TAYLOR, K., NÉMETH, A., SZABÓ, T. G., PÁLÓCZI, K., SÓDAR, B., KITTEL, Á., GYÖRGY, B., PÁLLINGER, É., MATKÓ, J. & BUZÁS, E. I. 2015. Improved Characterization of EV Preparations Based on Protein to Lipid Ratio and Lipid Properties. *PLOS ONE*, 10, e0121184.
- OSTROWSKI, M., CARMO, N. B., KRUMEICH, S., FANGET, I., RAPOSO, G., SAVINA, A., MOITA, C. F., SCHAUER, K., HUME, A. N., FREITAS, R. P., GOUD, B., BENARROCH, P., HACOEN, N., FUKUDA, M., DESNOS, C., SEABRA, M. C., DARCHEN, F., AMIGORENA, S., MOITA, L. F. & THERY, C. 2010. Rab27a and Rab27b control different steps of the exosome secretion pathway. *Nat Cell Biol*, 12, 19-30; sup pp 1-13.

References

- PAGET, S. 1989. The distribution of secondary growths in cancer of the breast. 1889. *Cancer Metastasis Rev*, 8, 98-101.
- PARDO, A. & SELMAN, M. 2005. MMP-1: the elder of the family. *The International Journal of Biochemistry & Cell Biology*, 37, 283-288.
- PAROLINI, I., FEDERICI, C., RAGGI, C., LUGINI, L., PALLESCHI, S., DE MILITO, A., COSCIA, C., IESSI, E., LOGOZZI, M., MOLINARI, A., COLONE, M., TATTI, M., SARGIACOMO, M. & FAIS, S. 2009. Microenvironmental pH is a key factor for exosome traffic in tumor cells. *The Journal of biological chemistry*, 284, 34211-34222.
- PASQUALON, T., LUE, H., GROENING, S., PRUESSMEYER, J., JAHR, H., DENECKE, B., BERNHAGEN, J. & LUDWIG, A. 2016. Cell surface syndecan-1 contributes to binding and function of macrophage migration inhibitory factor (MIF) on epithelial tumor cells. *Biochimica et Biophysica Acta (BBA) - Molecular Cell Research*, 1863, 717-726.
- PATHAN, M., FONSEKA, P., CHITTI, S. V., KANG, T., SANWLANI, R., VAN DEUN, J., HENDRIX, A. & MATHIVANAN, S. 2019. Vesiclepedia 2019: a compendium of RNA, proteins, lipids and metabolites in extracellular vesicles. *Nucleic Acids Res*, 47, D516-d519.
- PEINADO, H., ALEČKOVIĆ, M., LAVOTSHKIN, S., MATEI, I., COSTA-SILVA, B., MORENO-BUENO, G., HERGUETA-REDONDO, M., WILLIAMS, C., GARCÍA-SANTOS, G., GHAJAR, C., NITADORI-HOSHINO, A., HOFFMAN, C., BADAL, K., GARCIA, B. A., CALLAHAN, M. K., YUAN, J., MARTINS, V. R., SKOG, J., KAPLAN, R. N., BRADY, M. S., WOLCHOK, J. D., CHAPMAN, P. B., KANG, Y., BROMBERG, J. & LYDEN, D. 2012. Melanoma exosomes educate bone marrow progenitor cells toward a pro-metastatic phenotype through MET. *Nature medicine*, 18, 883-891.
- PEREZ-HERNANDEZ, D., GUTIÉRREZ-VÁZQUEZ, C., JORGE, I., LÓPEZ-MARTÍN, S., URSA, A., SÁNCHEZ-MADRID, F., VÁZQUEZ, J. & YÁÑEZ-MÓ, M. 2013. The intracellular interactome of tetraspanin-enriched microdomains reveals their function as sorting machineries toward exosomes. *The Journal of biological chemistry*, 288, 11649-11661.
- PETRERA, A., VON TOERNE, C., BEHLER, J., HUTH, C., THORAND, B., HILGENDORFF, A. & HAUCK, S. M. 2021. Multiplatform Approach for Plasma Proteomics: Complementarity of Olink Proximity Extension Assay Technology to Mass Spectrometry-Based Protein Profiling. *J Proteome Res*, 20, 751-762.
- PETROVA, V., ANNICCHIARICO-PETRUZZELLI, M., MELINO, G. & AMELIO, I. 2018. The hypoxic tumour microenvironment. *Oncogenesis*, 7, 10.
- PETTERSEN, J. S., FUENTES-DUCULAN, J., SUÁREZ-FARIÑAS, M., PIERSON, K. C., PITTSKIEFER, A., FAN, L., BELKIN, D. A., WANG, C. Q., BHUVANENDRAN, S., JOHNSON-HUANG, L. M., BLUTH, M. J., KRUEGER, J. G., LOWES, M. A. & CARUCCI, J. A. 2011. Tumor-associated macrophages in the cutaneous SCC microenvironment are heterogeneously activated. *J Invest Dermatol*, 131, 1322-30.
- PLEBANEK, M. P., ANGELONI, N. L., VINOKOUR, E., LI, J., HENKIN, A., MARTINEZ-MARIN, D., FILLEUR, S., BHOWMICK, R., HENKIN, J., MILLER, S. D., IFERGAN, I., LEE, Y., OSMAN, I., THAXTON, C. S. & VOLPERT, O. V. 2017. Pre-metastatic cancer exosomes induce immune surveillance by patrolling monocytes at the metastatic niche. *Nature Communications*, 8, 1319.

- POCSFALVI, G., STANLY, C., VILASI, A., FIUME, I., CAPASSO, G., TURIÁK, L., BUZAS, E. I. & VÉKEY, K. 2016. Mass spectrometry of extracellular vesicles. *Mass Spectrometry Reviews*, 35, 3-21.
- POGGIO, M., HU, T., PAI, C.-C., CHU, B., BELAIR, C. D., CHANG, A., MONTABANA, E., LANG, U. E., FU, Q., FONG, L. & BLELLOCH, R. 2019. Suppression of Exosomal PD-L1 Induces Systemic Anti-tumor Immunity and Memory. *Cell*, 177, 414-427.e13.
- PRESTA, M., MOSCATELLI, D., JOSEPH-SILVERSTEIN, J. & RIFKIN, D. B. 1986. Purification from a human hepatoma cell line of a basic fibroblast growth factor-like molecule that stimulates capillary endothelial cell plasminogen activator production, DNA synthesis, and migration. *Molecular and cellular biology*, 6, 4060-4066.
- PROUDFOOT, A. E. I., HANDEL, T. M., JOHNSON, Z., LAU, E. K., LIWANG, P., CLARK-LEWIS, I., BORLAT, F., WELLS, T. N. C. & KOSCO-VILBOIS, M. H. 2003. Glycosaminoglycan binding and oligomerization are essential for the in vivo activity of certain chemokines. *Proceedings of the National Academy of Sciences*, 100, 1885.
- PSAILA, B. & LYDEN, D. 2009. The metastatic niche: adapting the foreign soil. *Nature Reviews Cancer*, 9, 285-293.
- PURUSHOTHAMAN, A., BANDARI, S. K., LIU, J., MOBLEY, J. A., BROWN, E. E. & SANDERSON, R. D. 2016. Fibronectin on the Surface of Myeloma Cell-derived Exosomes Mediates Exosome-Cell Interactions. *The Journal of biological chemistry*, 291, 1652-1663.
- PURUSHOTHAMAN, A., CHEN, L., YANG, Y. & SANDERSON, R. D. 2008. Heparanase stimulation of protease expression implicates it as a master regulator of the aggressive tumor phenotype in myeloma. *J Biol Chem*, 283, 32628-36.
- PURUSHOTHAMAN, A., UYAMA, T., KOBAYASHI, F., YAMADA, S., SUGAHARA, K., RAPRAEGER, A. C. & SANDERSON, R. D. 2010. Heparanase-enhanced shedding of syndecan-1 by myeloma cells promotes endothelial invasion and angiogenesis. *Blood*, 115, 2449-2457.
- QIAN, B.-Z. & POLLARD, J. W. 2010. Macrophage diversity enhances tumor progression and metastasis. *Cell*, 141, 39-51.
- RABE, D. C., RUSTANDY, F. D., LEE, J. & ROSNER, M. R. 2018. Tumor extracellular vesicles are required for tumor-associated macrophage programming. *bioRxiv*, 375022.
- RAMANI, V. C., PRUETT, P. S., THOMPSON, C. A., DELUCAS, L. D. & SANDERSON, R. D. 2012. Heparan Sulfate Chains of Syndecan-1 Regulate Ectodomain Shedding *. *Journal of Biological Chemistry*, 287, 9952-9961.
- RAMTEKE, A., TING, H., AGARWAL, C., MATEEN, S., SOMASAGARA, R., HUSSAIN, A., GRANER, M., FREDERICK, B., AGARWAL, R. & DEEP, G. 2015. Exosomes secreted under hypoxia enhance invasiveness and stemness of prostate cancer cells by targeting adherens junction molecules. *Molecular carcinogenesis*, 54, 554-565.
- RANA, S., YUE, S., STADEL, D. & ZÖLLER, M. 2012. Toward tailored exosomes: The exosomal tetraspanin web contributes to target cell selection. *The International Journal of Biochemistry & Cell Biology*, 44, 1574-1584.
- RAO, S. K., HUYNH, C., PROUX-GILLARDEAUX, V., GALLI, T. & ANDREWS, N. W. 2004. Identification of SNAREs involved in synaptotagmin VII-regulated lysosomal exocytosis. *J Biol Chem*, 279, 20471-9.

References

- RAPOSO, G., NIJMAN, H. W., STOORVOGEL, W., LIEJENDEKKER, R., HARDING, C. V., MELIEF, C. J. & GEUZE, H. J. 1996. B lymphocytes secrete antigen-presenting vesicles. *J Exp Med*, 183, 1161-72.
- RAPOSO, G. & STOORVOGEL, W. 2013. Extracellular vesicles: Exosomes, microvesicles, and friends. *The Journal of Cell Biology*, 200, 373-383.
- RAPRAEGER, A. C., KRUFKA, A. & OLWIN, B. B. 1991. Requirement of heparan sulfate for bFGF-mediated fibroblast growth and myoblast differentiation. *Science*, 252, 1705-8.
- RATAJCZAK, J., MIEKUS, K., KUCIA, M., ZHANG, J., RECA, R., DVORAK, P. & RATAJCZAK, M. Z. 2006. Embryonic stem cell-derived microvesicles reprogram hematopoietic progenitors: evidence for horizontal transfer of mRNA and protein delivery. *Leukemia*, 20, 847-856.
- REÁTEGUI, E., VAN DER VOS, K. E., LAI, C. P., ZEINALI, M., ATAI, N. A., ALDIKACTI, B., FLOYD, F. P., H. KHANKHEL, A., THAPAR, V., HOCHBERG, F. H., SEQUIST, L. V., NAHED, B. V., S. CARTER, B., TONER, M., BALAJ, L., T. TING, D., BREAKFIELD, X. O. & STOTT, S. L. 2018. Engineered nanointerfaces for microfluidic isolation and molecular profiling of tumor-specific extracellular vesicles. *Nature Communications*, 9, 175.
- REILAND, J., KEMPF, D., ROY, M., DENKINS, Y. & MARCHETTI, D. 2006. FGF2 binding, signaling, and angiogenesis are modulated by heparanase in metastatic melanoma cells. *Neoplasia (New York, N.Y.)*, 8, 596-606.
- RICKLEFS, F. L., ALAYO, Q., KRENZLIN, H., MAHMOUD, A. B., SPERANZA, M. C., NAKASHIMA, H., HAYES, J. L., LEE, K., BALAJ, L., PASSARO, C., ROOJ, A. K., KRASEMANN, S., CARTER, B. S., CHEN, C. C., STEED, T., TREIBER, J., RODIG, S., YANG, K., NAKANO, I., LEE, H., WEISSLEDER, R., BREAKFIELD, X. O., GODLEWSKI, J., WESTPHAL, M., LAMSZUS, K., FREEMAN, G. J., BRONISZ, A., LAWLER, S. E. & CHIOCCA, E. A. 2018. Immune evasion mediated by PD-L1 on glioblastoma-derived extracellular vesicles. *Science Advances*, 4, eaar2766.
- RIDER, P., CARMİ, Y., VORONOV, E. & APTE, R. N. 2013. Interleukin-1 α . *Seminars in Immunology*, 25, 430-438.
- ROBERTS-DALTON, H. D., COCKS, A., FALCON-PEREZ, J. M., SAYERS, E. J., WEBBER, J. P., WATSON, P., CLAYTON, A. & JONES, A. T. 2017. Fluorescence labelling of extracellular vesicles using a novel thiol-based strategy for quantitative analysis of cellular delivery and intracellular traffic. *Nanoscale*, 9, 13693-13706.
- ROBINSON, C. J., MULLOY, B., GALLAGHER, J. T. & STRINGER, S. E. 2006. VEGF165-binding sites within heparan sulfate encompass two highly sulfated domains and can be liberated by K5 lyase. *J Biol Chem*, 281, 1731-40.
- ROMAGNANI, P., ANNUNZIATO, F., LAZZERI, E., COSMI, L., BELTRAME, C., LASAGNI, L., GALLI, G., FRANCALANCI, M., MANETTI, R., MARRA, F., VANINI, V., MAGGI, E. & ROMAGNANI, S. 2001. Interferon-inducible protein 10, monokine induced by interferon gamma, and interferon-inducible T-cell alpha chemoattractant are produced by thymic epithelial cells and attract T-cell receptor (TCR) alphabeta+ CD8+ single-positive T cells, TCRgammadelta+ T cells, and natural killer-type cells in human thymus. *Blood*, 97, 601-7.
- RØNNOV-JESSEN, L. & PETERSEN, O. W. 1993. Induction of alpha-smooth muscle actin by transforming growth factor-beta 1 in quiescent human breast gland

- fibroblasts. Implications for myofibroblast generation in breast neoplasia. *Lab Invest*, 68, 696-707.
- ROUCOURT, B., MEEUSSEN, S., BAO, J., ZIMMERMANN, P. & DAVID, G. 2015. Heparanase activates the syndecan-syntenin-ALIX exosome pathway. *Cell Research*, 25, 412-428.
- RUFFELL, B., CHANG-STRACHAN, D., CHAN, V., ROSENBUSCH, A., HO, C. M. T., PRYER, N., DANIEL, D., HWANG, E. S., RUGO, H. S. & COUSSENS, L. M. 2014. Macrophage IL-10 blocks CD8+ T cell-dependent responses to chemotherapy by suppressing IL-12 expression in intratumoral dendritic cells. *Cancer cell*, 26, 623-637.
- SADIR, R., IMBERTY, A., BALEUX, F. & LORTAT-JACOB, H. 2004. Heparan sulfate/heparin oligosaccharides protect stromal cell-derived factor-1 (SDF-1)/CXCL12 against proteolysis induced by CD26/dipeptidyl peptidase IV. *J Biol Chem*, 279, 43854-60.
- SALCEDO, R., PONCE, M. L., YOUNG, H. A., WASSERMAN, K., WARD, J. M., KLEINMAN, H. K., OPPENHEIM, J. J. & MURPHY, W. J. 2000. Human endothelial cells express CCR2 and respond to MCP-1: direct role of MCP-1 in angiogenesis and tumor progression. *Blood*, 96, 34-40.
- SÁNCHEZ, C. A., ANDAHUR, E. I., VALENZUELA, R., CASTELLÓN, E. A., FULLÁ, J. A., RAMOS, C. G. & TRIVIÑO, J. C. 2016. Exosomes from bulk and stem cells from human prostate cancer have a differential microRNA content that contributes cooperatively over local and pre-metastatic niche. *Oncotarget*, 7, 3993-4008.
- SANDERSON, R. D., BANDARI, S. K. & VLODAVSKY, I. 2019. Proteases and glycosidases on the surface of exosomes: Newly discovered mechanisms for extracellular remodeling. *Matrix Biology*, 75-76, 160-169.
- SANDERSON, R. D., YANG, Y., KELLY, T., MACLEOD, V., DAI, Y. & THEUS, A. 2005. Enzymatic remodeling of heparan sulfate proteoglycans within the tumor microenvironment: growth regulation and the prospect of new cancer therapies. *J Cell Biochem*, 96, 897-905.
- SANSONE, P., SAVINI, C., KURELAC, I., CHANG, Q., AMATO, L. B., STRILLACCI, A., STEPANOVA, A., IOMMARINI, L., MASTROLEO, C., DALY, L., GALKIN, A., THAKUR, B. K., SOPLOP, N., URYU, K., HOSHINO, A., NORTON, L., BONAFÉ, M., CRICCA, M., GASPARRE, G., LYDEN, D. & BROMBERG, J. 2017. Packaging and transfer of mitochondrial DNA via exosomes regulate escape from dormancy in hormonal therapy-resistant breast cancer. *Proceedings of the National Academy of Sciences*, 114, E9066.
- SARRAZIN, S., LAMANNA, W. C. & ESKO, J. D. 2011. Heparan sulfate proteoglycans. *Cold Spring Harbor perspectives in biology*, 3, a004952.
- SASISEKHARAN, R., LOHSE DANIEL, L., COONEY CHARLES, L., LINHARDT ROBERT, J. & LANGER ROBERT, S. 1995. *Purification Of Heparinase I, Ii, And Iii From Flavobacterium Heparinum*. US patent application US 98336792 A. 1995/02/14.
- SAVINA, A., VIDAL, M. & COLOMBO, M. I. 2002. The exosome pathway in K562 cells is regulated by Rab11. *J Cell Sci*, 115, 2505-15.
- SAWA-WEJKSZA, K., DUDEK, A., LEMIESZEK, M., KAŁAWAJ, K. & KANDEFER-SZERSZEŃ, M. 2018. Colon cancer-derived conditioned medium induces differentiation of THP-1 monocytes into a mixed population of M1/M2 cells. *Tumor Biology*, 40, 1010428318797880.

References

- SCHÄFER, T., ZENTGRAF, H., ZEHE, C., BRÜGGER, B., BERNHAGEN, J. & NICKEL, W. 2004. Unconventional Secretion of Fibroblast Growth Factor 2 Is Mediated by Direct Translocation across the Plasma Membrane of Mammalian Cells. *Journal of Biological Chemistry*, 279, 6244-6251.
- SCHWENDE, H., FITZKE, E., AMBS, P. & DIETER, P. 1996. Differences in the state of differentiation of THP-1 cells induced by phorbol ester and 1,25-dihydroxyvitamin D3. *J Leukoc Biol*, 59, 555-61.
- SEELENMEYER, C., STEGMAYER, C. & NICKEL, W. 2008. Unconventional secretion of fibroblast growth factor 2 and galectin-1 does not require shedding of plasma membrane-derived vesicles. *FEBS Letters*, 582, 1362-1368.
- SEGURA, E., GUÉRIN, C., HOGG, N., AMIGORENA, S. & THÉRY, C. 2007. CD8+ dendritic cells use LFA-1 to capture MHC-peptide complexes from exosomes in vivo. *J Immunol*, 179, 1489-96.
- SHELDON, H., HEIKAMP, E., TURLEY, H., DRAGOVIC, R., THOMAS, P., OON, C. E., LEEK, R., EDELMANN, M., KESSLER, B., SAINSON, R. C. A., SARGENT, I., LI, J.-L. & HARRIS, A. L. 2010. New mechanism for Notch signaling to endothelium at a distance by Delta-like 4 incorporation into exosomes. *Blood*, 116, 2385-2394.
- SHINOHARA, H., KURANAGA, Y., KUMAZAKI, M., SUGITO, N., YOSHIKAWA, Y., TAKAI, T., TANIGUCHI, K., ITO, Y. & AKAO, Y. 2017. Regulated Polarization of Tumor-Associated Macrophages by miR-145 via Colorectal Cancer-Derived Extracellular Vesicles. *The Journal of Immunology*, 199, 1505.
- SHIRATORI, H., FEINWEBER, C., LUCKHARDT, S., LINKE, B., RESCH, E., GEISSLINGER, G., WEIGERT, A. & PARNHAM, M. J. 2017. THP-1 and human peripheral blood mononuclear cell-derived macrophages differ in their capacity to polarize in vitro. *Molecular Immunology*, 88, 58-68.
- SIMON DAVIS, D. A. & PARISH, C. R. 2013. Heparan Sulfate: A Ubiquitous Glycosaminoglycan with Multiple Roles in Immunity. *Frontiers in Immunology*, 4.
- SINGH, R., POCHAMPALLY, R., WATABE, K., LU, Z. & MO, Y.-Y. 2014. Exosome-mediated transfer of miR-10b promotes cell invasion in breast cancer. *Molecular Cancer*, 13, 256.
- SKOG, J., WÜRDINGER, T., VAN RIJN, S., MEIJER, D. H., GAINCHE, L., CURRY, W. T., CARTER, B. S., KRICHEVSKY, A. M. & BREAKEFIELD, X. O. 2008. Glioblastoma microvesicles transport RNA and proteins that promote tumour growth and provide diagnostic biomarkers. *Nature Cell Biology*, 10, 1470-1476.
- STARR, T., BAULER, T. J., MALIK-KALE, P. & STEELE-MORTIMER, O. 2018. The phorbol 12-myristate-13-acetate differentiation protocol is critical to the interaction of THP-1 macrophages with Salmonella Typhimurium. *PLOS ONE*, 13, e0193601.
- STEINBACH, F. & THIELE, B. 1994. Phenotypic investigation of mononuclear phagocytes by flow cytometry. *Journal of Immunological Methods*, 174, 109-122.
- STOICA, G. E., KUO, A., POWERS, C., BOWDEN, E. T., SALE, E. B., RIEGEL, A. T. & WELLSTEIN, A. 2002. Midkine Binds to Anaplastic Lymphoma Kinase (ALK) and Acts as a Growth Factor for Different Cell Types*. *Journal of Biological Chemistry*, 277, 35990-35998.
- STONE, K. R., MICKEY, D. D., WUNDERLI, H., MICKEY, G. H. & PAULSON, D. F. 1978. Isolation of a human prostate carcinoma cell line (DU 145). *Int J Cancer*, 21, 274-81.

- STOORVOGEL, W., STROUS, G. J., GEUZE, H. J., OORSCHOT, V. & SCHWARTZT, A. L. 1991. Late endosomes derive from early endosomes by maturation. *Cell*, 65, 417-427.
- STRINGER, S. E., FORSTER, M. J., MULLOY, B., BISHOP, C. R., GRAHAM, G. J. & GALLAGHER, J. T. 2002. Characterization of the binding site on heparan sulfate for macrophage inflammatory protein 1 α . *Blood*, 100, 1543-1550.
- STUFFERS, S., SEM WEGNER, C., STENMARK, H. & BRECH, A. 2009. Multivesicular Endosome Biogenesis in the Absence of ESCRTs. *Traffic*, 10, 925-937.
- SULLIVAN, R., MARESH, G., ZHANG, X., SALOMON, C., HOOPER, J., MARGOLIN, D. & LI, L. 2017. The Emerging Roles of Extracellular Vesicles As Communication Vehicles within the Tumor Microenvironment and Beyond. *Frontiers in Endocrinology*, 8.
- SUMI, Y., MURAMATSU, H., TAKEI, Y., HATA, K.-I., UEDA, M. & MURAMATSU, T. 2002. Midkine, a heparin-binding growth factor, promotes growth and glycosaminoglycan synthesis of endothelial cells through its action on smooth muscle cells in an artificial blood vessel model. *Journal of Cell Science*, 115, 2659-2667.
- SUN, Z. J., WANG, Y., CAI, Z., CHEN, P. P., TONG, X. J. & XIE, D. 2008. Involvement of Cyr61 in growth, migration, and metastasis of prostate cancer cells. *British journal of cancer*, 99, 1656-1667.
- SVENSSON, K. J., CHRISTIANSON, H. C., WITTRUP, A., BOURSEAU-GUILMAIN, E., LINDQVIST, E., SVENSSON, L. M., MÖRGELIN, M. & BELTING, M. 2013. Exosome uptake depends on ERK1/2-heat shock protein 27 signaling and lipid Raft-mediated endocytosis negatively regulated by caveolin-1. *The Journal of biological chemistry*, 288, 17713-17724.
- TADOKORO, H., HIRAYAMA, A., KUDO, R., HASEBE, M., YOSHIOKA, Y., MATSUZAKI, J., YAMAMOTO, Y., SUGIMOTO, M., SOGA, T. & OCHIYA, T. 2020. Adenosine leakage from perforin-burst extracellular vesicles inhibits perforin secretion by cytotoxic T-lymphocytes. *PLOS ONE*, 15, e0231430.
- TAKAHASHI, H., SAKAKURA, K., KUDO, T., TOYODA, M., KAIRA, K., OYAMA, T. & CHIKAMATSU, K. 2017. Cancer-associated fibroblasts promote an immunosuppressive microenvironment through the induction and accumulation of protumoral macrophages. *Oncotarget*, 8, 8633-8647.
- TAURO, B. J., GREENING, D. W., MATHIAS, R. A., MATHIVANAN, S., JI, H. & SIMPSON, R. J. 2013. Two distinct populations of exosomes are released from LIM1863 colon carcinoma cell-derived organoids. *Molecular & cellular proteomics : MCP*, 12, 587-598.
- TAYLOR, D. D., GERÇEL-TAYLOR, C., LYONS, K. S., STANSON, J. & WHITESIDE, T. L. 2003. T-cell apoptosis and suppression of T-cell receptor/CD3-zeta by Fas ligand-containing membrane vesicles shed from ovarian tumors. *Clin Cancer Res*, 9, 5113-9.
- TEDESCO, S., DE MAJO, F., KIM, J., TRENTI, A., TREVISI, L., FADINI, G. P., BOLEGO, C., ZANDSTRA, P. W., CIGNARELLA, A. & VITIELLO, L. 2018. Convenience versus Biological Significance: Are PMA-Differentiated THP-1 Cells a Reliable Substitute for Blood-Derived Macrophages When Studying in Vitro Polarization? *Frontiers in Pharmacology*, 9.
- THAKUR, B. K., ZHANG, H., BECKER, A., MATEI, I., HUANG, Y., COSTA-SILVA, B., ZHENG, Y., HOSHINO, A., BRAZIER, H., XIANG, J., WILLIAMS, C., RODRIGUEZ-BARRUECO, R., SILVA, J. M., ZHANG, W., HEARN, S., ELEMENTO, O., PAKNEJAD, N., MANOVA-

References

- TODOROVA, K., WELTE, K., BROMBERG, J., PEINADO, H. & LYDEN, D. 2014. Double-stranded DNA in exosomes: a novel biomarker in cancer detection. *Cell Research*, 24, 766-769.
- THEOCHARIS, A. D., SKANDALIS, S. S., GIALELI, C. & KARAMANOS, N. K. 2016. Extracellular matrix structure. *Advanced Drug Delivery Reviews*, 97, 4-27.
- THEODORAKI, M. N., HOFFMANN, T. K. & WHITESIDE, T. L. 2018. Separation of plasma-derived exosomes into CD3(+) and CD3(-) fractions allows for association of immune cell and tumour cell markers with disease activity in HNSCC patients. *Clinical and experimental immunology*, 192, 271-283.
- THÉRY, C., AMIGORENA, S., RAPOSO, G. & CLAYTON, A. 2006. Isolation and Characterization of Exosomes from Cell Culture Supernatants and Biological Fluids. *Current Protocols in Cell Biology*, 30, 3.22.1-3.22.29.
- THÉRY, C., BOUSSAC, M., VÉRON, P., RICCIARDI-CASTAGNOLI, P., RAPOSO, G., GARIN, J. & AMIGORENA, S. 2001. Proteomic Analysis of Dendritic Cell-Derived Exosomes: A Secreted Subcellular Compartment Distinct from Apoptotic Vesicles. *The Journal of Immunology*, 166, 7309.
- THÉRY, C., REGNAULT, A., GARIN, J., WOLFERS, J., ZITVOGEL, L., RICCIARDI-CASTAGNOLI, P., RAPOSO, G. & AMIGORENA, S. 1999. Molecular characterization of dendritic cell-derived exosomes. Selective accumulation of the heat shock protein hsc73. *J Cell Biol*, 147, 599-610.
- THÉRY, C., WITWER, K. W., AIKAWA, E., ALCARAZ, M. J., ANDERSON, J. D., ANDRIANTSITOHAINA, R., ANTONIOU, A., ARAB, T., ARCHER, F., ATKIN-SMITH, G. K., AYRE, D. C., BACH, J.-M., BACHURSKI, D., BAHARVAND, H., BALAJ, L., BALDACCHINO, S., BAUER, N. N., BAXTER, A. A., BEBAWY, M., BECKHAM, C., BEDINA ZAVEC, A., BENMOUSSA, A., BERARDI, A. C., BERGESE, P., BIELSKA, E., BLENKIRON, C., BOBIS-WOZOWICZ, S., BOILARD, E., BOIREAU, W., BONGIOVANNI, A., BORRÀS, F. E., BOSCH, S., BOULANGER, C. M., BREAKFIELD, X., BREGGIO, A. M., BRENNAN, M. Á., BRIGSTOCK, D. R., BRISSON, A., BROEKMAN, M. L. D., BROMBERG, J. F., BRYL-GÓRZECKA, P., BUCH, S., BUCK, A. H., BURGER, D., BUSATTO, S., BUSCHMANN, D., BUSSOLATI, B., BUZÁS, E. I., BYRD, J. B., CAMUSSI, G., CARTER, D. R. F., CARUSO, S., CHAMLEY, L. W., CHANG, Y.-T., CHEN, C., CHEN, S., CHENG, L., CHIN, A. R., CLAYTON, A., CLERICI, S. P., COCKS, A., COCUCCI, E., COFFEY, R. J., CORDEIRO-DA-SILVA, A., COUCH, Y., COUMANS, F. A. W., COYLE, B., CRESCITELLI, R., CRIADO, M. F., D'SOUZA-SCHOREY, C., DAS, S., DATTA CHAUDHURI, A., DE CANDIA, P., DE SANTANA, E. F., DE WEVER, O., DEL PORTILLO, H. A., DEMARET, T., DEVILLE, S., DEVITT, A., DHONDT, B., DI VIZIO, D., DIETERICH, L. C., DOLO, V., DOMINGUEZ RUBIO, A. P., DOMINICI, M., DOURADO, M. R., DRIEDONKS, T. A. P., DUARTE, F. V., DUNCAN, H. M., EICHENBERGER, R. M., EKSTRÖM, K., EL ANDALOUSSI, S., ELIE-CAILLE, C., ERDBRÜGGER, U., FALCÓN-PÉREZ, J. M., FATIMA, F., FISH, J. E., FLORES-BELLVER, M., FÖRSÖNITS, A., FRELET-BARRAND, A., et al. 2018. Minimal information for studies of extracellular vesicles 2018 (MISEV2018): a position statement of the International Society for Extracellular Vesicles and update of the MISEV2014 guidelines. *Journal of Extracellular Vesicles*, 7, 1535750.
- THOMAS, D. A. & MASSAGUÉ, J. 2005. TGF-beta directly targets cytotoxic T cell functions during tumor evasion of immune surveillance. *Cancer Cell*, 8, 369-80.

- THOMPSON, C. A., PURUSHOTHAMAN, A., RAMANI, V. C., VLODAVSKY, I. & SANDERSON, R. D. 2013. Heparanase Regulates Secretion, Composition, and Function of Tumor Cell-derived Exosomes*♦. *Journal of Biological Chemistry*, 288, 10093-10099.
- TIAN, T., ZHU, Y.-L., HU, F.-H., WANG, Y.-Y., HUANG, N.-P. & XIAO, Z.-D. 2013. Dynamics of exosome internalization and trafficking. *Journal of Cellular Physiology*, 228, 1487-1495.
- TIETJEN, G. T., GONG, Z., CHEN, C. H., VARGAS, E., CROOKS, J. E., CAO, K. D., HEFFERN, C. T., HENDERSON, J. M., MERON, M., LIN, B., ROUX, B., SCHLOSSMAN, M. L., STECK, T. L., LEE, K. Y. & ADAMS, E. J. 2014. Molecular mechanism for differential recognition of membrane phosphatidylserine by the immune regulatory receptor Tim4. *Proc Natl Acad Sci U S A*, 111, E1463-72.
- TOMASEK, J. J., GABBIANI, G., HINZ, B., CHAPONNIER, C. & BROWN, R. A. 2002. Myofibroblasts and mechano-regulation of connective tissue remodelling. *Nature Reviews Molecular Cell Biology*, 3, 349-363.
- TOMINAGA, N., KOSAKA, N., ONO, M., KATSUDA, T., YOSHIOKA, Y., TAMURA, K., LÖTVALL, J., NAKAGAMA, H. & OCHIYA, T. 2015. Brain metastatic cancer cells release microRNA-181c-containing extracellular vesicles capable of destructing blood-brain barrier. *Nature communications*, 6, 6716-6716.
- TORREGGIANI, E., RONCUZZI, L., PERUT, F., ZINI, N. & BALDINI, N. 2016. Multimodal transfer of MDR by exosomes in human osteosarcoma. *Int J Oncol*, 49, 189-96.
- TORRES, S., BARTOLOMÉ, R. A., MENDES, M., BARDERAS, R., FERNANDEZ-ACEÑERO, M. J., PELÁEZ-GARCÍA, A., PEÑA, C., LOPEZ-LUCENDO, M., VILLAR-VÁZQUEZ, R., DE HERREROS, A. G., BONILLA, F. & CASAL, J. I. 2013. Proteome Profiling of Cancer-Associated Fibroblasts Identifies Novel Proinflammatory Signatures and Prognostic Markers for Colorectal Cancer. *Clinical Cancer Research*, 19, 6006.
- TRAJKOVIC, K., HSU, C., CHIANTIA, S., RAJENDRAN, L., WENZEL, D., WIELAND, F., SCHWILLE, P., BRÜGGER, B. & SIMONS, M. 2008. Ceramide Triggers Budding of Exosome Vesicles into Multivesicular Endosomes. *Science*, 319, 1244.
- TRAMS, E. G., LAUTER, C. J., NORMAN SALEM, JR. & HEINE, U. 1981. Exfoliation of membrane ecto-enzymes in the form of micro-vesicles. *Biochimica et Biophysica Acta (BBA) - Biomembranes*, 645, 63-70.
- TUXHORN, J. A., AYALA, G. E., SMITH, M. J., SMITH, V. C., DANG, T. D. & ROWLEY, D. R. 2002. Reactive stroma in human prostate cancer: induction of myofibroblast phenotype and extracellular matrix remodeling. *Clin Cancer Res*, 8, 2912-23.
- UCHIMURA, K., MORIMOTO-TOMITA, M., BISTRUP, A., LI, J., LYON, M., GALLAGHER, J., WERB, Z. & ROSEN, S. D. 2006. HSulf-2, an extracellular endoglucosamine-6-sulfatase, selectively mobilizes heparin-bound growth factors and chemokines: effects on VEGF, FGF-1, and SDF-1. *BMC biochemistry*, 7, 2-2.
- UENO, M., YAMADA, S., ZAKO, M., BERNFIELD, M. & SUGAHARA, K. 2001. Structural Characterization of Heparan Sulfate and Chondroitin Sulfate of Syndecan-1 Purified from Normal Murine Mammary Gland Epithelial Cells: COMMON PHOSPHORYLATION OF XYLOSE AND DIFFERENTIAL SULFATION OF GALACTOSE IN THE PROTEIN LINKAGE REGION TETRASACCHARIDE SEQUENCE*. *Journal of Biological Chemistry*, 276, 29134-29140.
- UMEZU, T., TADOKORO, H., AZUMA, K., YOSHIZAWA, S., OHYASHIKI, K. & OHYASHIKI, J. H. 2014. Exosomal miR-135b shed from hypoxic multiple myeloma cells

References

- enhances angiogenesis by targeting factor-inhibiting HIF-1. *Blood*, 124, 3748-3757.
- VALADI, H., EKSTROM, K., BOSSIOS, A., SJOSTRAND, M., LEE, J. J. & LOTVALL, J. O. 2007. Exosome-mediated transfer of mRNAs and microRNAs is a novel mechanism of genetic exchange between cells. *Nat Cell Biol*, 9, 654-9.
- VALLABHANENI, K. C., PENFORNIS, P., DHULE, S., GUILLONNEAU, F., ADAMS, K. V., YUAN MO, Y., XU, R., LIU, Y., WATABE, K., VEMURI, M. C. & POCHAMPALLY, R. 2014. Extracellular vesicles from bone marrow mesenchymal stem/stromal cells transport tumor regulatory microRNA, proteins, and metabolites. *Oncotarget*, 6.
- VAN BALKOM, B. W. M., EISELE, A. S., PEGTEL, D. M., BERVOETS, S. & VERHAAR, M. C. 2015. Quantitative and qualitative analysis of small RNAs in human endothelial cells and exosomes provides insights into localized RNA processing, degradation and sorting. *Journal of Extracellular Vesicles*, 4, 26760.
- VAN DEUN, J., MESTDAGH, P., AGOSTINIS, P., AKAY, Ö., ANAND, S., ANCKAERT, J., MARTINEZ, Z. A., BAETENS, T., BEGHEIN, E., BERTIER, L., BERX, G., BOERE, J., BOUKOURIS, S., BREMER, M., BUSCHMANN, D., BYRD, J. B., CASERT, C., CHENG, L., CMOCH, A., DAVELOOSE, D., DE SMEDT, E., DEMIRSOY, S., DEPOORTER, V., DHONDT, B., DRIEDONKS, T. A. P., DUDEK, A., ELSHARAWY, A., FLORIS, I., FOERS, A. D., GÄRTNER, K., GARG, A. D., GEEURICKX, E., GETTEMANS, J., GHAZAVI, F., GIEBEL, B., KORMELINK, T. G., HANCOCK, G., HELSMOORTELE, H., HILL, A. F., HYENNE, V., KALRA, H., KIM, D., KOWAL, J., KRAEMER, S., LEIDINGER, P., LEONELLI, C., LIANG, Y., LIPPENS, L., LIU, S., LO CICERO, A., MARTIN, S., MATHIVANAN, S., MATHIYALAGAN, P., MATUSEK, T., MILANI, G., MONGUIÓ-TORTAJADA, M., MUS, L. M., MUTH, D. C., NÉMETH, A., NOLTE-'T HOEN, E. N. M., O'DRISCOLL, L., PALMULLI, R., PFAFFL, M. W., PRIMDAL-BENGTSON, B., ROMANO, E., ROUSSEAU, Q., SAHOO, S., SAMPAIO, N., SAMUEL, M., SCICLUNA, B., SOEN, B., STEELS, A., SWINNEN, J. V., TAKATALO, M., THAMINY, S., THÉRY, C., TULKENS, J., VAN AUDENHOVE, I., VAN DER GREIN, S., VAN GOETHEM, A., VAN HERWIJNEN, M. J., VAN NIEL, G., VAN ROY, N., VAN VLIET, A. R., VANDAMME, N., VANHAUWAERT, S., VERGAUWEN, G., VERWEIJ, F., WALLAERT, A., WAUBEN, M., WITWER, K. W., ZONNEVELD, M. I., DE WEVER, O., VANDESOMPELE, J., HENDRIX, A. & CONSORTIUM, E.-T. 2017. EV-TRACK: transparent reporting and centralizing knowledge in extracellular vesicle research. *Nature Methods*, 14, 228-232.
- VAN NIEL, G., D'ANGELO, G. & RAPOSO, G. 2018. Shedding light on the cell biology of extracellular vesicles. *Nature Reviews Molecular Cell Biology*, 19, 213-228.
- VÉRON, P., SEGURA, E., SUGANO, G., AMIGORENA, S. & THÉRY, C. 2005. Accumulation of MFG-E8/lactadherin on exosomes from immature dendritic cells. *Blood Cells, Molecules, and Diseases*, 35, 81-88.
- VERONA, E. V., ELKAHLOUN, A. G., YANG, J., BANDYOPADHYAY, A., YEH, I. T. & SUN, L.-Z. 2007. Transforming Growth Factor- β Signaling in Prostate Stromal Cells Supports Prostate Carcinoma Growth by Up-regulating Stromal Genes Related to Tissue Remodeling. *Cancer Research*, 67, 5737.
- VERWEIJ, F. J., BEBELMAN, M. P., JIMENEZ, C. R., GARCIA-VALLEJO, J. J., JANSSEN, H., NEEFJES, J., KNOL, J. C., DE GOEIJ-DE HAAS, R., PIERSMA, S. R., BAGLIO, S. R., VERHAGE, M., MIDDELDORP, J. M., ZOMER, A., VAN RHEENEN, J., COPPOLINO, M. G., HURBAIN, I., RAPOSO, G., SMIT, M. J., TOONEN, R. F. G., VAN NIEL, G. &

- PEGTEL, D. M. 2018. Quantifying exosome secretion from single cells reveals a modulatory role for GPCR signaling. *Journal of Cell Biology*, 217, 1129-1142.
- VICENTE, C. M., LIMA, M. A., NADER, H. B. & TOMA, L. 2015. SULF2 overexpression positively regulates tumorigenicity of human prostate cancer cells. *J Exp Clin Cancer Res*, 34, 25.
- WEBBER, J. & CLAYTON, A. 2013. How pure are your vesicles? *Journal of Extracellular Vesicles*, 2, 10.3402/jev.v2i0.19861.
- WEBBER, J., STEADMAN, R., MASON, M. D., TABI, Z. & CLAYTON, A. 2010. Cancer exosomes trigger fibroblast to myofibroblast differentiation. *Cancer Res*, 70, 9621-30.
- WEBBER, J., STONE, T. C., KATILIUS, E., SMITH, B. C., GORDON, B., MASON, M. D., TABI, Z., BREWIS, I. A. & CLAYTON, A. 2014. Proteomics analysis of cancer exosomes using a novel modified aptamer-based array (SOMAscan) platform. *Mol Cell Proteomics*, 13, 1050-64.
- WEBBER, J., YEUNG, V. & CLAYTON, A. 2015a. Extracellular vesicles as modulators of the cancer microenvironment. *Seminars in Cell & Developmental Biology*, 40, 27-34.
- WEBBER, J. P., SPARY, L. K., SANDERS, A. J., CHOWDHURY, R., JIANG, W. G., STEADMAN, R., WYMANT, J., JONES, A. T., KYNASTON, H., MASON, M. D., TABI, Z. & CLAYTON, A. 2015b. Differentiation of tumour-promoting stromal myofibroblasts by cancer exosomes. *Oncogene*, 34, 290-302.
- WEI, X., LIU, C., WANG, H., WANG, L., XIAO, F., GUO, Z. & ZHANG, H. 2016. Surface Phosphatidylserine Is Responsible for the Internalization on Microvesicles Derived from Hypoxia-Induced Human Bone Marrow Mesenchymal Stem Cells into Human Endothelial Cells. *PLoS One*, 11, e0147360.
- WEI, Y., WANG, D., JIN, F., BIAN, Z., LI, L., LIANG, H., LI, M., SHI, L., PAN, C., ZHU, D., CHEN, X., HU, G., LIU, Y., ZHANG, C. Y. & ZEN, K. 2017. Pyruvate kinase type M2 promotes tumour cell exosome release via phosphorylating synaptosome-associated protein 23. *Nat Commun*, 8, 14041.
- WELSH, J. B., SAPINOSO, L. M., KERN, S. G., BROWN, D. A., LIU, T., BAUSKIN, A. R., WARD, R. L., HAWKINS, N. J., QUINN, D. I., RUSSELL, P. J., SUTHERLAND, R. L., BREIT, S. N., MOSKALUK, C. A., FRIERSON, H. F. & HAMPTON, G. M. 2003. Large-scale delineation of secreted protein biomarkers overexpressed in cancer tissue and serum. *Proceedings of the National Academy of Sciences*, 100, 3410.
- WELTON, J. L., WEBBER, J. P., BOTOS, L.-A., JONES, M. & CLAYTON, A. 2015. Ready-made chromatography columns for extracellular vesicle isolation from plasma. *Journal of Extracellular Vesicles*, 4, 27269.
- WIECKOWSKI, E. U., VISUS, C., SZAJNIK, M., SZCZEPANSKI, M. J., STORKUS, W. J. & WHITESIDE, T. L. 2009. Tumor-Derived Microvesicles Promote Regulatory T Cell Expansion and Induce Apoptosis in Tumor-Reactive Activated CD8⁺ T Lymphocytes. *The Journal of Immunology*, 183, 3720.
- WINKLER, J., ABISOYE-OGUNNIYAN, A., METCALF, K. J. & WERB, Z. 2020. Concepts of extracellular matrix remodelling in tumour progression and metastasis. *Nature Communications*, 11, 5120.
- WITTRUP, A., ZHANG, S.-H., TEN DAM, G. B., VAN KUPPEVELT, T. H., BENGTON, P., JOHANSSON, M., WELCH, J., MÖRGELIN, M. & BELTING, M. 2009. ScFv Antibody-

References

- induced Translocation of Cell-surface Heparan Sulfate Proteoglycan to Endocytic Vesicles. *Journal of Biological Chemistry*, 284, 32959-32967.
- WITWER, K. W., BUZÁS, E. I., BEMIS, L. T., BORA, A., LÄSSER, C., LÖTVALL, J., NOLTE-'T HOEN, E. N., PIPER, M. G., SIVARAMAN, S., SKOG, J., THÉRY, C., WAUBEN, M. H. & HOCHBERG, F. 2013. Standardization of sample collection, isolation and analysis methods in extracellular vesicle research. *Journal of extracellular vesicles*, 2, 10.3402/jev.v2i0.20360.
- WOLF, P. 1967. The Nature and Significance of Platelet Products in Human Plasma. *British Journal of Haematology*, 13, 269-288.
- WOLFERS, J., LOZIER, A., RAPOSO, G., REGNAULT, A., THÉRY, C., MASURIER, C., FLAMENT, C., POUZIEUX, S., FAURE, F., TURSZ, T., ANGEVIN, E., AMIGORENA, S. & ZITVOGEL, L. 2001. Tumor-derived exosomes are a source of shared tumor rejection antigens for CTL cross-priming. *Nat Med*, 7, 297-303.
- WU, T.-H., LI, Y.-Y., WU, T.-L., CHANG, J. W. C., CHOU, W.-C., HSIEH, L.-L., CHEN, J.-R. & YE, K.-Y. 2014. Culture supernatants of different colon cancer cell lines induce specific phenotype switching and functional alteration of THP-1 cells. *Cellular Immunology*, 290, 107-115.
- WYCKOFF, J., WANG, W., LIN, E. Y., WANG, Y., PIXLEY, F., STANLEY, E. R., GRAF, T., POLLARD, J. W., SEGALL, J. & CONDEELIS, J. 2004. A paracrine loop between tumor cells and macrophages is required for tumor cell migration in mammary tumors. *Cancer Res*, 64, 7022-9.
- YANG, E., WANG, X., GONG, Z., YU, M., WU, H. & ZHANG, D. 2020. Exosome-mediated metabolic reprogramming: the emerging role in tumor microenvironment remodeling and its influence on cancer progression. *Signal Transduction and Targeted Therapy*, 5, 242.
- YANG, N. & FRIEDL, A. 2016. Syndecan-1-Induced ECM Fiber Alignment Requires Integrin $\alpha\beta 3$ and Syndecan-1 Ectodomain and Heparan Sulfate Chains. *PLOS ONE*, 11, e0150132.
- YANG, Y., MACLEOD, V., MIAO, H. Q., THEUS, A., ZHAN, F., SHAUGHNESSY, J. D., JR., SAWYER, J., LI, J. P., ZCHARIA, E., VLODAVSKY, I. & SANDERSON, R. D. 2007. Heparanase enhances syndecan-1 shedding: a novel mechanism for stimulation of tumor growth and metastasis. *J Biol Chem*, 282, 13326-33.
- YANG, Y., YACCOBY, S., LIU, W., LANGFORD, J. K., PUMPHREY, C. Y., THEUS, A., EPSTEIN, J. & SANDERSON, R. D. 2002. Soluble syndecan-1 promotes growth of myeloma tumors in vivo. *Blood*, 100, 610-7.
- YAYON, A., KLAGSBRUN, M., ESKO, J. D., LEDER, P. & ORNITZ, D. M. 1991. Cell surface, heparin-like molecules are required for binding of basic fibroblast growth factor to its high affinity receptor. *Cell*, 64, 841-848.
- YEUNG, V., WEBBER, J. P., DUNLOP, E. A., MORGAN, H., HUTTON, J., GURNEY, M., JONES, E., FALCON-PEREZ, J., TABI, Z., ERRINGTON, R. & CLAYTON, A. 2018. Rab35-dependent extracellular nanovesicles are required for induction of tumour supporting stroma. *Nanoscale*, 10, 8547-8559.
- YING, X., WU, Q., WU, X., ZHU, Q., WANG, X., JIANG, L., CHEN, X. & WANG, X. 2016. Epithelial ovarian cancer-secreted exosomal miR-222-3p induces polarization of tumor-associated macrophages. *Oncotarget*, 7, 43076-43087.
- YURCHENCO, P. D. & SCHITTNY, J. C. 1990. Molecular architecture of basement membranes. *Faseb j*, 4, 1577-90.

- ZABEO, D., CVJETKOVIC, A., LÄSSER, C., SCHORB, M., LÖTVALL, J. & HÖÖG, J. L. 2017. Exosomes purified from a single cell type have diverse morphology. *Journal of extracellular vesicles*, 6, 1329476-1329476.
- ZABOROWSKI, M. P., BALAJ, L., BREAKEFIELD, X. O. & LAI, C. P. 2015. Extracellular Vesicles: Composition, Biological Relevance, and Methods of Study. *BioScience*, 65, 783-797.
- ZEHE, C., ENGLING, A., WEGEHINGEL, S., SCHÄFER, T. & NICKEL, W. 2006. Cell-surface heparan sulfate proteoglycans are essential components of the unconventional export machinery of FGF-2. *Proc Natl Acad Sci U S A*, 103, 15479-84.
- ZHANG, H., FREITAS, D., KIM, H. S., FABIJANIC, K., LI, Z., CHEN, H., MARK, M. T., MOLINA, H., MARTIN, A. B., BOJMAR, L., FANG, J., RAMPERSAUD, S., HOSHINO, A., MATEI, I., KENIFIC, C. M., NAKAJIMA, M., MUTVEI, A. P., SANSONE, P., BUEHRING, W., WANG, H., JIMENEZ, J. P., COHEN-GOULD, L., PAKNEJAD, N., BRENDDEL, M., MANOVA-TODOROVA, K., MAGALHÃES, A., FERREIRA, J. A., OSÓRIO, H., SILVA, A. M., MASSEY, A., CUBILLOS-RUIZ, J. R., GALLETTI, G., GIANNAKAKOU, P., CUERVO, A. M., BLENIS, J., SCHWARTZ, R., BRADY, M. S., PEINADO, H., BROMBERG, J., MATSUI, H., REIS, C. A. & LYDEN, D. 2018. Identification of distinct nanoparticles and subsets of extracellular vesicles by asymmetric flow field-flow fractionation. *Nature cell biology*, 20, 332-343.
- ZHANG, H. & LYDEN, D. 2019. Asymmetric-flow field-flow fractionation technology for exomere and small extracellular vesicle separation and characterization. *Nature protocols*, 14, 1027-1053.
- ZHANG, L. & YU, D. 2019. Exosomes in cancer development, metastasis, and immunity. *Biochimica et biophysica acta. Reviews on cancer*, 1871, 455-468.
- ZHANG, P., ZHOU, X., HE, M., SHANG, Y., TETLOW, A. L., GODWIN, A. K. & ZENG, Y. 2019. Ultrasensitive detection of circulating exosomes with a 3D-nanopatterned microfluidic chip. *Nature Biomedical Engineering*, 3, 438-451.
- ZHAO, H., YANG, L., BADDOUR, J., ACHREJA, A., BERNARD, V., MOSS, T., MARINI, J. C., TUDAWE, T., SEVIOUR, E. G., SAN LUCAS, F. A., ALVAREZ, H., GUPTA, S., MAITI, S. N., COOPER, L., PEEHL, D., RAM, P. T., MAITRA, A. & NAGRATH, D. 2016. Tumor microenvironment derived exosomes pleiotropically modulate cancer cell metabolism. *Elife*, 5, e10250.
- ZHOU, W., FONG, MIRANDA Y., MIN, Y., SOMLO, G., LIU, L., PALOMARES, MELANIE R., YU, Y., CHOW, A., O'CONNOR, SEAN TIMOTHY F., CHIN, ANDREW R., YEN, Y., WANG, Y., MARCUSSON, ERIC G., CHU, P., WU, J., WU, X., LI, ARTHUR X., LI, Z., GAO, H., REN, X., BOLDIN, MARK P., LIN, PENGNIAN C. & WANG, SHIZHEN E. 2014. Cancer-Secreted miR-105 Destroys Vascular Endothelial Barriers to Promote Metastasis. *Cancer Cell*, 25, 501-515.
- ZITVOGEL, L., REGNAULT, A., LOZIER, A., WOLFERS, J., FLAMENT, C., TENZA, D., RICCIARDI-CASTAGNOLI, P., RAPOSO, G. & AMIGORENA, S. 1998. Eradication of established murine tumors using a novel cell-free vaccine: dendritic cell derived exosomes. *Nature Medicine*, 4, 594-600.